

**Development of Organocatalytic Methods for Activity-  
Directed Bioactive Molecule Discovery**

Jacob Masters

Submitted in accordance with the requirements for the degree of

Doctor of Philosophy

The University of Leeds

School of Chemistry

April 2019

The candidate confirms that the work submitted is his/her own, except where work which has formed part of jointly-authored publications has been included. The contribution of the candidate and the other authors to this work has been explicitly indicated below. The candidate confirms that appropriate credit has been given within the thesis where reference has been made to the work of others.

“Realisation of small molecule libraries based on frameworks distantly related to natural products” A. Aimon, G. Karageorgis, J. Masters, M. Dow, P. G. E. Craven, M. Ohsten, A. Willaume, R. Morgentin, N. Ruiz-Llamas, H. Lemoine, T. Kalliokoski, A. J. Eatherton, D. J. Foley, S. P. Marsden and A. Nelson, *Org. Biomol. Chem.*, 2018, **16**, 3160–3167.

This copy has been supplied on the understanding that it is copyright material and that no quotation from the thesis may be published without proper acknowledgement.

The right of Jacob Masters to be identified as Author of this work has been asserted by him in accordance with the Copyright, Designs and Patents Act 1988.

## Acknowledgements

The opportunity to work on this project has been extremely rewarding, and I would like to thank my supervisors Adam and Stuart for all their help and guidance they have provided me with throughout the last three and a half years. I will always be grateful for their help in my professional development.

I would also like to thank my industrial supervisor Andy Eatherton who has been very supportive, especially during a rewarding placement at AstraZeneca. Dr George Karageorgis has been highly useful throughout the project, and his help has been invaluable. I have to give a mention to Dr Sri Sridharan – an ever-present force of nature throughout my seven and a half years at the School of Chemistry in Leeds. The scary organic wizard shouting at me in my first year of undergraduate labs has become a dear friend, who has supported me immensely both academically and personally.

My colleagues in the Nelson lab at the University of Leeds are exceptionally intelligent people who will no doubt go on to great successes in the future. All past and current PhDs/post-docs have been of great value, but I would notably like to thank Adam, Chloe, Joan, Shiao, Chris and Luke – you have been terrifically fun to work with. I could write loads here, but I'm not sure any of it is appropriate for what is supposed to be a professional document.

Despite being complete strangers while doing our undergraduate degrees at Leeds, Sam Liver has become one of my closest friends. The friendship forged with him while working on this project has been one of the main highlights of the process. Additionally, Bobby Lowe has now seen out seven and a half years as both a colleague and a friend in Leeds, and his presence has frequently managed to turn bad days around. Ly bros x.

Finally, my girlfriend Megan and my family have been vital, especially during some of the more challenging periods. They are loving, kind and ambitious people who inspire me to fulfil my potential, and I will always be grateful for their unconditional love and support.

## Abstract

Conventional approaches for the discovery of bioactive small molecules typically follow a cycle of design, synthesis, purification and testing. This workflow usually employs a narrow toolkit of robust chemical reactions, and places equal value on every chemical entity regardless of bioactivity. Consequently, significant effort is invested into designing, making and purifying large numbers of compounds with low levels of bioactivity.

Activity-Directed Synthesis (ADS) places the focus exclusively on bioactive molecules during the discovery phase, using activity to guide syntheses through an iterative discovery cycle. ADS exploits chemistry that may yield multiple product outcomes and are not commonly integrated into traditional discovery workflows. The process is structure-blind and function-driven, permitting the discovery of bioactive small molecules and their associated synthetic routes in parallel, mimicking elements of the process in which small molecule natural products are produced *via* biosynthetic pathways in nature.

Integration of new chemistries into the ADS workflow would permit exploration of more diverse areas of chemical space using the approach. Organocatalysis was recognised to have potential to generate a wide range of scaffolds in a combinatorial manner and is robust enough to tolerate the miniaturised high-throughput format required for ADS. The potential for the use of organocatalysis in ADS was explored and successfully translated into a micro-scale format for application in ADS. Additionally, protocols were developed to remove undesirable functional groups from product mixtures prior to screening.

The miniaturised organocatalytic chemistry was then applied in ADS to reaction arrays, seeking to use organocatalysis in ADS to discover novel androgen receptor agonists. Different strategies for reaction array design were developed, in addition to protocols for efficient execution of reaction arrays. Both conversion and bioactivity of product mixtures were assessed

using a TR-FRET assay and NMR, highlighting issues that significantly decreased the number of reactions that yielded intermolecular products. However, successful identification of bioactive components within product mixtures that were not the result of intermolecular reactions demonstrated the potential for the protocols developed to be successful in identifying bioactive small molecules. Consequently, ADS is now poised to utilise organocatalysis to attempt to generate bioactive molecules for alternative biological targets.

## Table of Contents

<b>Acknowledgements</b>		<b>iii</b>
<b>Abstract</b>		<b>iv</b>
<b>Abbreviations</b>		<b>ix</b>
<b>1 Introduction</b>		<b>1</b>
1.1 Current Approaches to Bioactive Molecule Discovery		3
1.1.1 Current Medicinal Chemistry Toolbox		3
1.1.2 High-Throughput Screening of Diverse Libraries		5
1.1.3 Diversity- and Lead-Oriented Synthesis		8
1.1.4 Structure-Based Design		12
1.1.5 Fragment-Based Discovery		14
1.1.6 Emerging High-Throughput Discovery Methods		17
1.2 Activity-Directed Synthesis (ADS)		21
1.2.1 Natural Product Biosynthesis		21
1.2.2 Strategy Underpinning ADS		23
1.2.3 ADS Case Study		25
1.2.4 Other Function-Driven Approaches to Bioactive Molecule Discovery		29
1.3 Androgen Receptor		30
1.3.1 Biology of the Androgen Receptor		30
1.3.2 Known Androgen Receptor Modulators		31
1.4 Overview of Covalent Organocatalysis		34
1.4.1 Enamine Catalysis		35
1.4.2 Iminium Catalysis		37
1.4.3 <i>N</i> -Heterocyclic Carbene Catalysis		39
1.5 Project Outline		42
1.5.1 Objective 1: Configuration of Organocatalysis for ADS		42
1.5.2 Objective 2: Exploring the Value of Organocatalysis in ADS		43
<b>2 Configuration of Organocatalytic Chemistry for ADS</b>		<b>44</b>

2.1	Selection and Synthesis of Organocatalysts .....	44
2.3	Identification of Exemplar Organocatalytic Chemistry .....	47
2.3.1	Amine-Catalysed Reactions.....	47
2.3.2	<i>N</i> -Heterocyclic Carbene Catalysed Reactions .....	51
2.3.3	Transfer of Chemistry to Microwell Plate Format .....	55
2.4	Development of Post-Reaction Protocols .....	58
2.4.1	Reduction with Sodium Borohydride.....	58
2.4.2	Reductive Amination .....	61
2.5	Summary of Configuration of Organocatalysis for ADS .....	63
<b>3</b>	<b>Exploring the Value of Organocatalysis in ADS.....</b>	<b>64</b>
3.1	Configuration of TR-FRET Androgen Receptor Assay.....	64
3.2	Design and Execution of an Exhaustive ADS Reaction Array	67
3.2.1	Design of Round 1 ADS Reaction Array.....	67
3.2.2	Synthesis of Armed Substrates.....	69
3.2.3	Selection of Co-Substrates .....	71
3.2.4	Execution of Mock Array .....	73
3.2.5	Execution of Exhaustive Reaction Array .....	79
3.3	Design and Execution of a Targeted ADS Reaction Array.....	84
3.3.1	Design of Targeted Reaction Array .....	84
3.3.2	Execution of Targeted Reaction Array.....	87
3.4	Design and Execution of Second Exhaustive ADS Reaction Array.....	93
3.4.1	Synthesis of Co-Substrates .....	94
3.4.2	Execution of Second Exhaustive ADS Reaction Array ...	96
3.5	Evaluation of Product Mixtures from Organocatalytic ADS..	100
3.5.1	Validation of Conversion and Bioactivity .....	100
3.5.2	Scale-Up and Identification of Products .....	105
<b>4</b>	<b>Conclusions and Future Work .....</b>	<b>109</b>
4.1	Analysis of Value of Organocatalysis in ADS .....	110
4.2	Future Scope for Application of Organocatalysis in ADS .....	111

<b>5</b>	<b>Appendix: Synthesis of Compounds Accessible using a Top-Down Lead-Oriented Synthesis Approach .....</b>	<b>112</b>
<b>6</b>	<b>Experimental Procedures .....</b>	<b>114</b>
6.1	General Information .....	114
6.2	Chemistry Experimental Procedures.....	115
6.2.1	Synthesis of Catalysts .....	115
6.2.2	Synthesis of Exemplar Reactions from Literature .....	119
6.2.3	Synthesis of Round 1 Substrates .....	130
6.2.4	Synthesis of Round 2 Co-substrates .....	134
6.2.5	Syntheses for Compounds Isolated from ADS.....	139
6.2.6	Synthesis of Exemplar Screening Compounds.....	142
6.3	Procedures for Transfer to Plate Format .....	155
6.4	Procedures for Post-Reaction Protocol Development.....	159
6.5	Procedures for Assembly of ADS Reaction Arrays .....	160
6.5.1	Stock Solutions of Reaction Components .....	160
6.5.2	Mock Array.....	160
6.5.3	Reaction Arrays .....	161
6.6	Assay Experimental Procedures .....	163
6.6.1	General Assay Procedure.....	163
6.6.2	Procedure for Dose-Response Assay .....	165
6.6.3	Procedure for Single Point Assays .....	165
6.7	Structural Data used for Cheminformatics Pipeline.....	166
6.8	Full Data for Round 1 Exhaustively Designed ADS Arrays..	167
6.8.1	Round 1 Validation Study.....	177
6.9	Design of Round 2 ADS Reaction Arrays .....	179
6.10	Methods for Evaluation and Scale-Up.....	184
6.10.1	NMR Analysis Reaction Tracing Experiments.....	184
6.10.2	Crude Dose-Response Experiments .....	185
6.10.3	Fractionation of Reactions .....	186
<b>7</b>	<b>References.....</b>	<b>189</b>



## Abbreviations

ADS	Activity-Directed Synthesis
AR	Androgen Receptor
CAS	Chemical Abstracts Service
COSY	Homonuclear Correlation Spectroscopy
DABCO	1,4-Diazabicyclo[2.2.2]octane
DBU	1,8-Diazabicyclo[5.4.0]undec-7-ene
DCM	Dichloromethane
DMF	<i>N,N</i> -Dimethylformamide
DMSO	Dimethyl Sulfoxide
DOS	Diversity-Oriented Synthesis
DOSP	( <i>p</i> -dodecylphenylsulfonyl)prolinato
DTT	Dithiothreitol
esp	$\alpha,\alpha,\alpha',\alpha'$ -tetramethyl-1,3-benzenedipropionate
FBDD	Fragment-Based Drug Discovery
GPCR	G-protein coupled receptors
GST	Glutathione S-transferase
HCV	Hepatitis C Virus
HIV	Human Immunodeficiency Virus
HMBC	Heteronuclear Multiple Bond Correlation
HOMO	Highest Occupied Molecular Orbital
HPLC	High Performance Liquid Chromatography
HRMS	High Resolution Mass Spectrometry
HSQC	Heteronuclear Single-Quantum correlation
HTS	High-Throughput Screening
IC <sub>50</sub>	Half-Maximal Inhibitory Concentration
IR	Infrared
LBD	Ligand Binding Domain
LC-MS	Liquid Chromatography-Mass Spectrometry
LE	Ligand Efficiency
LOS	Lead-Oriented Synthesis
LUMO	Lowest Unoccupied Molecular Energy
mCPBA	<i>meta</i> -Chloroperoxybenzoic acid

MS	Mass Spectrometry
NHC	<i>N</i> -Heterocyclic Carbene
NMO	<i>N</i> -Methylmorpholine <i>N</i> -oxide
NMR	Nuclear Magnetic Resonance
oct	Octanoate
SAR	Structure-Activity Relationship
SARMs	Selective-Androgen Receptor Modulators
SBDD	Structure-Based Drug Design
SUI	Stress Urinary Incontinence
TFA	Trifluoroacetic Acid
THF	Tetrahydrofuran
TLC	Thin Layer Chromatography
tpa	Triphenylacetate
TR-FRET	Time-Resolved Fluorescence Resonance Transfer
XRC	X-Ray Crystallography

## 1 Introduction

Nature has provided an invaluable number of biologically active small molecules that have served as great inspiration to medicinal chemists. The structural complexity and bioactive diversity of natural products is well documented, and their influence on drug design is evident. The FDA (US Food and Drug Administration) had approved a total of 547 natural products and associated derivatives as small molecule therapies by the end of 2013, representing more than one-third (38%) of all approved molecular entities.<sup>1</sup>

In contrast, the efficient exploration of diverse areas of chemical space by medicinal chemists in recent years has been less effective. It has been proposed that this is largely due to an over-reliance on a well-established but narrow set of synthetic methods, and compound libraries that have not managed to explore biologically relevant chemical space efficiently.<sup>2,3</sup> An analysis of the CAS registry suggested that around half of all known compounds are based upon 0.25% of known molecular frameworks, demonstrating an evident lack of diversity between known compounds, and by consequence their inefficient exploration of biologically relevant chemical space.

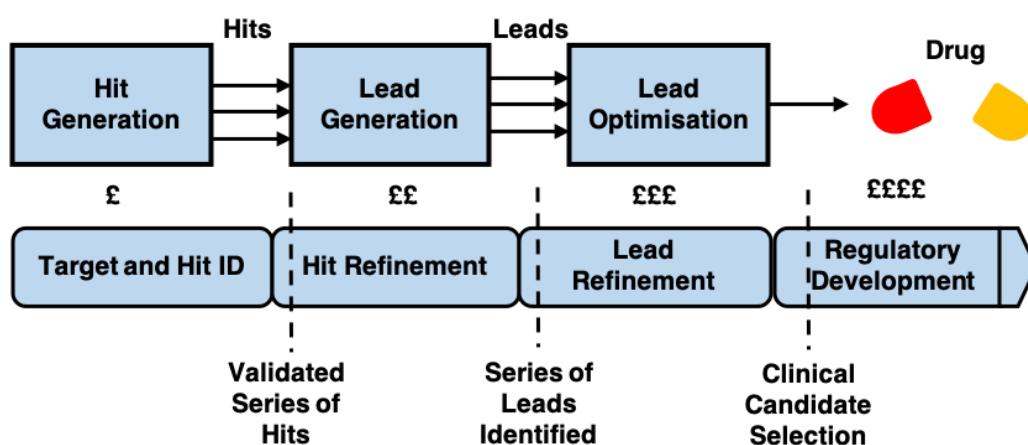


**Figure 1.1** – An overview of the pipeline for the discovery and development of new drugs.

As the total spend on research and development costs increases year on year, with ever increasing rates of attrition of clinical candidates (**Figure 1.1**), new strategies that result in the identification of high-quality bioactive hit molecules in the early stages of the drug discovery process are required. Higher quality starting points should help to avoid the massive expense of clinical candidate failures during the later stages of the drug discovery process.<sup>4</sup>

Natural products have been optimised *via* an evolutionary natural selection process to possess functional benefit for the host organism. This process often results in natural products that have structures with high affinity for their intended biological targets.<sup>5</sup> Analysis of the structural properties of natural products demonstrates there to be a greater number of chiral centres, bridgeheads, rings and rotatable bonds per molecule in natural products than in pharmaceutical compounds in development. This shows that they display more structural complexity in comparison to synthetic compounds designed by medicinal chemists.<sup>6</sup> This structural complexity leads to an innate tendency for natural products to display potent bioactivity, as they can explore more diverse areas of chemical space in contrast to synthetic compounds.

New strategies that increase the efficient development of bioactive molecules with similar characteristics to natural products are therefore of great importance, helping medicinal chemists move further away from compound libraries that do not explore chemical space efficiently. This introduction explores commonly used approaches that chemists use to discover bioactive molecules that are suitable as starting points in drug discovery. A new approach will then be discussed - Activity-Directed Synthesis (ADS): a function-driven, structure-blind approach to bioactive molecule discovery that mimics some aspects of the process used by nature to enable the emergence of natural products.

## 1.1 Current Approaches to Bioactive Molecule Discovery

To discover a bioactive small molecule that is a suitable clinical candidate as a therapy for a disease, a suitable chemical starting point must be identified using a lead generation strategy. Recent analysis of hit-to-candidate projects published in *J. Med. Chem.* in 2016-2017 shows that while 43% of clinical candidates were generated from previously known ligands, the remainder of clinical candidates were discovered using a range of *de novo* lead generation strategies.<sup>7</sup> A selection of these strategies will be more discussed in more detail.

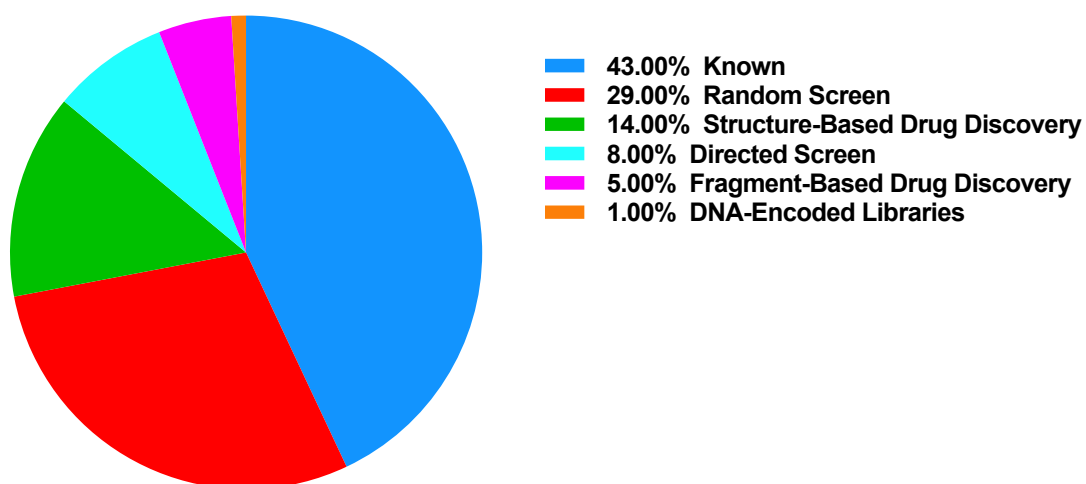


**Figure 1.2** – Sources of hit-to-candidate pairs from articles in *J. Med. Chem.* during the period 2016-2017 (n = 66). Figure adapted from referenced article.<sup>7</sup>

### 1.1.1 Current Medicinal Chemistry Toolbox

Medicinal chemists have gravitated towards the use of a narrow toolkit of reactions that prioritise synthetic accessibility and the ability to deliver compounds, over the efficient exploration of chemical space.<sup>2,8,9</sup> Despite unprecedented advances in the range of available synthetic methods, the reactions that medicinal chemists use during the drug discovery process have remained remarkably similar, demonstrating a high barrier to entry for new synthetic methodologies. The bias towards these reactions has led to development of compounds that have a low fraction of

$sp^3$ -hybridised carbon centres and are largely lipophilic: properties that are not usually observed in either successful drugs or natural products.<sup>10</sup> Medicinal chemists are also guided by Lipinski's work linking his 'Rule of 5' for physicochemical properties to oral absorption of drug molecules. These parameters are often at odds with the chemistries commonly used within drug discovery, as they feature aromatic or unsaturated functionality that tends to increase lipophilicity.<sup>11</sup>

As can be observed in **Figure 1.3**, an analysis of articles in the *Journal of Medicinal Chemistry* demonstrated that the palette of reactions that medicinal chemists have used has barely changed in 30 years. Of the top ten most commonly used reactions from articles in 2014, only the Suzuki-Miyaura coupling has been developed within the last 40 years. This clearly shows that uptake of newly discovered novel reactions has been poor, with the opportunity cost of this being structural diversity and potential bioactivity of compounds. Considering the extensive potential and novel reactivity of recently developed methods including, but not limited to, late-stage functionalisation, C-H activation and photoredox coupling; it is surprising that these chemistries have not been added to the palette of reactions commonly used by synthetic medicinal chemists.<sup>12-14</sup> However, there has been increased recognition that integration of such methods into discovery workflows could add significant value and lead to the accession of unexplored chemical space.<sup>15,16</sup>

Additionally, commercially available building blocks are reflective of the currently used chemistries, offering great diversity and availability for starting reagents, but often no or very little diversity for reagents that are required for new methodologies.<sup>2</sup> Analyses of molecular shape diversity have demonstrated that the limitations of the chemistry toolbox may have led to significant overpopulation of certain types of molecular shapes, hampering the structural diversity required to efficiently explore biologically relevant chemical space.

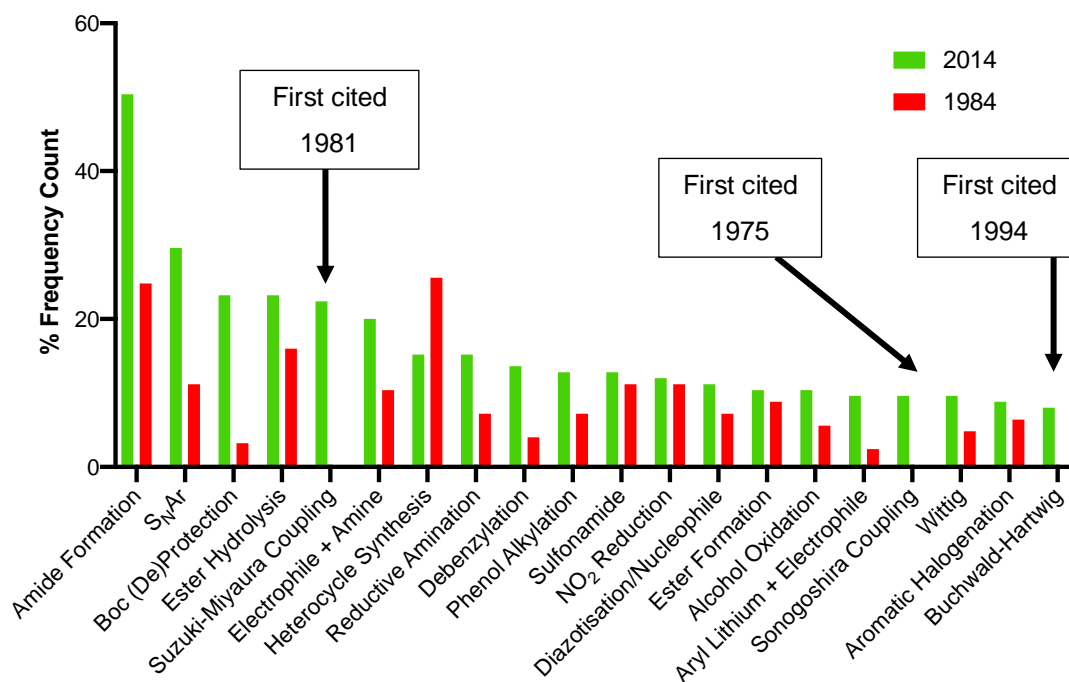


**Figure 1.3** - Occurrence of reaction classes, plotted as the percentage of which it shows up in at least one manuscript ( $n = 125$ ; representative data set taken from *J. Med. Chem.* in 2014 and 1984).<sup>8</sup> Figure adapted from *J. Med. Chem.*, 2016, 59, 4443–4458.

As such, it is essential that new approaches to discovering bioactive small molecules attempt to increase structural diversity by incorporating less commonly used synthetic methodology. This should consequently allow access to unexplored areas of chemical space that could lead to hits that would otherwise not be uncovered using chemistries currently employed in pharmaceutical discovery processes.

### 1.1.2 High-Throughput Screening of Diverse Libraries

Medicinal chemists have often initiated drug discovery programmes by screening large libraries of compounds using an *in vitro* biological assay, a process known as High-Throughput Screening (HTS).<sup>17</sup> HTS is the automated screening of a large numbers of molecules, with active hit compounds providing an entry point for drug discovery projects.<sup>18</sup> Each compound in the library is screened in a high-throughput assay, and the

activity of each compound reported. Further validation of any active compounds can provide an entry point for medicinal chemists into the drug discovery process. The total number of small molecule drugs that have been found to have originated from HTS is thought to be roughly 50%.<sup>19</sup> However, recent additions to the hit discovery toolbox may have decreased this reliance on HTS - a recent analysis of articles from the *Journal of Medicinal Chemistry* between 2016 and 2017 demonstrated that 31% of candidate starting points sampled were identified *via* a random HTS.<sup>7</sup>

One drug currently on the market that was the result of a successful HTS project is Sorafenib, a multi-kinase inhibitor used for the treatment of advanced renal cell carcinoma.<sup>20</sup> Raf serine/threonine kinase isoforms cRaf1, MEK1, or ERK2 were identified as suitable targets due to their vital role in the MAPK cascade involved in cellular proliferation and survival.<sup>21</sup> A scintillation proximity assay was used in the HTS campaign that allowed detection of inhibitors of the kinases cRaf1, MEK1, or ERK2.<sup>22</sup> A HTS campaign was initiated, screening around 200,000 compounds, with one compound identified as a promising hit with an IC<sub>50</sub> of 17  $\mu$ M (**Figure 1.4**). Optimisation of the hit by evolving the compound with a range of synthetic transformations, notably generation of a library of bis-aryl analogues via parallel synthesis, increased the potency. Structure-Activity Relationship (SAR) studies informed the design and synthesis of more analogues until Sorafenib was identified as a nanomolar modulator of Raf1.

The example shown in **Figure 1.4** is an example of extensive optimisation of HTS hits using a reliable toolkit of synthetic methods, and this process has led to the discovery of many effective drugs.<sup>23</sup> However, high clinical failure rates have led to escalating downstream costs and doubts as to the efficiency of this linear process.



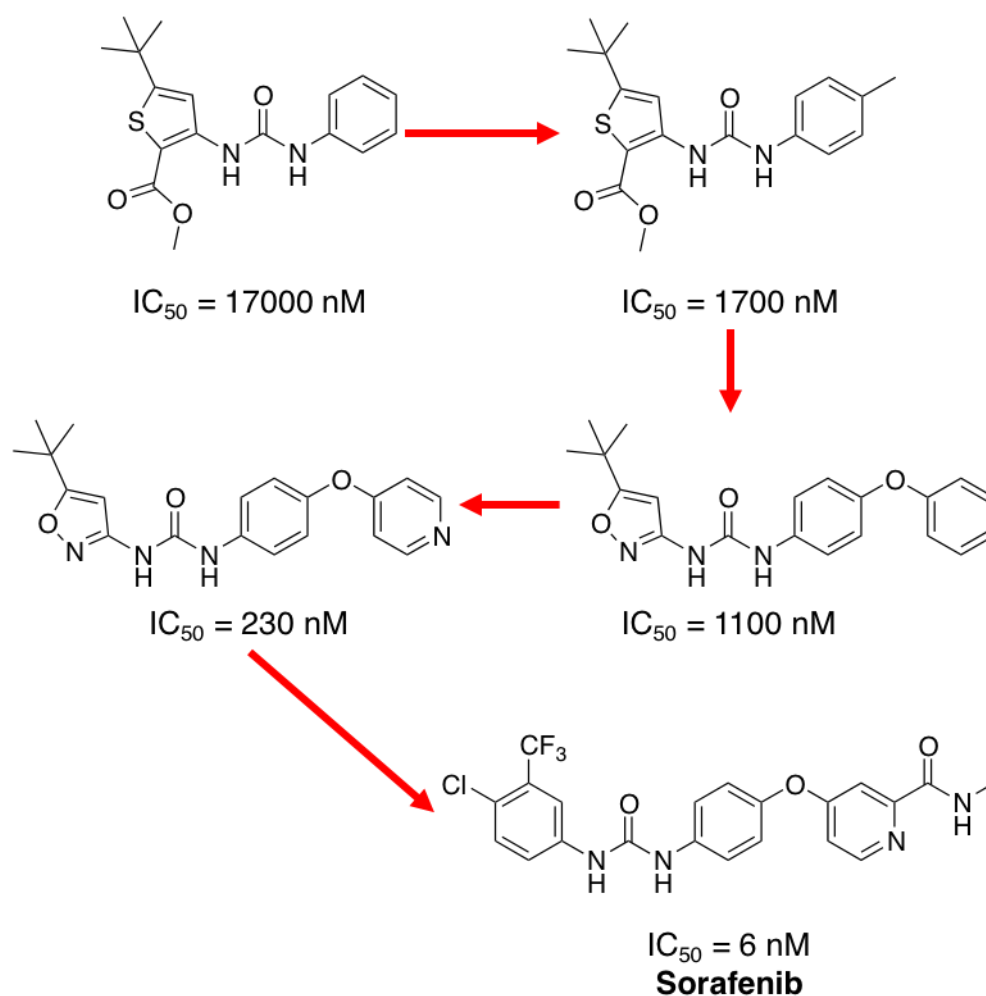


**Figure 1.4** – Overview of the discovery of Sorafenib utilising HTS and subsequent optimisation via SAR studies.<sup>20</sup>

The majority of compounds generated from HTS-initiated programs have also tended to be flat, aromatic and achiral; with high  $sp^2$  character.<sup>24</sup> This is speculated to be a result of the dependence upon the previously mentioned toolkit of reliable synthetic methods,<sup>2</sup> in addition to pressure to abide explicitly with guidelines to make compounds with lead-like properties. Emphasis appears to have been placed upon synthetic accessibility of scaffolds screened in biochemical assays rather than the true diversity of compound libraries, limiting the proportion of three-dimensional chemical space that can be explored.<sup>11</sup> One approach to tackle this issue is Lead-Oriented Synthesis which focuses on the synthesis of diverse compounds with lead-like molecular properties.

HTS clearly has value in generating excellent starting points for drug discovery, and ongoing curation of the libraries utilised is essential for it to continue to be a productive source of hits. Development of higher quality screening libraries that explore novel chemical space is therefore prudent to prevent declining productivity.<sup>25</sup>

### ***1.1.3 Diversity- and Lead-Oriented Synthesis***

Diversity-Oriented Synthesis (DOS) is a strategy facilitating the generation of novel and diverse combinatorial libraries that can be screened against a variety of targets in order to support the discovery of bioactive molecules.<sup>26,27</sup> In contrast to traditional target-oriented approaches that aim to access precise regions of chemical space with respect to a specified target, DOS utilises a range of synthetic strategies to obtain diverse novel scaffolds.<sup>28</sup> By maximising diversity in the molecular scaffold and its appendage, functional groups and stereochemistry, small DOS libraries of compounds that vary in structure can be generated to efficiently explore chemical space. These libraries aim to generate compounds with novel frameworks that can be added to screening libraries, offering diversity that does not currently exist in many HTS compound collections.

The strategies employed in DOS to achieve skeletal diversity utilise highly functionalised molecules, or molecules that contain functionality capable of forming numerous different scaffolds. When treated with reagents, functional groups pair within the molecule to form new scaffolds, or different reactions occur at the functionality dependent on the conditions employed (**Figure 1.5**).<sup>29</sup> Efficient, high yielding, and stereoselective reactions are used over a number of steps to assemble a small library of diverse compounds. By using a divergent strategy in which forward synthetic analysis is utilised, complex and diverse areas of chemical space can be explored.<sup>30</sup>

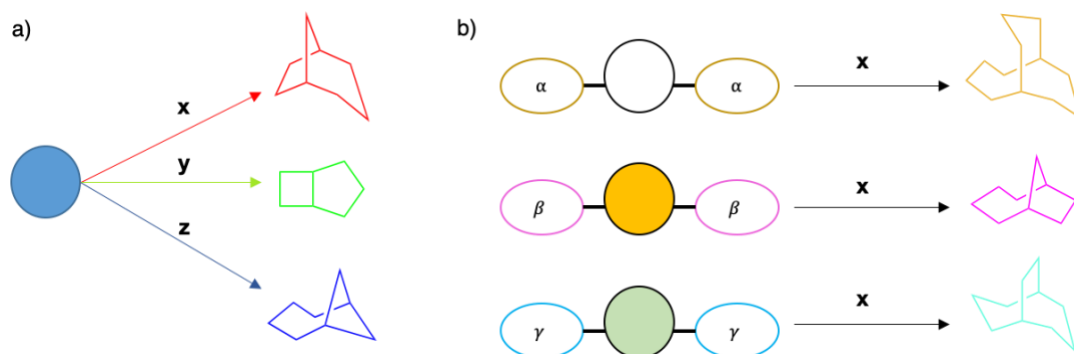
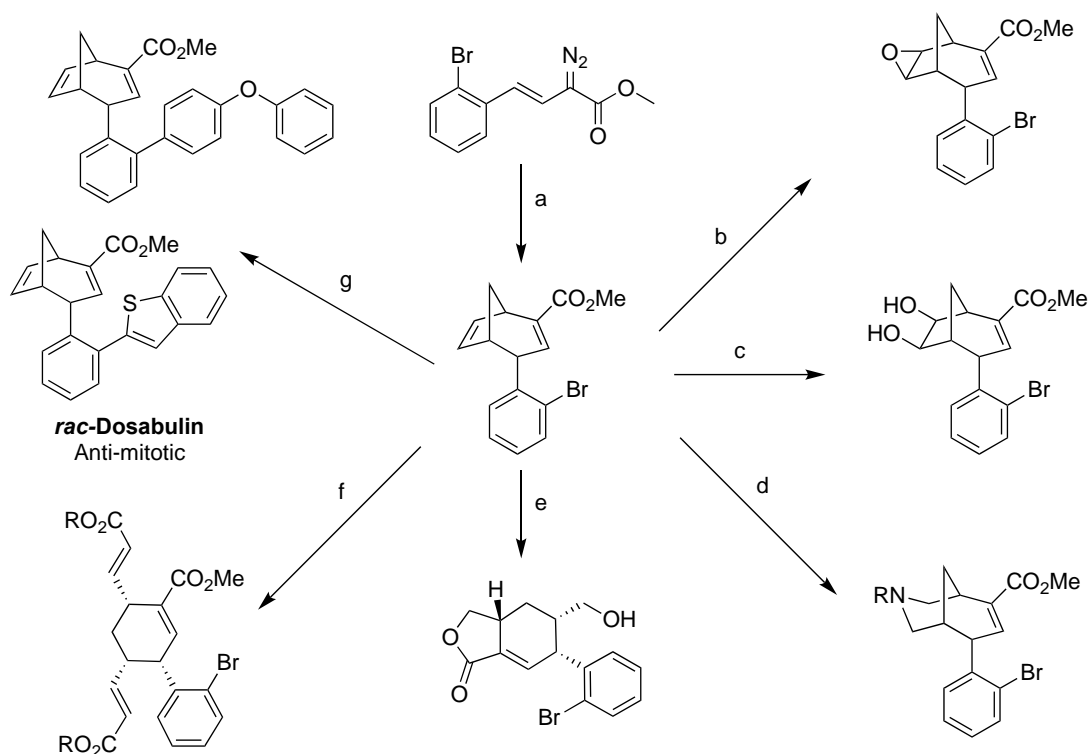


**Figure 1.5** – The two principal approaches to scaffold diversity in DOS. (a) Reagent-based approach in which different reagents (**x**, **y** and **z**) cause diverse scaffolds to be formed from the same starting material. (b) Substrate-based approach in which the same reaction conditions (**x**) are used, but different reactivity (**α**, **β** and **γ**) is encoded within the substrate.

Spring et al. synthesised a DOS compound library using rhodium-carbenoid chemistry.<sup>31</sup> Utilising a reagent-based approach, once a functionalised substrate had been generated, the group was able to synthesise 35 structurally diverse scaffolds by performing different transformations and couplings (**Scheme 1.1**). Screening of the compound collection revealed two compounds that displayed anti-mitotic activity in cells. Further modification of these compounds facilitated the identification of (S)-Dosabulin, a novel small molecule capable of arresting mitosis by depolymerising microtubules with sub-micromolar efficacy. This discovery validated DOS in tandem with phenotypic screening as an effective strategy for the identification of bioactive entities.

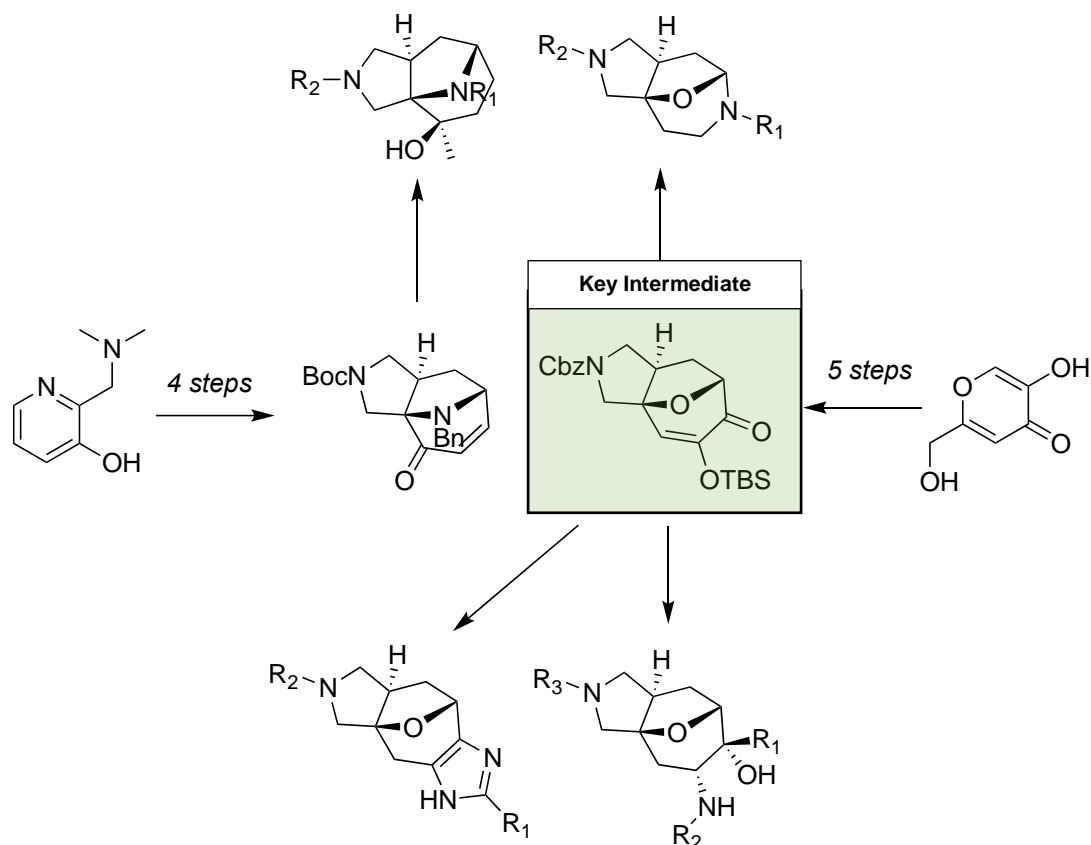
DOS is a highly efficient strategy in obtaining libraries of diverse compounds for use in screening, but the strategy still requires the synthesis and rational design of molecules that may not display activity in a target-driven approach. Additionally, synthetic and scaffold diversity is prioritised over the utility of the products made, with no consideration given to the molecular properties of the products formed.



**Scheme 1.1** - Selection of products generated in a diversity-oriented synthesis that enabled identification of a modulator of mitosis. By using a reagent-based approach, numerous diverse scaffolds were synthesised from a common starting material containing multiple functional groups. a) cyclopentadiene,  $\text{Rh}_2(\text{OAc})_4$  (1 mol%), DCM; b) *m*CPBA, DCM; c)  $\text{OsO}_4$  (2.5 mol%), NMO, acetone- $\text{H}_2\text{O}$  (9:1); d) 2,6-lutidine, NMO,  $\text{OsO}_4$  (2.5 mol%),  $\text{PhI}(\text{OAc})_2$ , acetone- $\text{H}_2\text{O}$  (10:1), then  $\text{NH}_2\text{R}$ ,  $\text{NaBH}(\text{OAc})_3$ , DCM; e) 2,6-lutidine, NMO,  $\text{OsO}_4$  (2.5 mol%),  $\text{PhI}(\text{OAc})_2$ , acetone- $\text{H}_2\text{O}$  (10:1), then  $\text{NaBH}_4$ , MeOH; f) alkene, Hoveyda-Grubbs (II) catalyst (10 mol%), ethylene, toluene,  $100^\circ\text{C}$ ; g)  $\text{Pd}(\text{OAc})_2$  (10 mol%),  $\text{PPh}_3$  (15 mol%),  $(\text{HO})_2\text{B}$ -Heterocycle, 2N  $\text{K}_2\text{CO}_3$ , toluene,  $90^\circ\text{C}$ ;

Lead-Oriented Synthesis (LOS) is a similar concept to DOS, that aims to deliver shape-diverse libraries of compounds. However, unlike DOS, compounds discovered *via* LOS must have specific lead-like molecular properties that give them higher utility in the drug discovery process.<sup>32</sup> Molecules should also be tolerant to a wide range of polar functional groups, be without residual reactive centres, and not be susceptible to  $\text{Log}P$  drift – a phenomenon whereby reactions tend to occur with higher efficiency with substrates that possess more non-polar functionality, making them more

synthetically tractable.<sup>33</sup> Additionally, synthetic routes to compounds must utilise cheap reagents and conditions, allowing easy translation of the chemistry into a drug discovery setting.



**Scheme 1.2** – Overview of a ‘top-down’ approach to LOS to develop a number of libraries based upon lead-like scaffolds.

Foley et. al. demonstrated an example of a ‘top-down’ LOS approach, in which compound libraries based on many diverse natural product-like scaffolds were synthesised (**Scheme 1.2**).<sup>34,35</sup> The approach used a [5+2] cycloaddition to obtain a cycloadduct, that was subjected to synthetic strategies such as cleavage, addition of new functionality and ring expansion, to generate 26 diverse scaffolds from the same key intermediate. Four of these scaffolds were subsequently decorated, enabling the production of over 2900 medicinally relevant screening compounds. Notably, the scaffolds had broad natural product-like features, but were only distantly related to specific natural products themselves, hence providing attractive starting points for drug discovery. This approach is discussed further in

**Chapter 5**, as my contributions to this project resulted in the delivery of a number of compounds that populated one of the synthesised libraries.

### 1.1.4 Structure-Based Design

Structure-Based Drug Design (SBDD) is a more rational approach to drug discovery than HTS, that uses the known structure of a biological target to direct the design of bioactive molecules (**Figure 1.6**). By determining the structure of the target protein, compounds or fragments can be docked into regions of the structure *in silico* and arbitrarily scored based on their predicted interactions with the target.<sup>36</sup> Acquisition of these compounds and testing *via* a biochemical assay allows experimental efficacy values to be obtained, which can be compared to the scoring functions generated by computer algorithms.

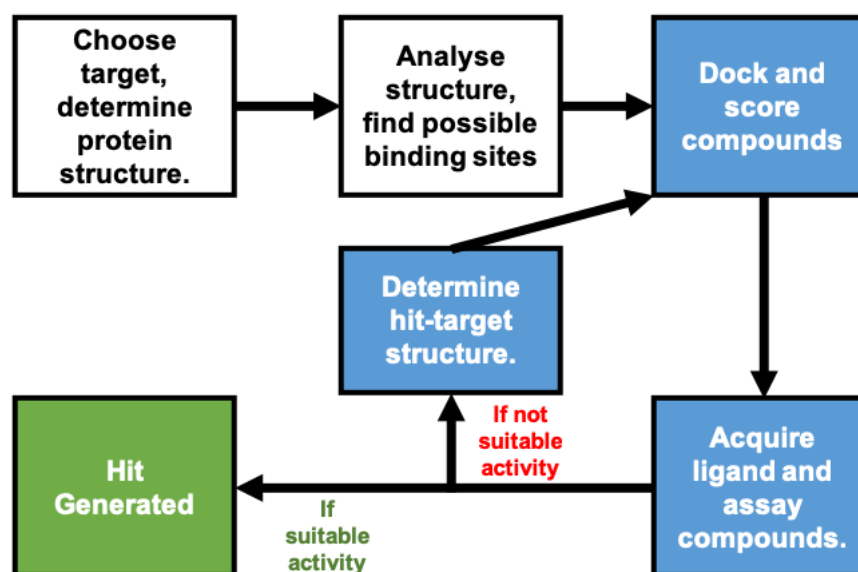
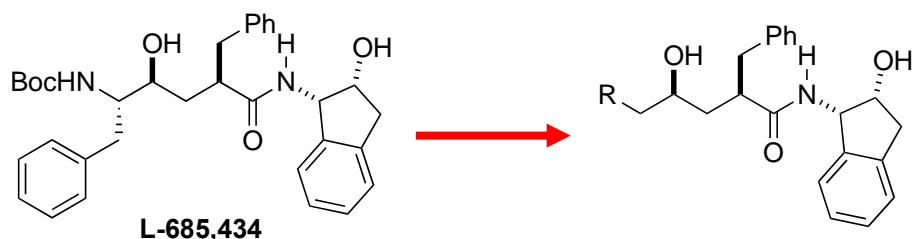


**Figure 1.6** - Flow chart demonstrating the a typical iterative process of a Structure-Based Drug Design campaign.<sup>36</sup>

The scoring functions produced by algorithms serve to prioritise compounds for synthesis and assaying, by attempting to reduce the volume of synthesis required to obtain active compounds. Structural determination of a modulator in complex with the target reveals potential sites for optimisation on the ligand that can be altered to increase potency. After several rounds of

this process, compounds with sufficiently high specificity and potency can be identified and taken forward in the drug discovery process as candidate molecules.



Compound	R	cIC <sub>95</sub> (nM)	IC <sub>50</sub> (nM)
3		400	7.8
11		1500	347
12		n.d.	80
13		>400	15
14 (L-732,747)		100	0.35

**Table 1.1** – Compounds investigated during the structure-guided optimisation of L-685,434 to L-732,747, an inhibitor of HIV protease.<sup>37</sup> cIC<sub>95</sub> = computationally predicted concentration to observe a 95% inhibitory effect.

**Table 1.1** details an example of a clinical candidate discovered with the aid of SBDD, the HIV protease inhibitor L-735,524.<sup>37</sup> Initial *in silico* modelling of the inhibitor L-685,434 in complex with HIV protease enabled structure guided optimisation of the hit compound, with the aim of designing

a more potent competitive inhibitor of the enzyme. L-685,434 lacked appropriate solubility and pharmacokinetic properties, and it was hypothesised that incorporating a basic amine into the structure of the compound could improve bioavailability and aqueous solubility. Incorporation of the amine into a ring would also limit the conformational freedom. A selection of the molecules designed *in silico*, synthesised and tested during the optimisation process are shown in **Table 1.1**. The information generated from the *in silico* docking and scoring was evidently efficiently used to increase the potency of the hit compound, enabling discovery of L-732,747.

The SBDD approach, when used in combination with hits provided from HTS screens, provides a powerful method of generating potent lead compounds, allowing faster access to a quantitative understanding of the interactions a ligand and the desired target.<sup>38</sup> However, there are inherent errors of the algorithms used in the docking and scoring process. *In silico* docking do not always correlate to experimental *in vitro* activity, but indicate a higher probability of discovering an active ligand.<sup>39</sup> This is in part due to failures to consider role of solvent in the binding site, desolvation of the inhibitor, and the conformational variability of the inhibitor and the target.<sup>40</sup> In addition, *in silico* scoring of fragments can only be initiated in cases where the biological target is fully defined. As such, it remains only a technique useful for guiding chemists in making rational decisions in the optimisation of lead compounds, rather than a strategy for generating novel scaffolds that explore new areas of chemical space.

### **1.1.5 Fragment-Based Discovery**

In 1996, Fesik et al. reported a new technique for identifying compounds with nanomolar affinities for their desired target, a method they described as “SAR by NMR”.<sup>41</sup> Weakly binding small organic molecule fragments (with millimolar/high-micromolar activity) were identified by detecting chemical shift changes in <sup>15</sup>N-labelled protein targets via heteronuclear single quantum coherence (HSQC) spectroscopy. Once several weakly binding fragments had been identified and optimised at



different, but proximal residues of the protein, X-ray crystallography was carried out to find the location and orientation of the fragments interacting with the target, and the weakly binding fragments linked together to obtain ligands with nanomolar affinities.

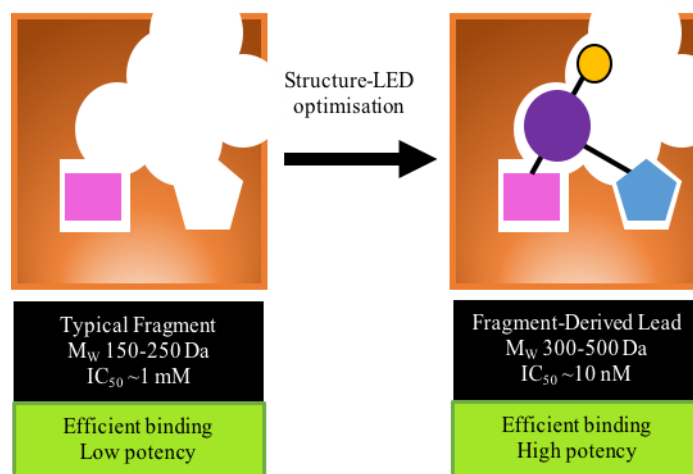


**Figure 1.7** – Overview of Fragment-Based Drug Discovery.

This technique has evolved into what is now commonly known as Fragment-Based Drug Discovery (FBDD), and has rapidly developed over the last 20 years into a popular and viable alternative to methods such as HTS (**Figure 1.7**).<sup>42</sup> By screening libraries of fragments, each with typically up to ~18 heavy atoms,<sup>43</sup> rather than much larger libraries of drug-like compounds with up to 30 heavy atoms, both the speed and efficiency of screening are increased. This is due to the observation that for each heavy atom added to a molecule, there are roughly an order of magnitude more molecules in chemical space that are possible to explore, hence the fragments sample chemical space much more efficiently.<sup>44</sup> Biological protein targets present complex surfaces for ligands to bind, and fragments are capable of exhibiting high-quality well-defined interactions with a target, despite demonstrating binding affinities in much higher millimolar ranges. For this reason, the concept of ligand efficiency (LE) was defined as the free energy of binding of a ligand divided by its heavy atom account, and is a common metric calculated to determine binding efficiency of a fragment.<sup>45</sup>

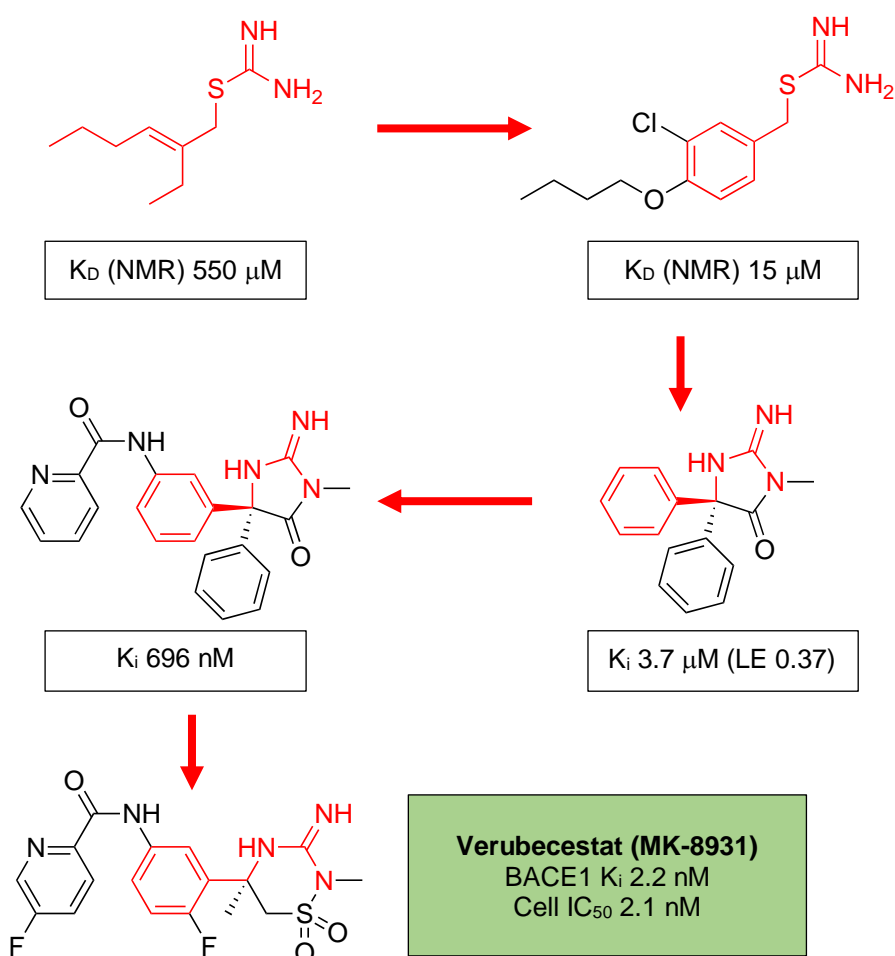


**Figure 1.8** – Overview of the discovery of Verubecestat, a BACE1 inhibitor, using a fragment-based approach.

Numerous FBDD leads have now been progressed into clinical trials,<sup>42,46</sup> showing the enthusiasm of academic groups and pharmaceutical companies in adopting the strategy. An example of a clinical candidate discovered *via* fragment-based drug discovery is the  $\beta$ -site amyloid precursor protein cleaving enzyme 1 (BACE1) inhibitor Verubecestat (**Figure 1.8**).<sup>47</sup> Beginning from a selection of isothiourea fragment hits, further development aided by SBDD provided insights that enabled optimisation of the pharmacophore, resulting in an iminohydantoin lead compound. The lead displayed high ligand efficiency, and improved binding, in part to the projection of the phenyl group into a hydrophobic pocket of the protein. Further optimisation enabled improved potency and selectivity, eventually resulting in the discovery of Verubecestat, which eventually progressed to be a clinical candidate targeting mild to moderate prodromal Alzheimer's disease.

### 1.1.6 Emerging High-Throughput Discovery Methods

Miniaturisation and parallel processing have allowed acceleration of drug discovery workflow. Such approaches have already been implemented effectively for high-throughput discovery of chemical reactions and reaction optimisation, in which arrays of catalysts and ligands with diverse mixtures of substrates have been assembled, in addition to methods that allow bioactive molecule discovery.

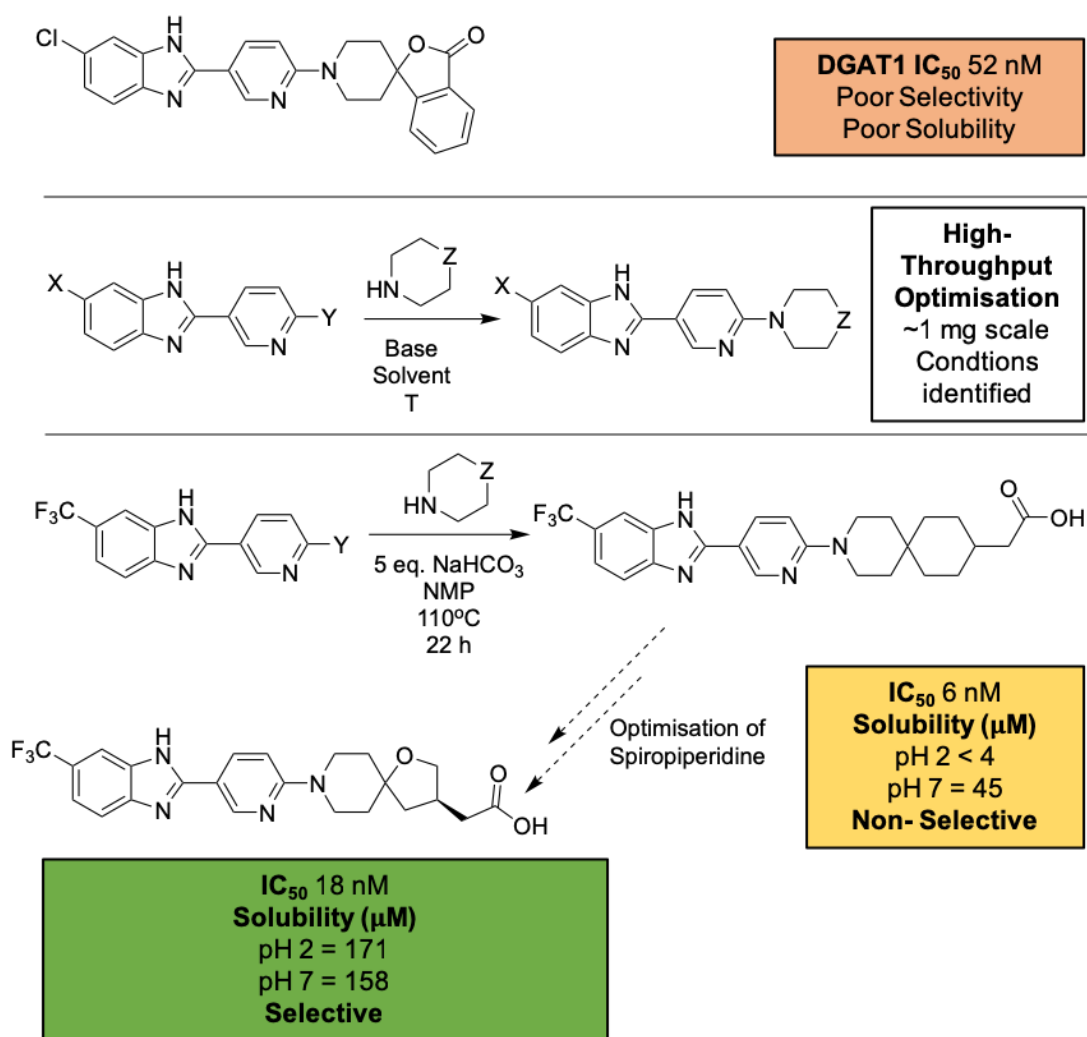


**Figure 1.9** – An overview of microscale high-throughput optimisation applied to the discovery of spiropiperidine DGAT1 inhibitors.

The processes of high-throughput chemical synthesis, reaction optimisation and screening on a biochemical assay have been integrated to good effect. Miniaturisation and parallel processing enabled the high-throughput optimisation of a lead compound that inhibited diacylglycerol

acyltransferase (DGAT1) (**Figure 1.9**).<sup>48</sup> The lead was a potent modulator of DGAT1, but exhibited poor selectivity and solubility. Miniaturised reaction arrays enabled optimisation of challenging  $S_NAr$  reactions: variation of base, solvent and substrate class enabled the discovery of robust synthetic conditions. These conditions enabled the synthesis of a spiropiperidine compound that exhibited good potency but poor solubility. A series of analogues was made that led to the discovery of a more potent, selective and soluble lead compound.

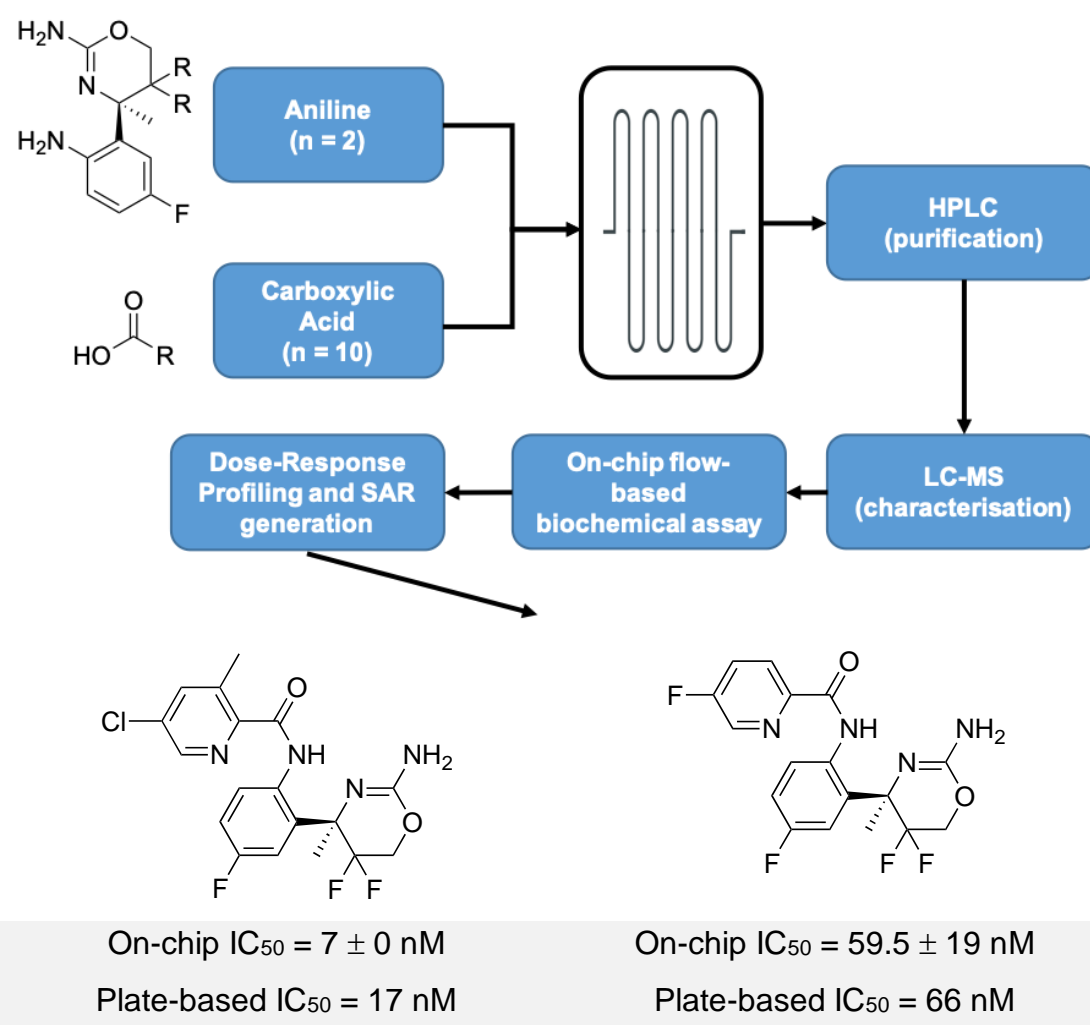


**Figure 1.10** – Overview of a flow-reaction and screening based workflow utilised to generate SAR for a series of inhibitors of BACE1.<sup>49</sup>

Technology that integrates both synthetic and biological evaluation in-flow has also been established. A notable example explored the SAR of a series of inhibitors of the protease beta-secretase 1 (BACE1), in which

aniline core fragments were coupled in flow to carboxylic acid building blocks (**Figure 1.10**).<sup>49</sup> The workflow facilitated the integrated synthesis, purification, and screening of each product made using an on-chip flow-based biochemical assay, altering the concentration gradient flowing through a capillary. The hit compounds demonstrated to be active using the flow system were screened individually using a plate-based assay, allowing validation of their activity. This workflow allowed dose-dependency to be rapidly established for each compound in around one hour, enabling the definition of SAR for a series of inhibitors.

Cernak et. al. described a method entitled NanoSAR, in which nanomole-scale Suzuki and C-N coupling reactions mixtures were screened on a label-free affinity-selection mass spectrometry bioassay to discover modulators for three kinase targets.<sup>50</sup> A known fragment was derivatised *via* nanoscale reactions, utilising a range of building blocks, with reaction conditions optimised to match each specific building block. Crude reaction mixtures were then analysed by ultra HPLC-mass-spectrometry to assess conversion and reaction efficiency, before being screened on an affinity-selection mass spectrometry bioassay. This allowed screening of a range of reaction conditions for each combination of building blocks used, and the affinities of the crude mixtures for the target were then ranked. Mixtures showing the highest affinity were then reproduced on a larger scale to identify products. Using this method, potent modulators of all three kinases were discovered using the nanoscale reactions that required minimal consumption of chemical matter. **Figure 1.11** demonstrates this workflow for one of the kinase targets, Checkpoint kinase 1 (CHK1).

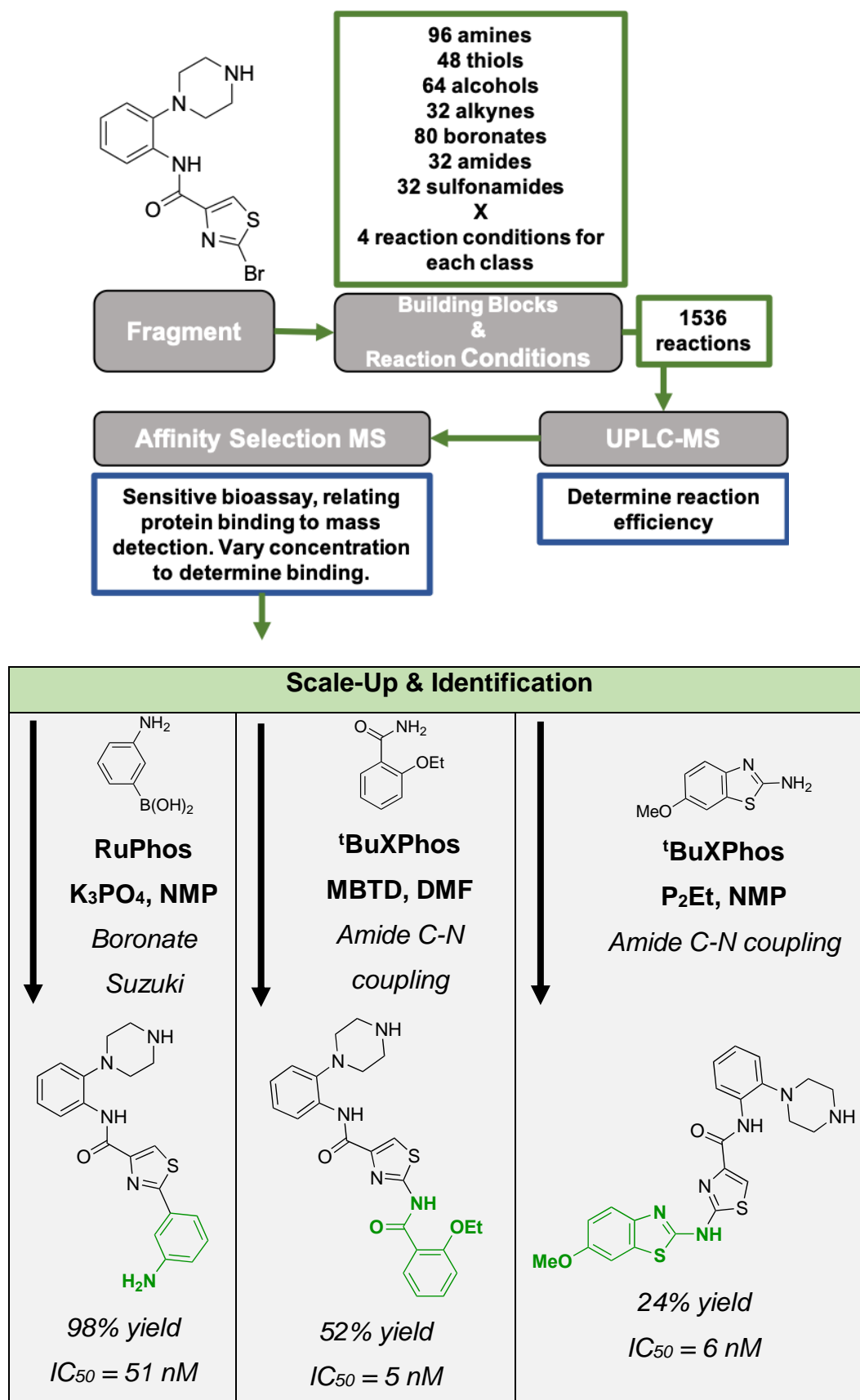


**Figure 1.11** – Overview of the discovery of inhibitors for CHK1 kinase, utilising the NanoSAR technique.

## 1.2 Activity-Directed Synthesis (ADS)

Activity-Directed Synthesis (ADS) is a novel bioactive molecule discovery approach in which molecule activity directs the emergence of an associated synthesis.<sup>51</sup> By exploring chemistries where alteration of the catalyst or conditions results in a diverse range of outcomes, a range of complex products can be formed enabling the exploration of a wider area of biologically relevant chemical space. Taking inspiration from the evolution of natural products, the focus is placed on molecules that are biologically active.

### 1.2.1 Natural Product Biosynthesis

Natural products have emerged to provide functional benefit to the host organism that produces them. Diverse substances produced as products in biosynthetic pathways within bacteria, plants, fungi, and other lower organisms that lack an immune system, or tend to inhabit competitive ecosystems. The complex and varied structures of these substances are produced by similarly sophisticated biosynthetic pathways that are driven by functional benefit to the host organism. It has been suggested that bioactive secondary metabolites are capable of boosting an organism's fitness for survival by increasing their ability to compete within an ecosystem.<sup>52</sup> The activity of a secondary metabolite is therefore a consequence of its structure, as natural selection results in the production of molecules whose activity has assisted their host organism's survival.<sup>53</sup> The evolution of biosynthetic pathways is therefore structure-blind and function-driven, which contrasts sharply with human-led ligand discovery approaches.

**Figure 1.12** outlines the biosynthetic pathway of terpenes, the largest class of natural products that are found in a variety of plants, animals and microorganisms.<sup>54</sup> The enzyme terpene cyclase produces a range of different structures by catalysing the cyclisation of different isoprenoid pyrophosphate units that are produced *via* the mevalonate pathway. Five-carbon building blocks such as isopentenyl pyrophosphate (IPP) and

dimethylallyl pyrophosphate (DMAPP) are precursors for primary metabolites like testosterone, the carotenoids and coenzyme Q. Other secondary metabolites are also produced: monoterpenes from geranyl pyrophosphate, sesquiterpenes from farnesyl pyrophosphate; and diterpenes from geranylgeranyl pyrophosphate. Terpene cyclases have very little primary sequence homology despite being structurally similar, suggesting the different classes have diverged rapidly from a common enzyme ancestor.

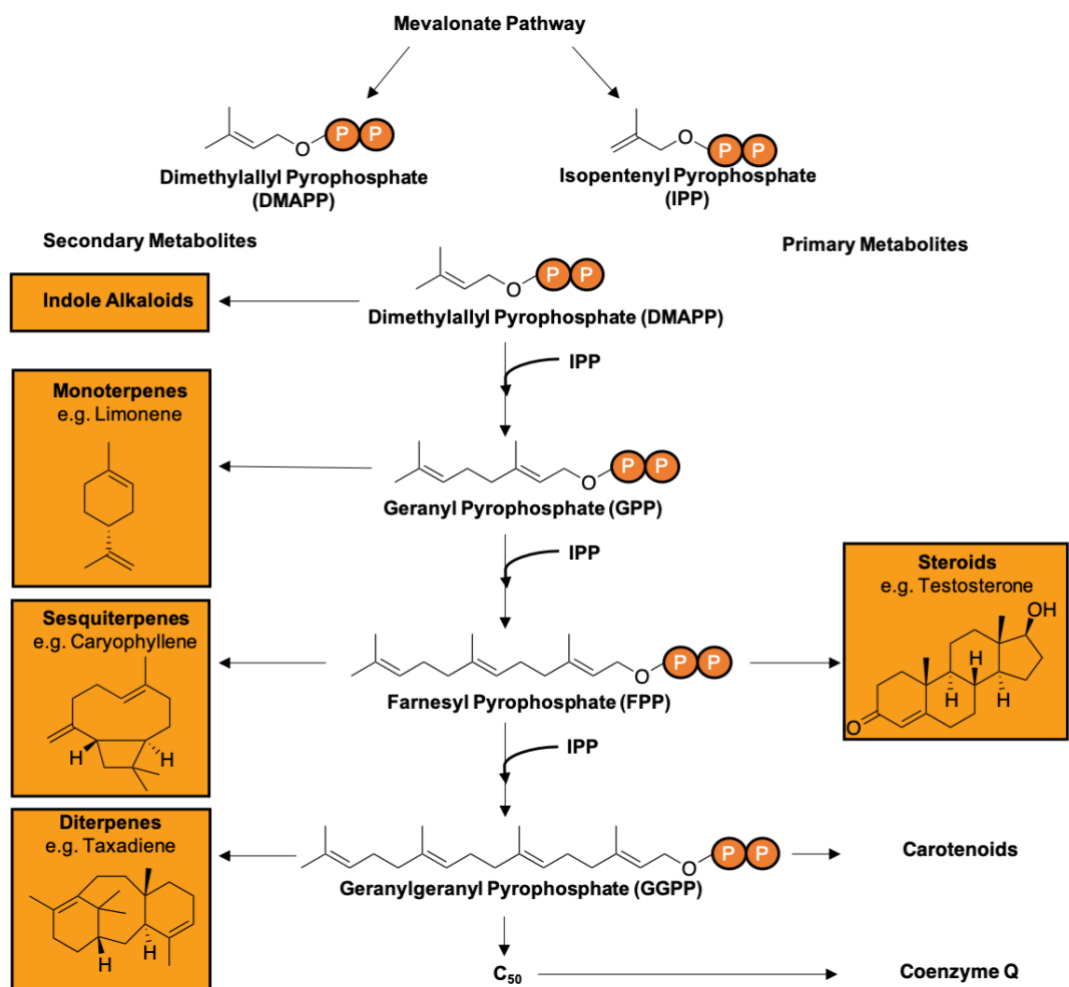


**Figure 1.12** – A schematic overview of terpene biosynthesis that yields a diverse range of functional natural products.<sup>54</sup>



### 1.2.2 Strategy Underpinning ADS

ADS is a structure-blind, function-driven iterative process in which arrays of reactions are designed with the purpose of combining the synthesis and screening process to inform the design of bioactive molecules.<sup>55</sup> By considering the reaction starting materials to be analogous to metabolites and the reagents and catalysts to be analogous to biosynthetic proteins, it is possible to mimic some aspects of the emergence of natural products in nature.

Using a microwell plate, reactions are carried out on a small scale (e.g. 100  $\mu\text{L}$ ) (see **Figure 1.13**). The substrates and catalyst in each well are varied in order to generate a range of products. Following the reaction, the catalysts and solvent are removed from each well, and the products dissolved in DMSO, then buffer, and screened using the selected assay. The data from screening are analysed and the results inform the design of a subsequent array of reactions. This subsequent reaction array can be screened at lower concentrations, incorporating selection pressures into the protocol. This process is repeated until a reaction yielding a sufficiently promising bioactive compound is found, at which point the reaction is scaled up, and the active product within the mixture of products isolated, characterised, and the biological activity verified and evaluated. Reactions with multiple possible outcomes are ideally used in ADS rather than optimised reactions with high yields and selectivity. This enables the screening of an array of diverse compounds against the desired biological target, allowing comparison of multiple chemotypes.

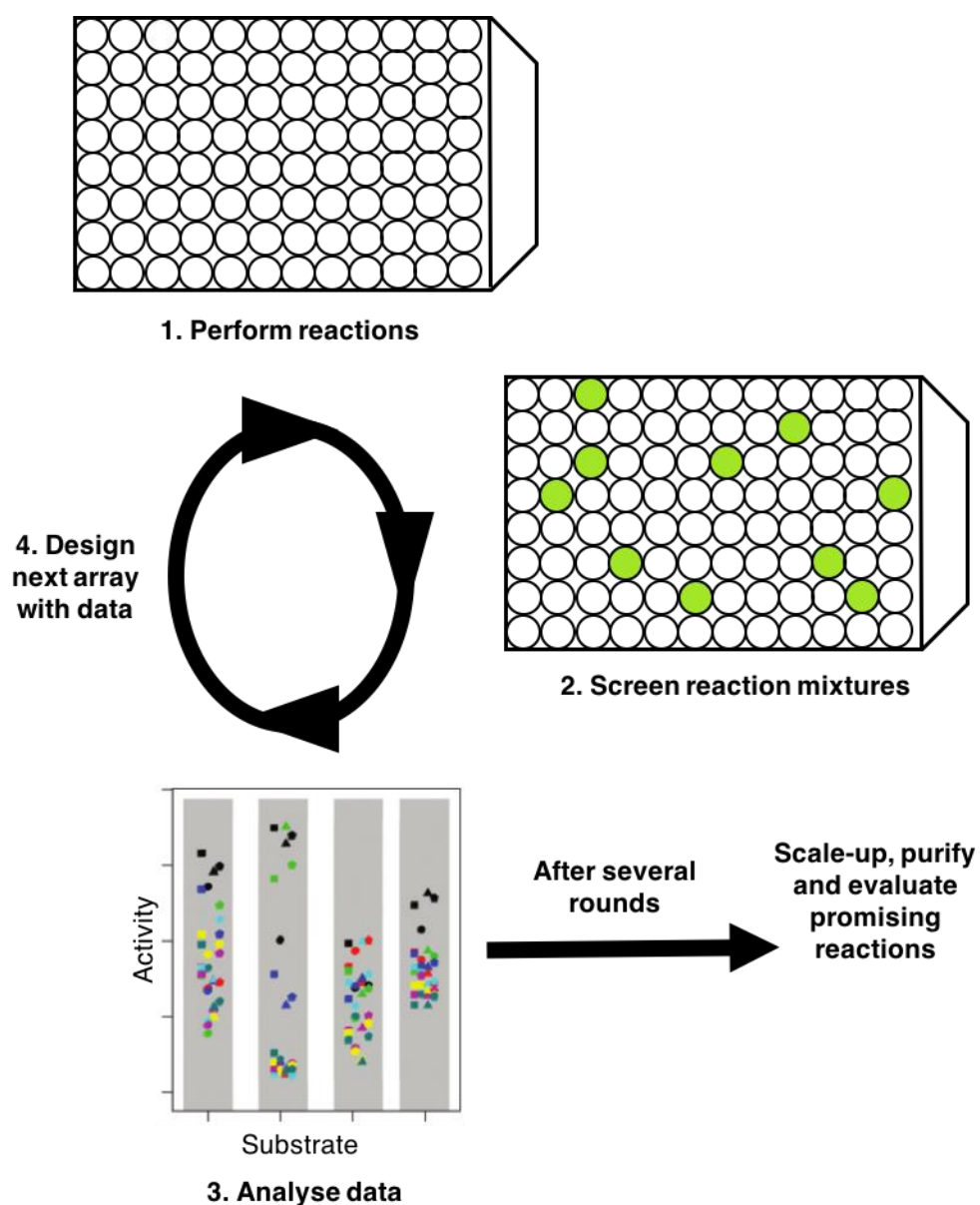
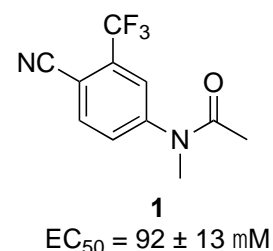


**Figure 1.13** - Overview of Activity-Directed Synthesis. Arrays of reactions are performed with variable substrates, catalyst and solvents. The resulting product mixtures are scavenged, then assayed to identify reactions yielding bioactive products. Analysis of each round of screening can inform the design of a subsequent array of reactions.

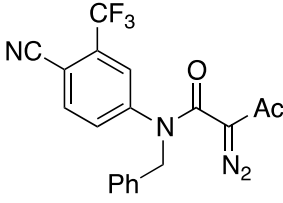
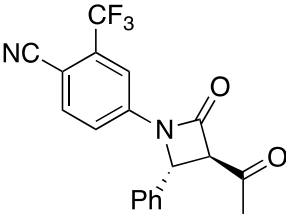
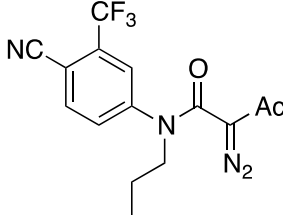
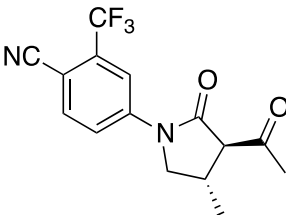
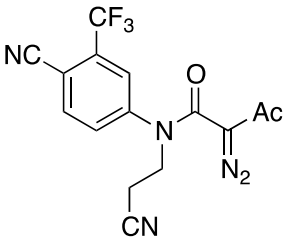
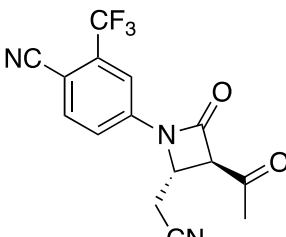
### 1.2.3 ADS Case Study

Initial work by Karageorgis et al. used metal-carbenoid chemistry to validate the ADS approach with intramolecular reactions, employing the Androgen Receptor as a model target.<sup>51</sup>  $\alpha$ -Diazo carbonyl compounds are able to participate in many intermolecular reactions<sup>56</sup> (C-H, N-H and O-H insertions; cycloadditions, cyclopropanation) in addition to intramolecular reactions forming various new rings from the existing substrate scaffold.<sup>57</sup> The designed diazo substrates contained aryl-amide motif **1**, adapted from a trifluoromethyl aryl fragment that had been identified in a previous report as a good starting point for AR agonist discovery, and were designed to maximise the range of outcomes possible with the chemistry.<sup>58</sup> The substrates were shown to have no activity under the conditions of the assay and catalyst scavenging methods were developed to prevent any effects of the metal catalysts on protein functionality or assay read-out. This ensured that any bioactivity observed was likely to stem from formation of a bioactive entity.



Arrays of reactions were executed that harnessed intramolecular reactivity. In the first ADS round, 12  $\alpha$ -diazo amides underwent reaction in the 96 well plate, with three different catalysts being varied. Screening of the array at a total product concentration of 10  $\mu$ M showed that four of the product mixtures yielded highly active products. The substrates and conditions used in these reactions informed the design of the next array, using variations of them to try to explore related chemical space. In addition, two substrates that had not yielded active product mixtures in the first round were included as a control. The second array of reactions varied the aforementioned six substrates, an expanded range of eight catalysts and four solvents, albeit screened at ten-fold lower concentration relative to products (1  $\mu$ M total product concentration) in the assay than the first array. The most active product mixtures arose when two of the active substrates from the first array (**Table** 1.2, starting material entries 1-6) were reacted with rhodium carboxylates in either DCM, toluene or EtOAc, and the

conditions employed in these reactions were used to inform the design of the following round. The third array exploited the two active substrates plus four structurally related substrates varied in the reaction mixtures, along with six varieties of rhodium carboxylate catalyst in three different solvents, screened at ten-fold lower concentration than the previous array (100 nM).

Starting Material	Reaction Conditions	Product	Yield (%)	EC <sub>50</sub> (nM)
	Rh <sub>2</sub> (esp) <sub>2</sub> (1 mol%), EtOAc		75	340 ± 30
	Rh <sub>2</sub> (oct) <sub>4</sub> (1 mol%), DCM		71	
	Rh <sub>2</sub> (OAc) <sub>4</sub> (1 mol%), DCM		68	
	Rh <sub>2</sub> (esp) <sub>2</sub> (1 mol%), DCM		90	470 ± 40
	Rh <sub>2</sub> (oct) <sub>4</sub> (1 mol%), DCM		88	
	Rh <sub>2</sub> (OAc) <sub>4</sub> (1 mol%), DCM		55	
	Rh <sub>2</sub> (esp) <sub>2</sub> (1 mol%), EtOAc		78	440 ± 60
	Rh <sub>2</sub> (tpa) <sub>4</sub> (1 mol%), Toluene		70	

**Table 1.2** - Synthesis, yield and activity of the bioactive intramolecular ADS products found by Karageorgis et al. <sup>51</sup>

For the eight most bioactive product mixtures from the third array, the structures for the products were elucidated, enabling identification of three major bioactive compounds. The purified compounds were evaluated for agonism of the AR independently (syntheses, structures and activities shown in **Table 1.2**). Three sub-micromolar novel agonists of the AR receptor were discovered from just three arrays of intramolecular reactions, with only three products requiring purification through the whole process.

Following the successful study of ADS using one substrate with intramolecular reactions, ADS using intermolecular reactions was investigated.<sup>59</sup> Using a variety of substrates that were *N*-substituted with groups that would disfavour intramolecular reactions, the rhodium-catalysed carbenoid chemistry could be utilised with a co-substrate to form new scaffolds between two molecules. In round one, 192 out of a possible 480 reactions were randomly chosen using four substrates, ten co-substrates, six catalysts and two solvents, screened at a 10  $\mu$ M total product concentration. The co-substrates were selected to ensure diversity when reacted with the substrates and catalysts. 192 reactions in round one yielded only two significantly active compounds, that informed design of the subsequent array. Round two focused on substrates **3** and **5**, Rh<sub>2</sub>((S)-DOSP)<sub>4</sub> and similar catalysts, and derivatives of co-substrates that yielded active products in round one: cyclohexene and indole, whilst also including other structurally related co-substrates and catalysts. 86 reactions were chosen from a possible 360 combinations of the two substrates, 18 co-substrates, five catalysts and DCM or toluene as solvents; screening at half the total product concentration of round one (5  $\mu$ M). Product mixtures utilising substrate **3** were identified as promising in combination with a selection of catalysts, with superior activities to both of the active product mixtures in round one. Round three combined substrate **3** with a range of 12 co-substrates and four catalysts in DCM, screening at a concentration of 1  $\mu$ M to further increase selection pressure, yielding two bioactive product mixtures. A selection of the bioactive products formed in all three rounds of the intermolecular experiments can be seen in **Table 1.3**.

SAR studies of the two bioactive compounds produced in the third round of intermolecular ADS permitted the identification of key structural features in each series, facilitating the discovery of novel chemotypes that acted as agonists of the AR. The activity of the original fragment **1** had been improved 125-fold in only three rounds of ADS, validating the strategy as an approach to explore chemical space efficiently and generate novel bioactive scaffolds suitable as starting points for drug discovery.

2, R = Ac 3, R=H		4, R = Ac 5, R=H		
R	Substrates	Catalyst	Product + Yield	EC <sub>50</sub> (μM)
1	3 +	Rh <sub>2</sub> ((S)-DOSP) <sub>4</sub>		8.8 ± 0.7
1	3 +	Rh <sub>2</sub> ((S)-DOSP) <sub>4</sub>		7.3 ± 0.2
2	5 +	Rh <sub>2</sub> (OAc) <sub>4</sub>		0.79 ± 0.06
2	3 +	Rh <sub>2</sub> ((S)-DOSP) <sub>4</sub>		4.7 ± 0.1
2	3 +	Rh <sub>2</sub> ((S)-DOSP) <sub>4</sub>		4.9 ± 0.1
2	3 +	Rh <sub>2</sub> (esp) <sub>2</sub>		3.8 ± 0.2
3	3 +	Rh <sub>2</sub> ((R)-DOSP) <sub>4</sub>		1.1 ± 0.1
3	3 +	Rh <sub>2</sub> (OAc) <sub>4</sub>		0.73 ± 0.03

**Table 1.3** – Intermolecular reactions yielding bioactive compounds from ADS with the respected activities of the products.<sup>59</sup> R = round of ADS the combination was discovered in.

### 1.2.4 Other Function-Driven Approaches to Bioactive Molecule Discovery

A similar function-drive approach, termed synthetic fermentation, emerged at around the same time as ADS, in which bioactive, unnatural peptides were developed from small building blocks using amide-forming ligations (**Figure 1.14**).<sup>60</sup> Arrays of reactions harnessed six different  $\alpha$ -ketoacid initiating monomers, eight elongating isoxazolidine monomers, and nine isoxazolidine monomers that had functionality rendering them as terminating groups. In each well, one initiator, three elongating monomers and one terminator were combined in order to generate oligomers, whose identity depended on the combination of monomers used.

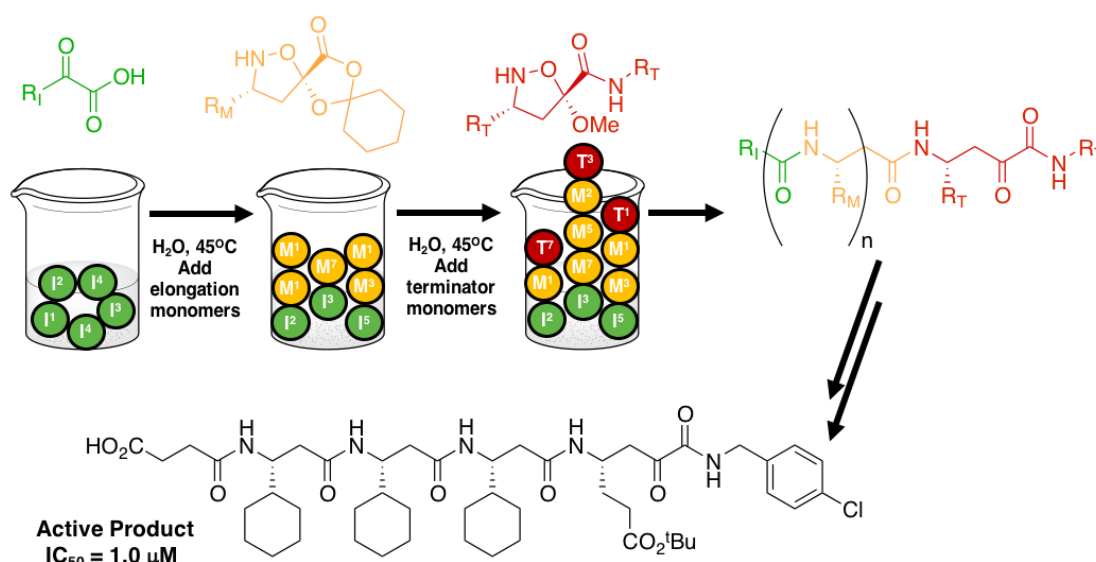


**Figure 1.14** - Overview of Synthetic Fermentation.<sup>60</sup> Oligomerisation of building blocks in mild aqueous conditions without the aid of reagents, organisms or enzymes, to form mixtures of peptide products in each synthetic culture. Initiating (I), elongating (M) and terminating (T) monomers are utilised to form peptide products that can be screened directly for biological activity.

The oligomeric products in each well were assayed directly against NS3/4A HCV protease, and if activity in a well in the array was observed, the contents of the well were determined. This method incorporated the principles of evolutionary feedback and selection pressures were implemented, leading to the fermentation of around 6000 peptidomimetics

from the 23 different monomers. Despite the successful identification and characterisation of a NS3/4A HCV protease inhibitor with an  $IC_{50}$  of  $1.0 \mu M$ , there are constraints on the range of products possible, as the underpinning peptide chemistry used in the platform is only capable of producing  $\beta$ -peptides.

### 1.3 Androgen Receptor

#### 1.3.1 Biology of the Androgen Receptor

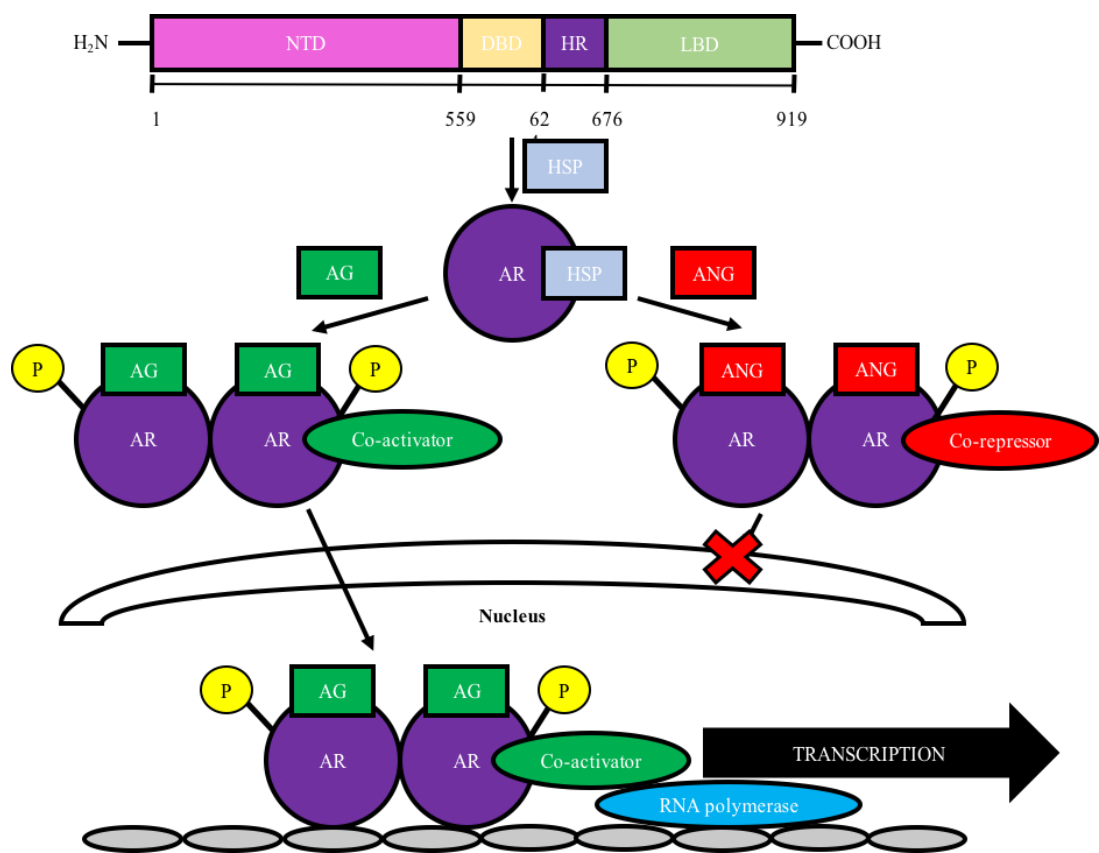


**Figure 1.15** – Overview of the transcriptional pathways activated/deactivated upon ligand binding to the AR receptor. NTD = *N*-terminal domain, DBD = DNA-binding domain, HR = hinge region, LBD = ligand binding domain, HSP = heat shock protein, AG = agonist, ANG = antagonist, P = phosphorylation.

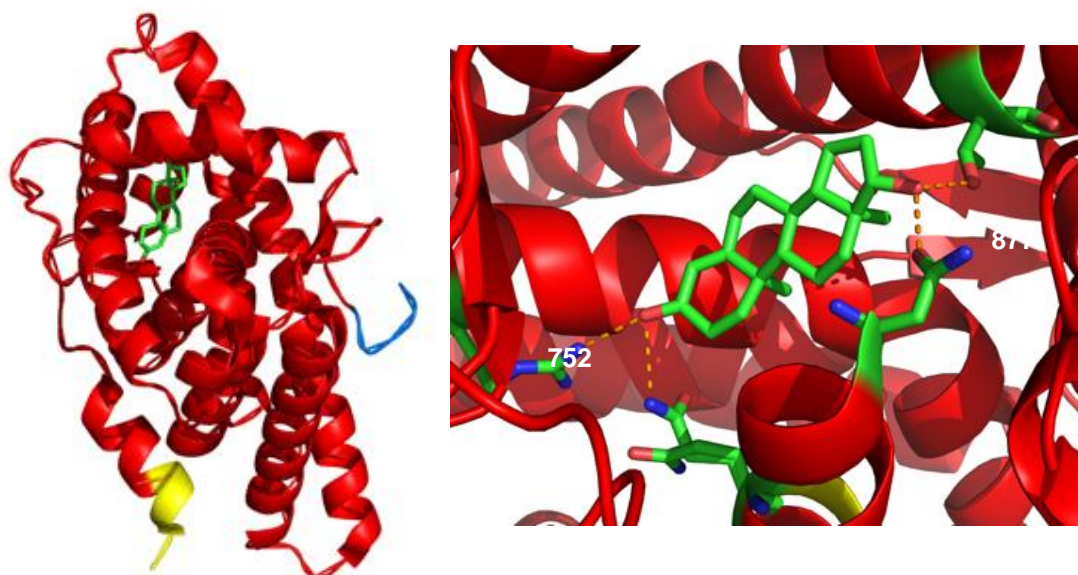
The androgen receptor (AR) is a member of the steroid and nuclear receptor superfamily. Binding of androgenic hormones to the AR regulates



its function, inducing conformational changes that affect receptor-DNA and receptor-protein interactions. Gene expression regulated by the AR is responsible for pubertal changes and sexual differentiation in males, in addition to organ tissue, muscle and bone production and maintenance throughout the body.<sup>61,62</sup>

**Figure 1.15** shows the transcriptional pathway induced when the AR is activated. When an agonist such as testosterone interacts with unbound AR in the cytoplasm, conformational changes in the ligand-binding domain form a surface that can interact with proteins that control transcription. The AR undergoes dimerisation, phosphorylation, and translocation into the nucleus. The resulting complex then binds to the promoter region of AR-responsive genes, resulting in the recruitment of transcriptional activator proteins and activation of gene expression. Diseases directly linked to AR dysfunction include prostate cancer and androgen insensitivity syndrome.<sup>62</sup>

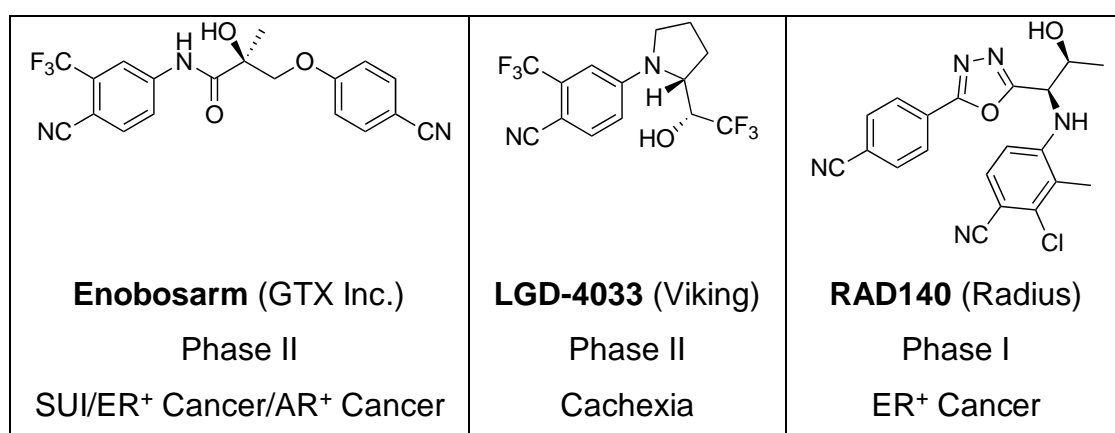
### 1.3.2 Known Androgen Receptor Modulators



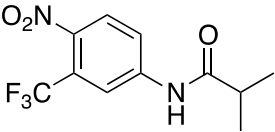
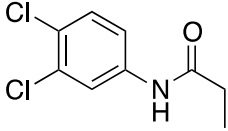
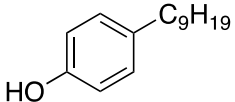
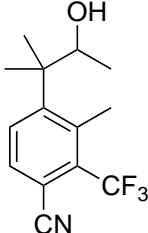
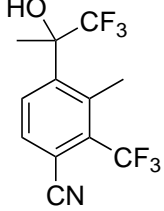
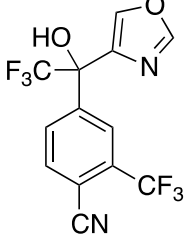
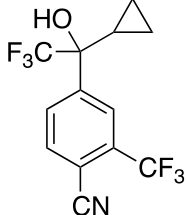
**Figure 1.16** – Crystal structure of the AR ligand-binding domain in complex with testosterone. (PDB: 2AM9). The 3-keto (H-bond to Arg752) and 17 $\beta$ -OH (two H-bonds to Thr877 and Asn705) groups of testosterone and their interactions to the protein are indicated.

The AR is one of the oldest known and frequently studied anabolic targets in mammalian systems, with work dating back to 1889.<sup>63</sup> Many different Selective Androgen Receptor Modulators (SARMs) have been identified, with a wide range of efficacies.<sup>64</sup> The scaffold of endogenous steroidal agonists such as testosterone and 5 $\alpha$ -dihydrotestosterone provide the ideal positioning for two key anchors for AR binding: the 3-keto (H-bond to Arg752) and 17 $\beta$ -OH (two H-bonds to Thr877 and Asn705) groups are essential for binding affinity (see **Figure 1.16**). SAR of the wider range of modulators outside of the steroid class shows general hydrophobicity of the ligands to be largely important.

Despite their efficacy, the use of steroids as therapies for disease are associated with significant side effects, and identification of alternative AR modulators is desirable. Many small molecule SARM candidates have been advanced to clinical studies that are more selective for the androgen receptor than other tissues, reducing the side effects commonly observed with steroid use. SARMs would be useful for a wide array of indications where stimulation of tissue growth would be a beneficial clinical outcome, such as Cachexia (muscle wastage), Duchenne Muscular Dystrophy, Osteoporosis, specific cancers and Stress Urinary Incontinence (SUI).<sup>65</sup> A number of SARM compounds are in the clinic for a range of indications, as shown in **Figure 1.17**.



**Figure 1.17** – A range of SARM clinical candidates.

Entry	Modulator	pEC <sub>50</sub>	Ref
1		7.09	49
2		7.29	49
3		7.94	49
4		7.80	51
5		8.40	51
6		8.90	51
7		9.80	51

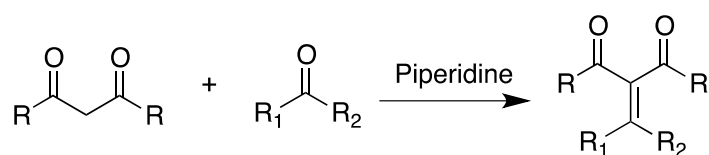
**Table 1.4** – Selected AR modulators.

**Table 1.4** shows a selection of modulators of the AR and their EC<sub>50</sub> values for the AR. Entries 1, 2 and 3 in **Table 1.4** were identified in a review by Sheehan et al. of natural and synthetic ligands that bind to the AR.<sup>64</sup> The efficacy values of the ligands were given as relative binding affinities in comparison to methyltrienolone in a competitive AR binding assay. Compounds featuring *para*- and *meta*-substituted aryl rings with some

hydrophobic character such as entries 1 and 2 were identified as suitable non-steroidal binders. *Para*-substituted phenols such as entry 3 were also identified as modulators. Entries 4, 5, 6 and 7 were identified by Handlon et al. as selective nanomolar androgen receptor modulators, and the aryl motif featured within the compounds is the same as featured in previous work on ADS.<sup>66</sup> These compounds do not feature a nitrogen atom adjacent to the aromatic ring, showing that amide functionality is not essential for compounds to be potent agonists.

#### 1.4 Overview of Covalent Organocatalysis

Organocatalysis is a burgeoning domain of organic chemistry, studying the use of small molecules as catalysts in synthetic transformations.<sup>67</sup> Organocatalysts can catalyse formation of diverse products, and the different classes of catalyst available have a range of reactivity capable of exploring many different ring systems. Organocatalysed reactions are generally insensitive to moisture and oxygen, with reactions that will generally run at room temperature, and are capable of forming products with high enantiomeric and diastereomeric ratios. Unlike the rhodium-catalysed chemistry used previously in ADS, the production of impurities related to toxic metal catalysts is avoided. These attributes may make organocatalysis a great selection for use in Activity Directed Synthesis.



**Scheme 1.3** - The Knoevenagel Condensation (1898)

The origins of organocatalysis can be traced back to Emil Knoevenagel, who used secondary amines as catalysts in aldol condensations between  $\beta$ -ketoesters with aldehydes or ketones (**Scheme 1.3**).<sup>68</sup> Following Knoevenagel's discovery, a variety of reactions in which amines, including natural products (primarily cinchona alkaloids), were found to catalyse product formation were discovered,<sup>69,70</sup> but the potential of

organocatalysis was not realised until the late 1990s when Macmillan, who discovered the organocatalysed Friedel-Crafts reaction,<sup>71</sup> coined the term. Numerous activation modes and methodologies exist, many of which may be suitable for exploitation in ADS.

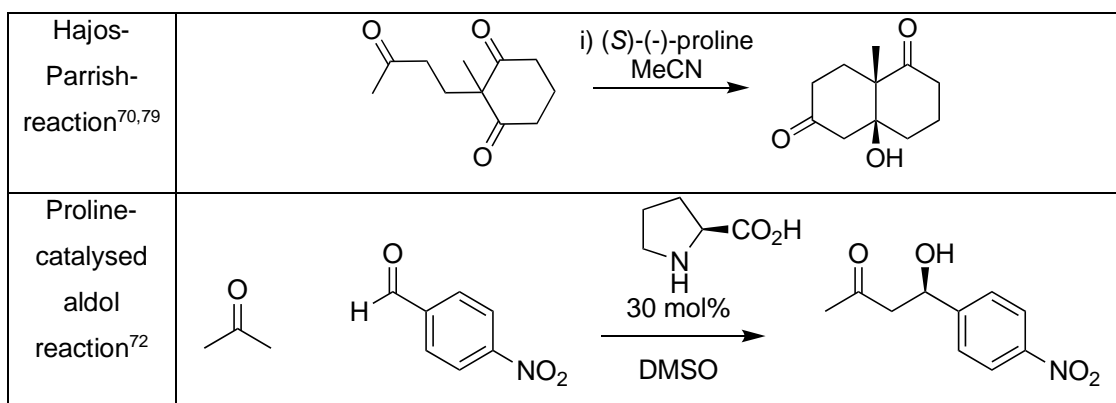
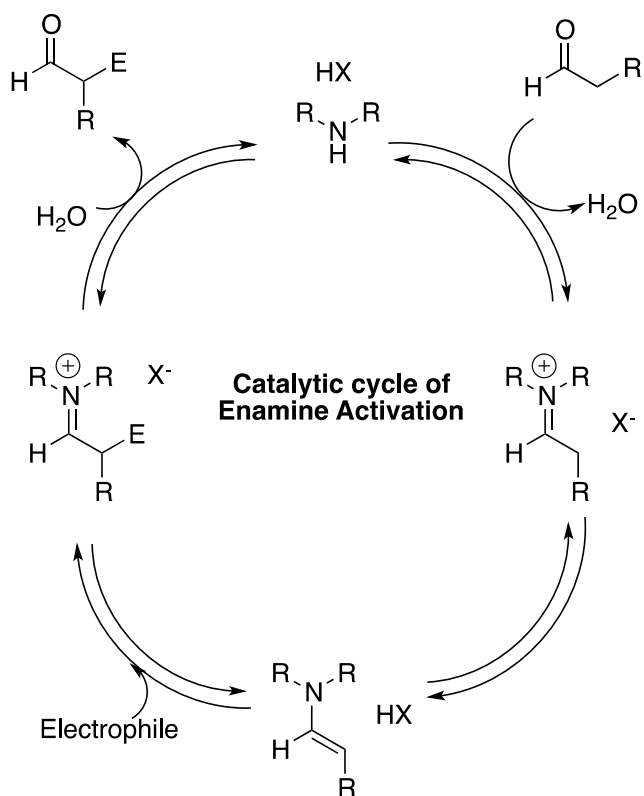
Amines are the most common class of organocatalyst, utilising primary and secondary amines to catalyse reactions. The field has seen a renaissance following the initial work in asymmetric organocatalysis by the likes of Hajos and Parrish decades ago,<sup>70</sup> with the simultaneous discovery of the proline-catalysed intermolecular aldol reaction and the Mannich reactions by List et al.,<sup>72,73</sup> and the chiral imidazolidinone-catalysed Diels-Alder reaction by Macmillan et al.<sup>74</sup>

#### 1.4.1 Enamine Catalysis

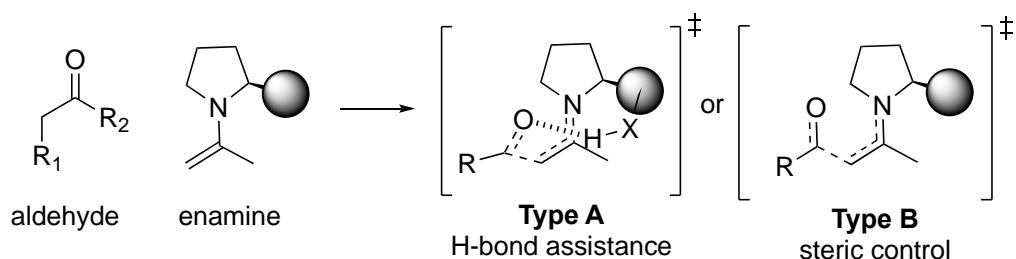
Enamines are among the most reactive neutral carbon nucleophiles, displaying rates of reaction comparable to some charged nucleophiles such as enolates.<sup>75</sup> Many enamines are sensitive to hydrolysis, making them hard to isolate, but this is advantageous in organocatalysis, where they are generated catalytically *in situ*. Brønsted acid-promoted condensation of an amine with a ketone or aldehyde initially affords an iminium ion, before deprotonation to form the enamine species.<sup>76</sup> The nucleophilic enamine attacks the electrophile, generating another iminium ion. Hydrolysis of the iminium species gives the  $\alpha$ -substituted product and regenerates the catalyst that can re-enter the catalytic cycle. The Brønsted acid, HX, can either be a protic solvent, an external added acid, or a functional group present in the amine catalyst. **Scheme 1.4** shows the catalytic cycle of enamine activation.

Chiral amine catalysts are capable of inducing high enantioselectivity in enamine-catalysed reactions (**Scheme 1.5**). Type A catalysts, such as proline, include an integrated H-bond donor that can activate the electrophile and orient its approach, and tend to be used to direct enantioselectivity in aldol, Mannich and  $\alpha$ -amination/oxygenation reactions.<sup>77</sup> Type B catalysts

include non-acidic bulky groups, and sterically block approach of electrophiles from one side, as in diarylprolinol silyl ether catalysts. They excel in reactions such as  $\alpha$ -halogenation and conjugate additions where H-bond assistance is not required, although are versatile enough to work with most enamine and iminium catalysed reactions.<sup>78</sup>



**Scheme 1.4** - The catalytic cycle of enamine catalysis, and examples of classic reactions where enamine catalysis is applied.



**Scheme 1.5** - The influence of steric control vs. hydrogen bonding control in amine catalysis.

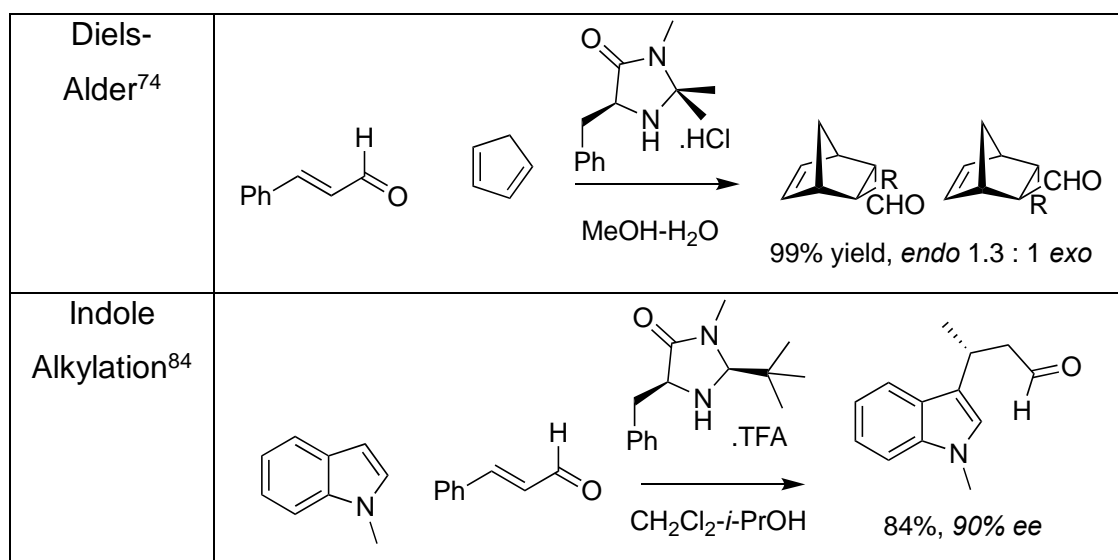
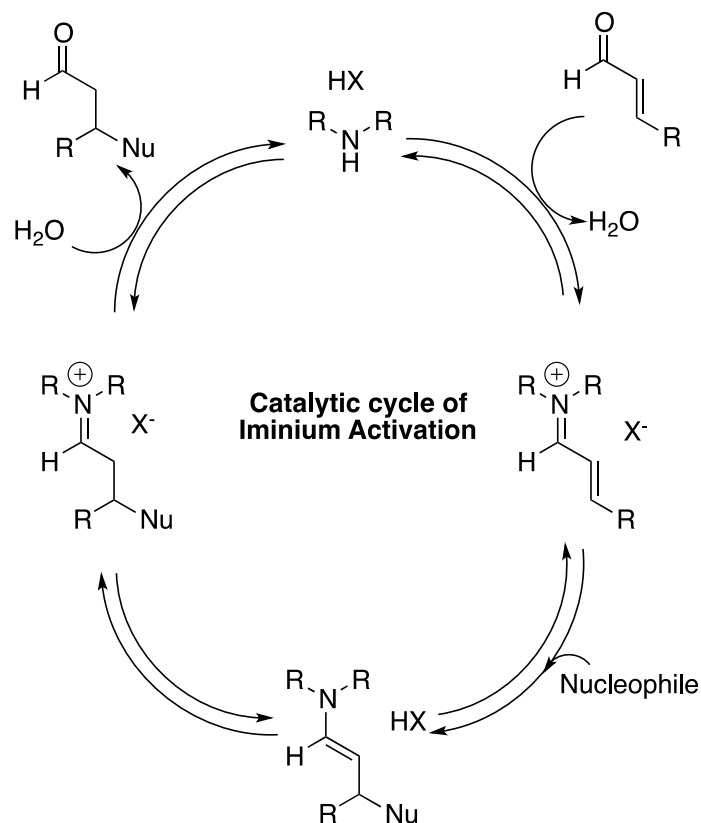
### 1.4.2 Iminium Catalysis

Iminium catalysis is another prominent activation mode in organocatalysis. Initial work on iminium catalysis focused on cycloadditions,<sup>74,80</sup> but the strategy was soon extended to Michael additions,<sup>71,81</sup> with iminium catalysis now being a well-established strategy for conjugate addition of nucleophiles to the  $\beta$ -position of  $\alpha,\beta$ -unsaturated aldehydes. Formation of the iminium ion has a similar activating effect of complexation of a carbonyl group to a Lewis acid, lowering the LUMO energy of the  $\pi$ -system in an  $\alpha,\beta$ -unsaturated aldehyde, increasing its electrophilicity.<sup>82</sup>

Following Brønsted acid-promoted condensation of the carbonyl and amine to form the iminium ion and a molecule of water, a nucleophile attacks at the  $\beta$ -position. This forms an enamine in equilibrium with the equivalent iminium intermediate, which can be hydrolysed to form the product and regenerate the catalyst that can re-enter the cycle. The generation of a molecule of water is noteworthy: unlike Lewis acid catalysed reactions, iminium catalysed reactions tend to be tolerant of moisture and air, increasing their practicality. **Scheme 1.6** shows the catalytic cycle of iminium catalysis.

Although amines with H-bond directing groups such as proline can be used,<sup>83</sup> better yields are generally obtained with bulky non-acidic groups, such as in the widely used imidazolidinone catalysts devised by

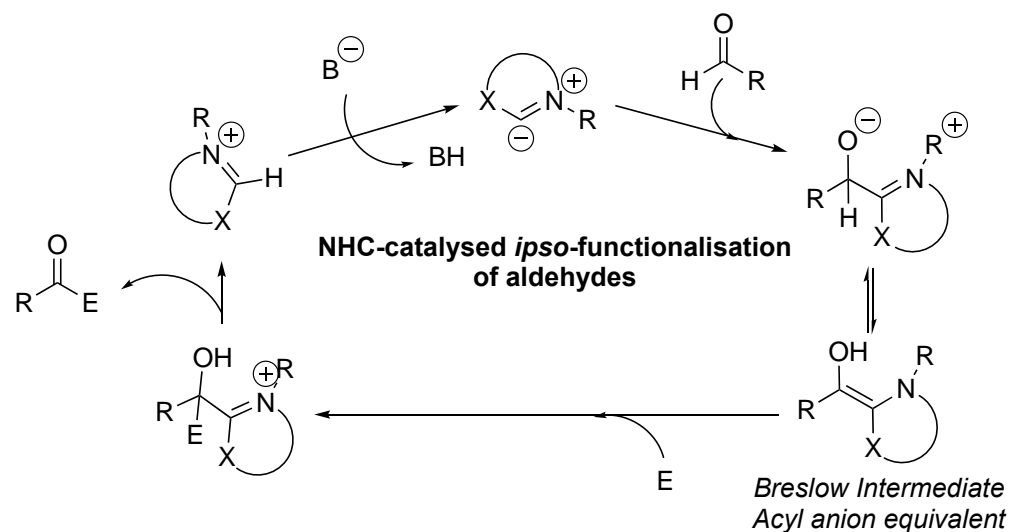
MacMillan.<sup>71,74</sup> As with enamine catalysis, chiral amine catalysts are capable of forming chiral products, with the steric bulk of substituents on the amine catalyst determining the conformation of the electrophilic  $\alpha,\beta$ -unsaturated iminium ion formed, as well as the face of nucleophilic attack.



**Scheme 1.6** - The catalytic cycle of iminium catalysis, and classic examples of Diels-Alder and Indole alkylations using iminium catalysis.



### 1.4.3 *N*-Heterocyclic Carbene Catalysis



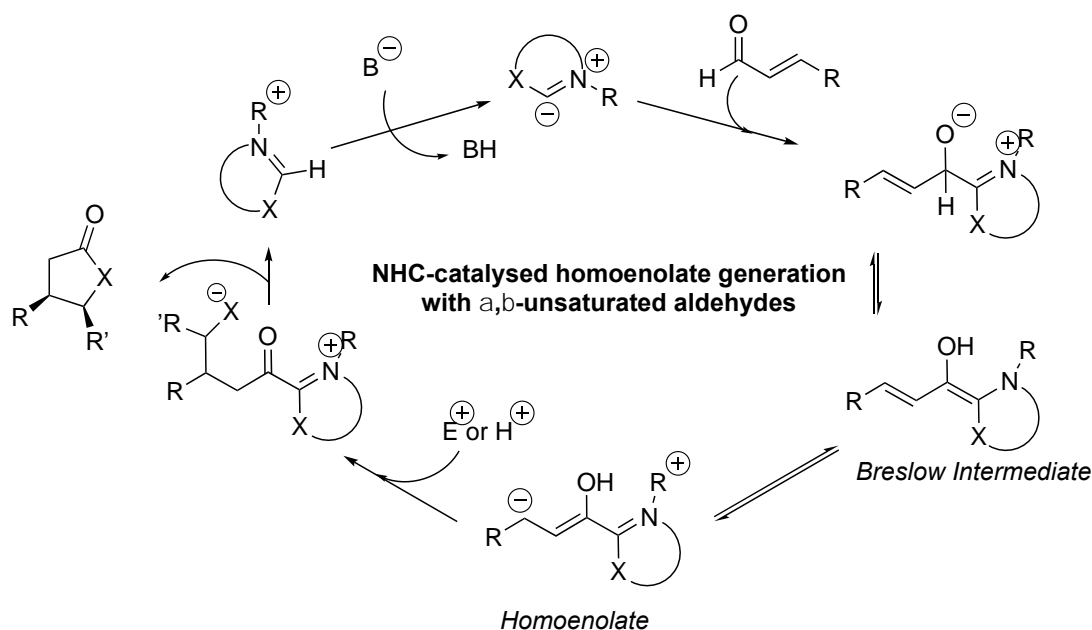
Benzoin Condensation <sup>85</sup>	<p style="text-align: center;">10 mol% NHC KO<sup>t</sup>Bu THF</p> <p style="text-align: center;">83%, 90% ee.</p>
Stetter Reaction <sup>86</sup>	<p style="text-align: center;">10 mol%</p> <p style="text-align: center;">NEt<sub>3</sub> EtOH</p>

**Scheme 1.7** - The catalytic cycle of NHC-catalysis for *ipso*-functionalisation *via* formation of an acyl anion equivalent.

Chiral *N*-heterocyclic carbenes (NHCs) are a class of Lewis basic catalysts capable of inverting the polarity of aldehyde substrates, generating nucleophiles *via* the premise of umpolung reactivity.<sup>87</sup> Although widely known as modifying ligands for transition metals following isolation of stable imidazolylidene carbenes by Arduengo,<sup>88</sup> their utility as organocatalysts was realised much later. Studies into NHC-catalysed reactions began with development of an asymmetric benzoin reaction by Sheehan et al.<sup>89</sup> using chiral thiazolium salt-derived NHCs. However, enantiomeric excesses exceeding 90% were not achieved until work by Enders et al. decades later, using a chiral triazolium salt-derived NHC.<sup>85</sup> Many NHC catalysts have been

developed that are complex chiral structures, capable of giving products in high enantiomeric excess, although several achiral catalysts are still successfully used in order to generate racemic mixtures of products with good yields – useful for application within ADS to maximise the number of products formed. Although many activation modes are possible, two fundamental modes of reactivity are catalysed by NHCs.

Pairing an NHC catalyst with an unconjugated aldehyde enables *ipso*-functionalisation (**Scheme 1.7**). Following deprotonation of the NHC salt-derived pre-catalyst, nucleophilic attack of the NHC on the aldehyde yields a zwitterionic intermediate that equilibrates via proton transfer to the Breslow intermediate, a nucleophilic enamino species.<sup>90</sup> Addition of an electrophile at the nucleophilic *ipso*-carbon of the newly formed acyl anion equivalent forms a cationic intermediate, which collapses to form the *ipso*-functionalised carbonyl and regenerates the carbene catalyst.



**Scheme 1.8** - The catalytic cycle involving homoenolate formation by reaction between NHCs and  $\alpha,\beta$ -unsaturated aldehydes. Examples of NHC-catalysed reactions *via* homoenolates can be seen in **Scheme 2.7** and **Scheme 2.8**.

The second reaction type catalysed by NHCs is the formation of activated homoenolates from  $\alpha,\beta$ -unsaturated aldehydes (**Scheme 1.8**). Following *in situ* deprotonation to form the active NHC species, nucleophilic attack of the NHC on the  $\alpha,\beta$ -unsaturated aldehydes yields the Breslow intermediate. Rearrangement leads to the formation of the homoenolate species, which is nucleophilic at the  $\beta$ -position. Nucleophilic attack on a suitable electrophile results in a  $\beta$ -functionalised species, whilst also regenerating the pre-catalyst which can re-enter the catalytic cycle.

## 1.5 Project Outline

The expansion of the synthetic toolkit that can be used with the approach is important to further validate ADS as a method for finding novel scaffolds. The robust nature of organocatalysis, and the structurally diverse products that the class of chemistry can mediate the formation of, appears to make it a feasible and potentially productive class of chemistry that can be applied to ADS. Consequently, this project had two major objectives:

### ***1.5.1 Objective 1: Configuration of Organocatalysis for ADS***

The first step towards the initial goal of configuring organocatalytic chemistry to be compatible with ADS is to identify exemplar organocatalytic reactions from the literature and replicate them in the laboratory. The reactions selected have to form products with a range of interesting scaffolds, with high  $sp^3$ -centre content where possible. A desirable outcome would be successful translation of a range of organocatalytic reactions into the microscale plate format required for ADS, and demonstration of their operational efficiency on this scale using a set of general conditions for each class of organocatalyst. This objective is the focus of Section **2.3.3** of this thesis.

Additionally, conditions for the treatment of product mixtures needed to be devised before carrying out the assay, that would allow removal of undesirable electrophilic functionality that may possibly interfere with assay readout. These conditions would ideally remove this functionality using simple and inexpensive reagents, or process them to add extra functionality into the products. A desirable outcome for this aim would be the identification of effective reductive conditions to remove undesirable electrophilic functionality, and quantifiable conversion upon a range of exemplar substrates. This objective is the focus of **Section 2.4** of this thesis.

### **1.5.2 Objective 2: Exploring the Value of Organocatalysis in ADS**

Following configuration of organocatalysis in a micro-scale plate format, the value of using the chemistry with the ADS format could be explored.

Approaches for the design of effective reaction arrays needed to be developed, that could explore diverse chemical space using a range of the organocatalytic reactivities outlined in **Section 1.4**. Ideally, the components used in these reactions would be selected using an efficient computational workflow, that would be developed to optimise the set of substrates selected for both reactivity and properties. Different strategies that balanced unpredictable reactivity that could create unexpected products, against conversion to products using literature precedent, would need to be explored in order to gain insight into best practices for execution of organocatalytic reaction arrays for future users. Additionally, once results were obtained from a reaction array, approaches for the design of subsequent reaction arrays would need to be developed. The development of these workflows would need to be supported by a robust high-throughput assay, that would have to be established so that activity within product mixtures could be identified.

Feedback for both of these objectives could be obtained by executing the reaction arrays, followed by screening reaction mixtures for functional products, which is the subject of **Chapter 3**. This would enable assessment of the value of organocatalysis in the context of activity-directed biomolecule discovery and enable future users of the ADS platform to employ it effectively.

## 2 Configuration of Organocatalytic Chemistry for ADS

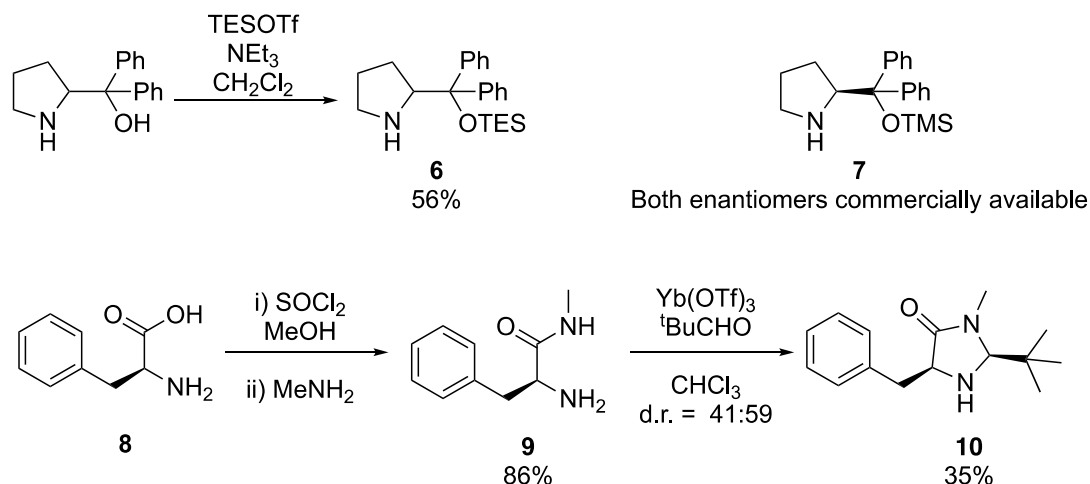
### 2.1 Selection and Synthesis of Organocatalysts

The catalysts used in ADS needed to be easily obtainable and had to possess a range of reactivities with diverse substrates and reaction types in order to create a varied range of products that can explore as much chemical space as possible. Racemic or achiral versions of the selected catalysts were desirable in order to explore activity of both enantiomeric series of products.

As the field of organocatalysis has advanced, many researchers have made attempts to optimise organocatalyst classes so that reactions with high stereoselectivity can be carried out, making the catalysts more complex to synthesise, and therefore more expensive to obtain if commercially available. By selecting simpler catalysts with broader reactivity, it may be possible to explore activity of more isomers of the potential products.

The Jørgensen-Hayashi class of catalyst is favoured in many amine-catalysed organocatalytic reactions due to diverse reactivity with a range of substrates. Triethylsilyl-protected diphenylprolinol **6** and trimethylsilyl-protected diphenylprolinol **7** (see **Scheme 2.1**), two of the variety of organocatalysts developed by Jørgensen and Hayashi, were selected as catalysts to explore enamine and iminium reactivity. The diarylprolinol silyl ethers that fall into this class are well established as efficient general organocatalysts, providing both HOMO activation (enamine), and LUMO activation (iminium), with good selectivity and reactivity.<sup>91</sup> The bulky substituent at the 2-position on the amine catalyst provides steric control in reactions, directing the electrophile towards the opposite face to the sterically large substituent of the catalyst. By using a racemic mixture of both enantiomers of the catalyst, both possible enantiomers of product will be present in successful reactions.

Catalyst **6** was obtained in one step from diphenylprolinol, by treatment with triethylsilyl trifluoromethanesulfonate and triethylamine in dichloromethane, with a yield of 56%. The use of the more sterically demanding triethylsilyl group in catalyst **6** increases the stability of the compound when compared to the more commonly seen trimethylsilyl-protected catalyst **7**.<sup>92</sup> **7** and its enantiomer are both commercially available.



**Scheme 2.1** – Synthesis of amine catalysts chosen to initially test the scope of literature reactions. Both enantiomers of the Macmillan imidazolidinone catalyst **10** were prepared.

Second generation Macmillan imidazolidinone catalysts are also widely exploited, often in combination with a trifluoroacetic acid co-catalyst.<sup>71,80,84</sup> The imidazolidinone catalyst (**10**) was produced in three steps, treating phenylalanine **8** with thionyl chloride in methanol, then adding methylamine to form the methyl amide **9**. The methyl amide **9** was then refluxed in chloroform with ytterbium (III) triflate and pivaldehyde, mediating a cyclisation that resulted in the production of a mixture of separable diastereomers in a yield of 85%, with the active catalytic *cis*-diastereomer obtained in an overall yield of 35%.<sup>93</sup>

The *N*-heterocyclic carbene catalysts for the project were selected to exploit ‘umpolung’ modes of activity with carbonyl substrates. Both **11**, 1,3-bis(2,4,6-trimethylphenyl)imidazolium chloride (iMes), and **12**, 2-mesityl-

2,5,6,7-tetrahydropyrrolo[2,1-c][1,2,4]triazol-4-ium chloride, are widely used, achiral, cheap and commercially available.

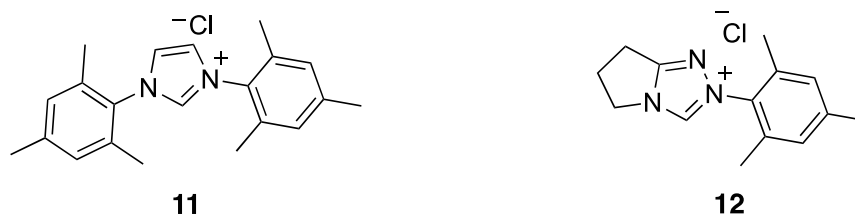


**Figure 2.1** – *N*-Heterocyclic carbene catalysts selected for use in ADS



## 2.3 Identification of Exemplar Organocatalytic Chemistry

Diverse examples of organocatalytic reactions from the literature needed to be identified that could be transferred into a micro-scale plate format suitable for ADS. The products of the reactions had to be representative of the kind of chemotypes that were to be explored with ADS. These reactions could then be reproduced, testing their viability in a miniaturised format essential for the platform to operate with the requisite throughput. Comparison of the outcomes of these micro-scale reactions with their full-scale counterparts could then allow comparison of their efficiency in producing the predicted products, enabling assessment of the success of the transfer to the micro-scale format.

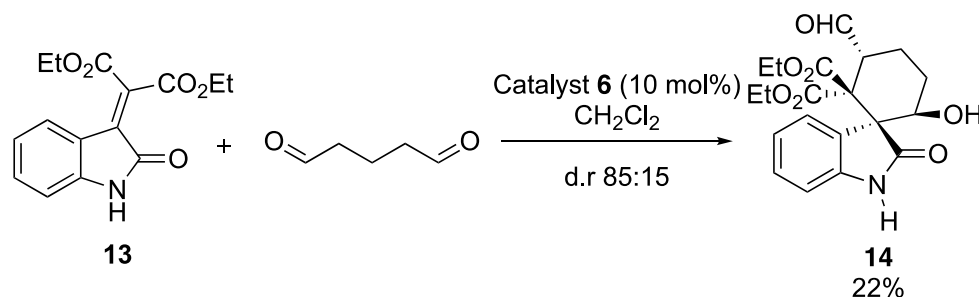
Using a range of the selected catalysts from **2.1**, reactions were selected that could demonstrate the diversity of the chemistry possible with organocatalysis, and the ability of the chemistry to yield complex structures that could sufficiently explore diverse areas of chemical space. The reactions had to require minimal additional components (such as acids/bases, oxidants) other than substrates and catalysts to permit operational simplicity when executing ADS arrays.

A range of complex catalysts are utilised throughout the literature, that are intended to optimise reactions to give products in high yields and enantioselectivity. As ADS requires operational simplicity, using the simpler catalysts detailed in **2.2** was important to gauge the efficiency of the selected reactions and to determine the diversity of the products that could be produced with the outlined palette of catalysts.

### 2.3.1 Amine-Catalysed Reactions

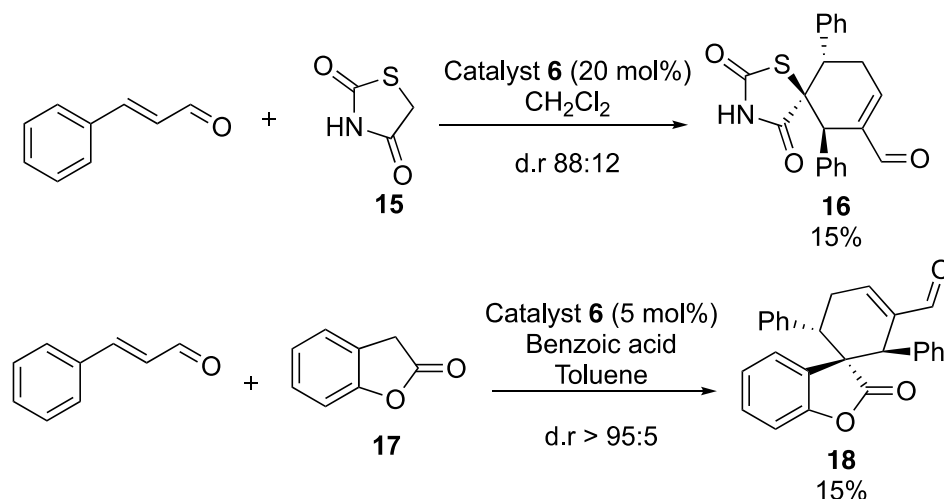
An organocatalytic Michael-aldol spiroannulation of an isatin-derived alkene with a linear dialdehyde was demonstrated by Huang *et al.* (**Scheme 2.2**).<sup>94</sup> This proceeded via an enamine catalysed Michael addition to the alkene, followed by cyclisation through an intramolecular aldol reaction. The

reaction reported in the literature used trimethylsilyl diarylprolinol catalyst **7** rather than catalyst **6**, which was used when recreating this reaction in the laboratory. Isatin-derived alkene **13** was stirred in DCM with diarylprolinol catalyst **6** (10 mol%), before adding 2.4 equivalents of a 50% aqueous solution of glutaraldehyde. Stirring for 14 hours and purification afforded the aldehyde **14** in a yield of 22%.

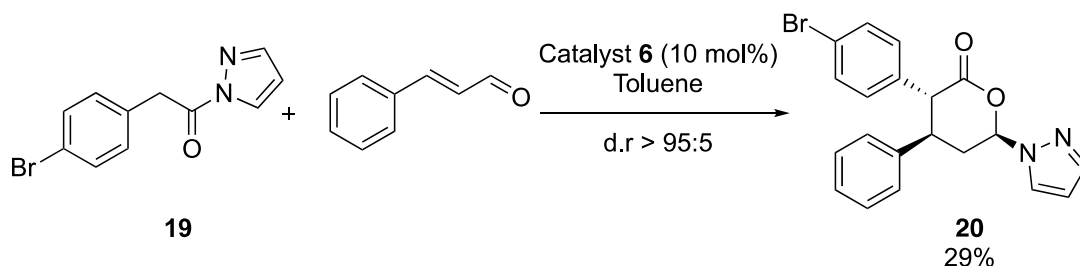


**Scheme 2.2** - Organocatalytic Michael-aldol spiroannulation of an isatin-derived alkene with glutaraldehyde.<sup>94</sup>

A pair of organocatalytic reactions proceeding by double Michael-Aldol cascade mechanisms was attempted (**Scheme 2.3**). Sequential double iminium-catalysed Michael-addition of the substrate to the  $\alpha,\beta$ -unsaturated aldehydes, followed by an enamine-catalysed intramolecular aldol reaction to close the ring generated spirocyclic products. Wang et al. used a thiazolidinedione substrate with a range of  $\alpha,\beta$ -unsaturated aldehydes to synthesise a range of spirocyclic thiazolidinedione derivatives. Melchiorre et al. generated spirocyclic benzofuranone derivatives using the same strategy, albeit under different conditions. To replicate these reactions, thiazolidinedione **15** or benzofuranone **17** was added to a solution of diphenylprolinol catalyst **6** (20 mol% for **16**, 5 mol% for **18**) in dichloromethane, before adding 3 equivalents of cinnamaldehyde, and in the case of **18**, a catalytic amount of benzoic acid. Following purification, the aldehydes **16** and **18** were both afforded in yields of 15%.



**Scheme 2.3** - Organocatalytic double Michael-aldol cascade reaction of thiazolidinedione/benzofuranone with  $\alpha,\beta$ -unsaturated aldehydes to form spirocyclic aldehyde products.<sup>95,96</sup>

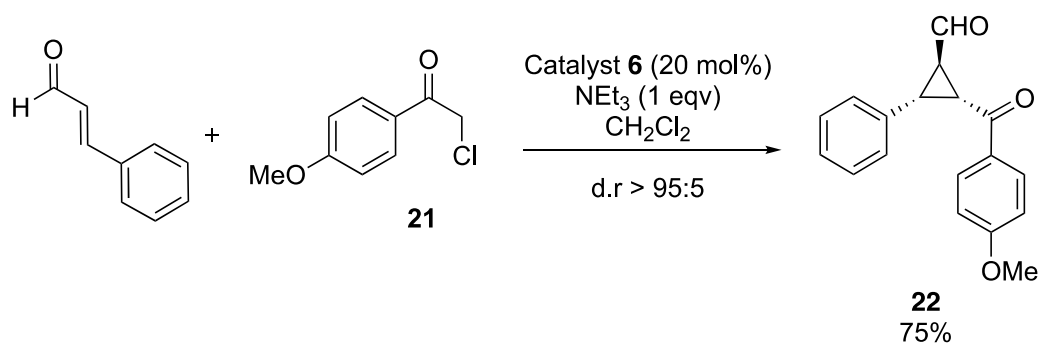


**Scheme 2.4** - Organocatalytic Michael-cyclisation cascade between a pyrazoleamide and cinnamaldehyde forming substituted  $\delta$ -lactones.<sup>97</sup>

Singh et al. developed a Michael-cyclisation approach to the synthesis of substituted  $\delta$ -lactones from a range of pyrazoleamides and  $\alpha,\beta$ -unsaturated aldehydes (**Scheme 2.4**). A large range of substituted phenyl substituents could in principle be used on either component, demonstrating good potential for the exploration of chemical space. Iminium-catalysed Michael addition of the pyrazoleamide to the  $\alpha,\beta$ -unsaturated aldehyde, hydrolysis of the pyrazole moiety, lactonisation, then nucleophilic addition of the pyrazole back into the compound leads to the formation of the highly substituted products. The pyrazoleamide **19** was added to a solution of catalyst **6** (10 mol%) in toluene, before addition of 1.5 equivalents of cinnamaldehyde. This mixture was stirred for 24 hours, and purification

afforded the lactone **20** in a yield of 29% (in comparison to a reported yield of 89% using the TMS catalyst **7**).

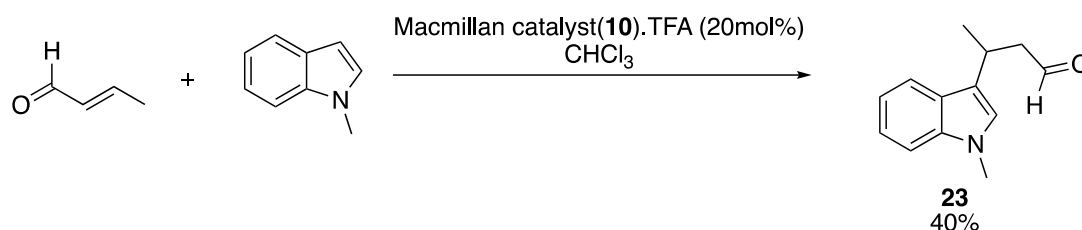
Ye et al. developed a reaction using chloroacetophenones and  $\alpha,\beta$ -unsaturated aldehydes to form cyclopropyl aldehydes, with each atom in the ring being a stereocentre (**Scheme 2.5**). Michael addition of the  $\alpha$ -chloro ketone to the iminium ion derived from the enal results in an enamine species which can then form a three-membered ring by alkylating at the  $\alpha$ -position. Cinnamaldehyde was stirred in DCM and an equivalent of triethylamine, before addition of 3 equivalents of  $\alpha$ -chloro ketone **21**, with catalyst **6** (10 mol%). After 24 hours of stirring at room temperature, purification afforded the cyclopropyl aldehyde **22** in a yield of 75% (in comparison to a literature yield of 93% using catalyst **7**).



**Scheme 2.5** - Organocatalytic Michael/ $\alpha$ -alkylation reaction between a chloroacetophenone and  $\alpha,\beta$ -unsaturated aldehyde to form a cyclopropyl aldehyde.<sup>98</sup>

An iminium-catalysed indole alkylation discovered by Austin et al. presented a good model reaction to test secondary amine catalysis using the Macmillan imidazolidinone catalyst (**Scheme 2.6**). Iminium-activation, with the imidazolidinone and a TFA co-catalyst, of the  $\alpha,\beta$ -unsaturated aldehyde facilitates attack of the indole nucleophile through the 3-position, generating a functionalised indole aldehyde. The literature reaction uses low temperature conditions ( $-87^\circ\text{C}$ ) and in a mixed solvent of dichloromethane and isopropanol, but the reaction was replicated at room temperature and using chloroform as the solvent. Three equivalents of *N*-methylindole were

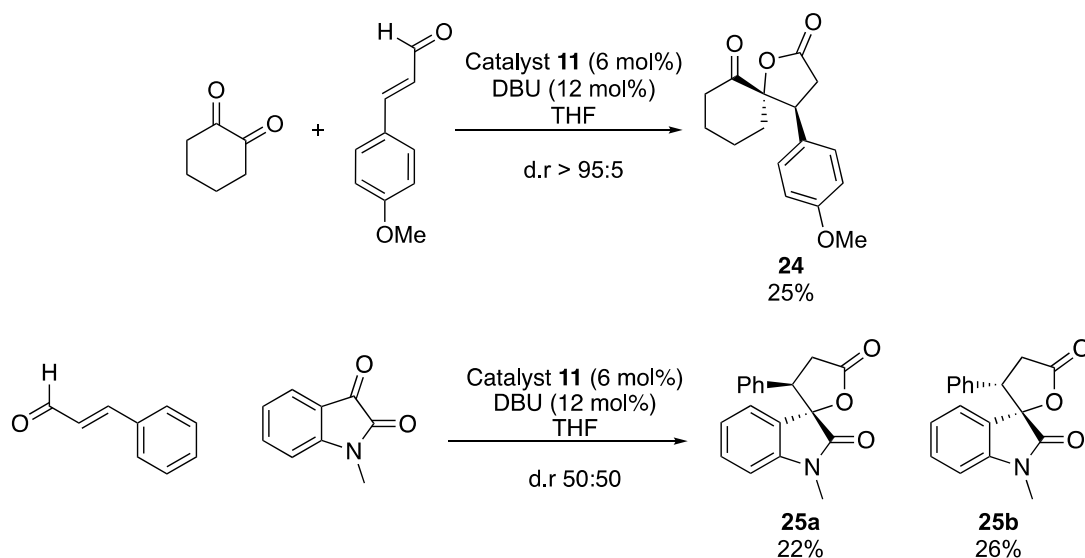
added to a stirred solution of crotonaldehyde, imidazolidinone (**10**) and TFA (20 mol%) in chloroform. After stirring for 24 hours, purification afforded the substituted indole **23** in a yield of 40% (literature yield was 82%, in which a much lower temperature was used).



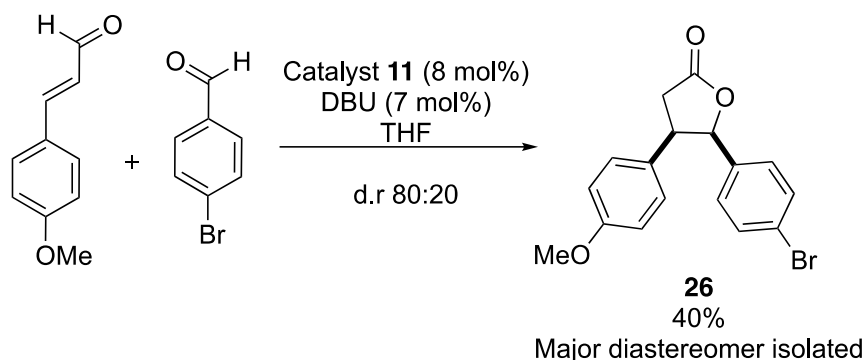
**Scheme 2.6** – Macmillan Imidazolidinone catalysed Michael-Addition of an indole to an  $\alpha,\beta$ -unsaturated aldehyde.<sup>84</sup>

### 2.3.2 *N*-Heterocyclic Carbene Catalysed Reactions

Nair et al. discovered an NHC-catalysed annulation of 1,2-dicarbonyl compounds (including isatins) with  $\alpha,\beta$ -unsaturated aldehydes capable of forming spiro  $\gamma$ -butyrolactones (**Scheme 2.7**). The catalyst forms the homoenolate species with the aldehyde, attacking the dicarbonyl through the  $\beta$ -position. The nucleophile formed can then attack back in to release the catalyst and form the spiro-products. In both reactions in **Scheme 2.7**, 1.5 equivalents of the relevant cinnamaldehyde was added to a stirred solution of imidazolium NHC catalyst **11** (6 mol%) and DBU in THF. The relevant 1,2-dicarbonyl compound was then added, and the reaction allowed to stir for 24 hours. Purification afforded the relevant spirocycle in variable yields. Lactone **24** was obtained in a 25% yield, comparable to the 92% yield demonstrated in the literature, while the spirocyclic oxindoles **25a** and **25b** were formed in yields of 22% and 26%. This reaction was of particular interest, as the isatin moiety is a constituent of a wide range of natural products, and is known to have a wide range of pharmacological activity against a range of biological targets.<sup>99</sup>

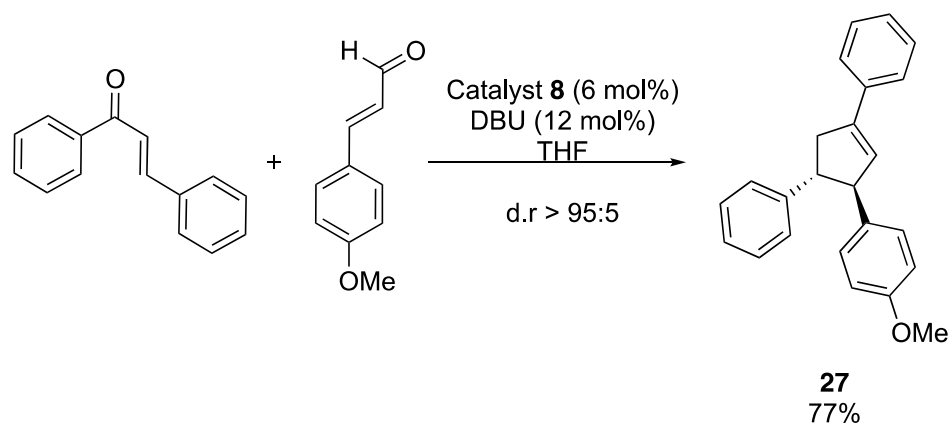


**Scheme 2.7** - Organocatalytic homoenolate addition involving an  $\alpha,\beta$ -unsaturated aldehyde and a 1,2-dicarbonyl.<sup>100</sup>



**Scheme 2.8** - Organocatalytic synthesis of disubstituted  $\gamma$ -butyrolactones via the direct annulation of  $\alpha,\beta$ -unsaturated aldehydes and benzaldehydes.<sup>101</sup>

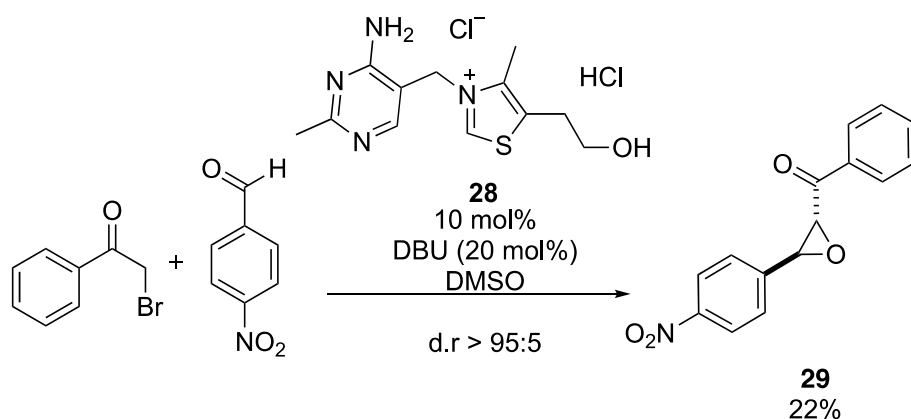
A variation of the reaction mechanism utilised by Nair et al. is shown in **Scheme 2.8**, a reaction class found by Bode et al.. Homo enolate addition of the enal into the aldehyde and then ring closure by the alkoxide releases the catalyst and forms the  $\gamma$ -butyrolactone product. Two equivalents of 4-bromobenzaldehyde was added to a stirred solution of 4-methoxycinnamaldehyde in THF, with imidazolium NHC catalyst **11** (8 mol%) and DBU. Following purification, the major diastereomer **26** was obtained in a 40% yield, with an isolated diastereomeric ratio of 89:11. In comparison to the literature procedure which reported a crude 80:20 d.r and 76% yield. Both substrates in this reaction could be varied to include various groups.



**Scheme 2.9** - Synthesis of 1,3,4-trisubstituted cyclopentenes using an NHC-catalysed reaction between chalcones and  $\alpha,\beta$ -unsaturated aldehydes via a homoenolate species.<sup>102</sup>

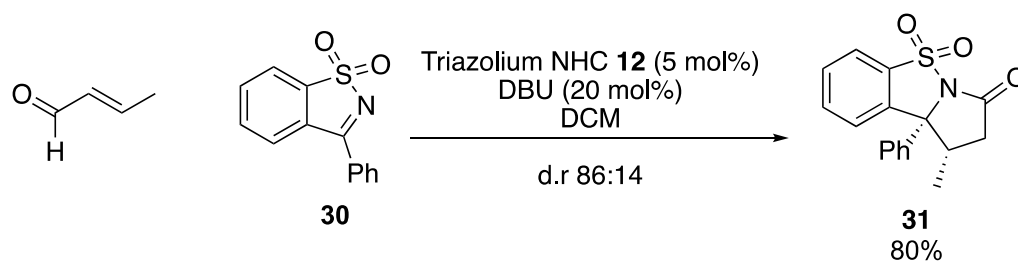
An iMes NHC-catalysed reaction forming substituted cyclopentene systems with two stereocentres was discovered by Nair et al. (**Scheme 2.9**). The homoenolate species adds into the  $\beta$ -position of the enone, then intramolecular aldol attack of the newly reformed enolate into the carbonyl enone then permits  $\beta$ -lactonisation to reform the catalyst and form the product. DBU was added to a suspension of the imidazolium NHC catalyst **11** (6 mol%) in THF, before addition of chalcone and 1.5 equivalents of 4-methoxycinnamaldehyde. Following purification, the cyclopentene **27** was obtained in a 77% yield, in comparison to 88% reported in the literature.

Sudalai et al. reported the NHC-catalysed oxidative coupling reaction shown in **Scheme 2.10**, which is catalysed by thiamine hydrochloride, another NHC catalyst structurally related to vitamin B<sub>1</sub>. The catalyst reacts with the  $\alpha$ -bromoketone, eliminating hydrogen bromide to form the ketodeoxy Breslow intermediate. This Breslow intermediate can attack the aldehyde, with the resulting species ejecting the catalyst and forming the  $\alpha,\beta$ -epoxyketone product. 4-Nitrobenzaldehyde and an excess of the 2-bromoacetophenone were added to a flask, followed by the thiamine hydrochloride NHC catalyst **28**. DMSO and DBU were added, and the mixture was stirred for 18 hours. Following purification, the epoxyketone **29** was obtained in a yield of 22% (in comparison to the reported literature yield of 78%).



**Scheme 2.10** - NHC-catalysed oxidative coupling of  $\alpha$ -bromoketones with aldehydes to form  $\alpha,\beta$ -epoxyketones.<sup>103</sup>

Rommel et al. reported a triazolium NHC-catalysed homoenolate addition of  $\alpha,\beta$ -unsaturated aldehydes to saccharin derivatives. The catalyst reacts with the  $\alpha,\beta$ -unsaturated aldehyde to form an activated *umpolung* Breslow intermediate, that reacts with the ketimine *via* a six-membered ene-like transition state. It is proposed that this transition state is stabilised by a hydrogen bond to the sulfonyl oxygen from the Breslow intermediate, allowing transfer of the acyl proton to the imine nitrogen atom, forming a new carbon-carbon bond. The reaction was reproduced by placing sulfonyl imine **30** in a flask, followed by 1.2 equivalents of crotonaldehyde. The triazolium NHC catalyst **12** was then added, followed by DCM and DBU. After stirring for 24 hours, purification afforded the  $\gamma$ -lactam major *cis*-product **31** in a yield of 80%, in comparison to the literature yield of 78%. The diastereomeric ratio of 86:14 in favour of the *cis*-isomer was identified by crude NMR, in comparison to the literature diastereomeric ratio of 75:25.



**Scheme 2.11** – Triazolium NHC-catalysed annulation of an  $\alpha,\beta$ -unsaturated aldehyde to saccharin derivatives.<sup>104</sup>



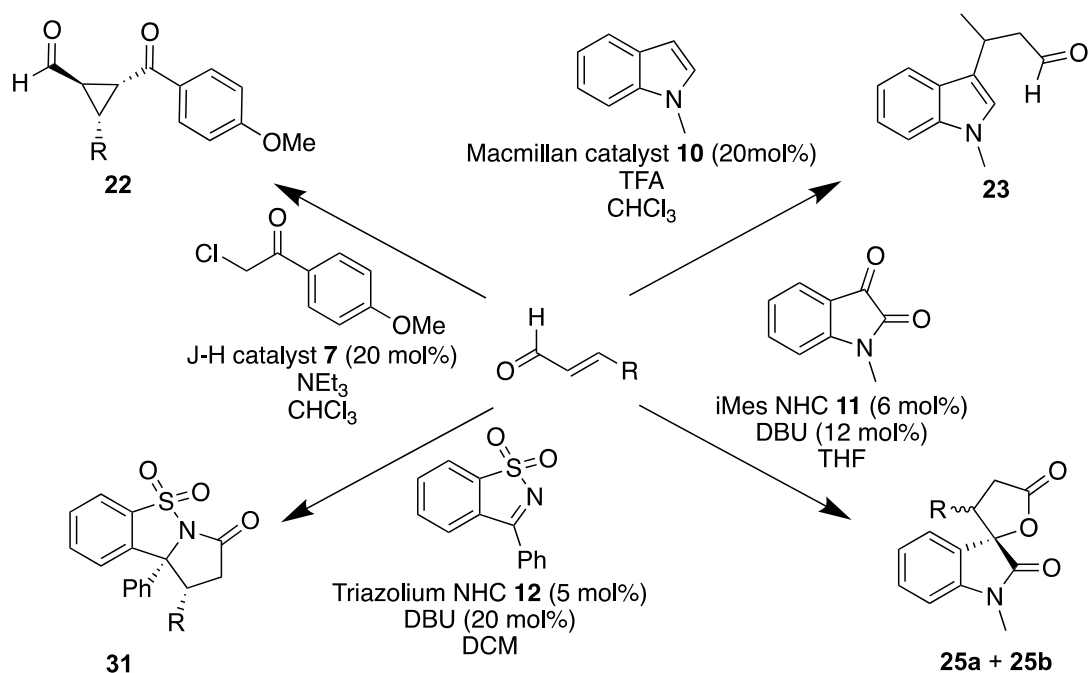
### **2.3.3 Transfer of Chemistry to Microwell Plate Format**

The exemplar reactions found and reproduced had all been carried out in a flask-based format on between 50-100 mg scale with regards to the limiting substrate. ADS is executed in a microwell plate format, where reactions are not stirred or agitated, are not under inert atmospheres, and the total reaction volumes are significantly reduced in order to fit inside low-volume reaction vials.

The viability of a selection of organocatalytic reactions compatible with this format had to be determined, and a set of general conditions that could be transferrable between reactions in the same organocatalytic class developed, so as to decrease the operational complexity of putting together complex reaction arrays.

To transition the chemistry from the full-scale flask to the micro-scale array format, a selection of the reactions explored in **2.2** were carried out in capped 100  $\mu$ L reaction vials in a 96-well plate, while maintaining the same overall concentration as the full-scale reactions (**Scheme 2.12**). The reactions selected captured the full range of organocatalysts described in **2.1**, exploring diverse reactivities that could generate a diverse range of scaffolds that were representative of the chemotypes that could be explored in organocatalytic ADS.

As the mass of the components to be used in the reactions was very small, stock solutions of the substrates were made, and the appropriate amounts added to reaction wells before allowing evaporation. Following evaporation, 100  $\mu$ L of a catalyst system containing the catalyst, solvent and any relevant additives was then added. The wells were then sealed with caps to prevent evaporation of solvents and left for 24 hours, before obtaining LC-MS analysis of the micro-scale crude reaction.



**Scheme 2.12** – the reactions selected to use to study compatibility with the plate format.

Alongside the micro-scale reaction, the procedure was also executed in a flask on a scale described in the literature. The LC-MS analysis of this mixture was also obtained, allowing comparison of the outcome to the micro-scale reaction. The full-scale reaction was then worked up and the crude products purified as in the literature protocol for each reaction, affording the pure product in each case. This allowed full analysis and characterisation of the relevant product, including LC-MS data indicating the relevant peak for the pure product on the LC-MS spectra. Comparing this LC-MS data to that of the crude mixtures of both the full-scale and micro-scale reactions allowed identification of the correct product in the reaction, demonstrating successful translation of the reaction from the full-scale to the micro-scale reaction.

**Table 2.1** provides a comparison of the LC-MS traces for the reaction in which the spiro  $\gamma$ -butyrolactone products **25a** and **25b** are formed by an NHC-catalysed annulation between an  $\alpha,\beta$ -unsaturated aldehyde and an isatin, as previously shown in **Scheme 2.7**. The LC-MS trace for the full-scale reaction shows a peak with mass corresponding to the anticipated product, and LC-MS of the isolated product, which was confirmed by NMR, demonstrated that to be correct. The same mass was found at the same

retention time in the microscale plate-based reaction, with the LC-MS trace appearing almost identical to that of the flask reaction. This confirmed that the reaction had been transferred successfully to the format required for ADS. Similar analyses for the other three reactions shown in **Scheme 2.12** can be found in the experimental, demonstrating successful transfer of the reactions to a plate format

Format	LC-MS Trace	Retention Time (Mins)	Mass Found
Flask		0.59 (1)	294.14
Isolated Product		0.59 (1)	293.93
Plate		0.59 (1)	294.14

**Table 2.1** – Comparison of a reaction performed in a flask, and on a 100  $\mu\text{L}$  scale in a vial. LC-MS data shows the expected product (calculated  $\text{M-H}^+$  294.11) isolated from the flask-based reaction is also present in the reaction vial used for the microscale reaction.

## 2.4 Development of Post-Reaction Protocols

Electrophilic functional groups such as aldehydes and Michael acceptors are undesirable in molecules in the early stages of the drug discovery process where large numbers of compounds are tested.<sup>105</sup> The unsuitability of these reactive groups stems from their potential to react with the protein of interest, thereby potentially interfering with the result of an *in vitro* assay.<sup>106</sup>

Many of the substrates in the reactions demonstrated in **Section 2.2** feature such functionality. Both aldehydes and  $\alpha,\beta$ -unsaturated aldehydes are electrophilic, and can potentially react with nucleophiles. It would therefore be beneficial to convert the substances containing these moieties to more benign products before screening of the product mixtures on the assay. A range of model compounds were selected for these experiments, featuring functionality representative of the kind that were likely to be observed in both substrates and products (**Figure 2.2**).

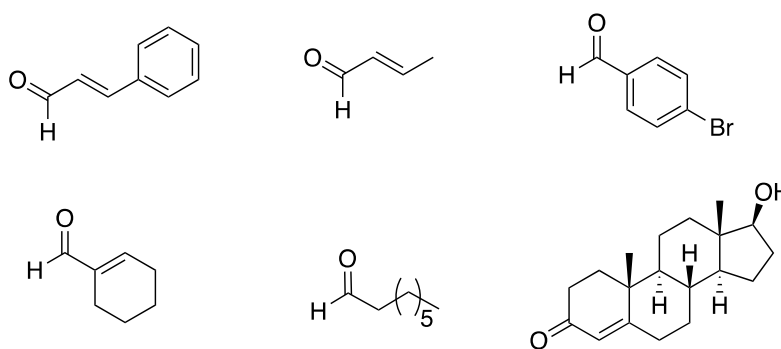


**Figure 2.2** – Range of model substrates selected for the development of post-reaction work-up protocols.

### 2.4.1 Reduction with Sodium Borohydride

Addition of a solution of sodium borohydride in methanol directly into a mixture was selected as a protocol to reduce electrophilic functionality. The substrates (0.035 mmol) were dissolved into deuterated chloroform with a known equimolar amount of an unreactive standard, 1,2,4-trichloro-5-

methoxybenzene. The solution was transferred into an NMR tube and an initial 400 MHz  $^1\text{H}$  NMR spectrum of the mixture was obtained. 40  $\mu\text{L}$  (0.0525 mmol, 1.5 equiv.) of a solution of sodium borohydride (11.92 mg in 240  $\mu\text{L}$ ) in methanol was added directly to the NMR tubes containing each of the six selected substrates and left for two hours before obtaining another 400 MHz  $^1\text{H}$  NMR spectrum. Conversion of the substrate to products could be observed by comparison of a distinguishable peak of a proton environment that experienced an upfield shift upon reduction in the NMR spectra ( $\delta \sim 10.0$  ppm for aldehydes, proton adjacent to carbonyl of ketone in testosterone) to the integral of the aromatic proton in the standard (see Appendices for an example).

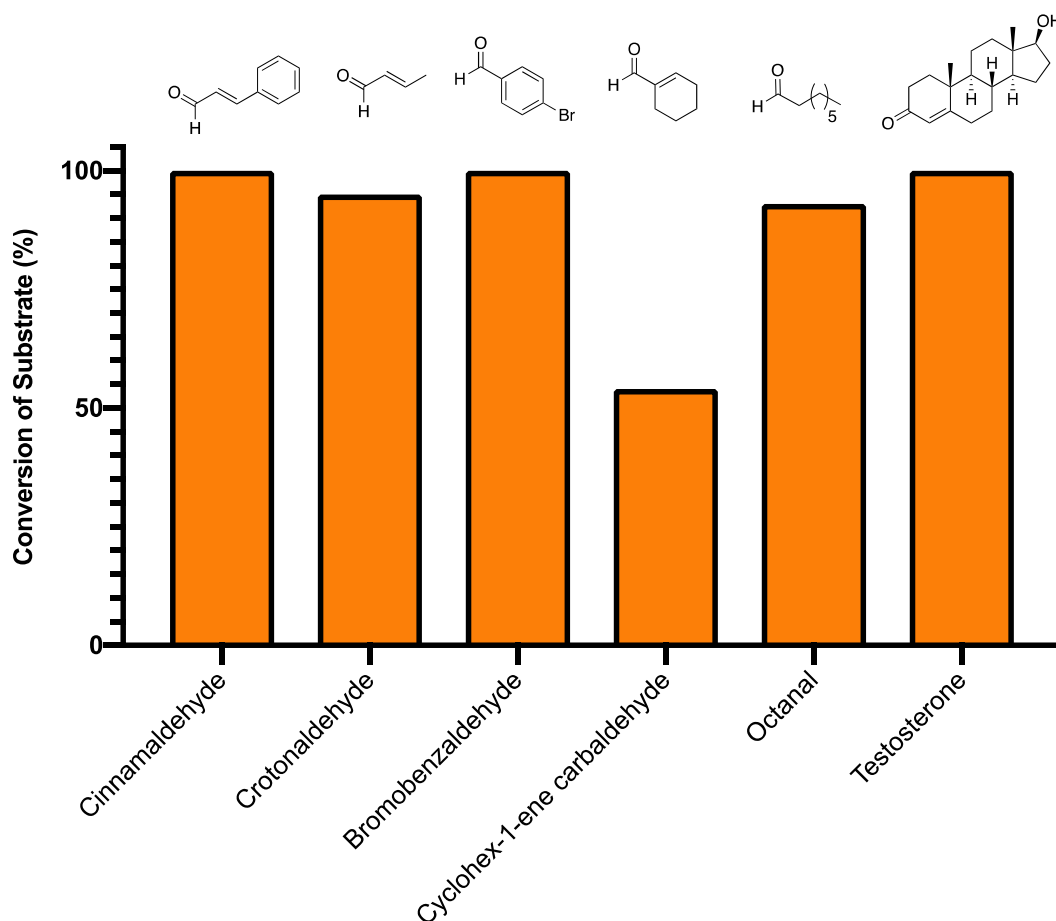


**Figure 2.3** – Conversion of the model substrates by treatment with the sodium borohydride reduction conditions.

As can be observed in **Figure 2.3**, these conditions provided excellent levels of conversion, eliminating electrophilic functionality such as

electrophilic aldehydes and Michael acceptors. NMR data for these transformations can be found in the experimental.

However, a concern regarded the potential for degradation of the sodium borohydride solution in methanol. Making a solution and adding it to a reaction array takes time, and for maximum efficiency of reduction, it was essential the solution used for the reduction did not degrade over the timescale of the reaction. Methanol reacts with the sodium borohydride to form methoxyborates, resulting in effervescence due to the reaction evolving four equivalents of hydrogen gas per equivalent of sodium borohydride when in an excess of the solvent.<sup>107</sup>

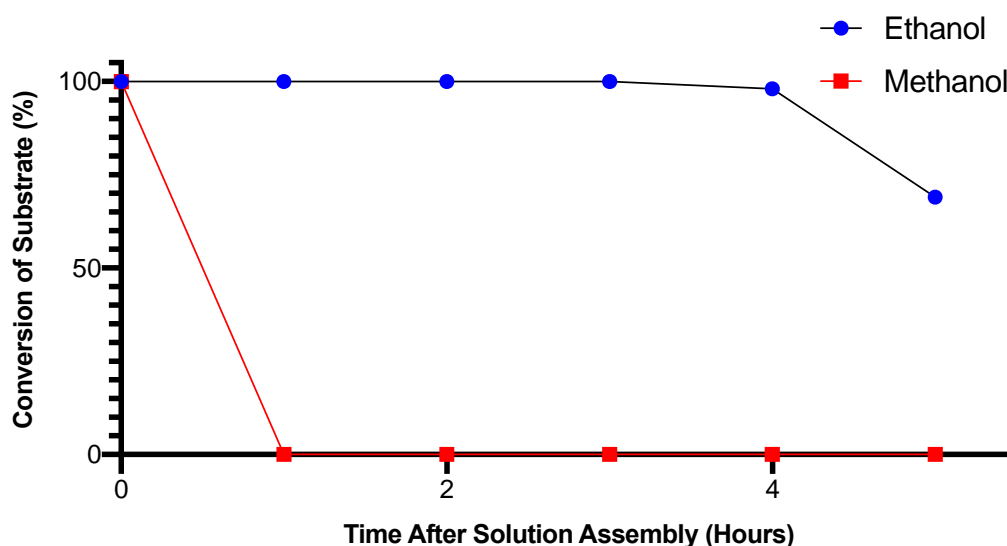


**Figure 2.4** – Conversion of cinnamaldehyde in reduction reactions, using sodium borohydride solutions at varying timepoints after their assembly.

The reduction efficiency of sodium borohydride in a selection of suitable alcohols (methanol, ethanol and propan-2-ol) over a five hour timescale was investigated in order to gauge which solvent was best to use. Cinnamaldehyde (0.027 mmol) was used as a model substrate to test the reducing power of the solutions, and was added to a vial containing an approximately equimolar amount of standard 1,2,4-trichloro-5-methoxybenzene (0.027mmol), followed by deuterated chloroform (400  $\mu$ L). Solutions of sodium borohydride (15.32 mg in 400  $\mu$ L of relevant alcohol) were made up, and 40  $\mu$ L of each solution (0.0405 mmol, 1.5 equiv.) added

to the reaction to determine conversion at one hour intervals over a 5 hour period. The resulting product mixtures were then analysed by 400 MHz  $^1\text{H}$  NMR spectroscopy after one hour reaction time. Propan-2-ol was ruled out as an option immediately, as the sodium borohydride was insoluble, and was therefore not suitable to use in the ADS workflow as a reductive protocol. **Figure 2.4** displays the results for remaining methanol and ethanol solutions.

Degradation of the reducing solution occurs much more slowly with ethanol rather than methanol. Ethanol was able to dissolve the sodium borohydride and showed much slower effervescence in comparison to the methanol solution, due to the slower reaction between ethanol and sodium borohydride forming the sodium tetraethoxyborate species and evolving hydrogen as a result. The ethanol solution was able to maintain a good level of reducing ability for well over 4 hours, providing a large enough window to give good conversion in reaction arrays over a suitable time period. Consequently, sodium borohydride in ethanol was used as the post-reaction protocol for reduction.

### **2.4.2 Reductive Amination**

An alternative reaction for processing of aldehyde products is reductive amination. Not only can the reactive groups be removed from potential bioactive products, but additional functionality can be added into the products by capping the carbonyl groups with amines, potentially increasing efficacy by adding another functional group into the molecule that can interact with the biological target. A selection of methods for reductive amination with dimethylamine as the model amine component in the reaction were considered; including sodium borohydride in tandem with phosphotungstic acid,<sup>108</sup> triethylsilane and TFA,<sup>109</sup> and  $\alpha$ -picoline borane in methanol.<sup>110</sup> However, a method using the desired secondary amine in addition to tetramethylammonium triacetoxyborohydride was selected.

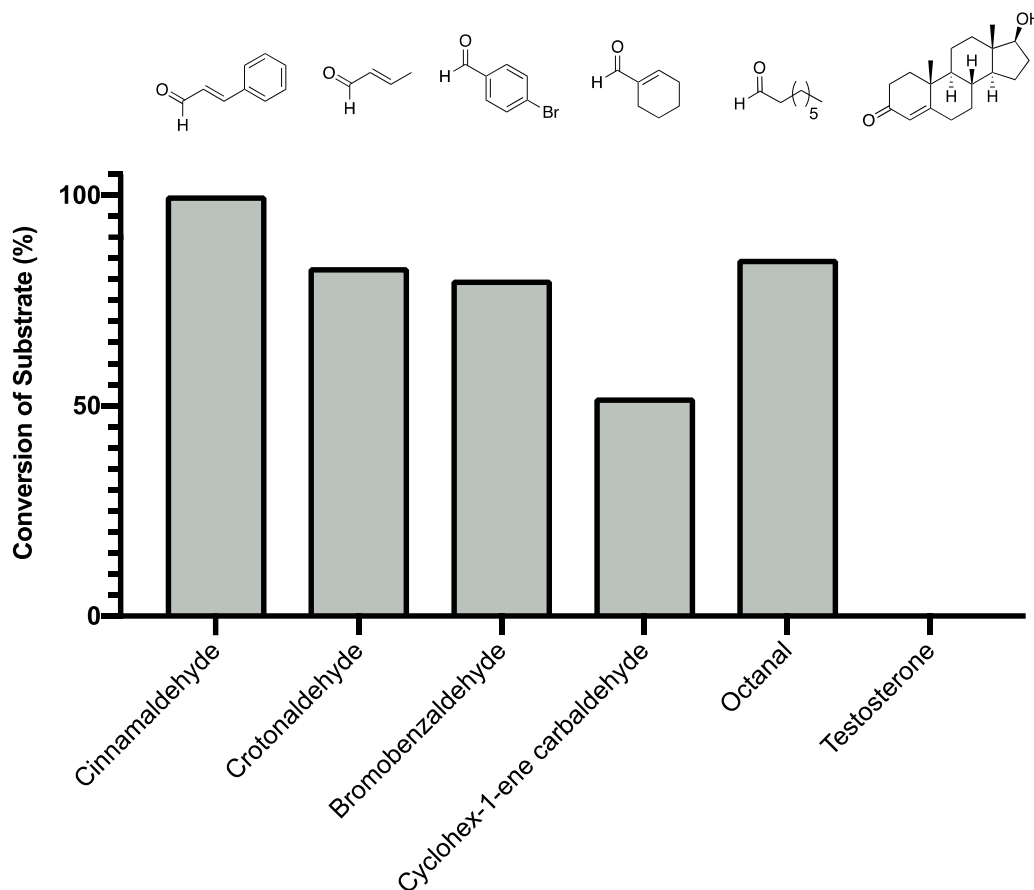


**Figure 2.5** – Conversion of the model substrates by treatment with dimethylamine, then tetramethylammoniumtriacetoxyborohydride 45 minutes later to reduce the imine.

The carbonyl substrates (0.027 mmol) and a known equimolar amount of 1,2,4-trichloro-5-methoxybenzene standard and were dissolved in deuterated chloroform before transferring the solution to an NMR tube. After a 300 MHz  $^1\text{H}$  NMR spectrum of the initial mixture had been obtained, the dimethylamine (0.030 mmol, 1.1 equiv.) was added to the NMR tube and allowed to potentially form an imine with a carbonyl species for 10 minutes. 40  $\mu\text{L}$  (0.0405 mmol, 1.5 eqv.) of a solution of tetramethylammonium triacetoxyborohydride (63.93 mg, 0.243 mmol) in acetic acid (240  $\mu\text{L}$ ) was then added. A 300 MHz  $^1\text{H}$  NMR spectrum of each mixture was obtained after 24 hours to monitor conversion, using the aldehyde proton signal ( $\delta \sim 10$  ppm) of the spectrum to measure conversion, while also observing new peak formation to identify products. Conversion to dimethylamine products was observed with all substrates, although reductive amination of testosterone, a



compound featuring a cyclic  $\alpha,\beta$ -unsaturated ketone, was unsuccessful (**Figure 2.5**).

To quench reductant potentially left over from the workup conditions that had the capability to interfere with further steps in the protocol, 5 equivalents of acetaldehyde were added to the product mixtures. The low boiling point of acetaldehyde (20.2°C) and its products from both work-up protocols, ethanol (78.4°C) and dimethylethylamine (36.5°C) meant that they would be evaporated before screening.

The conditions established instilled confidence that any highly electrophilic functionality within compounds present in product mixtures during ADS could be removed to generate species with less potential for *in vitro* assay interference.

## 2.5 Summary of Configuration of Organocatalysis for ADS

A wide range of organocatalysed reactions were identified that yielded diverse scaffolds and their viability was demonstrated. Following this, conditions were developed that allowed successful translation of organocatalysed reactions from a flask to a micro-scale format suitable for ADS. A selection of reactions that utilised a number of different organocatalysts across both amine and NHC classes were chosen to demonstrate this, and the outcomes of the miniaturised reactions were proven to be comparable to the outcomes of the same reactions in a flask. Post-reaction work-up protocols were then developed. A reduction with sodium borohydride, and a reductive amination with dimethylamine and morpholine with tetramethylammonium triacetoxyborohydride were efficient in removing electrophilic functionality that could be present in both the substrates and products of organocatalysed reactions.

With these methods in place, the focus could now move to exploring the value of organocatalysis in ADS, using alternative strategies to form intermolecular products with potential bioactivity.

### 3 Exploring the Value of Organocatalysis in ADS

With conditions for the execution of an ADS array based around organocatalysis chemistry devised, arrays of reactions could now be carried out to synthesise and identify bioactive products. Setting up a suitable high-throughput biochemical assay was essential to allow fast and efficient screening of products for any activity against the biological target. Following this, a number of different strategies for designing ADS reaction arrays utilising organocatalysis were explored.

#### 3.1 Configuration of TR-FRET Androgen Receptor Assay

A commercially-available TR-FRET (Time Resolved Fluorescence Resonance Energy Transfer) Androgen Receptor assay was selected to screen product mixtures generated from the reaction arrays for agonism of the Androgen Receptor. A FRET assay operates on the basis that when two fluorophores, a donor and acceptor, are in close proximity (roughly 10 nm)<sup>111</sup>, and their respective emission and excitation spectra overlap, the donor fluorophore can transfer energy to the acceptor fluorophore, leading to emission of fluorescence.<sup>112</sup> Time-resolved FRET utilises lanthanide metal donors that have much longer fluorescence lifetimes than standard FRET donors. This decreases the likelihood of assay interference often caused by screened organic compounds that have short fluorescence lifetimes.

In the context of the TR-FRET AR assay (see **Figure 3.1**), a terbium-labelled anti-GST antibody binds to the GST-labelled ligand binding domain of the AR protein (AR-LBD). Upon binding of an agonist ligand, a conformational change occurs around helix 12 in the AR-LBD, increasing its affinity for the fluorescein-labelled coactivator peptide, resulting in recruitment of the peptide. The resulting binding event between the AR-LBD and the fluorescein-labelled peptide brings the two fluorophores into mutual proximity.

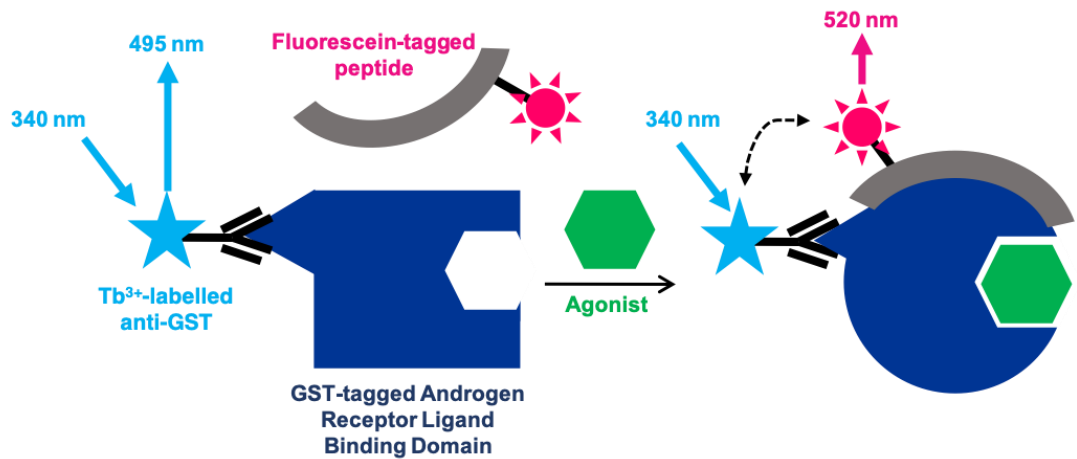


**Figure 3.1** – An overview of the TR-FRET AR assay. The GST-tagged AR-LBD binds to an anti-GST terbium-labelled antibody, the donor fluorophore. Upon binding of an agonist, a conformational change in the AR-LBD enables recruitment of the fluorescein-tagged peptide, the acceptor donor. Irradiation at 340 nm excites the terbium label, and the energy can be transferred to the fluorescein acceptor. The ratio between the emission intensities at 520 nm from the fluorescein, and 495 nm from the terbium label, can enable assessment of the bioactivity of the agonist.

The terbium label of the antibody can be excited by irradiation at 340 nm. The terbium label will emit this radiation at a wavelength of 495 nm if the energy is in the absence of a proximal acceptor fluorophore. However, if the donor terbium is proximal to the fluorescein acceptor as a result of a binding event between the peptide and the AR-LBD, the terbium label can transfer the absorbed energy to the fluorescein-labelled peptide, which emits at a wavelength of 520 nm. The ratio between the intensities of the emissions at the two wavelengths (520 nm/495 nm) correlates with the efficiency of energy transfer between donor and acceptor fluorophores, which allow determination of the extent of agonism. The assay can be executed to determine dose-dependent effects of specific ligands and determine  $EC_{50}$  values. Alternatively, ligands can be screened at a single concentration to determine activity in comparison to a positive control, such as testosterone, a known potent AR agonist.

To establish the assay, a 12-point three-fold serial dilution of testosterone was assayed, with concentrations of ligand ranging from 5  $\mu\text{M}$  down to 28.2 pM in pH 7.5 buffer, with a final concentration of 1% DMSO. Once the 12-point three-fold serial dilution of a 500  $\mu\text{M}$  DMSO solution of testosterone had been completed, each of the solutions was diluted 50-fold with buffer, and then added to the assay plate in triplicate. AR-LBD solution was then added at a concentration of 112 nM, followed by a solution of the terbium-labelled antibody at 20 nM and the fluorescein-labelled peptide at 2  $\mu\text{M}$ . After 4 hours, the emission intensities at 520 nm and 495 nm of each well was measured on a Perkin-Elmer Envision 2103 Multilabel reader. This enabled an  $\text{EC}_{50}$  value of 17.4 nM to be obtained for testosterone that was concordant with previously reported values.<sup>113</sup>

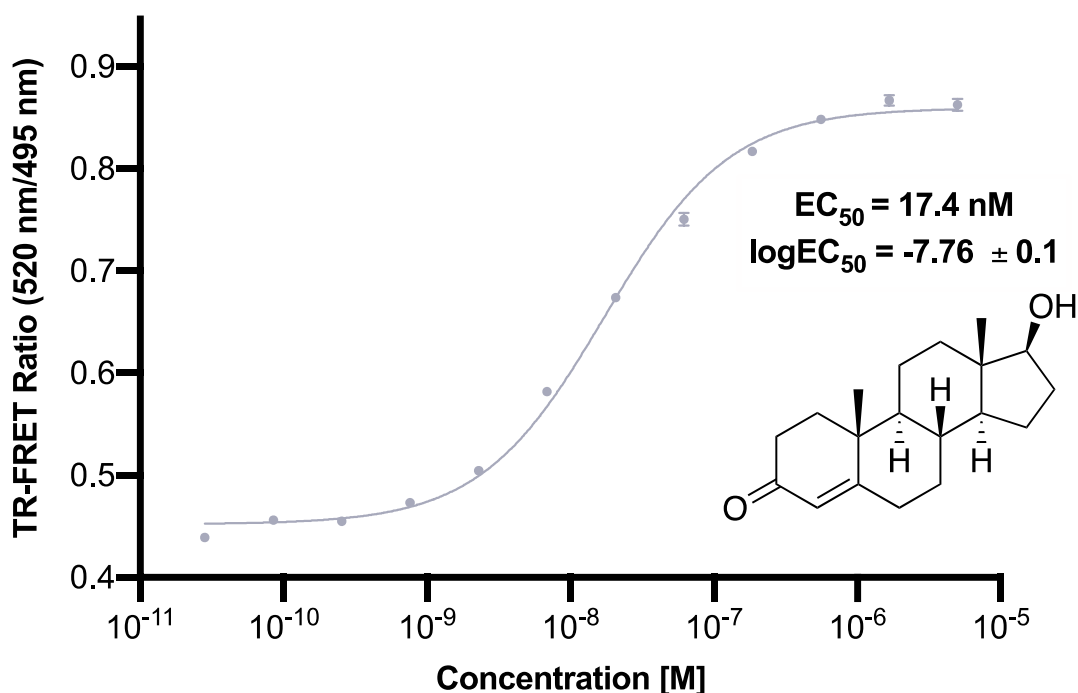


**Figure 3.2** – Dose-response curve obtained for Testosterone. Calculated  $\text{EC}_{50}$  value of 17.4 nM was consistent with literature values.

The concentration of the AR-LBD solution added to wells in the assay was variable, depending on which particular kit was being used during the project at the time, as there was significant batch-to-batch variation of the protein used. At a number of points in the project, consistency in obtaining a reasonable dynamic TR-FRET range was variable when using the assay, an observation that was likely due to batch-to-batch variation of the

commercially available assay kit. To address this, it was found that doubling the recommended final concentration of the terbium-labelled anti-GST antibody from 5 nM to 10 nM increased reliability, leading to a larger dynamic range. Assays in which higher concentrations of antibody were used are noted throughout the thesis.

## 3.2 Design and Execution of an Exhaustive ADS Reaction Array

### 3.2.1 Design of Round 1 ADS Reaction Array

Initially, a reaction array was designed to harness a wide range of complementary organocatalytic reactivities. The design of the reaction arrays that were planned for the first round is outlined in **Figure 3.3**. Using four different catalyst systems (**C1-C4**) in combination with 24 commercially-available diverse co-substrates (**B1-B24**) per plate; one 'armed' substrate (**A1-A5**) per plate could be utilised to simplify the set-up of an exhaustive array. There were two replicates of each plate of reactions, to enable the use of the two work-up procedures devised in the previous chapter: one plate using a sodium borohydride reductive work-up, and the other using a reductive amination work-up with dimethylamine. As five armed substrates were made for use in Round 1, this resulted in a total of 960 product mixtures to screen in Round 1.

The first round array was designed to be exhaustive, using every possible combination of substrate, co-substrate, catalyst and work-up protocol. It was envisaged that this approach would maximise the amount of chemical space that could potentially be explored. This approach inevitably led to the exploration of many combinations for which there was no literature precedent. However, this may add a degree of unpredictability to the discovery of bioactive products, as unexpected outcomes could emerge from productive reaction mixtures. This would increase the diversity of potential products so that they are outside the scope of known literature and enable the potential discovery of novel chemotypes and reactions. To maximise the probability of this occurring, functional groups known to exhibit reactivity

in organocatalytic reactions needed to be integrated into the substrates used.

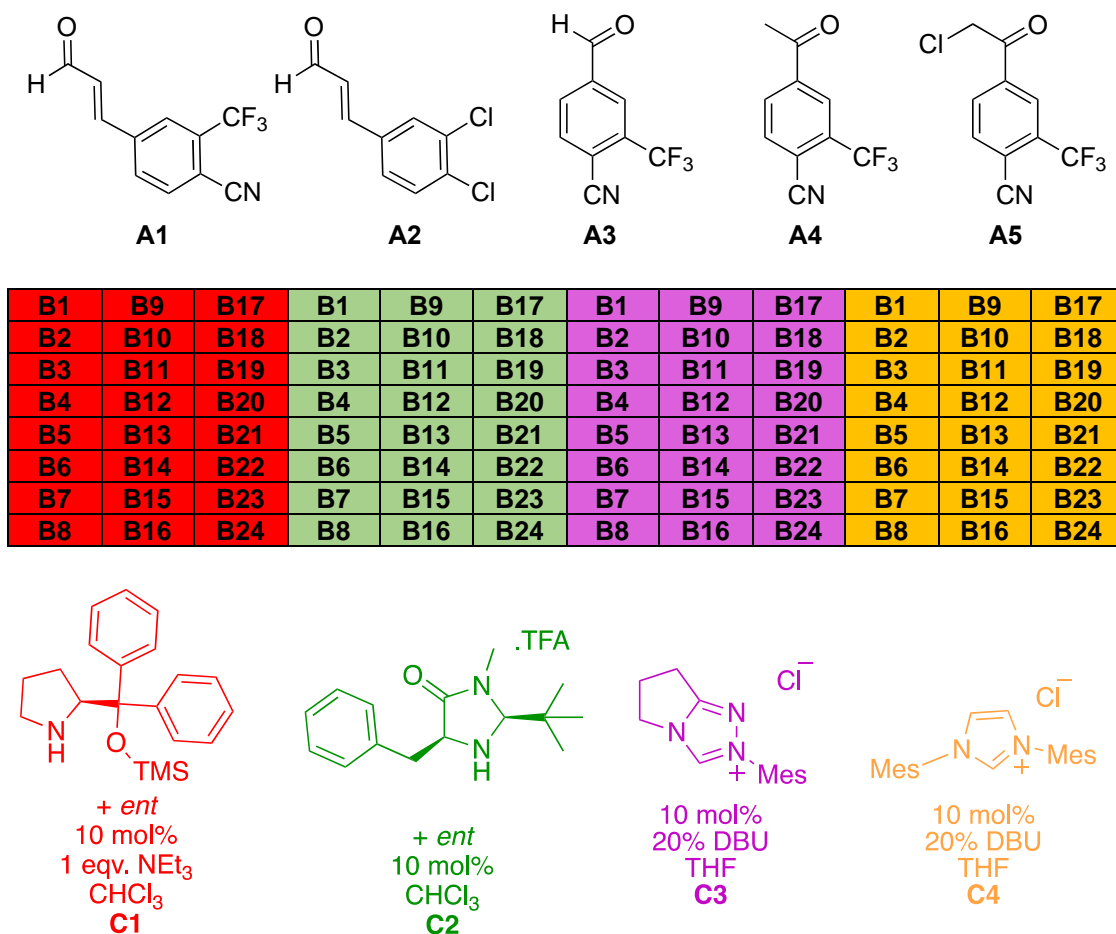


**Figure 3.3** - Design of the reaction arrays for the first round of ADS. Each of the ten 96-well plates that were to be executed corresponded to one of the five armed substrates (**A1–A5**) with one of the two work-up procedures (sodium borohydride reduction, or dimethylamine reductive amination). There were to be 24 co-substrates (represented by **B1–B24**) and 4 catalyst systems **C1–C4**) in use on each plate, resulting in a total of 960 first round reactions.

As in the previous AR project, it was decided that a set of substrates ‘armed’ with warhead moieties known to modulate the AR (noted in **Section 1.3.2**) would provide a good starting point for developing novel bioactive compounds, permitting a range of scaffolds to be built around these groups, providing functionality that could enable increased bioactivity. The structures of the armed substrates (**A1–A5**) are noted in Figure 3.3, and each feature a

functional group that was known to have reactivity with an organocatalyst, as well as a motif known to modulate the AR: either a 4-cyano-3-trifluoromethylphenyl group, or a 4,3-dichlorophenyl group.

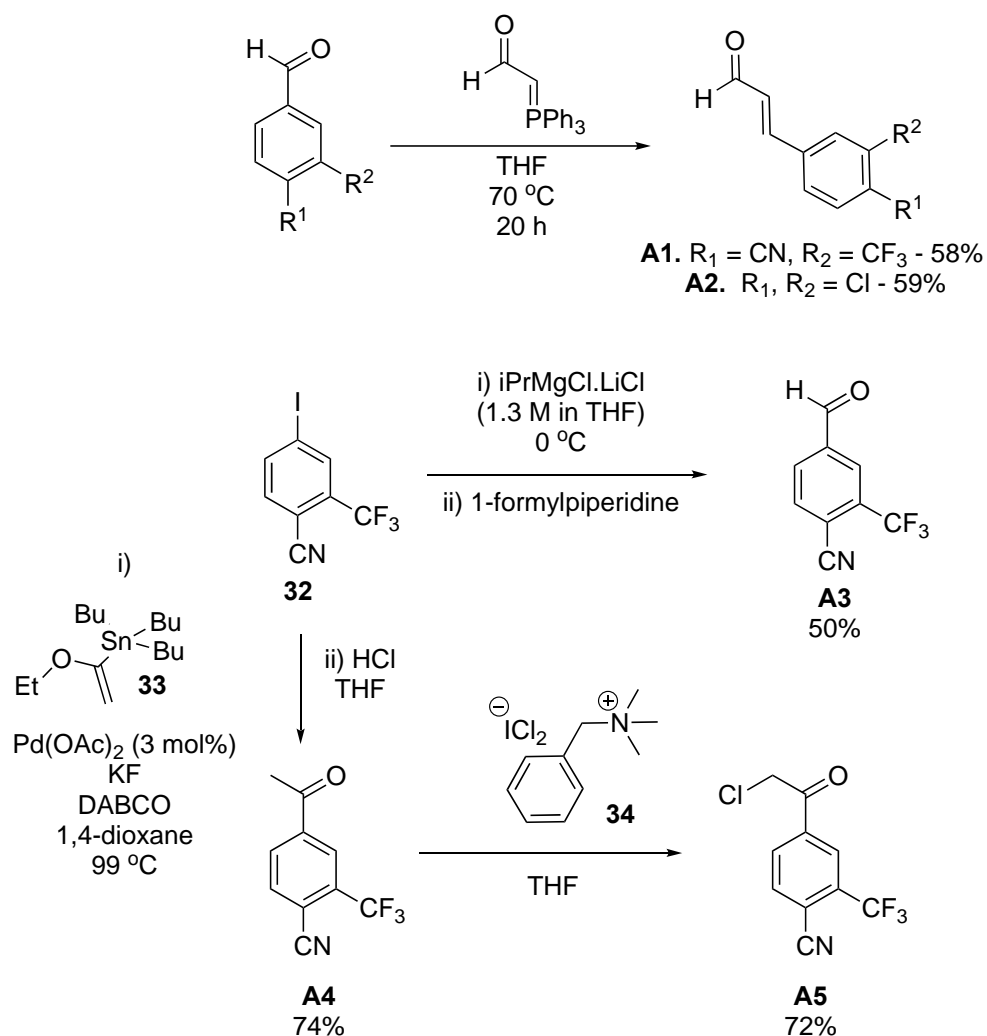
The substrates capture all of the reactivity modes outlined in **Section 1.4** – the enal ( $\alpha,\beta$ -unsaturated aldehyde) class of substrate (**A1** and **A2**) can capture both iminium (**Scheme 1.6**) and homoenolate (**Scheme 1.8**) reactivities with amine and NHC catalyst classes respectively. The benzaldehyde **A3** was the precursor for the required  $\alpha,\beta$ -unsaturated aldehyde **A1**, and had the capability to be activated with an NHC catalyst to generate a potent nucleophile (**Scheme 1.7**), in addition to being a suitable electrophile in reactions due to the carbonyl group. The methyl ketone **A4** could potentially be activated by an amine catalyst to form a nucleophilic enamine species (**Scheme 1.4**) that could react with a suitable electrophile, or the ketone functionality could be an electrophile for a suitable nucleophilic partner. The  $\alpha$ -chloroketone **A5** could be made in one simple step from the methyl ketone **A4**, and had potential utility as an electrophile capable of forming interesting small membered ring scaffolds, bringing extra diversity to the potential product set.<sup>98</sup>

### 3.2.2 Synthesis of Armed Substrates

Synthesis of the benzaldehyde **A3** was executed by slow addition of isopropylmagnesium chloride lithium chloride complex in THF (the 'turbo Grignard' reagent) to relevant aryl iodide at 0 °C. Formyl-1-piperidine was then added to act as the formyl donor, and after purification by flash column chromatography, the benzaldehyde **A3** was afforded in a yield of 50% (**Scheme 3.1**).<sup>66</sup>

The methyl ketone **A4** was also synthesised from the aryl iodide **32**, but utilised palladium-catalysed Stille chemistry. The aryl iodide was refluxed for 24 hours with tributyl(1-ethoxyvinyl)tin (**33**) in the presence of palladium (II) acetate, potassium iodide and DABCO in dioxane. The solution was then cooled, filtered through celite and evaporated, before treating the resulting

residue with hydrochloric acid and THF. Following purification by flash column chromatography, this afforded methyl ketone **A4** in a yield of 74%. Synthesis of the methyl ketone enabled the synthesis of chloroacetophenone **A5**. The methyl ketone **A4** was stirred overnight with benzyltrimethylammonium dichloriodate (**34**) in THF. Purification of the crude product by flash column chromatography afforded the  $\alpha$ -chloro ketone **A5** in a yield of 72%.



**Scheme 3.1** – Synthesis of the armed substrates.

The  $\alpha,\beta$ -unsaturated aldehydes **A1** and **A2** were synthesised via a one-step Wittig procedure. A slight excess of 1.1 equivalents of (triphenylphosphoranylidene)acetaldehyde was added to a flask with the relevant benzaldehyde and refluxed in THF for 20 hours. Following purification by flash column chromatography, this afforded enal **A1** in a yield of 58%, and **A2** in a yield of 59%.



### 3.2.3 Selection of Co-Substrates

A computational approach was used to aid selection of 24 co-substrates for use in the first round of the exhaustive project. The cheminformatics platforms Pipeline Pilot and KNIME were used to, allowing filtering of large databases of over 250,000 compounds from commercial suppliers to smaller sets of compounds with reactive functional groups, optimised physiochemical properties and maximal diversity.

The workflow began with filtering compounds in the database for functionality that had some precedent to react with at least one of the ‘armed’ substrates when paired with an organocatalyst – the sub-structures that were used as the filters can be found in **Section 6.7**. Physical parameters for each compound were then calculated, and the set filtered to obtain compounds with desirable characteristics. Molecular weight and rotatable bonds were limited, and AlogP was set between -1 and 3 to prevent the synthesis of overly heavy, greasy or polar compounds. Financial expenditure was controlled for filtering using pricing and quantity information, available from both suppliers, allowing exclusion of compounds that were more expensive than £100 per gram of material. This resulted in a set of compounds with potential reactive functionality, that had appropriate molecular properties for drug-like compounds.

The lists of different classes of compounds were then merged, and a native Pipeline Pilot module was used to select 35 diverse compounds from this combined set, using their structural fingerprints as the basis for diversity (**Figure 3.4**). This was a larger selection than the 24 co-substrates proposed in the initial design, as we anticipated some of the compounds may be unsuitable due to potential poor solubility, assay interference or lack of current commercial supply. These traits, if identified, led to their exclusion from the array, allowing trimming of the set down to 24 co-substrates.

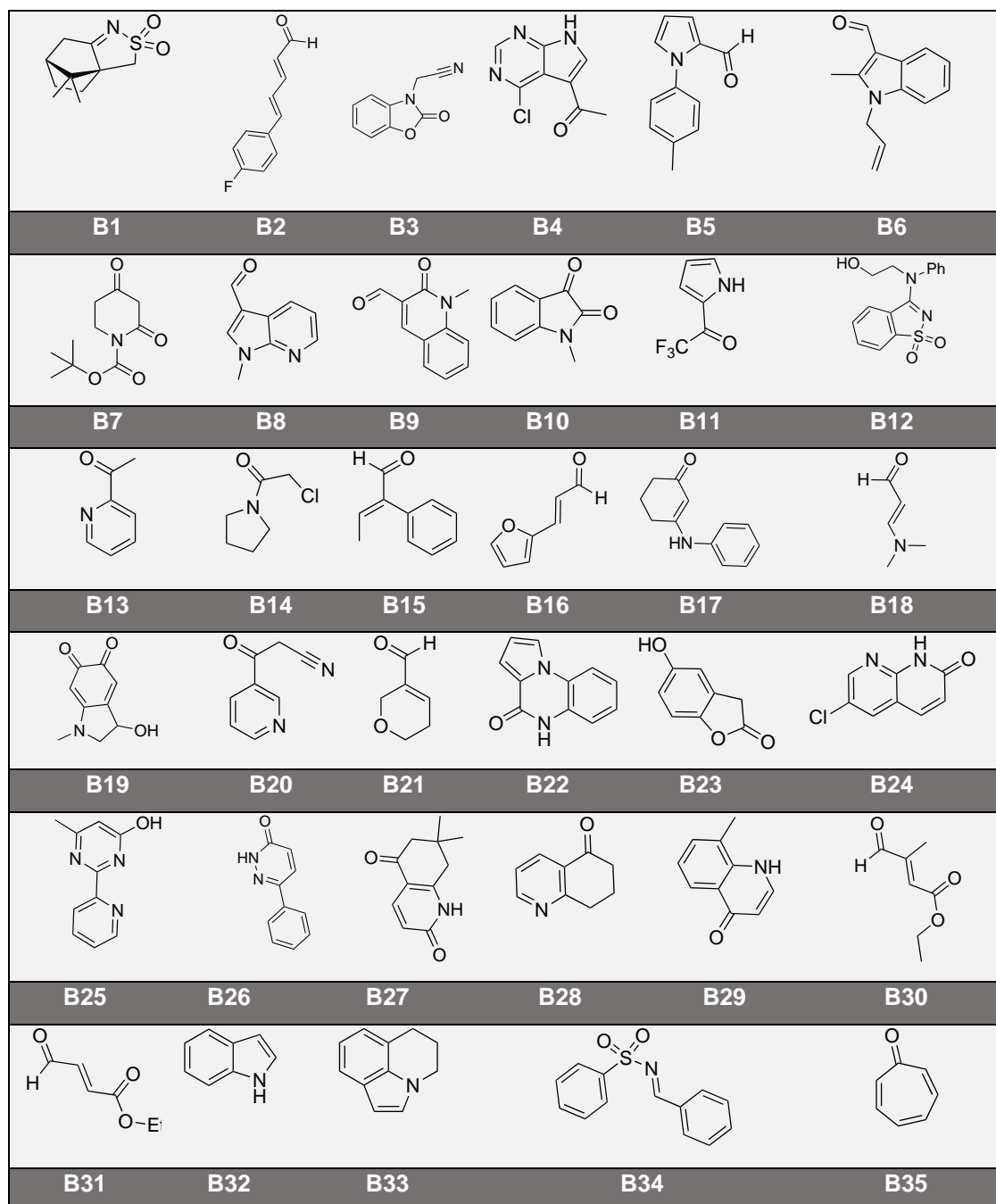
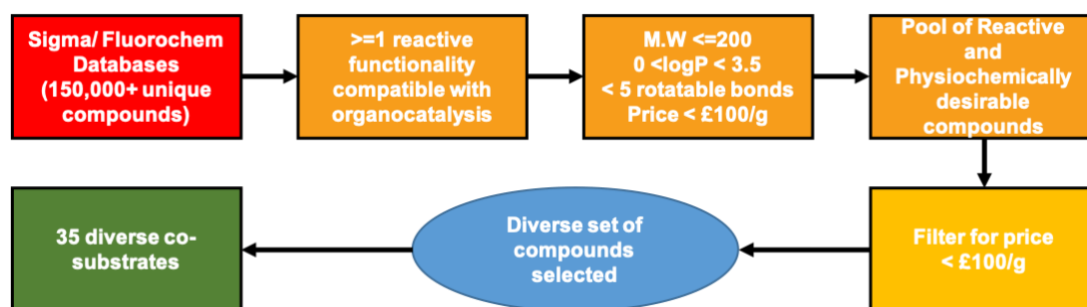


**Figure 3.4** – The 35 co-substrates selected using the cheminformatics workflow.

### 3.2.4 Execution of Mock Array

With all of the components for Round 1 obtained, a mock array was executed to determine if any individual components to be included in the array would cause assay interference or have solubility issues. Stock solutions were made up at the exact specification that would be used in the reaction array, and each individual component taken through each of the work-up procedures (reduction and reductive amination) separately. Each of these crude products was then screened using a single-point assay to determine the relative activities of each component. By normalising the results relative to the testosterone positive control, activity data for the component could be obtained, and its likelihood of assay interference determined.<sup>106</sup> The mock array was completed at a screening concentration of 10  $\mu\text{M}$  relative to the armed substrate; hence the co-substrates were being screened at 20  $\mu\text{M}$  due to their relative excess in the reaction mixtures (assay readout in experimental).

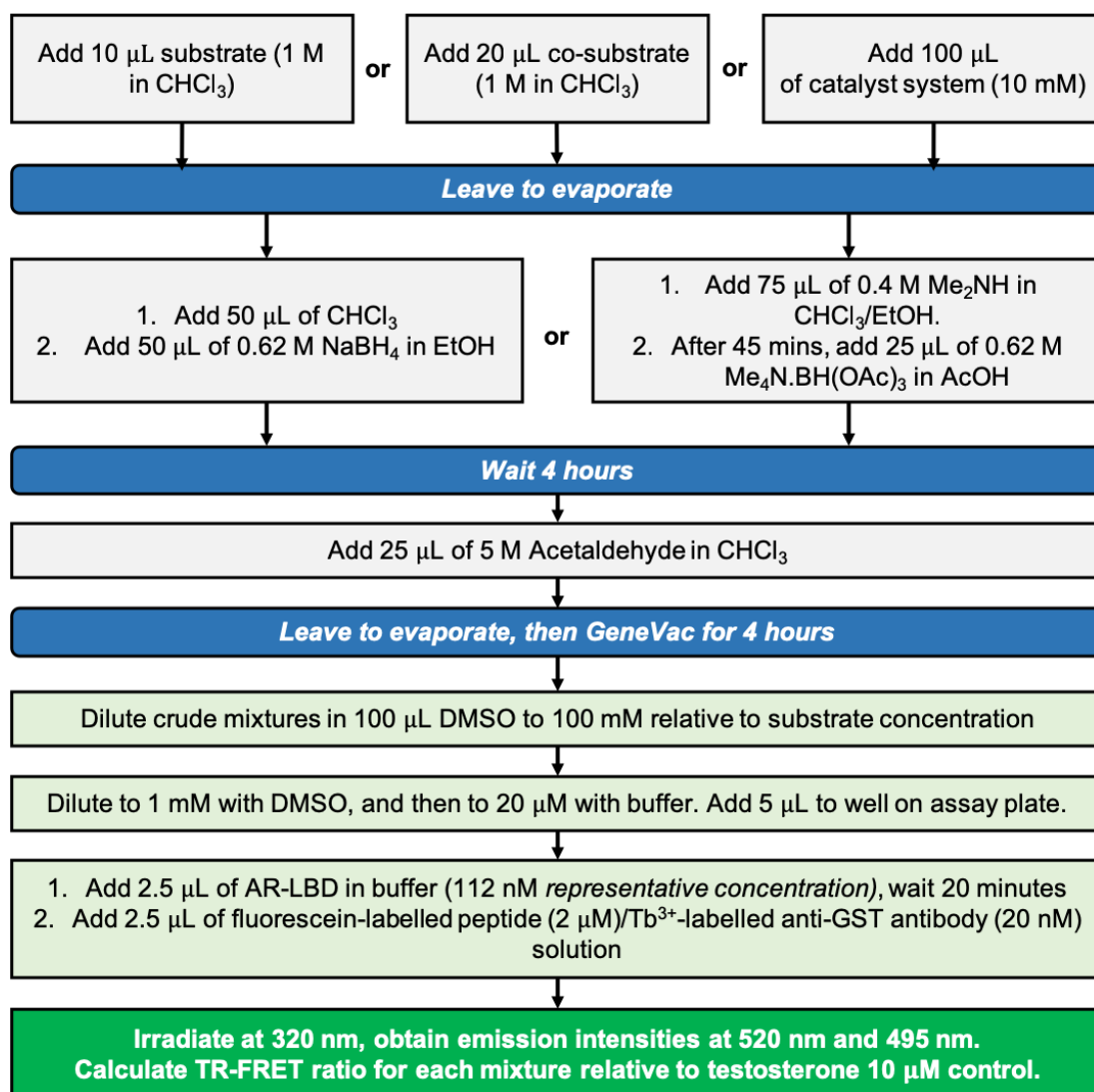
A survey of the previously compiled reaction library found that most of the organocatalytic reactions in the literature tended to proceed at their highest reported efficiency at reaction concentrations ranging from 50 mM to 300 mM relative to the limiting substrate. The reaction concentration was therefore set to 100 mM with respect to the limiting reagent, the armed substrate. The final co-substrate concentration in the reactions was set to 200 mM, and the catalyst loading 10 mol% (10 mM). The order of these components was also of importance – by adding the smaller volumes of the substrate components and allowing the evaporation of the 30  $\mu\text{L}$  total volume of the solutions, 100  $\mu\text{L}$  of the catalyst system could then be added and the reaction wells sealed, resulting in minimal solvent loss during the 24 hour reaction time during the execution of the ADS reaction arrays.

An overview of the workflow for the execution of the mock array process is shown in **Figure 3.5**. Each component solution was made as it would be in a reaction array, at the identical concentration to be used, allowing easy identification of components with solubility issues or readout

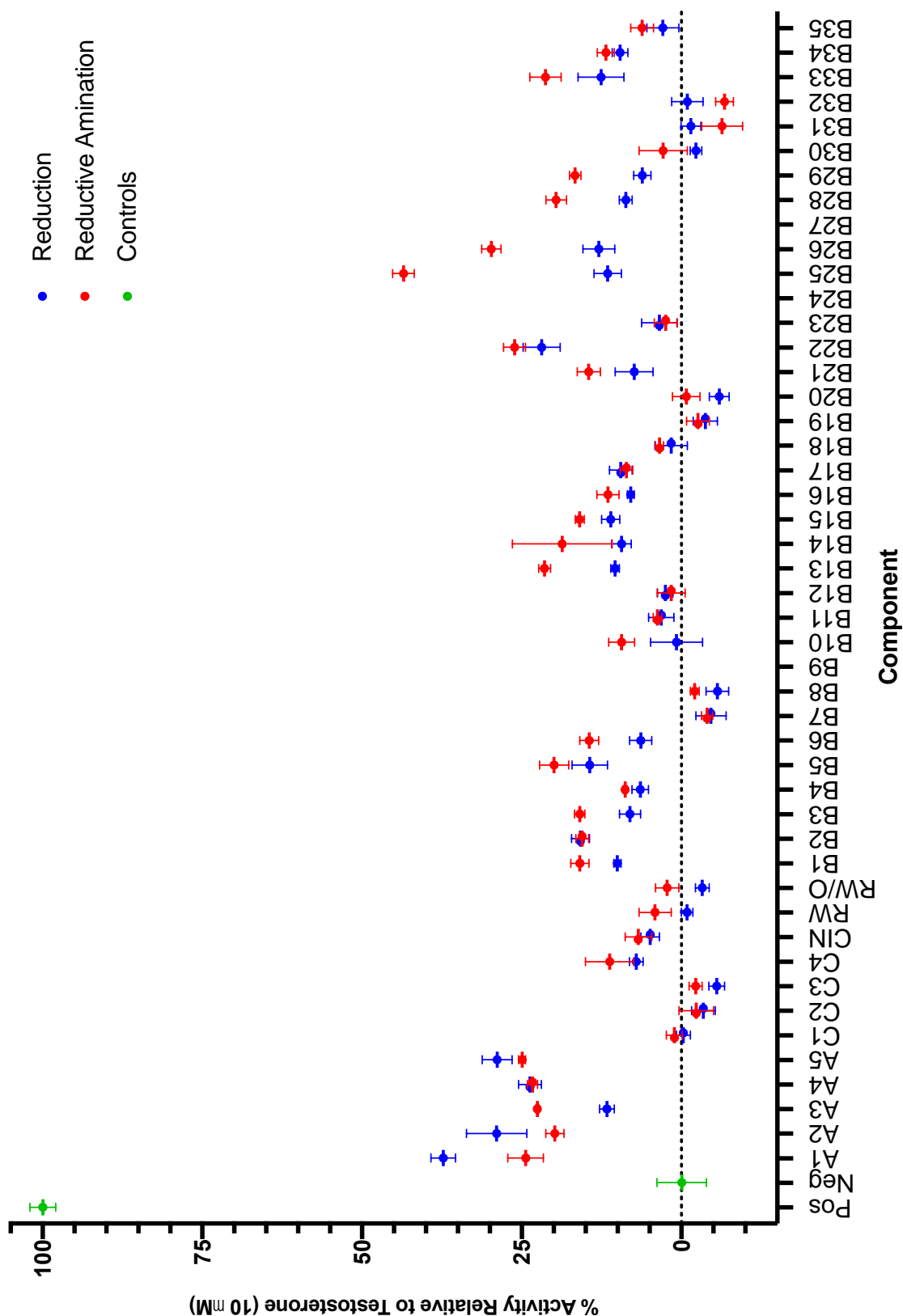
interference. Each component was added to its own well in two separate plates (corresponding to the two different work-up conditions being implemented), then left to allow solvent evaporation, before subjecting the components to the work-up protocols. Additional controls were also carried out, performing the work-ups on empty wells to determine whether the conditions would cause interference. The plates were then evaporated in a GeneVac, and each well then diluted with DMSO to 100 mM concentration relative to Substrate A concentration, and further diluted with DMSO and buffer to 20  $\mu\text{M}$  solutions that were screened using a single-point assay procedure at a final concentration of 10  $\mu\text{M}$  relative to the limiting substrate.

The single point assay procedure screened mixtures in triplicate, adding 5  $\mu\text{L}$  of the buffer solutions to the relevant wells of the assay plate. Once the relevant negative and positive (testosterone at a final concentration of 10  $\mu\text{M}$ ) controls were added, this was followed by addition of 2.5  $\mu\text{L}$  of a solution of AR-LBD, and after 20 mins, 2.5  $\mu\text{L}$  of a Fluorescein-labelled peptide/ $\text{Tb}^{3+}$ -labelled anti-GST antibody complex solution (concentration for both of these solutions specified on the individual assay kit). Incubation for four hours and reading of the plate using a Perkin-Elmer Envision 2103 Multilabel reader allowed TR-FRET ratios to be obtained for each well, and thus bioactivity could be calculated for each single-point well relative to the testosterone positive control. The assay readout for the mock array executed can be seen in **Figure 3.6**.

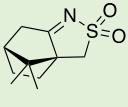
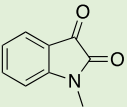
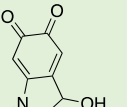
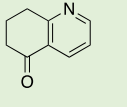
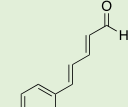
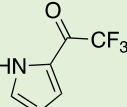
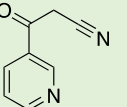
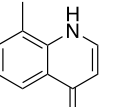
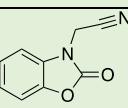
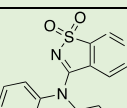
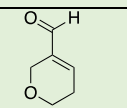
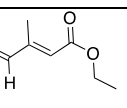
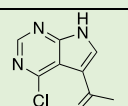
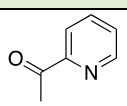
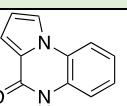
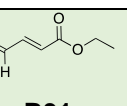
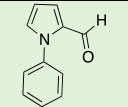
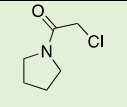
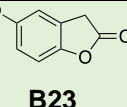
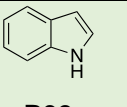
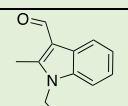
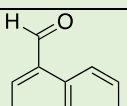
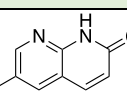
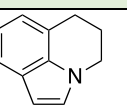
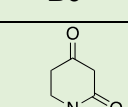
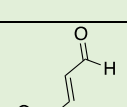
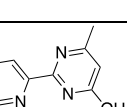
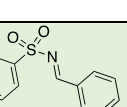
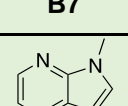
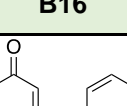
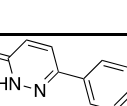
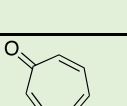
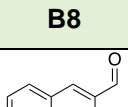
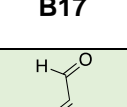
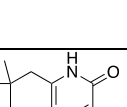
A number of components exhibited poor solubility or indicated interference; resulting in their exclusion from the first round (**Table 3.1**). Of those excluded, a number of them exhibited activity that highlighted assay interference, and a number also had solubility issues. From the remaining compounds, a number were eliminated due to similarity to other components in the set. The green highlighted compounds shown in **Table 3.1** were selected for inclusion in the first round of ADS. The results of the mock array led to the finalised design of round 1 outlined in **Figure 3.7**.



**Figure 3.5** – An overview of the workflow when used during the screening of the mock array. Each individual component solution was added to the same well in two different plates, at the concentration that was to be used in the first round reaction array. Evaporation was allowed, before subjecting to each plate to one of the two specified work-up conditions. Following quenching with acetaldehyde, the solutions were evaporated, before dissolving into DMSO, and then buffer to allow assay of the processed component.



**Figure 3.6** – Assay readout for the control screen of components. This enabled the removal of co-substrates that could potentially interfere with results (highlighted in red). An empty column indicates the component was insufficiently soluble in chloroform. CIN = cinnamaldehyde. RW = work-up with cinnamaldehyde. RW/O = work-up without cinnamaldehyde.

Molecule	%	Molecule	%	Molecule	%	Molecule	%
 <b>B1</b>	14 20	 <b>B10</b>	5 13	 <b>B19</b>	1 2	 <b>B28</b>	13 23
 <b>B2</b>	20 19	 <b>B11</b>	7 8	 <b>B20</b>	-1 4	 <b>B29</b>	10 20
 <b>B3</b>	12 20	 <b>B12</b>	7 6	 <b>B21</b>	11 18	 <b>B30</b>	2 7
 <b>B4</b>	10 13	 <b>B13</b>	14 25	 <b>B22</b>	25 29	 <b>B31</b>	3 -2
 <b>B5</b>	18 23	 <b>B14</b>	13 22	 <b>B23</b>	8 7	 <b>B32</b>	3 -2
 <b>B6</b>	2 19	 <b>B15</b>	15 20	 <b>B24</b>	x	 <b>B33</b>	16 25
 <b>B7</b>	0 0	 <b>B16</b>	12 15	 <b>B25</b>	15 46	 <b>B34</b>	14 16
 <b>B8</b>	-1 2	 <b>B17</b>	13 13	 <b>B26</b>	17 33	 <b>B35</b>	7 10
 <b>B9</b>	x	 <b>B18</b>	6 8	 <b>B27</b>	x		

**Table 3.1** – Activity data for co-substrates screened in the mock array. Top = sodium borohydride reduction, bottom = reductive amination. x = insoluble and not tested. Components used highlighted in green.

Substrate						
	<b>A1</b>	<b>A2</b>	<b>A3</b>	<b>A4</b>	<b>A5</b>	
Co-substrate						
	<b>B1</b>	<b>B2</b>	<b>B3</b>	<b>B4</b>	<b>B5</b>	<b>B6</b>
	<b>B7</b>	<b>B8</b>	<b>B10</b>	<b>B11</b>	<b>B12</b>	<b>B14</b>
	<b>B15</b>	<b>B16</b>	<b>B18</b>	<b>B19</b>	<b>B20</b>	<b>B21</b>
	<b>B23</b>	<b>B28</b>	<b>B31</b>	<b>B32</b>	<b>B34</b>	<b>B35</b>
	Catalyst	 10 mol% 1 eqv. NEt <sub>3</sub> CHCl <sub>3</sub>	 10 mol% CHCl <sub>3</sub>	 10 mol% 20% DBU THF	 10 mol% 20% DBU THF	
		<b>C1</b>	<b>C2</b>	<b>C3</b>	<b>C4</b>	
W.U		<b>NaBH<sub>4</sub> Reduction</b>		<b>Me<sub>2</sub>NH Reductive Amination</b>		

**Figure 3.7** – Components used in the Round 1 exhaustive array. Every combination of Substrate A, Substrate B, Catalyst and Work-Up was executed to generate a total of 960 reaction mixtures.



### 3.2.5 Execution of Exhaustive Reaction Array

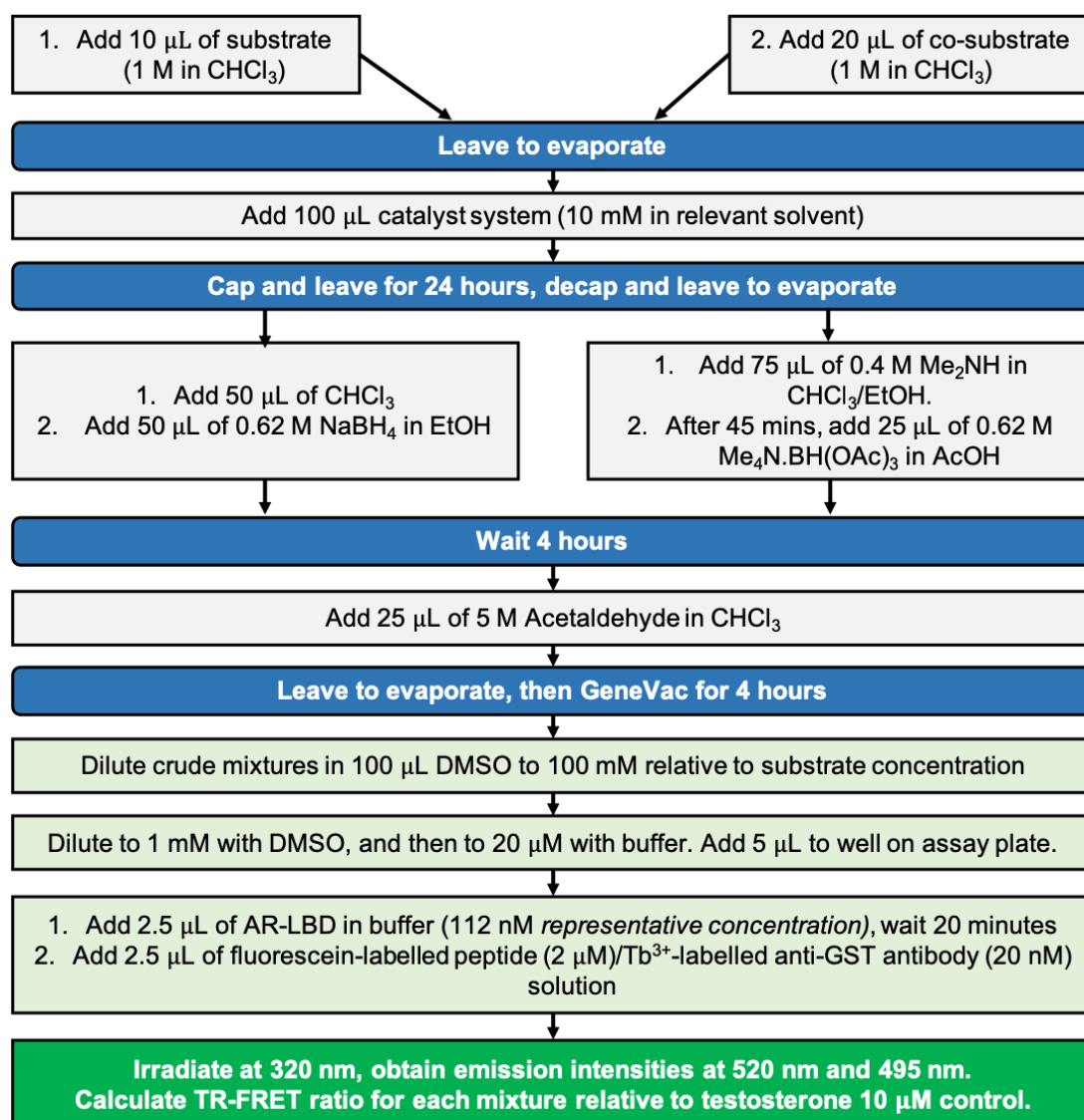


**Figure 3.8** - Overview of the workflow used during the assembly and screening of the exhaustive arrays. Substrate A and B solutions were added to the relevant well on the assay plate, before allowing evaporation. The catalyst/additive/solvent solution was then added, before capping the wells for 24 hours of reaction time. Evaporation was allowed, before subjecting to each plate to one of the two specified work-up conditions. Following quenching with acetaldehyde, the solutions were evaporated, before dissolving into DMSO, and then buffer to allow assay of the crude reaction mixtures.

The round 1 reaction array was carried out as described in the protocol in **Figure 3.8**. Armed substrate component solutions were added to the relevant reaction well, followed by the co-substrate component solution. The solvent was then allowed to evaporate in each well, before adding the catalyst system solution. The wells were then capped, and 24 hours of reaction time allowed (**Figure 3.9**). After uncapping and allowing solvent evaporation, before subjecting the components to the work-up protocols, quenching with an acetaldehyde solution. The plates were then allowed to evaporate naturally, then evaporated to dryness in a GeneVac, and each well diluted with DMSO to 100 mM concentration relative to the substrate concentration. Wells were then diluted further initially with DMSO, and then with pH 7.5 buffer, to 20  $\mu$ M solutions relative to the limiting substrate. These solutions were added to the assay plate and screened at a concentration of 10  $\mu$ M relative to the substrate concentration, using the single-point assay procedure described in **Section 6.6.3**, with a final concentration of 1% DMSO in each well. The TR-FRET ratio of emissions at 520 nm and 495 nm were measured for each well, allowing an indication as to the level of agonism for each mixture in relation to the testosterone positive control.

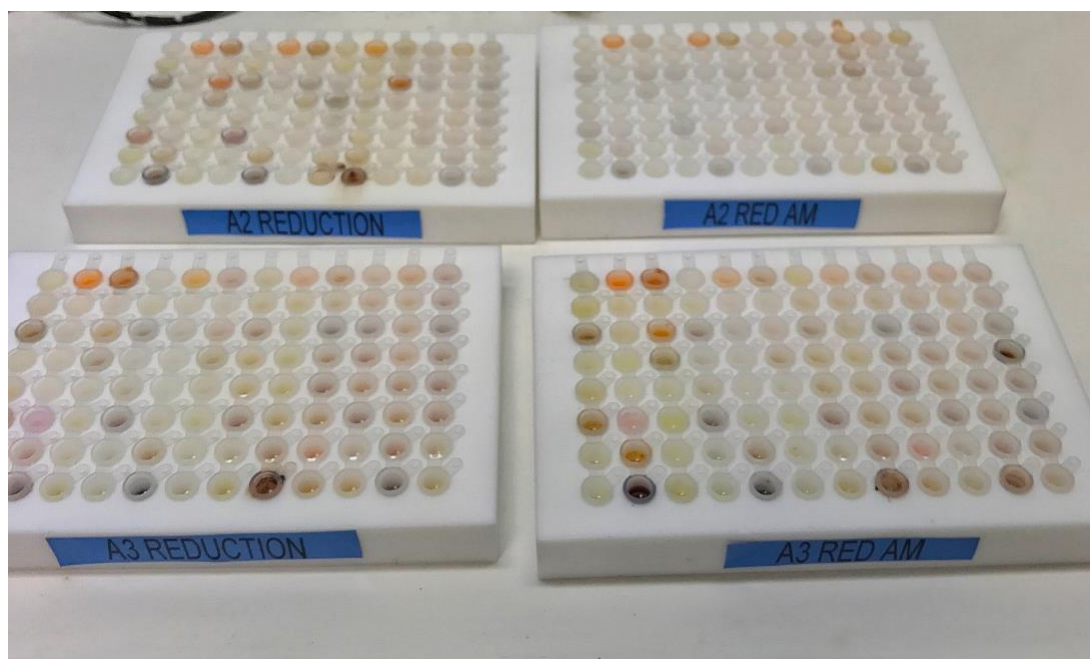
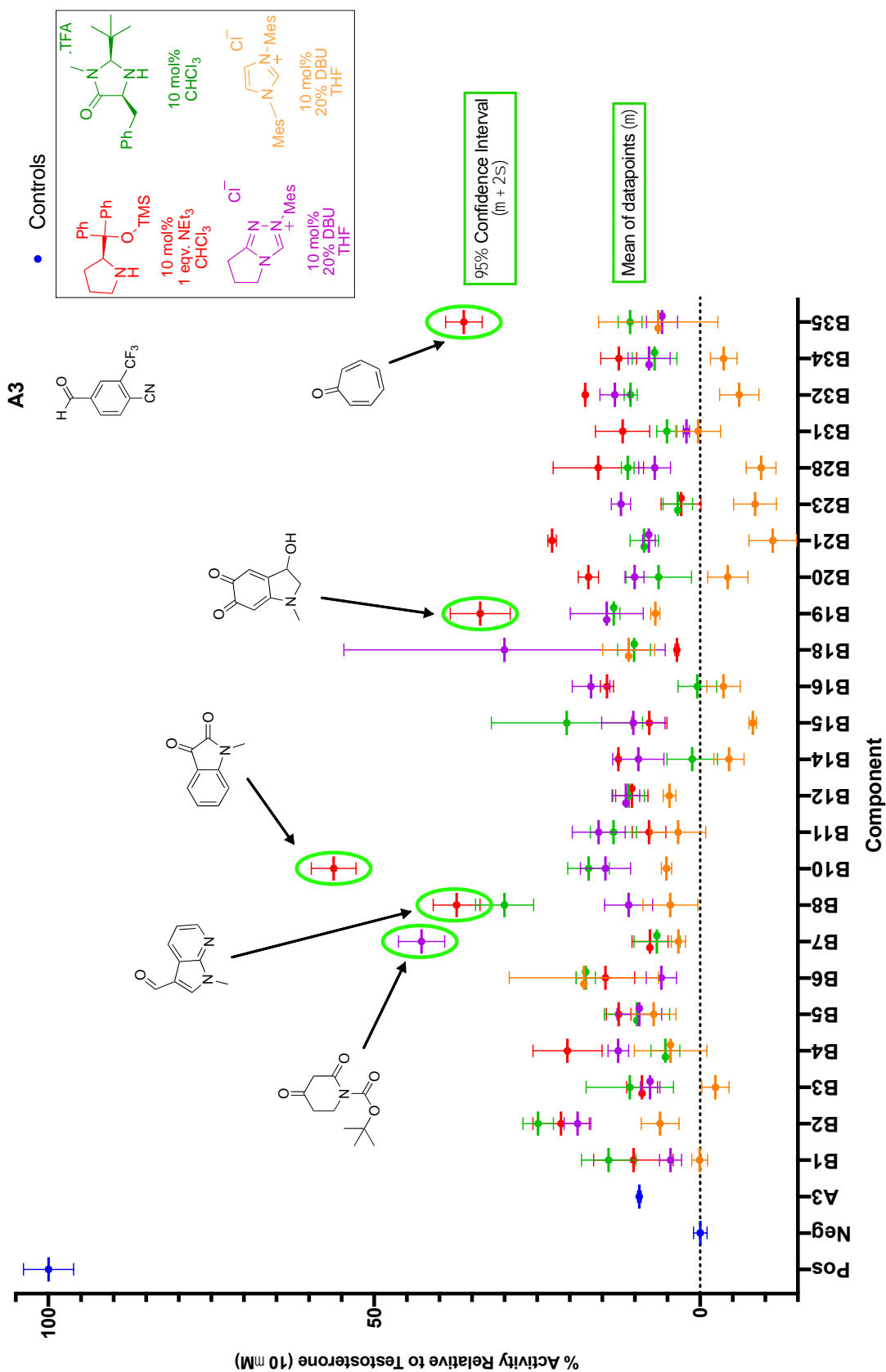


**Figure 3.9** – Experimental setup for the Round 1 reaction arrays. 96-well PTFE blocks were sealed with plastic caps.

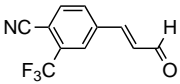
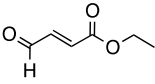
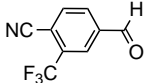
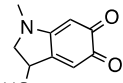
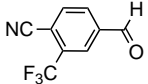
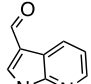
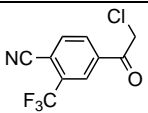
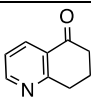
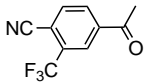
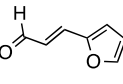
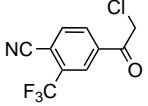
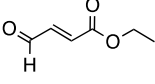
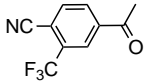
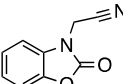
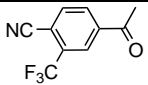
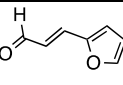
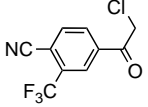
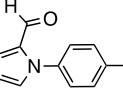
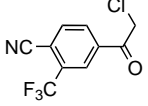
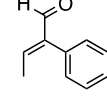
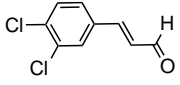
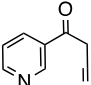
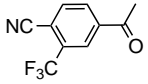
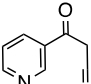
Product mixtures with bioactivity at least two standard deviations ( $2\sigma$ ) from the mean of the bioactivities of all product mixtures on a plate were considered as significant hits, corresponding to a 95% confidence interval ( $p=0.05$ ). An example of this criteria being applied per assay can be seen in **Figure 3.10**, wherein the data for the plate utilising armed substrate **A3** that was subjected to the reduction work-up protocol can be observed. From the ten 96-well plates that were initially screened, 47 of the 960 product mixtures showed activity that was statistically significant using our criteria, with respect to each plate. The assay readout for every plate from Round 1 can be observed in **Section 6.8** of the experimental.

As there were many crude mixtures to consider from this initial screen, hit validation was carried out on the 47 reactions that had exceeded the statistical criteria for each plate. The original reactions were repeated identically as they had been in the first round, including work-ups, and screened again at the same relative product concentration in order to validate the originally observed activity. This also helped to triage the initial results to a smaller set of productive combinations that could be used to design a second reaction array. 12 of the 47 mixtures retained comparable levels of activity observed in the original screen. The composition of the 12 mixtures are summarised in **Table 3.2**, and the assay data for the Round 1 Validation array observed in **Section 6.8.1**.

**Table 3.2** demonstrated that some of the combinations observed may have been related as they featured similar co-substrates. The majority of validated points utilised the reduction work-up, although two utilised the reductive amination procedure. All four of the catalysts were involved, suggesting diversity in the reactivity of the productive combinations, and potentially diversity in products being formed.



**Figure 3.10** – Illustrative assay readout data for the reaction array involving A3 treated with sodium borohydride. Statistical criteria used to filter hits is indicated.

Mixture	Substrate	Co-Substrate	Catalyst	Work-Up	%Activity
A1B31C1R			J-H C1	NaBH <sub>4</sub> Reduction	29
A3B19C1R			J-H C1	NaBH <sub>4</sub> Reduction	28
A3B8C2R			Macmillan C2	NaBH <sub>4</sub> Reduction	40
A5B28C2R			Macmillan C2	NaBH <sub>4</sub> Reduction	23
A4B16C3R			Triazolium C3	NaBH <sub>4</sub> Reduction	33
A5B31C3R			Triazolium C3	NaBH <sub>4</sub> Reduction	27
A4B3C3R			Triazolium C3	NaBH <sub>4</sub> Reduction	27
A4B16C4R			iMes C4	NaBH <sub>4</sub> Reduction	32
A5B5C4R			iMes C4	NaBH <sub>4</sub> Reduction	21
A5B15C4R			iMes C4	NaBH <sub>4</sub> Reduction	26
A2B20C1RA			J-H C1	Me <sub>2</sub> NH RA	70
A4B20C3RA			iMes C4	Me <sub>2</sub> NH RA	49

**Table 3.2** - Combinations from the validation array that displayed agonism of the AR at 10  $\mu$ M relative to the limiting substrate. % activity is the bioactivity of the combination in relation to testosterone (10  $\mu$ M).

### 3.3 Design and Execution of a Targeted ADS Reaction Array

#### 3.3.1 Design of Targeted Reaction Array

As the aim of using the organocatalytic chemistry was to ultimately generate new scaffolds, limiting the variance from the literature with respect to the components used was likely to yield more reactions that formed intermolecular products. By electing to only use reactively compatible substrates pairings that had been shown to generate new scaffolds in previous literature, designing arrays of targeted reactions that were likely to proceed to form products in each well presented itself as an attractive approach.

In previous work using metal-carbenoid chemistry, a diazo substrate could be activated via the catalyst to generate a species that is likely to react with many different substrates (**Figure 3.11a**). The chemistry used generates products cleanly and requires no work-up procedure that adds additional complexity to the mixture. Due to this, an exhaustive approach works well, producing diverse arrays of complex but clean mixtures of potential bioactive products from a relatively small palette of substrates.

In contrast, organocatalysis may require very specific combinations of substrates and catalyst to convert to new scaffolds, and the design of the array therefore has to be adjusted accordingly (**Figure 3.11b**). Specific combinations of substrate, co-substrate and catalyst classes were used, based on literature precedent, with the vision that this would enable generation of new scaffolds and therefore products. For example, an NHC catalyst only has precedent to activate aldehyde species, and iminium activation will only occur with an  $\alpha,\beta$ -unsaturated aldehyde. When compared to the exhaustive approach described in **Section 3.2**, the new proposed 'targeted' strategy offered increased probability of intermolecular product generation, but removed a large degree of the serendipitous discovery that had initially been expected from the exhaustively designed reaction arrays.

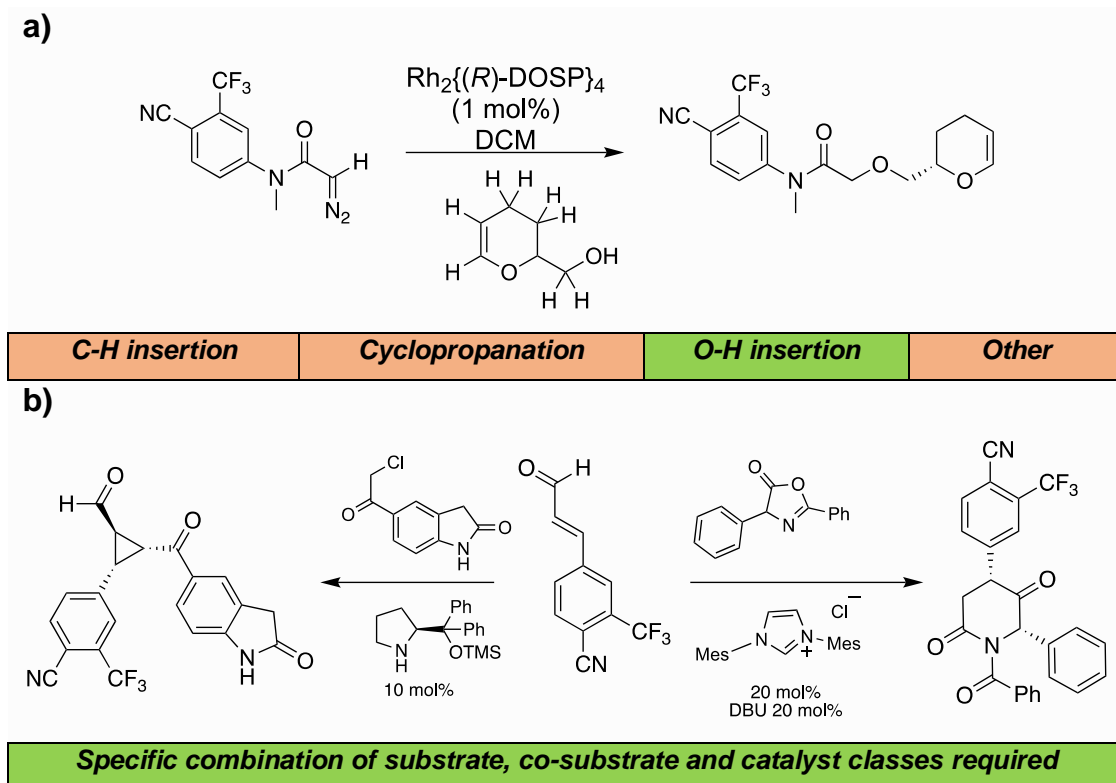


**Figure 3.11** – Comparison of the diazo chemical toolbox to the organocatalytic chemical toolbox. The diazo toolkit (a) was used to elaborate a fragment by pairing with a catalyst and co-substrate, with pairings where a reaction was very likely and probable to proceed to products *via* one of multiple possible outcomes, regardless of the combination. On the other hand, the organocatalytic toolkit (b) may require very specific pairings of components in order to generate intermolecular products.

With the aim of forming diverse new scaffolds using precedented chemistry in mind, an initial first array of 192 diverse reactions was devised, utilising 30 different scaffold forming reactions. In a similar format to that of the exhaustively designed array, armed  $\alpha,\beta$ -unsaturated aldehyde substrates featuring the 4-cyano-3-trifluoromethylphenyl (**A1**) and 3,4-dichlorophenyl (**A2**) motifs provided the basis for each reaction. Pairing of the enals to both a compatible co-substrate class and organocatalytic system that had literature precedent would increase the probability of reactions proceeding to form products when compared to reactions in the exhaustively designed reaction array.

Substrate							
	A1			A2			
Co-substrate							
	<b>TB2</b>	<b>TB3</b>	<b>TB4</b>	<b>TB18</b>	<b>TB19</b>	<b>TB20</b>	
	<b>TB5</b>	<b>TB6</b>	<b>TB7</b>	<b>TB21</b>	<b>TB22</b>	<b>TB23</b>	
	<b>TB8</b>	<b>TB9</b>	<b>TB10</b>	<b>TB24</b>	<b>TB25</b>	<b>TB26</b>	
	<b>TB11</b>	<b>TB12</b>	<b>TB13</b>	<b>TB27</b>	<b>TB28</b>	<b>TB29</b>	
	<b>TB14</b>	<b>TB15</b>	<b>TB16</b>	<b>TB30</b>	<b>TB31</b>	<b>TB32</b>	
	Catalyst						
		<b>C1</b>			<b>C3</b>		<b>C4</b>
	W.U	NaBH <sub>4</sub> Reduction			Me <sub>2</sub> NH Reductive Amination		

**Figure 3.12** – Overview of the design of the targeted array. Specific sets of co-substrates were matched to each catalyst class. **TB2 –16** were selected to pair with amine catalyst **C1**, **TB18-32** were selected to pair with NHC catalysts **C3 + C4**.



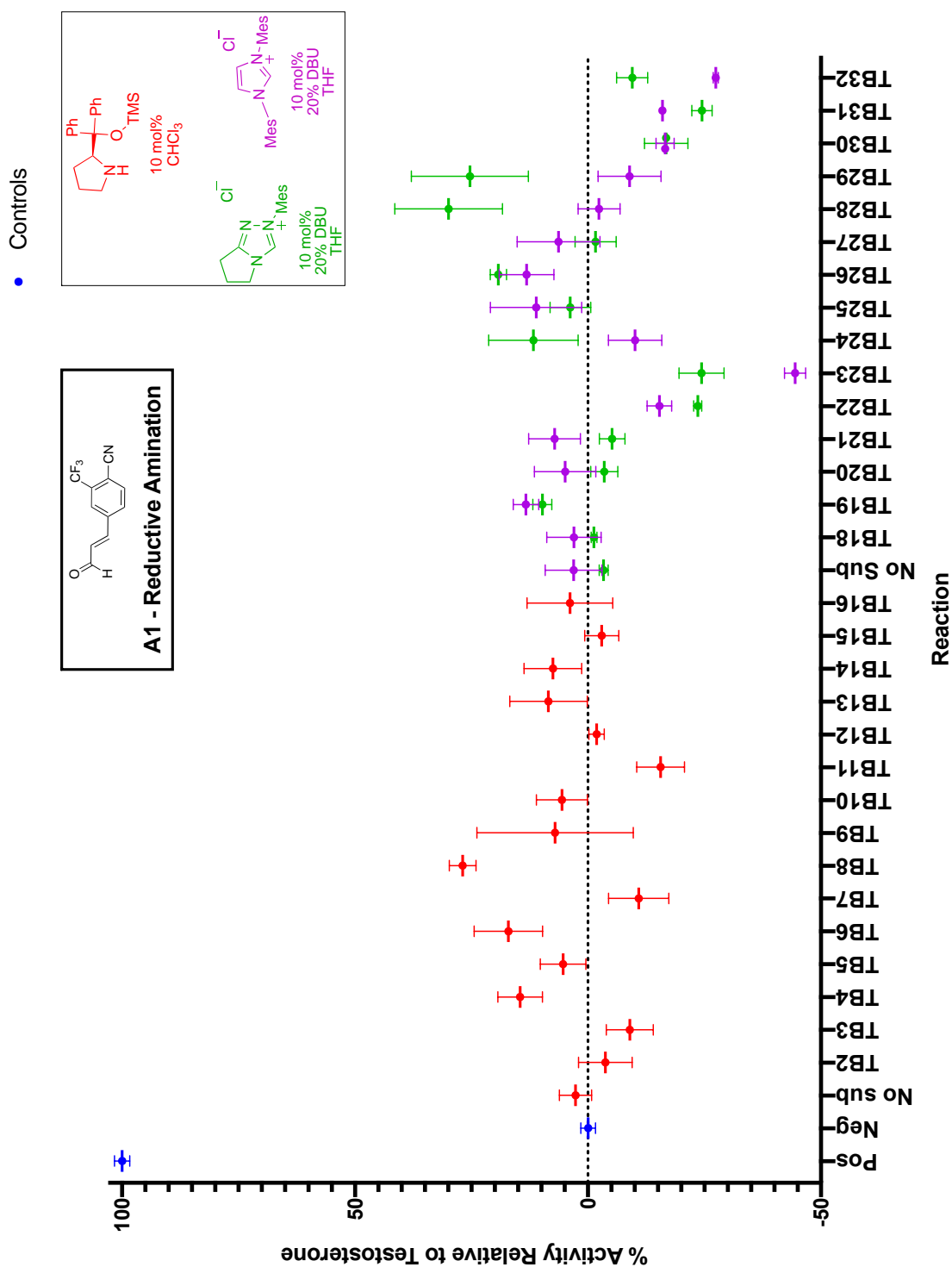
It was elected to select two subsets of co-substrates: 15 that were compatible with the amine organocatalyst class, and 15 that were compatible with the NHC organocatalyst class. In both cases, these sets were selected using the cheminformatics workflow previously described in **Figure 3.5**. The co-substrates were commercially available, filtered for appropriate molecular properties, and contained functionality that had direct literature precedent to react with an  $\alpha,\beta$ -unsaturated aldehyde and either an amine or an NHC organocatalyst.

Each of these 48 reactions were to be conducted in duplicate, with each of the duplicates being subjected to either the sodium borohydride work-up procedure, or the reductive amination work-up procedure with dimethylamine. Taking into account the two armed substrates, this resulted in 196 reactions in total. All reactions were to be quenched with acetaldehyde, before screening at 10  $\mu$ M concentration in a single-point assay for agonism of the AR. The design of the targeted array is summarised in **Figure 3.12**.

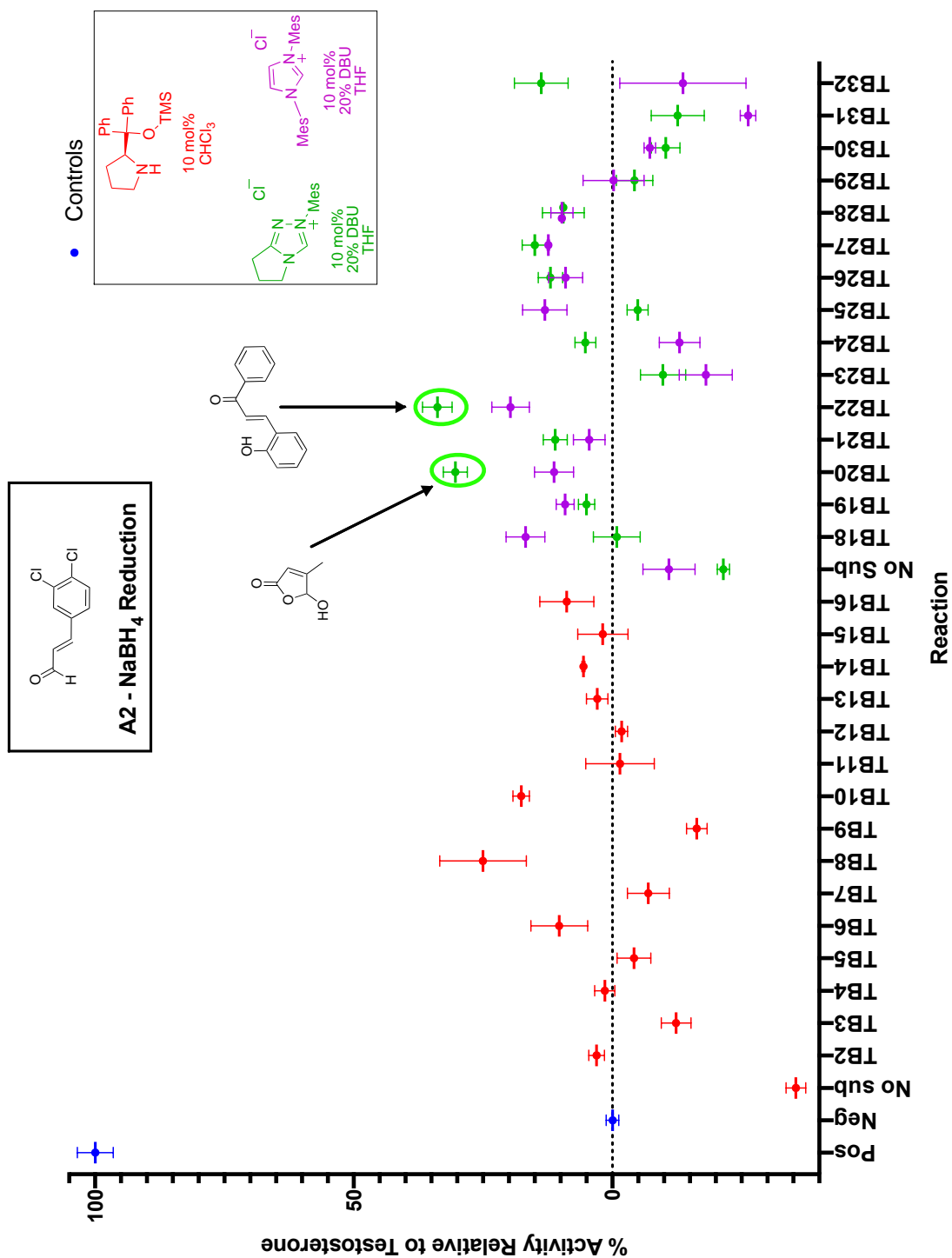
### ***3.3.2 Execution of Targeted Reaction Array***

In a similar fashion to the exhaustive array, reaction arrays began with the addition of 10  $\mu$ L of the armed substrate 1 M solution, followed by 20  $\mu$ L of the 1 M co-substrate solution to each well. The wells were allowed to evaporate, then 100  $\mu$ L of the appropriate 100 mM catalyst/solvent solution was added to the wells before capping each vial and leaving the reactions for 24 hours. The wells were then uncapped to allow evaporation to dry crude mixtures, before employing the appropriate work-up conditions. The wells were then quenched with a 5 M acetaldehyde solution, and the plates allowed to evaporate naturally, before evaporating to dryness in a GeneVac. Each well was then diluted with DMSO to 100 mM concentration relative to Substrate A concentration, and further diluted with DMSO and buffer to 20  $\mu$ M solutions (2x) that were screened using the single-point assay procedure at 10  $\mu$ M described in **Section 6.6.3**.

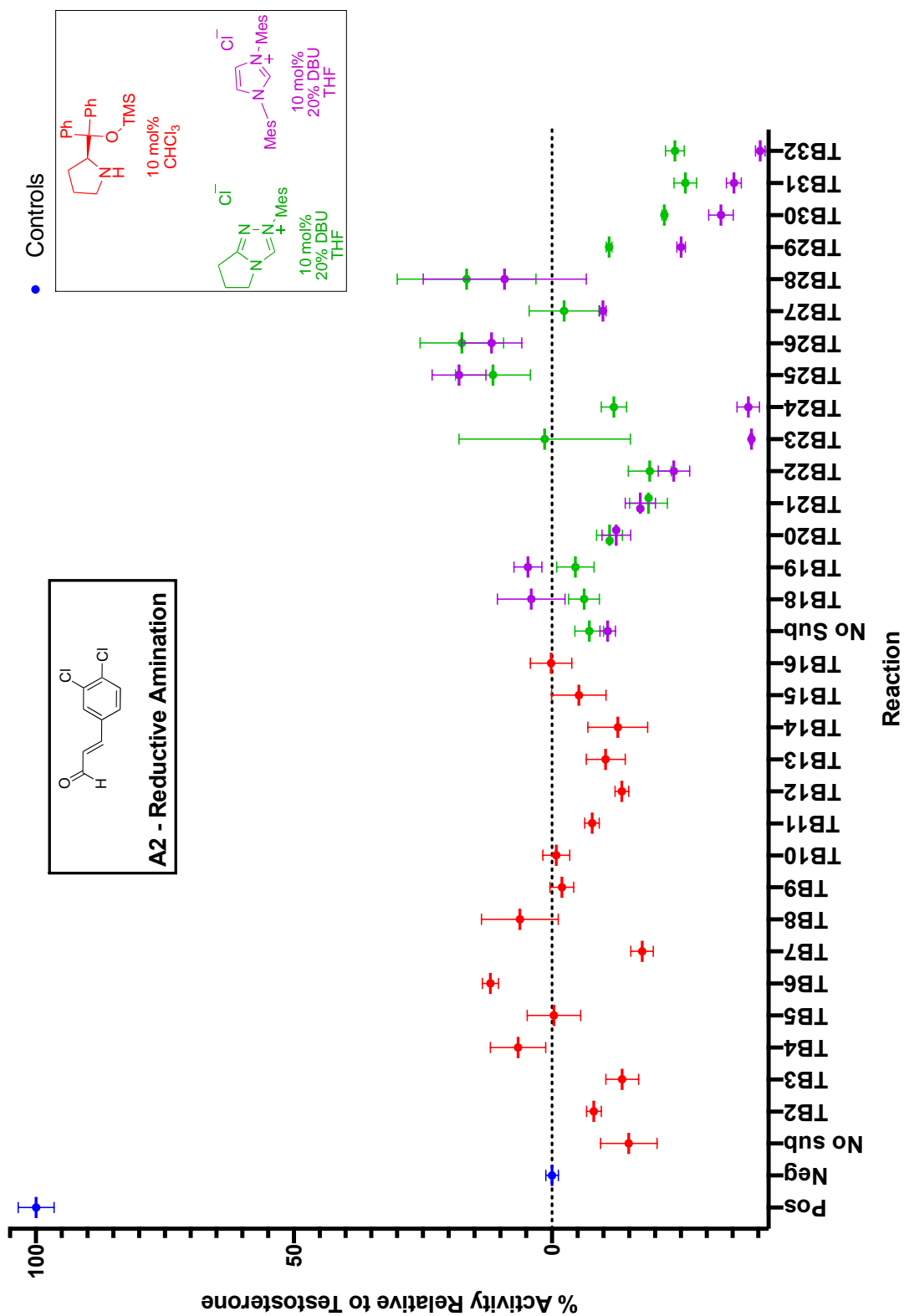




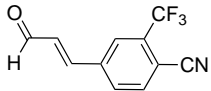
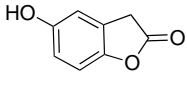
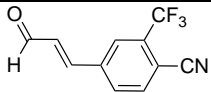
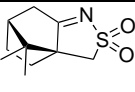
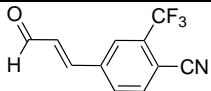
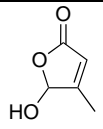
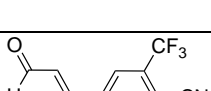
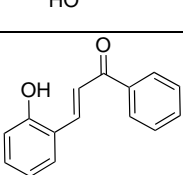
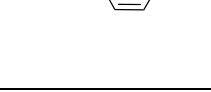
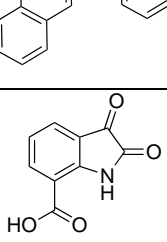
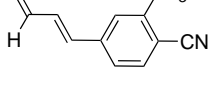
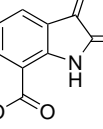
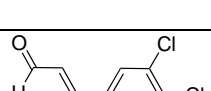
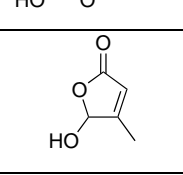
**Figure 3.14** – Assay readout for the targeted array of reactions featuring the armed substrate **A1**, that was subjected to the reductive amination work-up protocol.



**Figure 3.15** - Assay readout for the targeted array of reactions featuring the armed substrate **A2**, that was subjected to the reduction work-up protocol.



**Figure 3.16** - Assay readout for the targeted array of reactions featuring the armed substrate **A2**, that was subjected to the reductive amination work-up protocol.

Mixture	Substrate	Co-Substrate	Catalyst	Work-Up	%Activity
A1TB6C1R			J-H C1	NaBH <sub>4</sub> Reduction	31
A1TB8C1R			J-H C1	NaBH <sub>4</sub> Reduction	33
A1TB20C3R			Triazolium NHC C3	NaBH <sub>4</sub> Reduction	33
A1TB22C3R			Triazolium NHC C3	NaBH <sub>4</sub> Reduction	41
A1TB32C3R			Triazolium NHC C3	NaBH <sub>4</sub> Reduction	34
A2TB20C3R			Triazolium NHC C3	NaBH <sub>4</sub> Reduction	30
A2TB22C3R			Triazolium NHC C3	NaBH <sub>4</sub> Reduction	34

**Table 3.3** – Reaction combinations with bioactivity at least two standard deviations ( $2\sigma$ ) from the mean of the bioactivities of all product mixtures on each of the two plate were considered significant, corresponding to a 95% confidence interval ( $p=0.05$ ).

The assay readout for the targeted arrays can be seen in **Figure Figure 3.13-Figure 3.16**, and **Table 3.3** shows a summary of the reaction mixtures that exhibited bioactivity exceeding the statistical criteria of lying at least two standard deviations ( $2\sigma$ ) from the mean of the bioactivities of all product mixtures on each plate. None of the 192 product mixtures exhibited activity greater than 50% of the activity of testosterone ( $10 \mu\text{M}$ )

### 3.4 Design and Execution of Second Exhaustive ADS Reaction Array

With a selection of productive combinations from two different first round design strategies in hand, the design of a second round of ADS was considered. The most promising product mixtures with respect to activity were identified in the exhaustive project (outlined in **Table 3.2**). For this reason, it was decided that a design approach for elaborating these hits would be developed, allowing further investigation of the chemical space that each combination of components explored.

It was decided that for each combination found in Round 1, only the co-substrate and catalyst would be significantly varied for the combinations in Round 2. The armed substrate and work-up for each combination would be fixed and would not change, however catalyst would be varied within each class i.e. any hits with an amine organocatalyst would utilise both the Jorgensen-Hayashi and Macmillan catalysts, and any NHC catalysts hits would use both the iMes and triazolium catalysts. Each variation around a combination identified to be productive from round one can be thought of as a mini array – exploring the possibilities from the original combination, maintaining a level of commonality with it but utilising an expanded range of co-substrates to attempt to optimise the combination.

Similarly to Round 1, a cheminformatics workflow was used, selecting for reactive functionality similar to the co-substrate in the Round 1 combination, and physiochemical parameters. Using the databases and cheminformatics workflow denoted in **Figure 3.4**, appropriate co-substrates were found for most combinations. However, it was found that interesting variations of the important  $\alpha,\beta$ -unsaturated aldehyde class were not prevalent in commercial chemical catalogues. This class of compound were components in a number of the validated productive combinations from Round 1, so a selection of interesting derivatives that sought to improve the bioactivity of the resulting product were essential for the execution of an efficient second reaction array. To aid practical assembly, the reaction array was designed so that alongside the original combination that gave promising

reactivity, there would be up to 7 new co-substrates based around the productive Round 1 combination, allowing each combination variation to take up one column on the 96-well reaction plate. This would result in up to 14 new variations of each reaction based upon the original Round 1 hit.

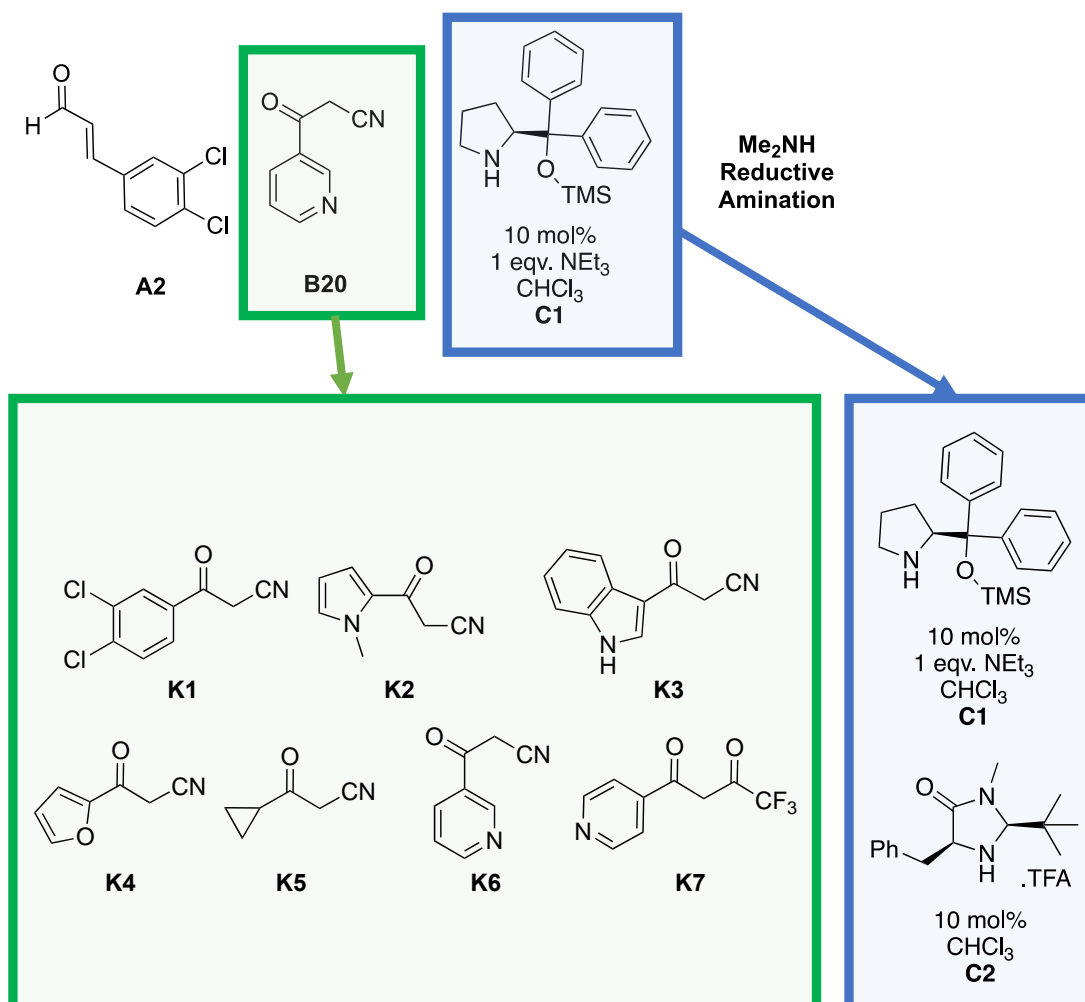


**Figure 3.17** – Schematic showing the logic behind design of Round 2 mixtures. Co-substrate was altered for each combination, as well as using the alternative catalyst in each organocatalyst class.

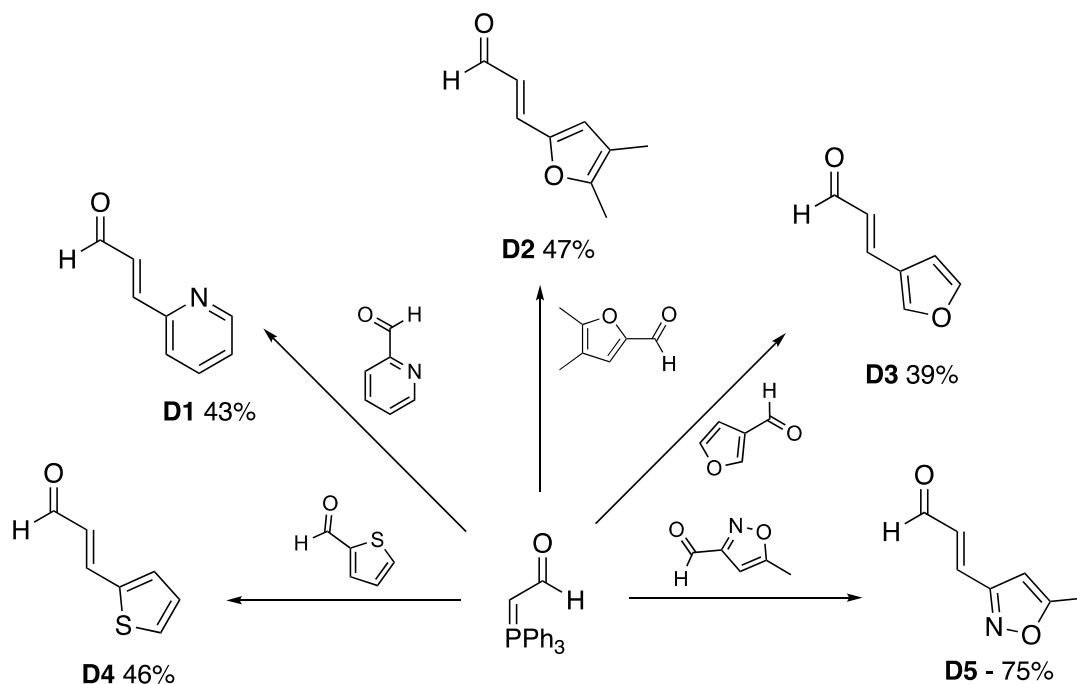
### 3.4.1 Synthesis of Co-Substrates

Synthesis of diverse heterocyclic analogues of  $\alpha,\beta$ -unsaturated aldehydes were carried out, using not only the Wittig method used previously when making **A1** and **A2** for Round 1, but also a Vilsmeier-Haack reaction to make the enals **D6** and **D7** (see **Scheme 3.2**). For the Wittig

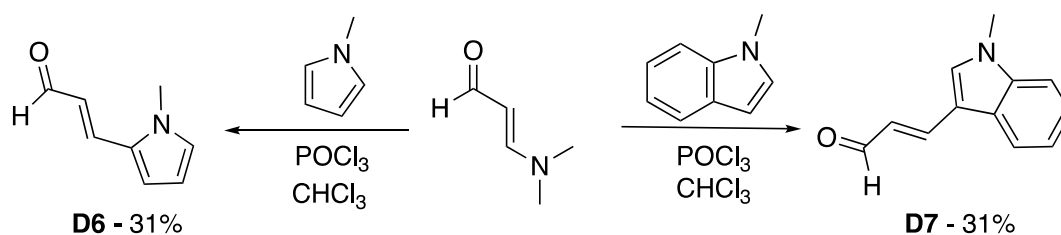


reactions, the respective aromatic aldehyde required was refluxed with either THF or toluene, with a slight excess of (triphenylphosphoranylidene)acetaldehyde for 24 hours. Conversion was observed in all cases, with the  $\alpha,\beta$ -unsaturated aldehydes (**D1-D5**) being synthesised with variable yields.

a)



b)



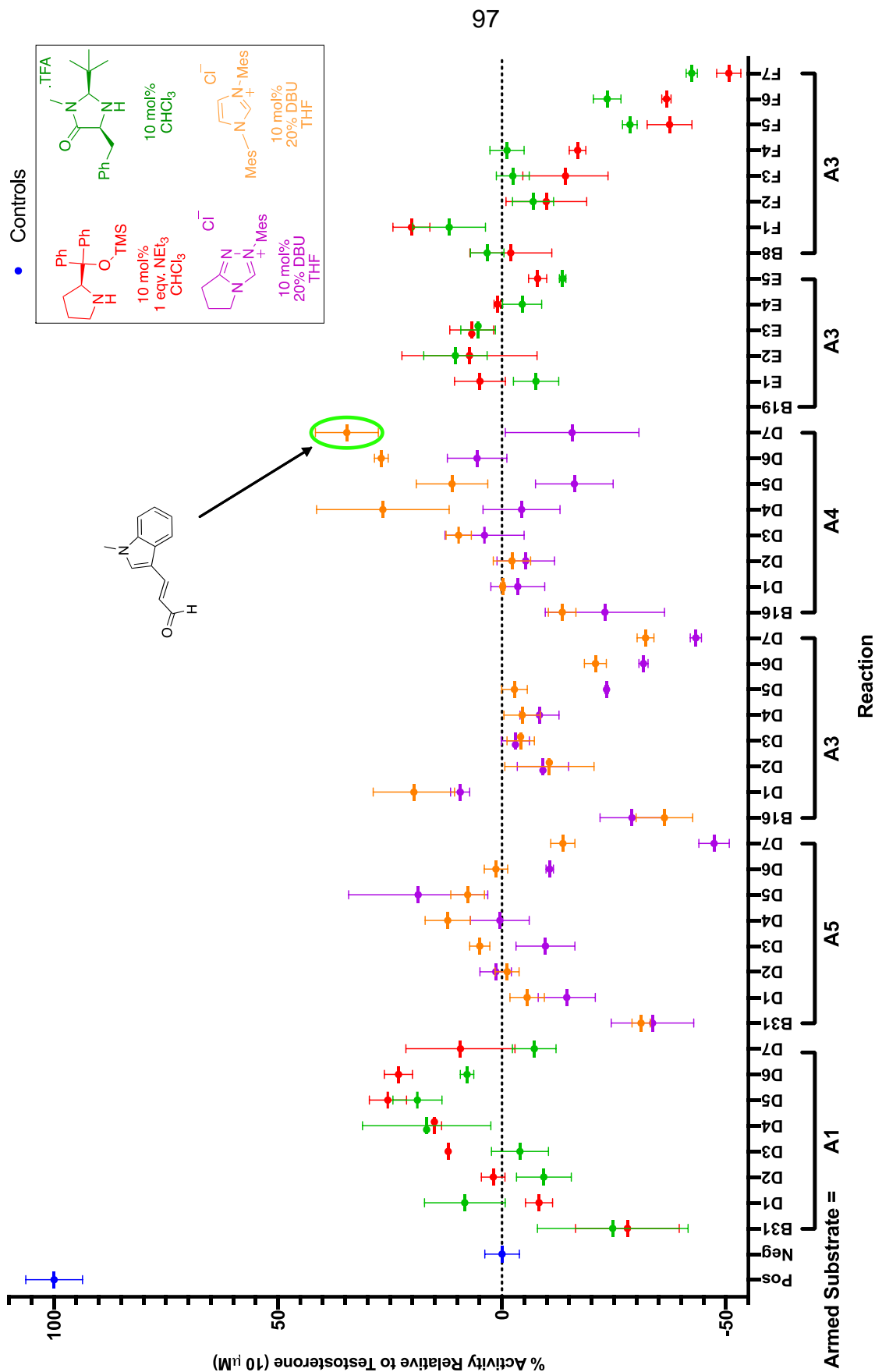
**Scheme 3.2** - Synthesis of a selection of  $\alpha,\beta$ -unsaturated aldehydes for use as co-substrates in Round 2 of ADS. a) The selection of  $\alpha,\beta$ -unsaturated aldehydes synthesised using the Wittig chemistry. All reactions executed in either THF or toluene at reflux. b) The pair of  $\alpha,\beta$ -unsaturated aldehydes synthesised using the Vilsmeier-Haack reaction.

For the Vilsmeier-Haack reaction, 3-dimethylaminoacrolein was added to phosphoryl chloride, resulting in formation of a  $\gamma$ -chlorinated amine intermediate. Addition of a suitable heterocycle enabled electrophilic aromatic substitution, forming the desired  $\alpha,\beta$ -unsaturated aldehyde product following hydrolysis.

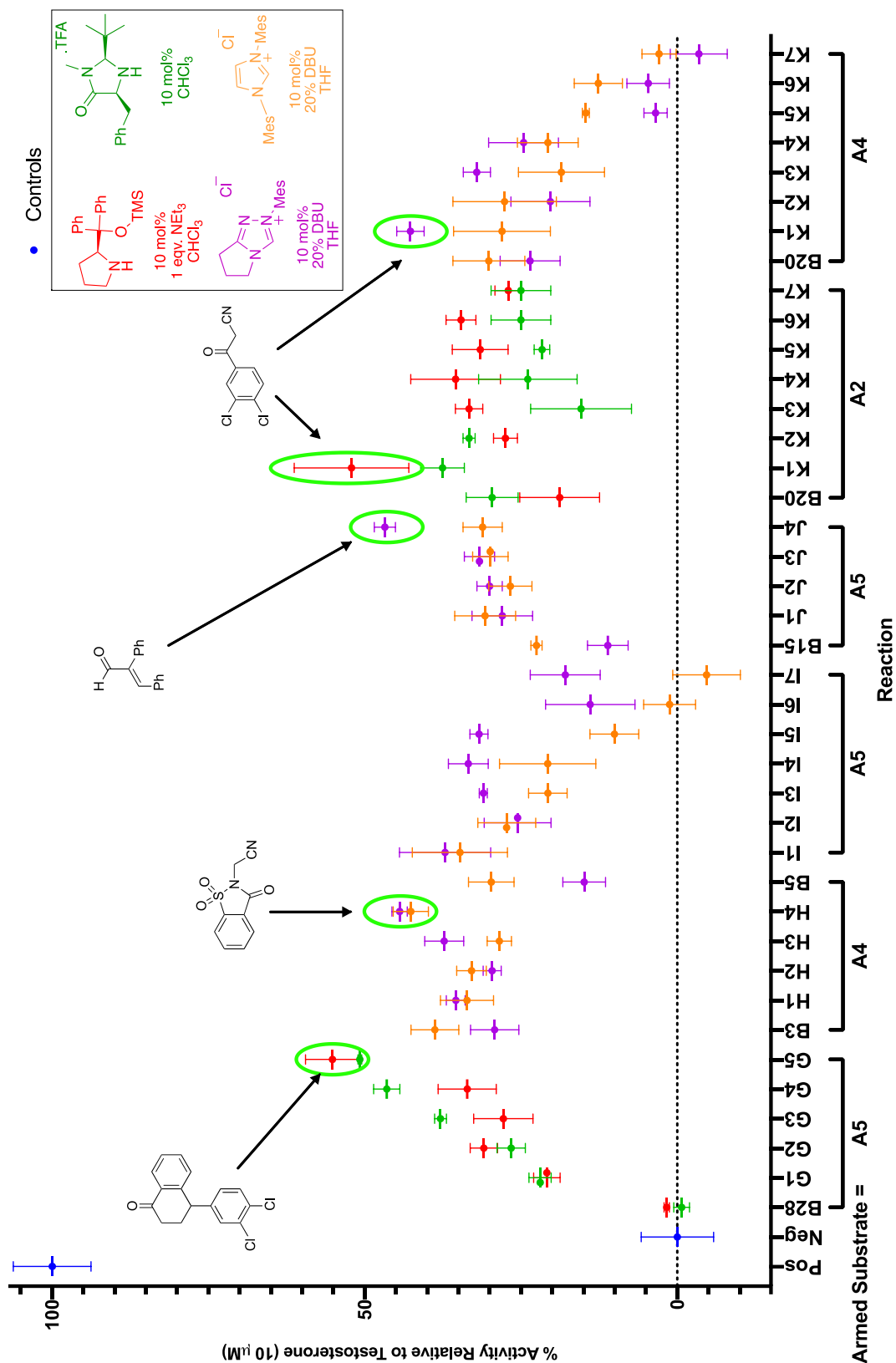
### **3.4.2 Execution of Second Exhaustive ADS Reaction Array**

The final layout of the Round 2 reaction arrays consisted of 170 reactions, using two 96-well reaction plates. Each pair of columns on the plate contained variations of reactions based around the same original productive Round 1 combination, with each column in a pair utilising a different catalyst. A mock array for the Round 2 components was executed, and no significant activity at the 1  $\mu$ M concentration was observed, with the exception of a few co-substrates exhibiting low TR-FRET ratios relative to the testosterone 10  $\mu$ M control. A full schematic for the layout of the Round 2 reaction arrays can be observed in the experimental, in addition to a full specification of the components used across the 170 reactions explored.

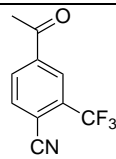
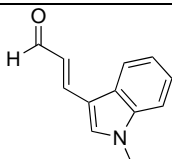
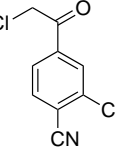
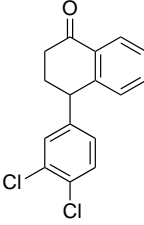
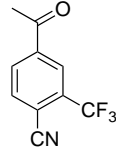
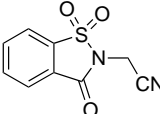
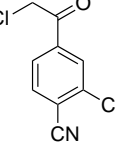
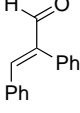
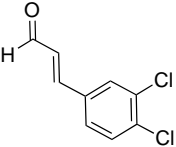
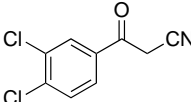
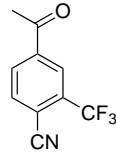
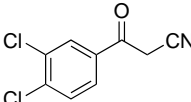
The Round 2 reaction array was conducted identically to the workflow denoted in **Figure 3.8**, except focusing on a more concentrated selection of combinations. The mixtures were initially screened at a concentration of 10  $\mu$ M, but baseline activity for all of the mixtures was too high, resulting in a very large spread of activity. For this reason, the mixtures from Round 2 were screened at 1  $\mu$ M relative to the concentration of the substrate, an order of magnitude lower than in Round 1, ensuring only the most productive bioactive combinations would be identified in Round 2. A number of combinations from Round 2 were prioritised, based on bioactivity shown in the assay. These combinations are highlighted on the assay readout which can be observed in the **Figure 3.18** and **Figure 3.19**, and summarised in **Table 3.4**.



**Figure 3.18** – Assay readout for Plate 1 of the second round of ADS, screened at a concentration of 1  $\mu\text{M}$  relative to the substrate, with activity assessed relative to a 10  $\mu\text{M}$  Testosterone control. All of these combinations utilised the sodium borohydride reduction workup.



**Figure 3.19** - Assay readout for Plate 2 of the second round of ADS, screened at a relative concentration of 1 μM relative to the substrate, with activity assessed relative to a 10 μM Testosterone control. All combinations utilised the sodium borohydride reduction work-up, with the exception of the highlighted combinations that used the reductive amination work-up.

Mixture	Substrate	Co-Substrate	Catalyst	Work-Up	%Activity
A4D7C4			iMes NHC <b>C4</b>	NaBH <sub>4</sub> Reduction	35
A5G5C1			Jorgensen-Hayashi <b>C1</b>	NaBH <sub>4</sub> Reduction	55
A4H4C3			Triazolium NHC <b>C3</b>	NaBH <sub>4</sub> Reduction	44
A5J4C3			Triazolium NHC <b>C3</b>	NaBH <sub>4</sub> Reduction	47
A2K1C1			Jorgensen-Hayashi <b>C1</b>	Me <sub>2</sub> NH Reductive Amination	52
A4K1C3			Triazolium NHC <b>C3</b>	Me <sub>2</sub> NH Reductive Amination	43

**Table 3.4** – A summary of mixtures from Round 2 that appeared to present bioactivity in a single point assay screen for agonism of the AR at 1  $\mu$ M concentration relative to the substrate in the reaction. % activity is the bioactivity of the combination in relation to testosterone (10  $\mu$ M).

### 3.5 Evaluation of Product Mixtures from Organocatalytic ADS

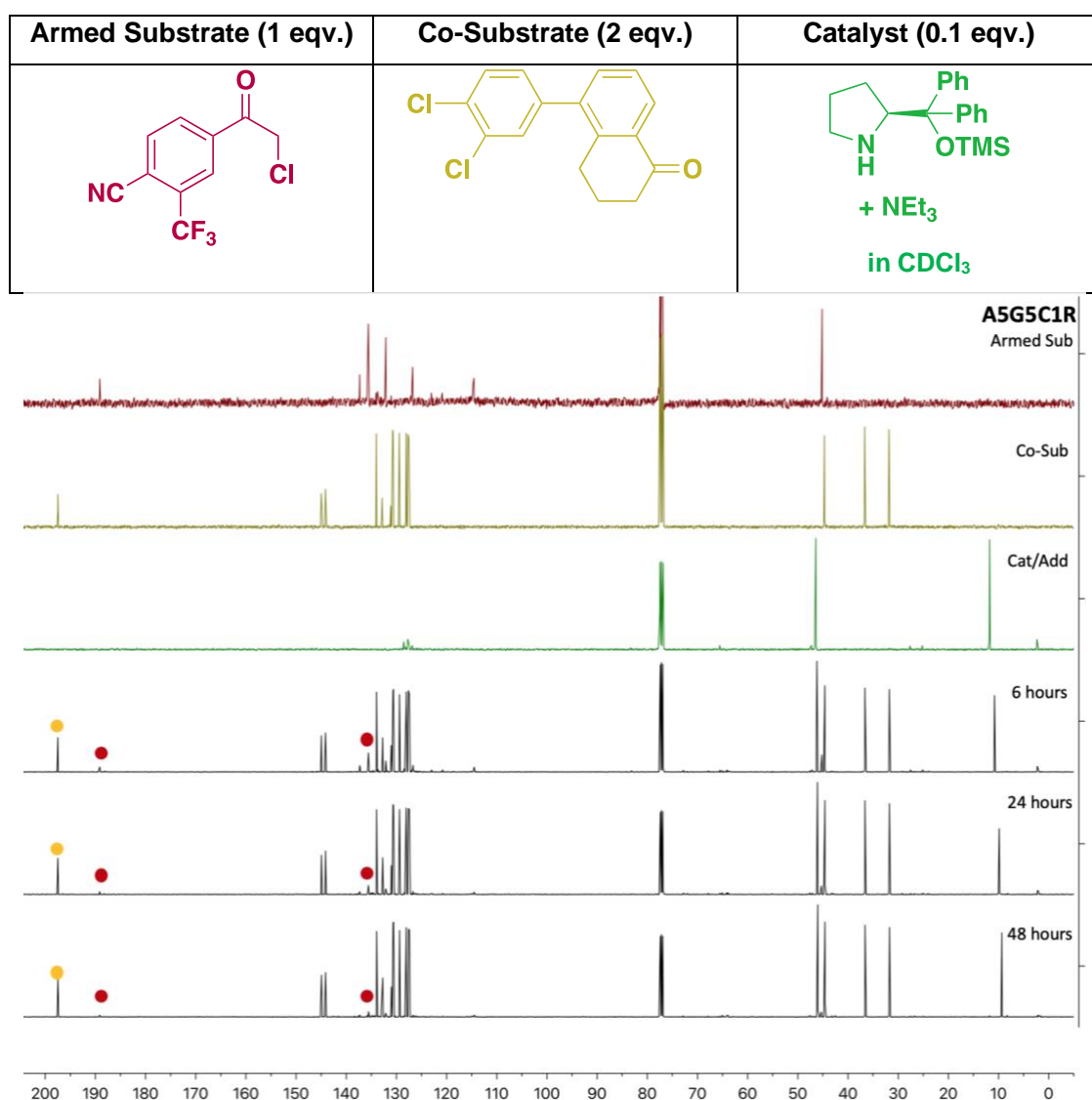
#### 3.5.1 Validation of Conversion and Bioactivity

At this stage, it was decided that more in-depth analysis of a selection of the reactions identified throughout the project was necessary in order to validate the hits discovered, and to gauge whether the chemistry had proceeded as anticipated. It was decided that two different approaches would be used to analyse the outcomes of these reactions: tracking the reactions by NMR and obtaining dose-response curves of the crude mixtures. This would allow confirmation of whether the reactions had generated intermolecular products, and whether the products were bioactive.

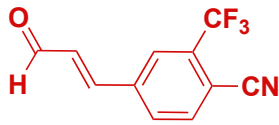
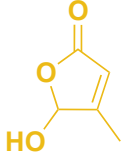
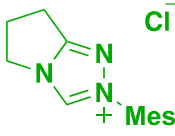
NMR experiments were carried out, tracking the reactions over a period of 48 hours, allowing analysis of the conversion of each reaction. The reactions were assembled as had been previously done in the reaction array, at identical concentrations to the round 2 reaction arrays, albeit scaled up by a factor of 5. Appropriate concentration stock solutions for all components were assembled and screened independently before adding into a mixture. Substrate and co-substrate solutions were added to a reaction vial and allowed to evaporate, before addition of the catalyst/deuterated solvent mixture, and transfer to an NMR tube, using  $^{13}\text{C}$  NMR (125 MHz) spectroscopy to analyse at timepoints of 6, 24 and 48 hours. This allowed a thorough assessment of reaction progress throughout the specified time period. Addition of the work-up at this point was unnecessary, as if the reaction did not produce intermolecular products pre-work up, any products produced afterwards were unlikely to be the result of intermolecular reactions and were likely to be a product of reducing the reaction mixture.

An example of the NMR analysis for the combination **A5G5C1R** (armed substrate **A5**, co-substrate **G5**, catalyst system **C1** and the sodium borohydride reduction protocol – this nomenclature will be used to refer to reactions from ADS arrays hereon) identified in the second round of the

exhaustively designed array can be seen in **Figure 3.20**, and shows that despite apparent consumption of the armed substrate **A5**, no new peaks are formed in the NMR spectra over a 24 hour time period. The consumption of the substrate **A5** may have been caused by it undergoing reaction with the amine catalyst **C1** to form a species that was insoluble in the NMR solvent, precipitating out and therefore not being observed in the NMR spectra. This led to the belief that the bioactivity identified in the reaction **A5G5C1R** stemmed from sodium borohydride reduction of the substrate, rather than an intermolecular reaction.



**Figure 3.20** – Analysis of the **A5G5C1R** combination *via* 500 MHz  $^{13}\text{C}$ -NMR demonstrated no formation of new intermolecular products. Despite conversion of the **substrate**, the **co-substrate** remains.

Armed Substrate (1 eqv.)	Co-Substrate (2 eqv.)	Catalyst (0.1 eqv.)
		 <b>10 mol%</b> <b>20% DBU</b> <b>in d<sup>8</sup>-THF</b>

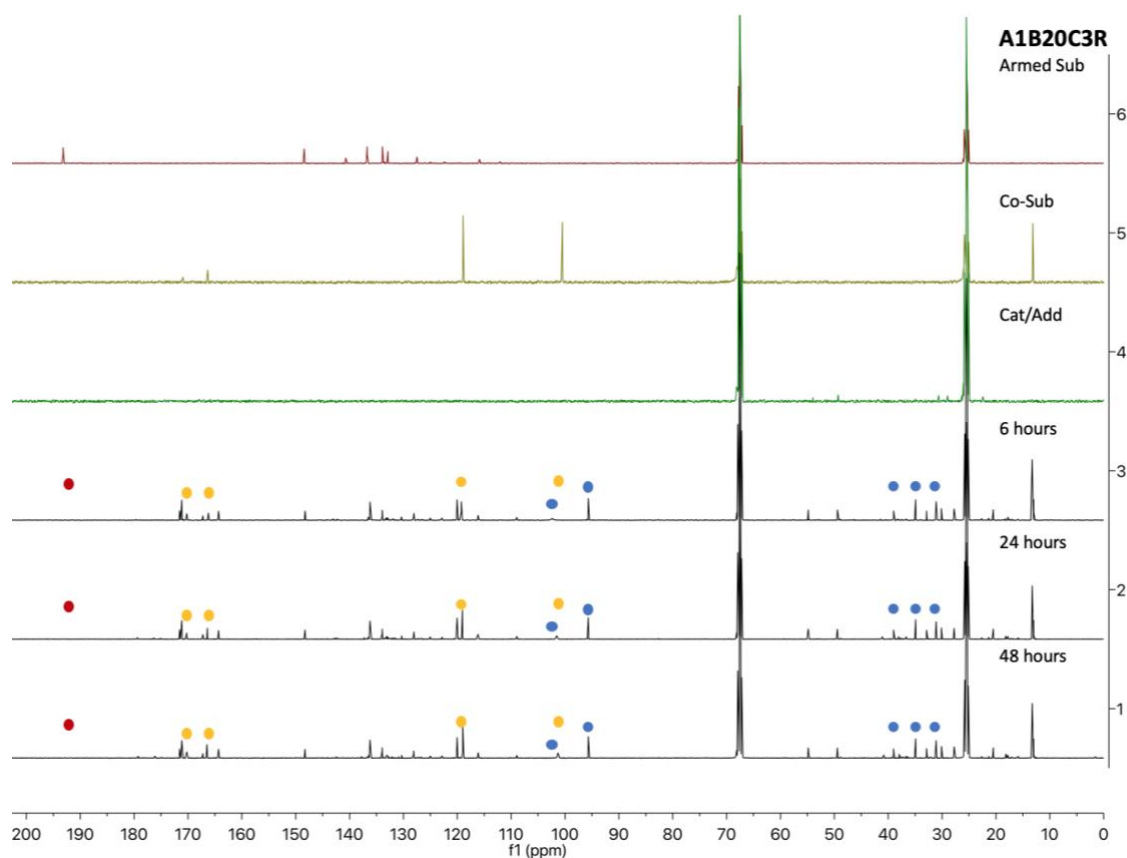


**Figure 3.21** - Analysis of the **A1TB20C3R** combination *via* 500 MHz <sup>13</sup>C-NMR demonstrated conversion of both **substrate** and **co-substrates**, and formation of new peaks prior to being subjected to the sodium borohydride reduction. This was also observed for the combination **A2TB20C3R** (Table 6.2). **Blue** dots indicate new peaks in NMR spectra.

Additionally, the NMR analysis of the two combinations from the targeted array, **A1TB20C3R** and **A2TB20C3R** (Table 6.2), demonstrated conversion of both substrate (**A1** or **A2**) and co-substrate (**TB20**) in the reaction, along with formation of new peaks that indicated formation of a new



product, which was potentially the consequence of an intermolecular reaction (**Figure 3.21**). Other reaction mixtures analysed from using the NMR analysis either demonstrated no conversion of either substrate, or generated product mixtures that were deemed too complex to deconvolute.

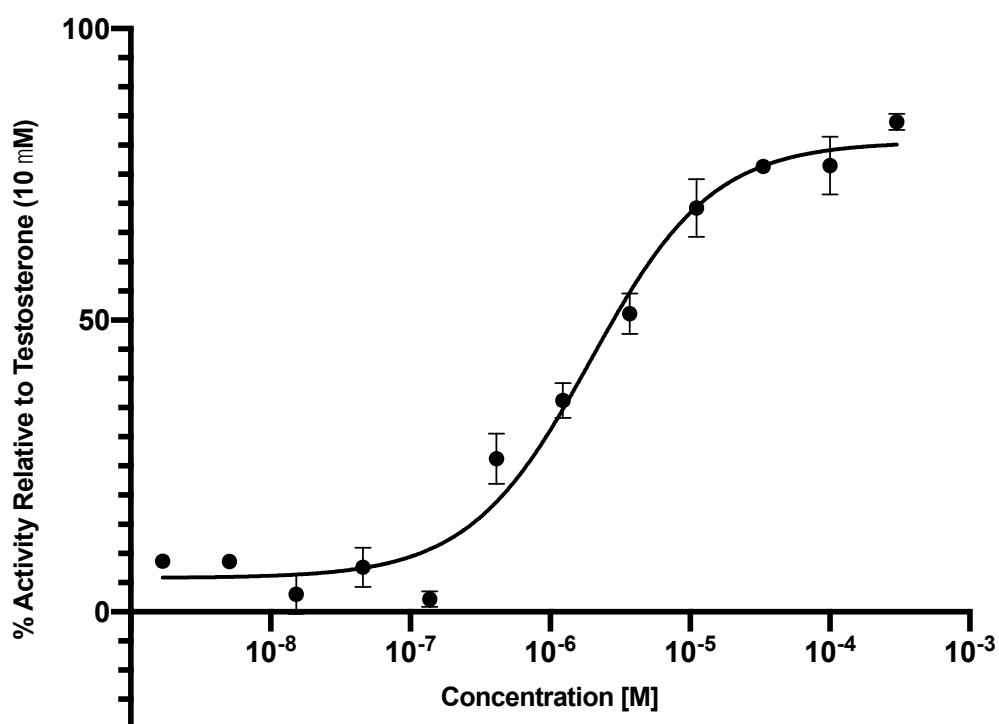
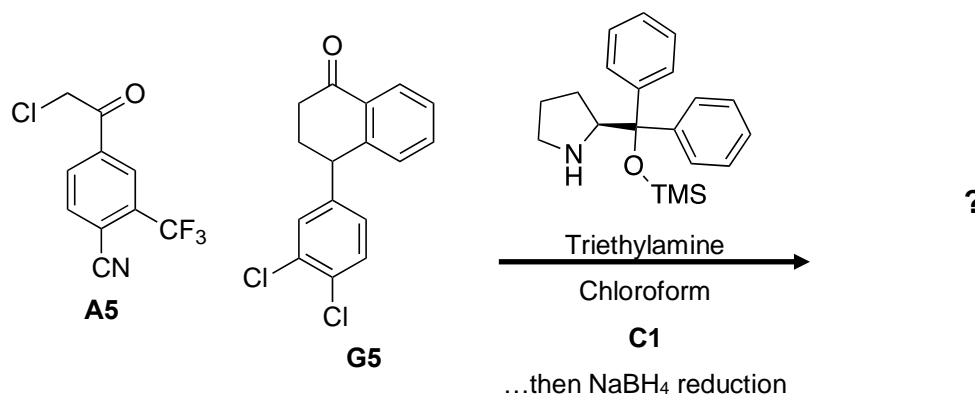


**Figure 3.22** – Dose-response curve for the crude mixture that was identified in the second round of ADS, for the combination between substrate **A5**, co-substrate **G5** and amine catalyst **C1**, followed by sodium borohydride reduction. The stated concentration is relative to the concentration of the substrate.

Alongside the NMR experiments, the crude mixtures were also screened for dose-dependency, obtaining dose-response curves. This allowed confirmation that the bioactivity in the mixture was being caused by a component with dose-dependent activity, rather than interference with the assay readout. A dose response curve was produced for each of them, as per the experimental in **6.6.2**. The dose-response experiment revealed that half maximal effect was observed at low micromolar total product concentrations of the mixture **A5G5C1R** relative to the concentration of the limiting substrate (**Figure 3.22**).

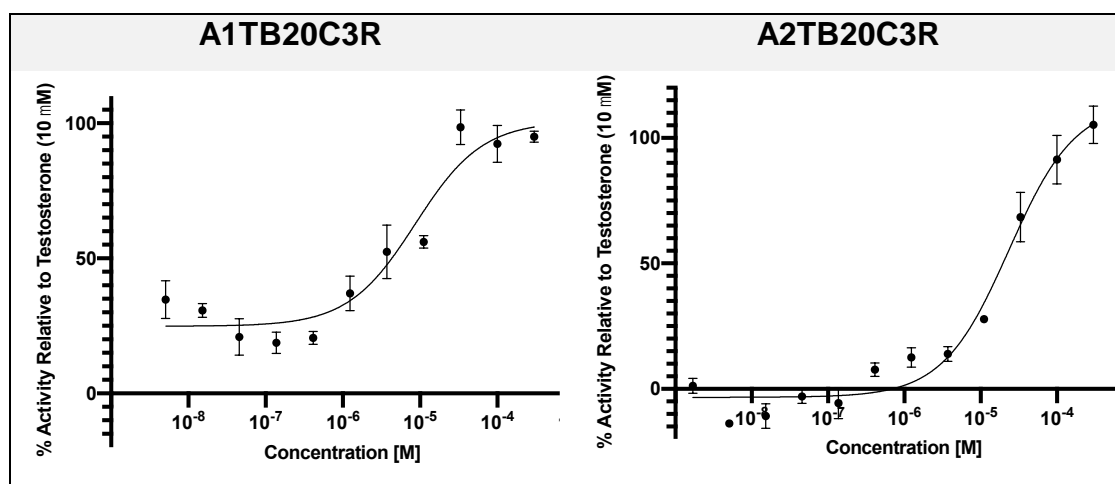
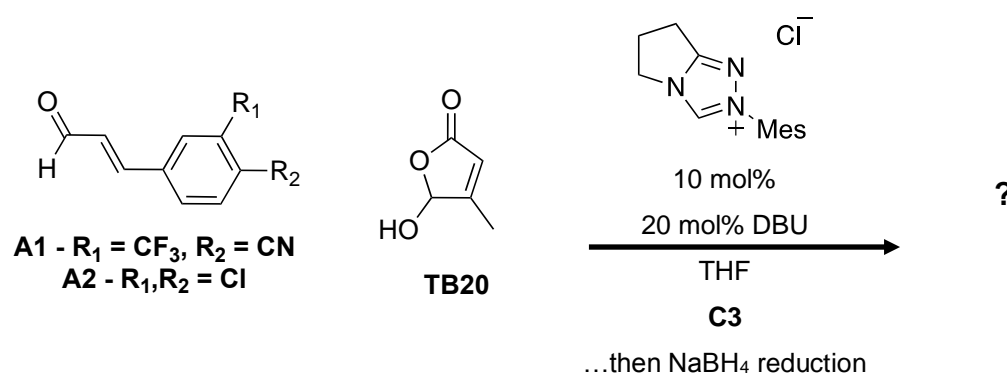


**Figure 3.23** - Dose-response curve for the crude mixtures that were identified in the targeted ADS reaction array, for the combinations **A1TB20C3R** and **A2TB20C3R**. The stated concentration is relative to the concentration of the substrate.

Dose-response of the crude mixtures **A1TB20C3R** and **A2TB20C3R** also indicated dose-dependent activity of components within them (**Figure**

3.23). Both of these combinations appeared to exhibit 50% of the maximal agonist activity in comparison to testosterone, suggesting they were partial agonists, in the region of 10  $\mu\text{M}$  activity.

Fractionation was carried out for these prioritised reactions, but also the other reactions highlighted in **Table 3.3** and **Table 3.4**. The reactions in these tables were replicated as they had been in the reaction arrays, but scaled up by a factor of 50. The crude mixtures were separated by fractionation *via* flash column chromatography. Screening of each of the isolated fractions individually at a concentration relative to the substrate of 20  $\mu\text{M}$  using the single-point procedure highlighted any significant activity. This allowed for facile identification of any fractions that contained bioactive entities in all of the reactions highlighted, and these fractions could then be highlighted for further investigation. This experiment highlighted only three reactions that yielded fractions with greater than 25% bioactivity at 20  $\mu\text{M}$  relative to a testosterone (10  $\mu\text{M}$ ) control – two fractions in **A5G5C1R** from the exhaustively designed reaction arrays, and **A1TB20C3R** and **A2TB20C3R** from the targeted arrays. These mixtures were the same as had been flagged by the NMR and dose-response validation approaches. The proposed compounds in each fraction were identified, and the reactions were scaled up to independently verify the identity of the component, and to validate the bioactivity.

### **3.5.2 Scale-Up and Identification of Products**

In order to identify the active components within **A5G5C1R**, 500 MHz  $^1\text{H}$  NMR spectra of the two fractions indicating bioactivity were obtained. By comparing to spectra from literature compounds, these initially appeared to be the two reduced diastereomers of the co-substrate (**G5** - 4-(3,4-dichlorophenyl)-1-tetralone). To verify that this was in fact the component responsible for causing bioactivity, an independent synthesis involving the direct sodium borohydride reduction of **G5** in methanol was carried out, and the two diastereomers were isolated independently. The identities and configuration of each of the diastereomers (37% *rac*-**35a**; 41% *rac*-**35b**) was

determined *via* NMR analysis and compared to the literature data for the known compounds.<sup>114</sup> Dose-response curves were obtained for both diastereomers, indicating that they both had low micromolar activity (**Figure 3.24**). Even though the reduced **G5** component was screened in the mock array for Round 2 at 1  $\mu\text{M}$  concentration, this co-substrate did not give a response that indicated that it was significantly active.

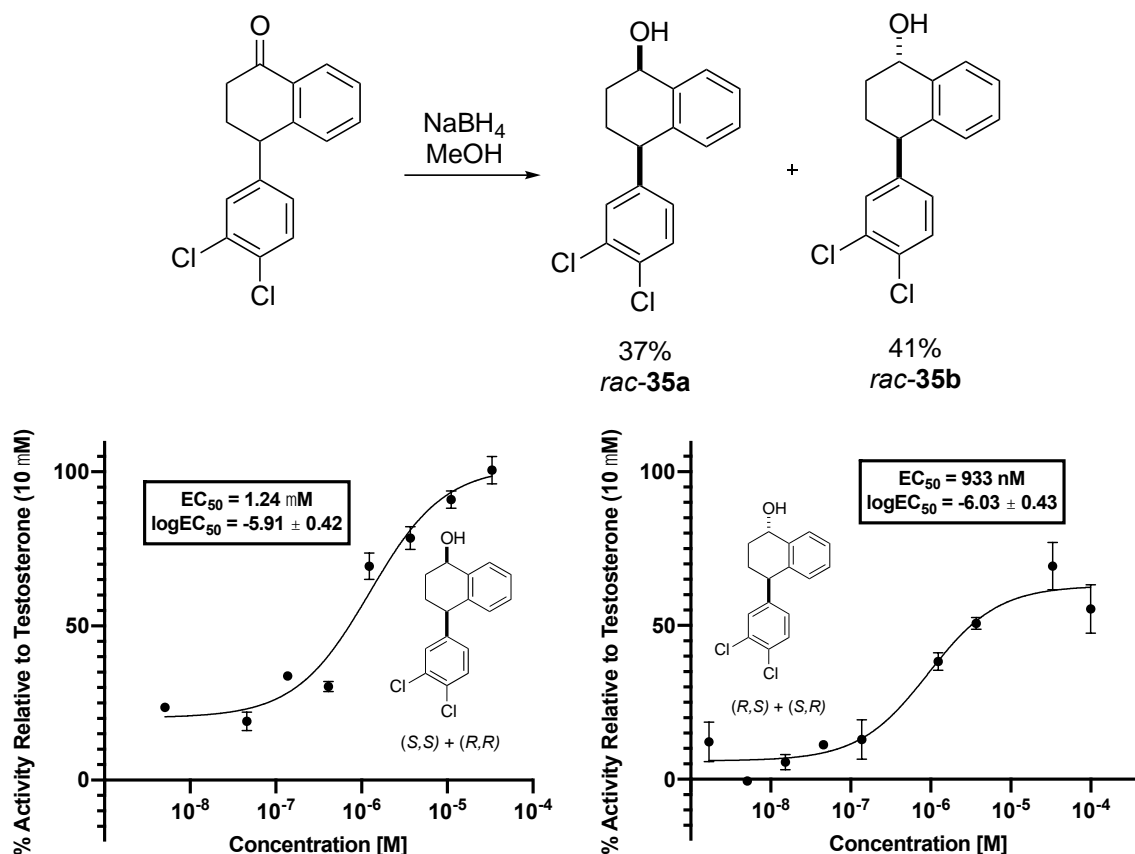


**Figure 3.24** – Dose-response for the racemic diastereomers for the reduced co-substrate in **A5G5C1R**. Both diastereomers exhibit low micromolar activity.

Similar analysis was carried out for the reactions **A1TB20C3R** and **A2TB20C3R**. 500 MHz  $^1\text{H}$  NMR spectra of the fractions that were found to display bioactivity from the fractionation indicated that the components causing the bioactivity were aliphatic alcohol reduction products **36** and **37** of the  $\alpha,\beta$ -unsaturated aldehyde substrates **A1** and **A2**.

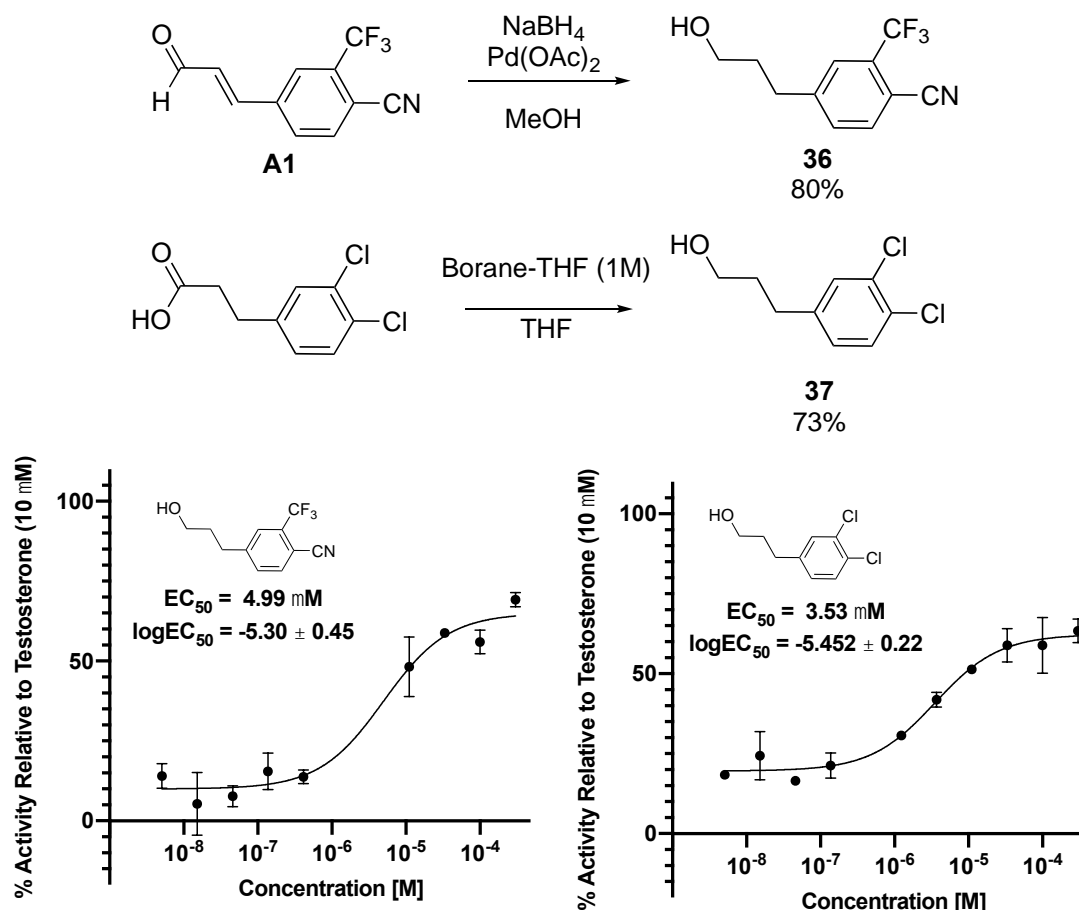


**Figure 3.25** - Dose-response for the aliphatic alcohol products of the reactions **A1TB20C3R** and **A2TB20C3R**. Both compounds display low micromolar level activity of the AR and appear to be partial agonists.

To verify that these compounds were bioactive, independent syntheses were carried out for the two materials.  $\alpha,\beta$ -unsaturated aldehyde **A1** was reduced in a flask with palladium(II) acetate and methanol, using sodium borohydride in a flask sealed with a balloon. The molecular hydrogen produced in the reduction of the aldehyde group is trapped in the reaction, resulting in palladium-catalysed reduction of the double bond, producing the aliphatic alcohol **36**, in a yield of 80%. In a separate method, 3-(3,4-dichlorophenyl)propanoic acid was reduced to the aliphatic alcohol using borane-THF complex (1M) to form the aliphatic alcohol **37** in a yield of 73%. The aliphatic alcohols **36** and **37** were compared to known literature to help confirm their identity.<sup>115,116</sup> Dose-response curves were obtained for both compounds, indicating that they both had micromolar activity as partial agonists (**Figure 3.25**).

As the sodium borohydride induced reduction of  $\alpha,\beta$ -unsaturated aldehydes is known to produce the allyl alcohol, as was discovered in the development of the work-up protocols described in **2.4.1**, it is proposed that activation of the  $\alpha,\beta$ -unsaturated aldehyde by the NHC resulted in a Breslow intermediate that had the ability to abstract a proton from the co-substrate. This results in the formation of the alkyl aldehyde once released from the catalyst, which can be subsequently reduced when the sodium borohydride work-up is applied to form the component which elicits agonism of the AR.

## 4 Conclusions and Future Work

The primary objective of the project was to expand the chemical toolbox compatible with ADS. Organocatalytic reactions that used a broad range of catalysts to generate a diverse range of products were identified. A selection of these reactions was miniaturised, and their outcomes to their full-scale literature counterparts, demonstrating their successful translation to the micro-scale format required for ADS. Work-up conditions were then developed that were able to reduce electrophilic functionalities to more benign functional groups, or reductively aminate them to add extra functionality. This work enabled organocatalysis to be primed as a useful option in the chemical toolbox available for ADS.

Following setup of a TR-FRET assay that screened for agonism of the androgen receptor, a number of strategies were then implemented to design ADS reaction arrays using the new chemical toolbox. A number of approaches were developed that allowed the design of reaction arrays that maximised diversity components, and therefore the products that could be generated. The exhaustively designed array promoted serendipitous discovery of bioactivity, only using the literature to loosely guide array design; whereas the targeted array focused more on conversion to new intermolecular products, using the literature to guide syntheses to known scaffolds. Workflows to follow up on any hits discovered from reaction arrays were developed, that included hit validation assays, fractionation of product mixtures, dose-response assays of crude mixtures and NMR analysis of reaction progression.

A reliance on activity to direct the synthesis of bioactive compounds comes with the caveat that the approach has no preconceptions regarding the structure of the products generated, as demonstrated with the isolation of the compounds identified in **Section 1.1**. No bioactive intermolecular products were isolated using either strategy, but products with micromolar levels of agonism that stemmed from substrates were identified,

demonstrating that novel intermolecular agonists can be identified using the workflow if they are generated.

#### 4.1 Analysis of Value of Organocatalysis in ADS

Organocatalysis appears to have useful attributes to be productive with ADS – robust and diverse reactions capable of forming a range of scaffolds with interesting stereochemistry. The setup of the chemistry in **Section 2.3.3** demonstrated that a range of simple but varied organocatalytic reactions could function on the microscale format required for ADS, using small volumes, no stirring and reactions open to the air. However, the strategies that were used to design arrays necessitated variance from the known literature reactions, particularly with regards to substrate scope, which was necessary to arm substrates with motifs known to have affinity for AR binding.

The lack of robustness when varying from the idealised conditions used in the seminal work that describes a new reaction is a problem for organic chemists, limiting synthetic utility of new reactions. It is well known that many organic reactions that are reported to work with relatively unfunctionalised substrates do not extend to work well in the synthesis of more complex functionalised target molecules.<sup>117</sup> A ‘robustness screen’ has been proposed as a solution to this issue. The screen assesses the tolerance of a set of reaction conditions to a range of functional groups, while simultaneously assessing the stability of the functional groups to the reaction conditions.<sup>118–120</sup> Parallel reaction processing using a small but efficiently selected range of functionalised additives and substrates can allow assessment as to the overall robustness of the reaction. Assessment of new synthetic methods with this screen and demonstrating their scope could potentially increase the speed at which new chemistries are adopted and allow for more complex synthetic problems to be solved.

ADS with organocatalysis has been applied to another project within the group that targets the p53/MDM2 protein-protein interaction. The project



utilised a targeted design approach as outlined in **Section 3.3**, in which 576 reactions were executed. No active intermolecular products were identified using this approach, but post-array analysis by LC-MS indicated that intermolecular products were formed in reactions that were inactive.

#### **4.2 Future Scope for Application of Organocatalysis in ADS**

A solution that could allow for successful demonstration of organocatalysis in ADS could be to attempt to generate compounds to screen using very simple substrates in reactions with strong literature precedent. These reaction arrays could then be screened against targets for which robust high-throughput assays are established but the selection of known small-molecule modulators is small. By starting with no preconceptions regarding target and not integrating affinity motifs into substrates, the approach would be truly target-agnostic, enabling the screening of a rapid number of chemotypes against targets for which there are little or no known modulating chemotypes, with a high probability of products being generated for every reaction in the array. This could provide valuable starting points for medicinal chemistry against difficult targets.

Additionally, extra quantitative validation methods embedded into the ADS workflow could successfully show intermolecular product formation. Development of robust high-throughput HPLC or LC-MS methods could help identification of intermolecular products in reactions that show activity on a high-throughput assay, allowing prioritisation of reactions.

In the early stage of its development, ADS has been demonstrated to have potential to be a fruitful method for developing bioactive molecules. Continuing to demonstrate its worth by using different varieties of chemistry against a range of biological targets could help to validate its position as an efficient bioactive hit molecule generation approach.

## 5 Appendix: Synthesis of Compounds Accessible using a Top-Down Lead-Oriented Synthesis Approach

The work completed during an industrial placement contributed to a project that focused on the 'top-down' LOS approach to a large number of novel scaffolds (an overview of the project is described in 1.1.3). This work contributed to the realisation of four distinct compound libraries based upon two cycloadduct starting materials were synthesised, decorating a number of the scaffolds as part of a collaborative effort to generate a library. Work was undertaken to demonstrate the synthesis of the key cycloadduct on a multigram scale, before validating the chemistry by making fused-imidazole and fused-pyrazine derivatives using routes previously developed within the group (**Figure 5.1**).

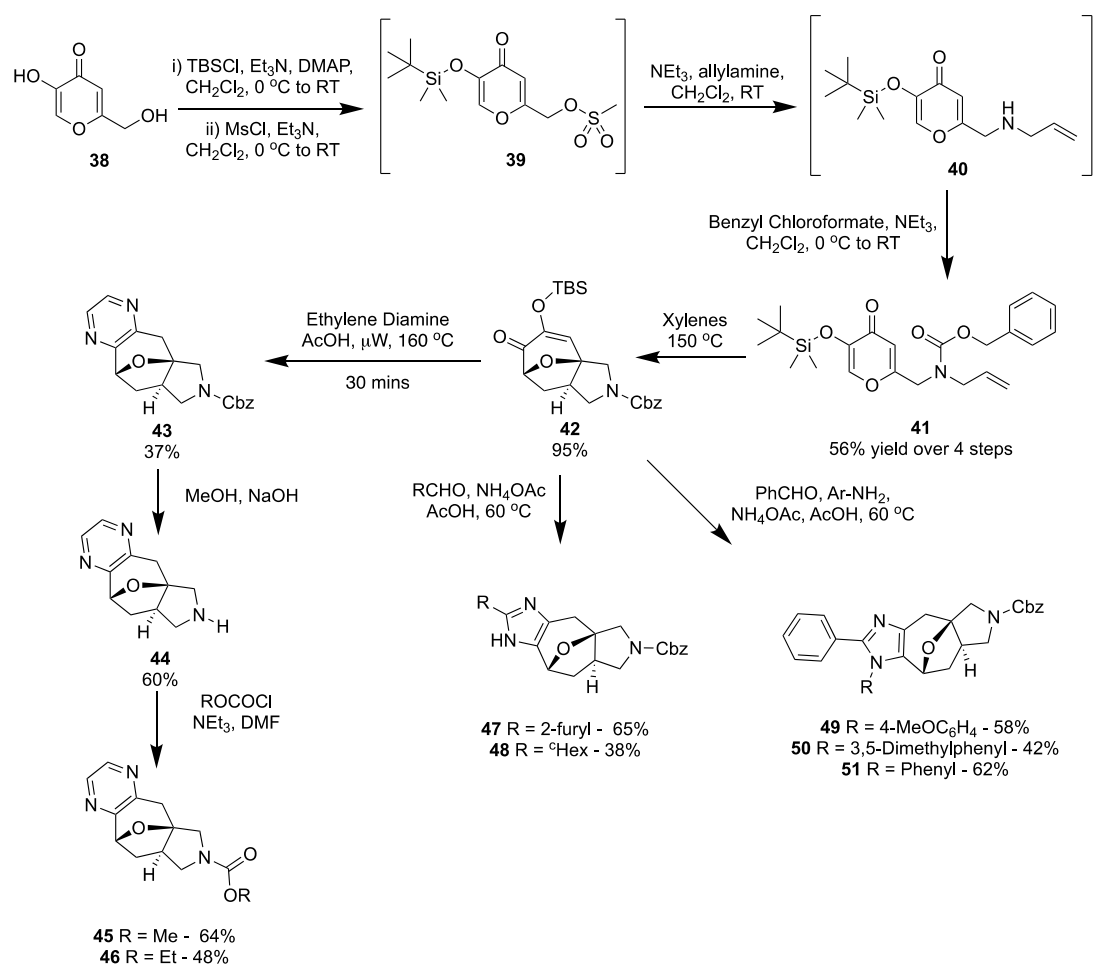


**Figure 5.1** – Chemistry undertaken to enable production of large screening libraries based on complex molecular scaffolds.

Initially, the multigram scale synthesis of cycloadduct **41** was demonstrated. Starting from 10 g of kojic acid **38**, the alcohol was treated in sequence with *tert*-butylchlorodimethylsilane and methanesulfonyl chloride to make **39**, that was used in the next step of the synthesis without purification. Allylamine was used to substitute the activated mesylate leaving group to make the amine **40**, which was once again used crude in the next step. The amine was then protected with a carboxybenzyl group to make carbamate **41** in an overall yield of 56% from the kojic acid starting material over 4 steps. The cycloadduct **41** was then refluxed in xylenes at 150 °C, initiating a [5+2] cycloaddition to form cycloadduct **42** in high yield, which was the key cycloadduct from which derivatives could be made.

Several imidazole derivatives (**47-51**) were generated from cycloadduct **42** *via* one-pot Debus-Radziszewski reactions, resulting in 5 novel analogues. Additionally, reaction of the cycloadduct **42** with ethylene diamine resulted in a fused pyrazine scaffold **43**. The fused pyrazine **43** could then be derivatised to substitute the nitrogen protecting group to generate novel analogues (**44-46**). This work demonstrated that the scaffolds could be readily functionalised to populate a library of screening compounds, and this was subsequently exploited by Edelris to generate a library of over 2900 compounds.

## 6 Experimental Procedures

### 6.1 General Information

Commercially available starting materials were obtained from Sigma-Aldrich, Fluorochem, Alfa Aesar, Fisher Scientific, Acros, Apollo Scientific and Insight Biotechnology. All non-aqueous reactions were carried out under an atmosphere of nitrogen in oven-dried glassware unless stated. Anhydrous DCM, anhydrous THF, anhydrous toluene, anhydrous diethyl ether, anhydrous methanol and anhydrous acetonitrile were obtained from a PureSolv MD5 purification system. All other anhydrous solvents were obtained from sealed bottles from the aforementioned suppliers. All other solvents were of analytical grade and used as supplied. Ether refers to diethyl ether and petrol refers to petroleum spirit (b.p. 40–60 °C) unless stated.

Solvents were removed under reduced pressure using a Büchi rotary evaporator and a Vacuubrand PC2001 Vario diaphragm pump. Reaction plated were evaporated where necessary with a GeneVac EZ-2 evaporator. Thin layer chromatography was carried out on pre-coated aluminium Merck SilicaGel 60 F254 plates, using ultraviolet light ( $\lambda_{\text{max}} = 254 \text{ nm}$ ) and  $\text{KMnO}_4$  for visualisation. Flash column chromatography was carried out using Merck Geduran SilicaGel (30–75  $\mu\text{M}$  particles).

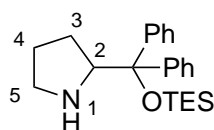
Analytical LC-MS was performed using an Agilent 1200 series LC system consisting of a Bruker HCT Ultra ion trap mass spec, a high vacuum degasser, a binary pump, a high performance autosampler and micro well plate autosampler, an autosampler thermostat, a thermostated column compartment and diode array detector. The system used a Phenomenex Luna C18 50 x 2mm 5 micron column and two solvent systems: MeCN/ $\text{H}_2\text{O}$  + 0.1% Formic acid or MeCN/ $\text{H}_2\text{O}$ . Accurate mass spectrometry was recorded using electrospray ionisation on a Bruker MaXis Impact spectrometer. Infrared spectroscopy was recorded on a Bruker Alpha-P ATR FT-IR spectrometer.

Proton ( $^1\text{H}$ ) and carbon ( $^{13}\text{C}$ ) NMR spectra were recorded on a Bruker 300, Bruker Ascend 400 Bruker Avance 500 spectrophotometer using an internal deuterium lock at 300 K unless stated. Chemical shifts are quoted in parts per million downfield of tetramethylsilane and coupling constants ( $J$ ) are reported in Hertz. Splitting patterns are abbreviated when reported: s (singlet), d (doublet), t (triplet), q (quartet), m (multiplet) app (apparent) and br (broad). DEPT 135, COSY, HMQC and HMBC pulse sequences were often used to aid spectral assignment.

## 6.2 Chemistry Experimental Procedures

### 6.2.1 Synthesis of Catalysts

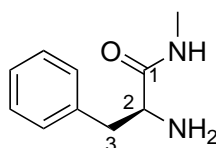
#### 2-{Diphenyl[(triethylsilyl)oxy]methyl}pyrrolidine (6)



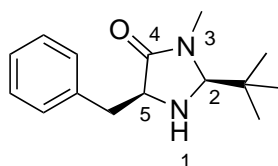
TESOTf (5.80 mL, 25.7 mmol) was added drop-wise to a solution of (*R*)-(+)-diphenyprolinol (2.50 g, 9.85 mmol) and (*S*)-(-)-diphenyprolinol (2.50 g, 9.85 mmol) and triethylamine (3.58 mL, 25.7 mmol) in DCM (35 mL) at 0 °C. Following the addition, the reaction mixture was warmed to room temperature and allowed to stir for 72 hours. Conversion of the starting material was confirmed by TLC analysis, and the mixture quenched with water (10 mL). The product was extracted with DCM (2 x 10 mL), washed with brine (2 x 5 mL) and dried over anhydrous  $\text{MgSO}_4$  before evaporation under reduced pressure to give the crude product as a yellow oil. The crude product was purified by flash column chromatography, eluting with 10:1–5:1 Hexane–EtOAc, to obtain the title compound<sup>121</sup> as a straw coloured, transparent viscous oil (3.22 g, 8.70 mmol, 44%).  $\delta_{\text{H}}$  (500MHz,  $\text{CDCl}_3$ ): 7.52–7.50 (2H, m, Ph), 7.40–7.38 (2H, m, Ph), 7.32–7.24 (6H, m, Ph), 4.05 (1H, t,  $J$  7.3, 2-H), 2.89–2.81 (1H, m, 5- $\text{H}_a$ ), 2.78–2.70 (1H, m, 5- $\text{H}_b$ ), 1.67–1.56 (3H, m, 4-H & 3- $\text{H}_{a/b}$ ), 1.29 (1H, m, 3- $\text{H}_{a/b}$ ), 0.89 (9H, t,  $J$  7.9,  $\text{CH}_2\text{CH}_3$ ), 0.39 (6H,

q,  $J$  8.0,  $\text{CH}_2\text{CH}_3$ );  $\delta_{\text{c}}$  (**125MHz**,  **$\text{CDCl}_3$** ): 146.7 (Ar), 145.5 (Ar), 128.8 (Ar), 128.0 (Ar), 127.5 (Ar), 127.3 (Ar), 126.9 (Ar), 126.9 (Ar), 82.9 (CO<sub>Si</sub>), 65.7 (C-2), 47.3 (C-5), 27.7 (C-3), 25.1 (C-4), 7.3 (C-7), 6.5 (C-8); **IR**  $\nu_{\text{max}}$  (**neat**)/ **$\text{cm}^{-1}$** : 3058.3, 3025.0, 2952.6, 2909.1, 2873.7, 1598.9;  **$R_f$**  = 0.03 (50:50 Hexane–EtOAc); **HRMS (ESI)**:  $\text{C}_{23}\text{H}_{33}\text{NOSi}$  requires  $[\text{M}+\text{H}]^+$  368.2410, found 368.2415.

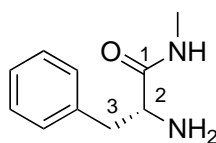
**(2S)-2-Amino-N-methyl-3-phenylpropanamide (9)**



Thionyl chloride (7.72 mL, 107 mmol) was added dropwise to a flask charged with L-phenylalanine (5.00 g, 30.3 mmol) in methanol (80 mL). After refluxing for 2 hours, the mixture was cooled to room temperature, and the reaction mixture was concentrated under reduced pressure. Methylamine (8M in ethanol, 7.8 mL, 60.6 mmol) was added along with additional ethanol (30 mL) and the mixture allowed to stir for 48 hours at room temperature. The reaction was then diluted with dichloromethane (50 mL) and water (25 mL), and the pH adjusted to 12 with saturated  $\text{K}_2\text{CO}_3$  solution. The layers were separated and the aqueous phase extracted with dichloromethane (2 x 5 mL). The separated organic layers were combined, dried over  $\text{Na}_2\text{SO}_4$ , and concentrated under reduced pressure to obtain the title compound<sup>93</sup> as a colourless amorphous solid (4.65 g, 26.1 mmol, 86%).  $\delta_{\text{H}}$  (**500MHz**,  **$\text{CDCl}_3$** ): 7.35-7.23 (5H, m, Ar-H), 3.62 (1H, dd,  $J$  9.4 and 4.0, 2-H), 3.30 (1H, dd,  $J$  13.8 and 4.0, 3- $\text{H}_{a/b}$ ), 2.83 (3H, d,  $J$  5.0, N- $\text{CH}_3$ ), 2.69 (1H, dd,  $J$  13.8 and 9.4, 3- $\text{H}_{a/b}$ );  $\delta_{\text{c}}$  (**125MHz**,  **$\text{CDCl}_3$** ): 174.8, 138.0, 129.3, 128.7, 126.8, 56.5, 41.1, 25.8; **IR**  $\nu_{\text{max}}$  (**neat**)/ **$\text{cm}^{-1}$** : 3367.7, 3354.7, 3084.6, 3060.2, 3030.7, 2959.6, 2943.0, 2919.4, 2866.7, 1673.1, 1603.6, 1581.5;  **$R_f$**  = 0.07 (75:25 EtOAc–Hexanes); **HRMS (ESI)**:  $\text{C}_{10}\text{H}_{14}\text{N}_2\text{O}$  requires  $[\text{M}+\text{H}]^+$  179.1179, found 179.1176.

**(2S,5S)-5-Benzyl-2-tert-butyl-3-methylimidazolidin-4-one (10)**

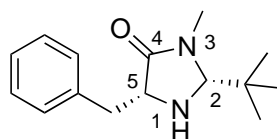
A solution of 2-amino-*N*-methyl-3-phenylpropanamide (500 mg, 2.80 mmol), pivaldehyde (0.610 mL, 5.60 mmol) and ytterbium (III) triflate (18 mg, 0.028 mmol, 1 mol%) in chloroform (30 mL) was refluxed for 16 hours to form a pale yellow solution. The reaction mixture was concentrated under reduced pressure, and the crude material purified by flash column chromatography, eluting with a gradient from 50:50 to 75:25 EtOAc–Petrol, to obtain the title compound<sup>93</sup> as a pale yellow flakey solid (245 mg, 0.99 mmol, 35%).  $\delta_{\text{H}}$  (500MHz,  $\text{CDCl}_3$ ): 7.31 – 7.07 (5H, m, Ar-H), 4.01 (1H, d, *J* 1.5, 2-H), 3.66 (1H, ddd, *J* 7.6, 4.0, 1.4, 5-H), 3.10 (1H, dd, *J* 13.8, 4.0, Benzyl  $\text{CH}_{\text{a/b}}$ ), 2.90 (1H, dd, *J* 13.8, 7.5, Benzyl  $\text{CH}_{\text{a/b}}$ ), 2.87 (3H, s,  $\text{NCH}_3$ ), 2.12 (1H, br s,  $\text{NH}$ ), 0.78 (9H, s,  $\text{CCH}_3$ );  $\delta_{\text{C}}$  (125MHz,  $\text{CDCl}_3$ ): 175.4, 137.6, 129.6, 128.7, 126.8, 83.6, 59.7, 38.7, 37.9, 31.4, 25.7; IR  $\nu_{\text{max}}$  (neat)/ $\text{cm}^{-1}$ : 3367.7, 3354.7, 3084.6, 3060.2, 3030.7, 2959.6, 2943.0, 2919.4, 2866.7, 1673.1;  $R_{\text{f}}$  = 0.36 (75:25 EtOAc–Petrol); HRMS (ESI):  $\text{C}_{15}\text{H}_{22}\text{N}_2\text{O}$  requires  $[\text{M}+\text{H}]^+$  247.1810, found 247.1812.

**(2R)-2-Amino-*N*-methyl-3-phenylpropanamide (ent-9)**

Thionyl chloride (3.86 mL, 52.9 mmol) was added dropwise to a flask charged with D-phenylalanine (2.50 g, 15.1 mmol) in methanol (40.0 mL). After refluxing for 2 hours, the mixture was cooled to room temperature, and the reaction mixture concentrated under reduced pressure. Methylamine (8M in ethanol, 4.00 mL, 32.0 mmol) was added and the mixture allowed to stir for 48 hours at room temperature. The reaction was then diluted with dichloromethane (25 mL) and water (12.5 mL), and the pH adjusted to 12

with saturated  $K_2CO_3$  solution. The layers were separated and the aqueous phase extracted with chloroform (2 x 5 mL). The separated organic layers were combined, dried over  $Na_2SO_4$ , and concentrated under reduced pressure to obtain the title compound<sup>93</sup> as a colourless amorphous solid (2.40 g, 9.7 mmol, 61%).  $\delta_H$  (**500MHz,  $CDCl_3$** ): 7.38 – 7.32 (2H, m, Ar 6'-H and 2'-H), 7.34 – 7.20 (3H, m, 3'-H, 4'-H and 5'-H), 3.64 (1H, dd, J 9.5, 3.9, 2-H), 3.32 (1H, dd, J 13.8, 3.9, 3- $H_{a/b}$ ), 2.85 (3H, dd, J 5.0, 1.3,  $NCH_3$ ), 2.71 (1H, dd, J 13.7, 9.4, 3- $H_{a/b}$ );  $\delta_C$  (**125MHz,  $CDCl_3$** ): 174.9, 138.1, 129.4, 128.8, 126.9, 56.6, 41.2, 25.9; **IR  $\nu_{max}$  (neat)/ $cm^{-1}$** : 3371.3, 3344.6, 3291.4, 3085.6, 3061.8, 3031.3, 2939.2, 2914.5, 2875.7, 1644.2, 1523.0;  **$R_f$  = 0.09** (75:25 EtOAc–Hexanes); **HRMS (ESI)**:  $C_{10}H_{14}N_2O$  requires  $[M+H]^+$  179.1179, found 179.1175.

**(2*R*,5*R*)-5-Benzyl-2-tert-butyl-3-methylimidazolidin-4-one (ent-10)**

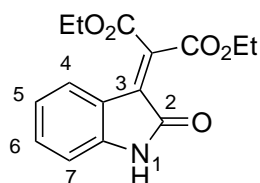


A solution of 2-amino-*N*-methyl-3-phenylpropanamide (2.00 g, 11.2 mmol), pivaldehyde (2.44 mL, 22.4 mmol) and ytterbium (III) triflate (69 mg, 0.11 mmol, 1 mol%) in chloroform (30 mL) was refluxed for 8 hours to form a pale yellow solution. The solvent was concentrated under reduced pressure, and the crude material purified by flash column chromatography, gradient eluting from 50:50 to 75:25 EtOAc–Petrol, to obtain the title compound<sup>93</sup> as a white amorphous solid (832 mg, 3.38 mmol, 30%).  $\delta_H$  (**500MHz,  $CDCl_3$** ): 7.26 – 7.03 (5H, m, Ar-H), 3.99 (1H, d, J 1.6, 2-H), 3.64 (1H, ddd, J 7.7, 4.0, 1.4, 5-H), 3.08 (1H, dd, J 13.7, 4.0, Benzyl  $CH_{a/b}$ ), 2.88 (1H, dd, J 13.7, 7.6, Benzyl  $CH_{a/b}$ ), 2.84 (3H, s,  $NCH_3$ ), 0.77 (9H, s,  $CCH_3$ );  $\delta_C$  (**125MHz,  $CDCl_3$** ): 175.4, 138.0, 129.7, 128.7, 126.8, 82.6, 59.5, 38.4, 35.1, 30.8, 25.5; **IR  $\nu_{max}$  (neat)/ $cm^{-1}$** : 3367.7, 3354.7, 3084.7, 3060.0, 3030.6, 2960.0, 2960.0, 2919.4, 2867.0, 1672.8;  **$R_f$  = 0.35** (75:25 EtOAc–Petrol); **HRMS (ESI)**:  $C_{15}H_{22}N_2O$  requires  $[M+Na]^+$  269.1624, found 269.1622.



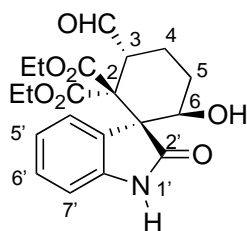
## 6.2.2 Synthesis of Exemplar Reactions from Literature

### 1,3-Diethyl 2-(2-oxo-2,3-dihydro-1H-indol-3-ylidene)propanedioate (13)



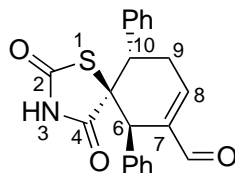
Diethyl malonate (325 mg, 2.03 mmol) and piperidine (0.22 mL, 2.24 mmol) were added to a solution of isatin (300 mg, 2.03 mmol) in EtOH (10 mL), and the mixture allowed to reflux for 24 hours. Following confirmation of conversion via TLC analysis, the resulting deep red mixture was evaporated to dryness under reduced pressure to obtain the title compound as a deep red powder (90 mg, 0.3 mmol, 15%).  $\delta_{\text{H}}$  (500MHz,  $\text{CDCl}_3$ ): 8.36 (1H, d,  $J$  7.8, 4-H), 8.04 (1H, br s, 1-H), 7.32 (1H, td,  $J$  7.8 and 1.3, 6-H), 7.02 (1H, td,  $J$  7.7 and 1.3, 5-H), 6.81 (1H, d,  $J$  7.8, 7-H), 4.43 (2H, q,  $J$  7.2,  $\text{CH}_2\text{CH}_3$ ), 4.38 (2H, q,  $J$  7.2,  $\text{CH}_2\text{CH}_3$ ), 1.38 (3H, t,  $J$  7.2,  $\text{CH}_2\text{CH}_3$ ), 1.37 (3H, t,  $J$  7.2,  $\text{CH}_2\text{CH}_3$ );  $\delta_{\text{C}}$  (125MHz,  $\text{CDCl}_3$ ): 167.7 (C-2), 165.3 (COOEt), 162.9 (COOEt), 143.5 (C-3), 134.6 (C-7a), 133.1 (C-3a), 129.6 (C-6), 129.0 (C-5), 122.8 (C-4), 119.8 (C-3a), 110.2 (C-7), 62.3 ( $\text{CH}_2\text{CH}_3$ ), 62.2 ( $\text{CH}_2\text{CH}_3$ ), 14.0 ( $\text{CH}_2\text{CH}_3$ ), 13.9 ( $\text{CH}_2\text{CH}_3$ );  $R_f$  = 0.28 (75:25 Hexane–EtOAc); HRMS (ESI):  $\text{C}_{15}\text{H}_{15}\text{NO}_5$  requires  $[\text{M}+\text{H}]^+$  290.1028, found 290.1023.

### 2,2-Diethyl-(1*R*\*,3*S*\*,6*S*\*)-3-formyl-6-hydroxy-2'-oxo-1',2'-dihydrospiro [cyclohexane-1,3'-indole]-2,2-dicarboxylate (14)



Gluteraldehyde solution (50% in H<sub>2</sub>O, 0.064 mL, 0.34 mmol) was added to a solution of diethyl 2-(2-oxoindolin-3-ylidene)malonate **13** (41 mg, 0.14 mmol) and 2-{diphenyl[(triethylsilyl)oxy]methyl}pyrrolidine **6** (0.25 mL, 5.0 mg, 0.014 mmol) in DCM (1 mL) at room temperature. The resulting mixture was stirred for 14 hours, and purified via flash column chromatography, eluting with 80:20-65:35 Petrol–EtOAc, to obtain the title compound<sup>94</sup> as an amorphous colourless solid (12 mg, 0.0308 mmol, 22%).  $\delta_{\text{H}}$  (500MHz, CDCl<sub>3</sub>): 9.81 (1H, d, *J* 1.5, CHO), 8.05 (1H, br s, 1-H), 7.31 (1H, d, *J* 7.7, 7'-H), 7.24 (1H, td, *J* 7.7 and 1.2, 6'-H), 7.02 (1H, td, *J* 7.7 and 1.2, 5'-H), 6.84 (1H, d, *J* 7.7, 4'-H), 4.78 (1H, dd, *J* 11.7 and 4.8, 6-H), 4.23 (2H, qd, *J* 7.2 and 1.6, ethyl CH<sub>2</sub>), 4.18 (1H, ddd, *J* 12.8, 3.8 and 1.5, 3-H), 3.94 (2H, qd, *J* 7.1 and 1.5, ethyl CH<sub>2</sub>), 2.30 (1H, qd, *J* 13.2 and 4.6, 4-H<sub>a/b</sub>), 2.11 (1H, dd, *J* 13.4 and 2.7, 4-H<sub>a/b</sub>), 2.01-1.90 (2H, m, 5-H), 1.23 (3H, t, *J* 7.2, ethyl CH<sub>3</sub>), 0.90 (3H, t, *J* 7.2, ethyl CH<sub>3</sub>);  $\delta_{\text{C}}$  (125MHz, CDCl<sub>3</sub>): 200.7 (C-CHO), 177.3 (C-2'), 168.5 (ester C=O), 168.2 (ester C=O), 142.5 (C-7'a), 130.2 (C-3'a), 128.8 (C-6'), 124.4 (C-4'), 122.8 (C-5'), 109.5 (C-7'), 72.4 (C-6), 62.2 (ethyl CH<sub>2</sub>), 62.1 (ethyl CH<sub>2</sub>) 61.6 (C-1), 57.3 (C-2), 49.1 (C-3), 26.6 (C-5), 21.0 (C-4), 13.9 (ethyl CH<sub>3</sub>), 13.4 (ethyl CH<sub>3</sub>); *R*<sub>f</sub> = 0.32 (50:50 Petrol–EtOAc); HRMS (ESI): C<sub>20</sub>H<sub>23</sub>NO<sub>7</sub> requires [M+H]<sup>+</sup> 390.1553, found 390.1551.

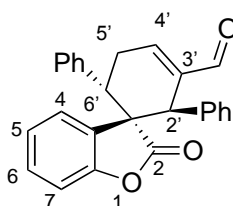
**(5*R*\*,6*S*\*,10*R*\*)-2,4-Dioxo-6,10-diphenyl-1-thia-3-azaspiro[4.5]dec-7-ene-7-carbaldehyde (**16**)**



Cinnamaldehyde (0.12 mL, 0.90 mmol) was added to a solution of 2-{diphenyl[(triethylsilyl)oxy]methyl}pyrrolidine **6** (22 mg, 0.06 mmol) and thiazolidinedione **15** (35 mg, 0.3 mmol) in dichloromethane (1 mL) and stirred at room temperature for 36 hours. Following evaporation of the solvent under reduced pressure, the crude product was purified by flash column chromatography, eluting with 90:10 Hexane–EtOAc, to afford a

mixture of white solid and deep orange oil, which was further purified by mass directed prep-HPLC to obtain the title compound<sup>95</sup> as a colourless amorphous solid (16 mg, 0.044 mmol, 15%).  $\delta_{\text{H}}$  (500MHz,  $\text{CDCl}_3$ ): 9.47 (1H, s, CHO), 7.22-7.37 (9H, m, 8-H; 2'-H, 3'-H, 4'-H, 6'-H), 7.14 (2H, dt, 4'-H), 4.43 (1H, s, 6-H), 3.52 (1H, dd,  $J$  11.2 and 5.9, 10-H), 3.39 (1H, dd,  $J$  20.5 and 11.2, 9- $\text{H}_{a/b}$ ), 3.03 (1H, dt,  $J$  20.5 and 5.3, 9- $\text{H}_{a/b}$ );  $\delta_{\text{C}}$  (125MHz,  $\text{CDCl}_3$ ): 191.47 (CHO), 174.94 (C-2), 168.15 (C-4), 149.48 (C-8), 139.89 (Ph), 137.83 (Ph), 137.23 (Ph), 130.52 (Ph), 129.35 (Ph), 128.61 (Ph), 128.52 (Ph), 128.41 (Ph), 128.35 (Ph), 67.63 (C-5), 46.62 (C-6), 44.39 (C-10), 32.19 (C-9);  $R_{\text{f}}$  = 0.07 (50:50 Hexane–Ethyl Acetate); HRMS (ESI):  $\text{C}_{21}\text{H}_{17}\text{NO}_3\text{S}$  requires  $[\text{M}-\text{H}]^-$  362.0856, found 362.0875.

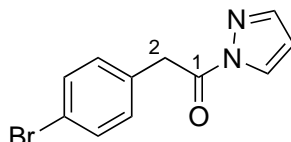
**(2'*R*\*,3'*R*\*,6'*S*\*)-2-Oxo-2',6'-diphenyl-2H-spiro[1-benzofuran-3,1'-cyclohexan]-3'-ene-3'-carbaldehyde (18)**



Cinnamaldehyde (0.17 mL, 1.35 mmol) was added to a solution of the catalyst 2-{diphenyl[(triethylsilyl)oxy]methyl}pyrrolidine **6** (9 mg, 0.0225 mmol) and coumaran-2-one **17** (60 mg, 0.45 mmol) stirring in toluene (1 mL) at room temperature. Benzoic acid (0.002 mL, 0.0225 mmol) was added, and the mixture allowed to stir for 24 hours at room temperature. The mixture was flushed through a plug of silica, and the solvent evaporated under reduced pressure, before purification by flash column chromatography, eluting with 84:16 Hexane–Diethyl Ether, to obtain the title compound<sup>96</sup> as a colourless amorphous solid (26 mg, 0.068 mmol, 15%).  $\delta_{\text{H}}$  (500MHz,  $\text{CDCl}_3$ ): 9.55 (1H, s, 3'-CHO), 7.46-7.19 (5H, m, Ar-H), 7.09-6.90 (6H, m, Ar-H), 6.79-6.70 (2H, m, Ar-H), 6.62 (1H, td,  $J$  8.0 and 0.8, Ar-H), 5.47 (1H, dd,  $J$  7.7 and 0.8, 4'-H) 4.12 (1H, s, 2'-H), 3.67 (1H, dd,  $J$  11.3 and 5.8, 6'-H), 3.47 (1H, m, 5'- $\text{H}_{a/b}$ ), 3.05 (1H, dt,  $J$  20.7 and 5.1, 5'- $\text{H}_{a/b}$ );  $\delta_{\text{C}}$  (125MHz,  $\text{CDCl}_3$ ): 192.2 (CHO), 177.1 (C-2), 152.5 (C-7a), 150.6 (C-3'),

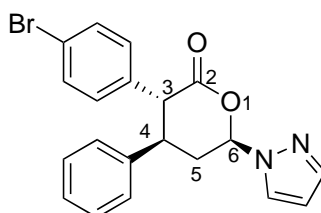
139.3 (Ar), 138.8 (Ar), 137.7 (C-4'), 128.7 (Ar), 128.5 (Ar), 128.2 (Ar), 128.1 (Ar), 127.5 (Ar), 127.3 (Ar), 126.8 (Ar), 122.6 (Ar), 110.0 (Ar), 53.5 (C-3), 46.0 (C-2'), 42.5 (C-6'), 31.3 (C-5');  $R_f = 0.17$  (50:50 Hexane–Diethyl Ether); **HRMS (ESI)**:  $C_{26}H_{20}O_3$  requires  $[M+H]^+$  381.1491, found 381.1488.

**2-(4-Bromophenyl)-1-(1H-pyrazol-1-yl)ethan-1-one (19)**



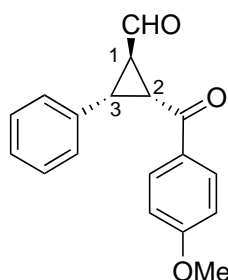
Thionyl chloride (0.28 mL, 3.80 mmol) was added dropwise to a solution of pyrazole (200 mg, 2.90 mmol), 4-bromophenylacetic acid (821 mg, 3.8 mmol) and triethylamine (1.64 mL, 11.8 mmol) in toluene (10 mL) at 0 °C. The reaction was stirred at room temperature for 24 hours before quenching with water (10 mL). The organic layer was washed sequentially with HCl (1M, 10 mL), NaOH (2M, 10 mL) and brine (10 mL), before drying over  $MgSO_4$  and evaporating under reduced pressure to obtain the title compound<sup>122</sup> as a pale pink amorphous solid (605 mg, 2.30 mmol, 79%).  $\delta_H$  (**500MHz,  $CDCl_3$** ): 8.26 (1H, d,  $J$  2.8, Pyrazole 3-H), 7.76 (1H, d,  $J$  1.4, Pyrazole 5-H), 7.52 – 7.47 (m, 2H, Ar-H), 7.28 – 7.25 (m, 2H, Ar-H), 6.48 (1H, dd,  $J$  2.9 and 1.5, Pyrazole 4-H), 4.43 (2H, s, 2-H);  $\delta_C$  (**125MHz,  $CDCl_3$** ): 169.5 (C-1), 144.4 (Pyrazole C-3), 132.4 (Ar), 131.9 (Ar), 131.6 (Ar), 128.7 (Pyrazole C-5), 121.6 (Ar), 110.3 (Pyrazole C-4), 40.0 (C-2); **IR**  $\nu_{max}/cm^{-1}$  (film) 3146, 2979, 1977, 1765, 1736, 1587, 1526, 1487; **HRMS (ESI)**:  $C_{11}H_9N_2OBr$  requires  $[M+Na]^+$  286.9790, found 286.9785.

**(3*R*\*,4*R*\*,6*R*\*)-3-(4-Bromophenyl)-4-phenyl-6-(1H-pyrazol-1-yl)oxan-2-one (20)**



Cinnamaldehyde (0.07 mL, 0.56 mmol) was added to a flask containing 2-(4-bromophenyl)-1-(1H-pyrazol-1-yl)ethanone **19** (100 mg, 0.37 mmol), 2-{diphenyl[(triethylsilyl)oxy]methyl}pyrrolidine **6** (14 mg, 0.037 mmol) and toluene (1 mL). The mixture was stirred for 24 hours at room temperature. Dichloromethane (10 mL) was added and the organic layer washed with saturated NaHCO<sub>3</sub> (2 x 10 mL) before drying over Na<sub>2</sub>SO<sub>4</sub> and evaporating under reduced pressure to give the crude product as a brown oil. The product was purified by flash column chromatography, eluting with 80:20 Hexane–EtOAc, to give the title compound<sup>97</sup> as an amorphous colourless solid (43 mg, 0.10 mmol, 29%).  $\delta_{\text{H}}$  (500MHz, CDCl<sub>3</sub>): 7.46 (2H, m, Ar-H), 7.14 – 7.11 (m, 2H, Ar-H), 7.06 – 6.97 (m, 3H, Ar-H), 6.86 – 6.83 (m, 2H, Ar-H), 6.68 - 6.65 (2H, m, Ar-H), 6.29 (1H, dd, *J* 10.7 and 3.9, 6'-H), 6.17 (1H, t, *J* 2.1, 4'-H), 3.74 (1H, d, *J* 12.0, 1H, 3-H), 3.19 (1H, td, *J* 12.0 and 3.1, 4-H), 3.01 (1H, m, 5-H<sub>a/b</sub>), 2.43 (1H, dt, *J* 14.1 and 3.5, 5-H<sub>a/b</sub>);  $\delta_{\text{C}}$  (125MHz, CDCl<sub>3</sub>): 170.0 (C-2), 141.4 (C-3'), 139.8 (Ar), 136.2 (Ar), 131.9 (Ar), 130.7 (Ar), 129.8 (Ar), 129.1 (Ar), 127.8 (Ar), 127.3 (Ar), 121.7 (Ar), 107.4 (C-4'), 87.4 (C-6), 55.0 (C-3), 45.0 (C-4), 35.3 (C-5); *R*<sub>f</sub> = 0.47 (40:60 EtOAc–Hexane); HRMS (ESI): C<sub>20</sub>H<sub>17</sub>BrN<sub>2</sub>O<sub>2</sub> requires [M+H]<sup>+</sup> 397.0552, found 397.0548.

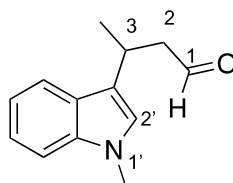
**(1R\*, 2R\*, 3R\*)-2-(4-Methoxybenzoyl)-3-phenylcyclopropane-1-carbaldehyde (22)**



4-Methoxyphenacylchloride **21** (110 mg, 0.60 mmol), cinnamaldehyde (25  $\mu$ L, 0.20 mmol), 2-{diphenyl[(trimethylsilyl)oxy]methyl}pyrrolidine **6** (12 mg, 0.04 mmol, 20 mol%) were dissolved in a flask of CH<sub>2</sub>Cl<sub>2</sub> (2 mL), followed by addition of triethylamine (30  $\mu$ L, 0.20 mmol). The reaction mixture was stirred at room temperature for 24 hours, then the solvent

removed under reduced pressure. Hydrochloric acid (5 mL, 1M) was added to the residue, and the reaction mixture extracted with  $\text{CH}_2\text{Cl}_2$  (5 mL x 3). The combined organic phases were dried over anhydrous sodium sulphate, filtered and evaporated under reduced pressure. The residue was purified by flash column chromatography, eluting with 95:5 Hexane–EtOAc, to yield the title compound<sup>98</sup> as a yellow oil (42 mg, 0.14 mmol, 75%).  $\delta_{\text{H}}$  (**400MHz**,  **$\text{CDCl}_3$** ): 9.87 (1H, d,  $J$  2.8, CHO), 7.96-7.91 (2H, m, Ar-H), 7.23-7.12 (5H, m, Ar-H), 6.94-6.88 (2H, m, Ar-H), 3.85 (3H, s,  $\text{H}_3\text{CO}$ ), 3.63 (1H, dd,  $J$  10.1 and 4.9, 3-H), 3.57-3.51 (1H, td,  $J$  5.5, 4.9 and 2.8, 1-H), 3.38 (1H, dd,  $J$  10.1 and 6.0, 2-H);  $\delta_{\text{C}}$  (**101MHz**,  **$\text{CDCl}_3$** ): 199.1 (CHO), 191.0 ( $\text{R}_2\text{CO}$ ), 163.9 (Ar), 133.7 (Ar), 130.7 (Ar), 129.1 (Ar), 128.8 (Ar), 128.4 (Ar), 127.5 (Ar), 114.0 (Ar), 55.6 ( $\text{H}_3\text{CO}$ ), 36.3 (C-2), 35.6 (C-3), 33.9 (C-1); **IR**  $\nu_{\text{max}}/\text{cm}^{-1}$  (**film**) 3063.1, 3027.4, 3016.6, 2935.4, 2840.8, 2250.3, 1708.6, 1661.3, 1596.2, 1573.7, 1510.2;  **$R_f$**  = 0.62 (50:50 Hexane–EtOAc); **HRMS (ESI)**:  $\text{C}_{18}\text{H}_{16}\text{O}_3$  requires  $[\text{M}+\text{H}]^+$  281.1172, found 281.1169.

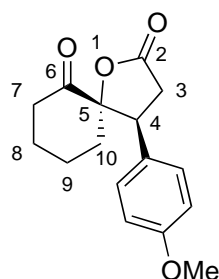
### 3-(1-Methyl-1H-indol-3-yl)butanal (23)



To a flask equipped with a magnetic stir bar containing *rac*-Macmillan catalyst (**10** and *ent*-**10**, 24 mg, 0.1 mmol) was added chloroform (1 mL) and TFA (8  $\mu\text{L}$ , 0.1 mmol). After stirring for 5 minutes, crotonaldehyde (124  $\mu\text{L}$ , 1.5 mmol) was added, before addition of methyl indole (63  $\mu\text{L}$ , 0.5 mmol) after another 10 minutes. The resulting suspension was stirred at ambient temperature for 24 hours. The reaction mixture was then passed through a silica gel plug with diethyl ether, before evaporation under reduced pressure. The resulting residue was purified by flash column chromatography (toluene) to afford the title compound<sup>84</sup> as a brown amorphous solid (38 mg, 0.19 mmol, 40%).  $\delta_{\text{H}}$  (**500MHz**,  **$\text{CDCl}_3$** ): 9.76 (1H, td,  $J$  2.3 and 0.5, 1-H), 7.65 (1H, dq,  $J$  7.9 and 0.9, Ar-H), 7.32 (1H, dq,  $J$  8.2 and 0.9, Ar-H), 7.29-7.23 (1H, m, Ar-H), 7.14 (1H, ddt,  $J$  7.9, 6.9 and 0.9, Ar-H), 6.85 (1H, s, 2'-H),

3.76 (3H, s,  $\text{NCH}_3$ ), 3.73 – 3.66 (1H, m, 3-H), 2.89 (1H, dddd,  $J$  16.3, 6.9, 2.4 and 0.6, 2- $\text{H}_a$ ), 2.72 (1H, dddd,  $J$  16.3, 7.0, 2.3 and 0.6, 2- $\text{H}_b$ ), 1.45 (3H, dd,  $J$  7.0 and 0.7, 4-H);  $\delta_c$  (**125MHz,  $\text{CDCl}_3$** ): 203.0 (C-1), 137.4 (Ar), 126.7 (Ar), 125.3 (C-2'), 121.9 (Ar), 119.2 (Ar), 119.0 (Ar), 118.9 (Ar), 109.5 (Ar), 51.1 (C-2), 32.8 ( $\text{NCH}_3$ ), 26.0 (C-3), 21.8 (C-4); **IR  $\nu_{\text{max}}/\text{cm}^{-1}$  (film)**: 3051.9, 2958.7, 2926.0, 2877.1, 2823.5, 2722.4, 1718.1, 1612.1, 1549.1;  **$R_f$**  = 0.35 (Toluene); **HRMS (ESI)**:  $\text{C}_{13}\text{H}_{15}\text{NO}$  requires  $[\text{M}+\text{Na}]^+$  224.1046, found 224.1041.

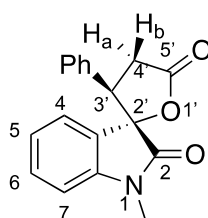
**(4*R*\*, 5*R*\*)-4-(4-methoxyphenyl)-1-oxaspiro[4.5]decane-2,6-dione (24)**



1,3-bis(2,4,6-trimethylphenyl)imidazolium chloride **11** (27 mg, 0.08 mmol, 6 mol%) in THF (1 mL) was added to a flask, followed by DBU (0.024 mL, 0.16 mmol). 4-methoxycinnamaldehyde (325 mg, 2.0 mmol) in THF (1 mL) added followed by 1,2-cyclohexanediol (150 mg, 1.3 mmol) in THF (3 mL). The reaction mixture was left at room temperature for 24 hours. Following TLC and LC-MS analysis, the reaction was filtered through celite and purified by column chromatography, eluting with 80:20 Hexane–EtOAc, to give the title compound<sup>100</sup> as an off-white amorphous solid (87 mg, 0.32 mmol, 25%).  $\delta_H$  (**400MHz,  $\text{CDCl}_3$** ): 7.11 (2H, d,  $J$  8.7, Ar), 6.85 (2H, d,  $J$  8.7, Ar), 3.79 (3H, s,  $\text{H}_3\text{CO}$ ), 3.67 (1H, t,  $J$  9.0, 4-H), 2.92 (2H, qd,  $J$  17.8 and 9.0, 3-H), 2.42-2.23 (2H, m, 10- $\text{H}_a$ , 7- $\text{H}_a$ ), 2.17 (1H, td,  $J$  12.8 and 4.3, 10- $\text{H}_b$ ), 1.87-1.49 (5H, m, 7- $\text{H}_b$ , 8-H, 9-H);  $\delta_c$  (**100MHz,  $\text{CDCl}_3$** ): 206.3 (C-6), 174.8 (C-2), 159.7 (p-Ar), 129.5 (Ar-H), 128.2 (i-Ar), 114.6 (Ar-H), 91.4 (C-5), 55.4 ( $\text{CH}_3$ ), 50.7 (C-4), 41.4 (C-7), 39.0 (C-10), 36.2 (C-3), 25.4 (C-8), 22.2 (C-9);  **$R_f$**  = 0.46 (50:50 Hexane–EtOAc); **HRMS (ESI)**:  $\text{C}_{16}\text{H}_{18}\text{O}_4$  requires  $[\text{M}+\text{H}]^+$  275.1278, found 275.1275.

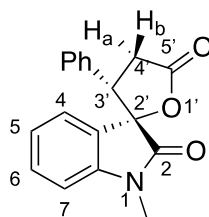
### 1-Methyl-3'-phenyl-1,2-dihydrospiro[indole-3,2'-oxolane]-2,5'-dione

DBU (9.0  $\mu$ L, 0.060 mmol) was added to a suspension of the iMes catalyst **11** (10 mg, 0.030 mmol) and methyl isatin (161 mg, 1.0 mmol) in THF. Cinnamaldehyde (66 mg, 0.50 mmol) was then added, and the reaction stirred at ambient temperature for 24 hours. The crude reaction mixture (d.r. 50:50 *via* NMR) was then passed through a short pad of Celite. After removal of the solvent, the residue was subjected to flash column chromatography (5:1, Hexane–EtOAc), resulting in the isolation of two separate diastereomers of the product.<sup>100</sup>



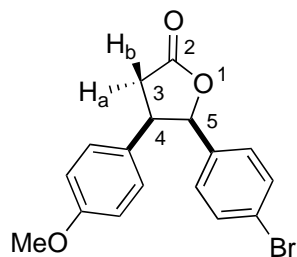
**(3*R*\*,3'*S*\*)-1-Methyl-3'-phenyl-1,2-dihydrospiro[indole-3,2'-oxolane]-2,5'-dione (25a)** (33 mg, 0.11 mmol, 22%) -  $\delta_{\text{H}}$  (**500MHz, CDCl<sub>3</sub>**): 7.54 (1H, ddd, *J* 7.4, 1.3 and 0.6, Ar-H), 7.38 (1H, td, *J* 7.8 and 1.3, Ar-H), 7.22 – 7.13 (4H, m, Ar-H), 6.94 – 6.90 (2H, m, Ar-H), 6.66 (1H, dt, *J* 7.9 and 0.7, Ar-H), 4.07 (1H, dd, *J* 13.7 and 8.0, 3'-H), 3.81 (1H, dd, *J* 16.8 and 13.7, 4'-H<sub>a</sub>), 2.91 (1H, dd, *J* 16.8 and 8.0, 4'-H<sub>b</sub>), 2.81 (3H, s, NCH<sub>3</sub>);  $\delta_{\text{C}}$  (**125MHz, CDCl<sub>3</sub>**): 175.0 (C-5'), 172.7 (C-2), 144.4 (Ar), 132.2 (Ar), 131.4 (Ar), 128.6 (Ar), 128.5 (Ar), 128.4 (Ar), 127.6 (Ar), 127.5 (Ar), 124.8 (Ar), 124.3 (Ar), 123.6 (Ar), 108.7 (Ar), 86.6 (C-3), 51.1 (C-3'), 32.3 (C-4'), 25.9 (NCH<sub>3</sub>); **IR**  $\nu_{\text{max}}$ /**cm<sup>-1</sup> (film)**: 3067.2, 2982.3, 2918.7, 2888.3, 2849.8, 1784.3, 1744.5, 1694.6, 1611.7, 1599.9; **R<sub>f</sub>** = 0.39 (65:35 Hexane–EtOAc); **HRMS (ESI)**: C<sub>18</sub>H<sub>15</sub>NO<sub>3</sub> requires [M+H]<sup>+</sup> 294.1125, found 294.1124.





**(3*R*\*,3'*R*\*)-1-Methyl-3'-phenyl-1,2-dihydrospiro[indole-3,2'-oxolane]-2,5'-dione (25b)** (37 mg, 0.13 mmol, 26%) -  $\delta_{\text{H}}$  (**500MHz, CDCl<sub>3</sub>**): 7.27 – 7.19 (4H, m, Ar-H), 7.04 – 6.95 (2H, m, Ar-H), 6.78 – 6.67 (2H, m, Ar-H), 6.27 (1H, ddd, *J* 7.6, 1.3 and 0.6, Ar-H), 3.97 (1H, dd, *J* 8.7 and 4.5, 3'-H), 3.71 (1H, ddd, *J* 17.6 and 8.7, 4'-H<sub>b</sub>), 3.21 (3H, s, NCH<sub>3</sub>), 3.07 (1H, dd, *J* 17.6 and 4.5, 4'-H<sub>a</sub>);  $\delta_{\text{C}}$  (**125MHz, CDCl<sub>3</sub>**): 176.16 (C-5'), 174.38 (C-2), 143.92 (Ar), 137.14 (Ar), 130.93 (Ar), 128.81 (Ar), 128.33 (Ar), 128.04 (Ar), 126.20 (Ar), 123.37 (Ar), 122.85 (Ar), 108.64 (Ar), 86.12 (C-3), 48.03 (C-3'), 34.33 (C-4'), 26.60 (NCH<sub>3</sub>); **IR**  $\nu_{\text{max}}/\text{cm}^{-1}$  (**film**): 2982.4, 2918.2, 2888.4, 1784.7, 1744.7, 1694.5, 1612.6, 1599.9; **R<sub>f</sub>** = 0.29 (65:35 Hexane–EtOAc); **HRMS (ESI)**: C<sub>18</sub>H<sub>15</sub>NO<sub>3</sub> requires [M+H]<sup>+</sup> 294.1125, found 294.1120.

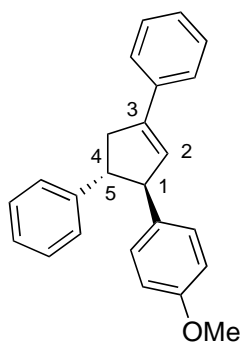
***cis*-5-(4-Bromophenyl)-4-(4-methoxyphenyl)oxolan-2-one (26)**



4-Bromobenzaldehyde (229 mg, 1.24 mmol), 4-methoxycinnamaldehyde (100 mg, 0.62 mmol) and 1,3-bis(2,4,6-trimethylphenyl)imidazolium chloride **11** (17.0 mg, 0.05 mmol, 8 mol%) added to flask, and THF (2 mL) added. DBU (10.0  $\mu\text{L}$ , 0.05 mmol, 7 mol%) added and solution left to stir for 24 hours at room temperature. The reaction mixture was concentrated under reduced pressure to give a crude oil (89:11 dr in favour of the syn product). The crude material was purified by flash column chromatography, eluting with 92:8 Hexane–EtOAc, to afford the title compound<sup>101</sup> (85 mg, 0.246 mmol).  $\delta_{\text{H}}$  (**400MHz, CDCl<sub>3</sub>**): 7.27 (2H, d, *J* 8.5,

5-Ph 3-H and 5-H), 6.77 (2H, d,  $J$  8.4, 5-Ph 2-H and 6-H), 6.72 (2H, d,  $J$  8.7, 4-Ph 2-H and 6-H), 6.66 (2H, d,  $J$  8.8, 6.72 (2H, d,  $J$  8.7, 4-Ph 3-H and 5-H), 5.72 (1H, d,  $J$  6.7, 5-H), 3.98 (1H, q,  $J$  6.2, 4-H), 3.72 (3H, s,  $OCH_3$ ), 3.02 (1H, dd,  $J$  17.4 and 8.2, 3-H<sub>a</sub>), 2.85 (1H, dd,  $J$  17.5 and 6.0, 3-H<sub>b</sub>);  $\delta_c$  (**125MHz, CDCl<sub>3</sub>**): 176.6 (C-2), 159.0 (Ar), 134.9 (Ar), 131.2 (Ar-H), 129.0 (Ar-H), 128.4 (Ar), 127.5 (Ar-H), 122.0 (Ar), 114.0 (Ar-H), 84.2 (C-5), 55.3 ( $H_3CO$ ), 46.1 (C-4), 35.3 (C-3);  $R_f$  = 0.11 (80:20 Hexane–EtOAc); **HRMS (ESI)**:  $C_{17}H_{15}BrO_3$  requires  $[M+H]^+$  347.0277, found 347.0275.

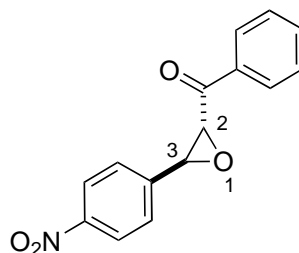
### 1-[(1*R*\*, 5*R*\*)-3,5-Diphenylcyclopent-2-en-1-yl]-4-methoxybenzene (27)



DBU (8.0  $\mu$ L, 0.04 mmol, 12 mol%) was added to a suspension of 1,3-bis(2,4,6-trimethylphenyl) imidazolium chloride **11** (11 mg, 0.02 mmol, 6 mol%) in THF (2 mL). This was followed by addition of 4-methoxycinnamaldehyde (79 mg, 0.48 mmol) and chalcone (100 mg, 0.34 mmol). The resulting solution was stirred for 8 hours at room temperature, with an initial green colour of the reaction changing to dark blue upon completion. The reaction mixture was passed through a short pad of Celite, the solvent removed, and the residue purified by column chromatography, eluting with 98:2 Hexane–EtOAc, to afford the title compound<sup>102</sup> as a viscous yellow oil (86 mg, 0.26 mmol, 77 %).  $\delta_H$  (**400MHz, CDCl<sub>3</sub>**): 7.48 (2H, dd,  $J$  7.0 and 1.6, Ar-H), 7.31 (2H, td,  $J$  7.6 and 1.7, Ar-H), 7.29-7.10 (6H, m, Ar-H), 7.02 (2H, dd,  $J$  8.6 and 1.9, Ar-H), 6.77 (2H, dd,  $J$  8.7 and 2.1, Ar-H), 6.19 (1H, t,  $J$  2.0, 2-H), 4.03 (1H, m, 1-H) 3.71 (3H, s,  $H_3CO$ ), 3.41-3.22 (2H, m, 4-H<sub>a/b</sub> and 5-H), 2.98-2.92 (1H, m, 4-H<sub>a/b</sub>);  $\delta_c$  (**100MHz, CDCl<sub>3</sub>**): 158.4 (Ar), 145.6 (Ar), 142.0 (Ar), 137.1 (Ar), 136.1 (Ar), 128.6 (Ar), 128.5 (Ar),

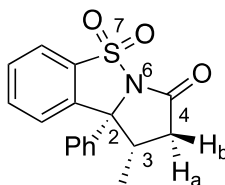
127.6 (Ar), 127.4 (C-2), 126.3 (Ar), 125.9 (Ar), 114.0 (Ar), 60.1 (C-1), 55.3 (H<sub>3</sub>CO), 54.8 (C-5), 42.0 (C-4); **R<sub>f</sub>** = 0.73 (50:50 Hexane–EtOAc); **HRMS (ESI)**: C<sub>24</sub>H<sub>22</sub>O requires [M+H]<sup>+</sup> 327.1743, found 327.1744.

**(2*R*\*, 3*S*\*)-2-benzoyl-3-(4-nitrophenyl)oxirane (29)**



$\alpha$ -bromoacetophenone (100 mg, 0.50 mmol), 4-nitrobenzaldehyde (83 mg, 0.55 mmol) and thiamine hydrochloride **28** (17 mg, 0.05 mmol) placed in a flask and flushed with nitrogen. DMSO-d<sub>6</sub> (2 mL) and DBU (0.015 mL, 0.10 mmol) added and left to stir at room temperature for 18 hours. Reaction quenched with water (10 mL) at 0 °C, then extracted with EtOAc (3 x 20 mL). Organic extracts washed with brine (3 x 20 mL), dried over sodium sulphate and evaporated to dryness, before purification by flash column chromatography, eluting with 75:25 Petrol–EtOAc, to give the title compound<sup>103</sup> as an amorphous off-white solid (36 mg, 0.11 mmol, 22%).  $\delta_{\text{H}}$  (500MHz, CDCl<sub>3</sub>): 8.27 (2H, d, *J* 8.8, Ar-H), 8.04 – 7.98 (2H, m, Ar-H), 7.67 – 7.63 (1H, m, Ar-H), 7.58 – 7.54 (2H, m, Ar-H), 7.53 – 7.49 (2H, m, Ar-H), 4.28 (1H, d, *J* 1.8, 2-H), 4.21 (1H, d, *J* 1.8, 3-H);  $\delta_{\text{C}}$  (125MHz, CDCl<sub>3</sub>): 192.1 (C-1), 149.8 (Ar), 142.9 (Ar), 135.4 (Ar), 134.50 (Ar), 129.18 (Ar), 128.57 (Ar), 126.8 (Ar), 124.2 (Ar), 61.0 (C-2), 58.2 (C-3); **R<sub>f</sub>** = 0.79 (34:66 EtOAc–Petrol); **HRMS (ESI)**: C<sub>15</sub>H<sub>11</sub>NO<sub>4</sub> requires [M+Na]<sup>+</sup> 292.0580, found 292.0583.

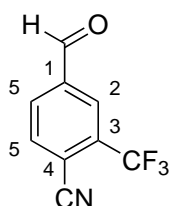
**(2*R*\*,3*S*\*)-3-methyl-2-phenyl-7λ<sup>6</sup>-thia-6-azatricyclo [6.4.0.0<sup>2,6</sup>] dodeca-1(12),8,10-triene-5,7,7-trione (31)**



To a flask with a magnetic stirrer bar was added 3-phenyl-1λ<sup>6</sup>,2-benzothiazole-1,1-dione **30** (98 mg, 0.40 mmol). Crotonaldehyde (36 μL, 0.44 mmol), DCM (1 mL) and a solution of the triazolium catalyst **12** (2.63 mg, 0.01 mmol) in DCM (1 mL) were added. Finally, DBU (12 μL, 0.080 mmol) was added, and the flask stirred at ambient temperature for 24 hours. The reaction mixture was then purified by flash column chromatography (25:50:1, Hexane–DCM–Acetone) to obtain the title compound<sup>104</sup> as an off white amorphous solid (96 mg, 0.32 mmol, 80%).  $\delta_{\text{H}}$  (**500MHz, CDCl<sub>3</sub>**): 7.87 (1H, dd, *J* 8.3 and 1.0, Ar-H), 7.78 – 7.74 (2H, m, Ar-H), 7.60 (1H, td, *J* 7.6 and 1.0, Ar-H), 7.51 – 7.47 (2H, m, Ar-H), 7.43 – 7.38 (2H, m, Ar-H), 7.37 – 7.32 (1H, m, Ar-H), 2.99 (1H, ddd, *J* 12.9, 7.5 and 6.7, 3-H), 2.69 (1H, dd, *J* 17.0 and 7.5, 4-H<sub>a</sub>), 2.50 (1H, dd, *J* 17.0 and 12.9, 4-H<sub>b</sub>), 1.11 (3H, d, *J* 6.7, CH<sub>3</sub>);  $\delta_{\text{C}}$  (**125MHz, CDCl<sub>3</sub>**): 170.4 (C-5), 141.9 (Ar), 136.4 (Ar), 135.3 (Ar), 133.8 (Ar), 130.1 (Ar), 129.0 (2 x Ar), 128.7 (Ar), 126.6 (2 x Ar), 123.9 (Ar), 122.4 (Ar), 75.1 (C-2), 42.3 (C-3), 40.4 (C-4), 16.5 (CH<sub>3</sub>); **IR**  $\nu_{\text{max}}$ /**cm<sup>-1</sup>** (**film**): 3066.7, 2981.8, 2922.2, 2887.7, 1744.3, 1694.0, 1598.8; **R<sub>f</sub>** = 0.41 (25:50:1 Hexane–DCM–Acetone); **HRMS (ESI)**: C<sub>17</sub>H<sub>15</sub>NO<sub>3</sub>S requires [M+H]<sup>+</sup> 314.0845, found 314.0847.

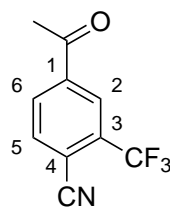
### 6.2.3 Synthesis of Round 1 Substrates

#### 4-Formyl-2-(trifluoromethyl)benzonitrile (A3)



To a solution of 4-iodo-2-(trifluoromethyl)benzonitrile (2.35 g, 5.05 mmol) in THF (31.6 mL) at 0 °C, isopropylmagnesium chloride lithium chloride (1.3 M solution in THF, 7.30 mL, 9.48 mmol) was added dropwise and the mixture stirred for 45 minutes. Piperidine-1-carbaldehyde (1.05 mL, 9.48 mmol) was added and stirring continued at 0 °C for 90 minutes. TLC analysis showed conversion to products. Saturated ammonium chloride solution (30 mL) was added to quench, and the mixture extracted with EtOAc (2 x 30 mL). The organic extracts were dried with magnesium sulphate, filtered and concentrated under reduced pressure, then purified by flash column chromatography (50:50, DCM-toluene) to give the title compound<sup>66</sup> as a brown amorphous solid (790 mg, 3.97 mmol, 50%).  $\delta_{\text{H}}$  (500MHz,  $\text{CDCl}_3$ ): 10.15 (1H, s, CHO), 8.30 (1H, d,  $J$  1.6, 3-H), 8.20 (1H, dd,  $J$  7.9 and 1.6, 5-H), 8.06 (1H, d,  $J$  7.9, 6-H);  $\delta_{\text{C}}$  (125MHz,  $\text{CDCl}_3$ ): 189.2 (C=O), 138.8 (C-4), 135.8 (C-6), 134.1 (q,  $J$  33.6, C-2), 132.9 (C-5), 127.2 (q,  $J$  4.6, C-3), 122.0 (q,  $J$  274.3,  $\text{CF}_3$ ), 115.0 (q,  $J$  2.1, C-1), 114.6 (CN); IR  $\nu_{\text{max}}$  (neat)/ $\text{cm}^{-1}$ : 3084.7, 3050.3, 2920.5, 2869.2, 2235.1, 1703.5, 1614.1;  $R_{\text{f}}$  = 0.33 (50:50 DCM-toluene).

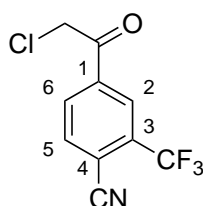
#### 4-Acetyl-2-(trifluoromethyl)benzonitrile (A4)



4-Iodo-2-trifluoromethylbenzonitrile (1.29 g, 4.34 mmol), tri-n-butyl-(1-ethoxyvinyl)tin (1.62 mL, 1.1 mmol), palladium(II) acetate (29 mg, 0.13 mmol, 3 mol%), DABCO (29 mg, 0.26 mmol), potassium fluoride (755 mg, 13.0 mmol) were stirred in 1,4-dioxane (16 mL) at 99 °C for 16 hours. The mixture was then cooled and filtered through celite, washing with ethyl acetate. The filtrate was then washed with water (25 mL) and brine (25 mL) before drying with magnesium sulphate, filtering and evaporating. Hydrochloric acid (2 M, 9 mL) and THF (25 mL) were added to the residue in the flask, and the solution stirred at room temperature overnight. Saturated

sodium hydrogen carbonate solution (25 mL) was added slowly, and the mixture extracted with ethyl acetate (2 x 20 mL). The organic extracts were dried with magnesium sulphate, filtered and evaporated, and the crude product purified by flash column chromatography, eluting with 70:28:2 Hexane–Ethyl Acetate–Triethylamine to obtain the *title compound* as pale orange amorphous solid (686 mg, 3.22 mmol, 74%).  $\delta_{\text{H}}$  (500MHz,  $\text{CDCl}_3$ ): 8.34 (1H, d,  $J$  1.6, 2-H), 8.22 (1H, dd,  $J$  8.1 and 1.6, 5-H), 7.98 (1H, d,  $J$  8.1, 6-H), 2.69 (3H, s,  $\text{CH}_3$ );  $\delta_{\text{C}}$  (125MHz,  $\text{CDCl}_3$ ): 195.1 (C=O), 140.1 (C-4), 135.5 (C-6), 133.6 (q,  $J$  33.4, C-2), 131.7 (C-5), 126.3 (q,  $J$  4.7, C-3), 122.1 (q,  $J$  274.3,  $\text{CF}_3$ ), 114.8 (CN), 113.9 (m, C-1), 26.9 ( $\text{CH}_3$ ); IR  $\nu_{\text{max}}$  (neat)/ $\text{cm}^{-1}$ : 3117.1, 3089.8, 3053.5, 2924.8, 2233.1, 1693.7, 1611.4, 1572.5;  $R_{\text{f}}$  = 0.25 (75:25 Hexanes–Ethyl Acetate); HRMS (ESI):  $\text{C}_{10}\text{H}_6\text{F}_3\text{NO}$  requires  $[\text{M}+\text{H}]^+$  214.0474, found 214.0471.

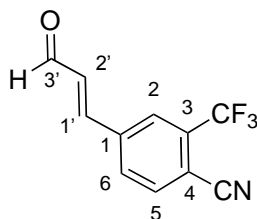
#### 1-(Chloroacetyl)-2-(trifluoromethyl)benzonitrile (A5)



4-Acetyl-2-(trifluoromethyl)benzonitrile (345 mg, 1.62 mmol) and benzyltrimethylammonium dichloriodate (1.13 mg, 3.24 mmol) were dissolved in THF (8 mL) and stirred for 24 hours at room temperature. The reaction mixture was then evaporated, and ethyl acetate (20 mL) and sodium thiosulphate solution (5% w/v, 20 mL) were added to the residue. The layers were separated, and the organic layer dried over magnesium sulphate, filtered and concentrated under reduced pressure. The crude product was then purified by flash column chromatography, eluting with 84:16 Hexane–Ethyl Acetate to give the *title compound* as a straw coloured amorphous solid (290 mg, 1.17 mmol, 72%).  $\delta_{\text{H}}$  (500MHz,  $\text{CDCl}_3$ ): 8.35 (1H, d,  $J$  1.8, 3-H), 8.26 (1H, dd,  $J$  8.1 and 1.8, 5-H), 8.02 (1H, d,  $J$  8.1, 6-H), 4.68 (2H, s,  $\text{CH}_2$ );  $\delta_{\text{C}}$  (125MHz,  $\text{CDCl}_3$ ): 189.0 (C=O), 137.2 (C-4), 135.5 (C-6), 133.9 (C-2), 132.0 (C-5), 126.6 (q,  $J$  4.8, C-3), 121.8 (q,  $J$  274.0,  $\text{CF}_3$ ), 114.7

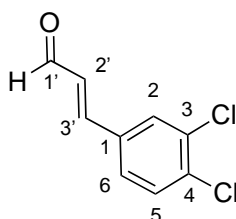
(m, C-1), 114.4 (CN), 45.0 (CH<sub>2</sub>Cl); **IR**  $\nu_{\max}$  (neat)/cm<sup>-1</sup>: 3112.0, 3077.5, 3048.4, 2939.2, 2233.8, 1715.9, 1611.8, 1569.4; **R<sub>f</sub>** = 0.39 (75:25 Hexane–Ethyl Acetate); **HRMS (ESI)**: C<sub>10</sub>H<sub>5</sub>ClF<sub>3</sub>NO requires [M+H]<sup>+</sup> 248.0085, found 248.0081.

#### 4-[(1*E*)-3-Oxoprop-1-en-1-yl]-2-(trifluoromethyl)benzonitrile (A1)



4-Formyl-2-(trifluoromethyl)benzonitrile (290 mg, 1.46 mmol) and triphenylphosphoranylidene acetaldehyde (444 mg, 1.46 mmol) were dissolved in toluene (5 mL) and stirred at 70 °C for 20 hours. Conversion to products was confirmed by TLC and the mixture concentrated under reduced pressure, then purified by flash column chromatography (50:50, Toluene–DCM) to obtain the *title compound* as an amorphous pale orange solid (192 mg, 0.85 mmol, 58%).  $\delta_{\text{H}}$  (500MHz, CDCl<sub>3</sub>): 9.79 (1H, d, *J* 7.3, 3'-H), 7.95 (1H, s, 3-H), 7.92 (1H, d, *J* 8.1, 5-H), 7.86 (1H, d, *J* 8.1, 6-H), 7.51 (1H, d, *J* 16.1, 1'-H), 6.83 (1H, dd, *J* 16.1, 7.3, 2'-H);  $\delta_{\text{C}}$  (125MHz, CDCl<sub>3</sub>): 192.4 (C-3'), 147.4 (C-1'), 138.8 (C-4), 135.6 (C-2'), 134.0 (q, *J* 33.0, C-2), 132.6 (C-5), 131.3 (C-6), 126.3 (q, *J* 4.6, C-3), 122.1 (q, *J* 274.0, CF<sub>3</sub>), 115.0 (CN), 111.7 (m, C-1); **IR**  $\nu_{\max}$  (neat)/cm<sup>-1</sup>: 3059.7, 2918.3, 2823.5, 2750.1, 2232.2, 1673.0, 1627.1, 1561.2, 1497.7; **R<sub>f</sub>** = 0.27 (50:50 Toluene–DCM); **HRMS (ESI)**: C<sub>11</sub>H<sub>6</sub>F<sub>3</sub>NO requires [M+H]<sup>+</sup> 226.0474, found 226.0471.

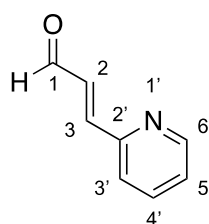
#### (2*E*)-3-(3,4-Dichlorophenyl)prop-2-enal (A2)



3,4-Dichlorobenzaldehyde (1.00 g, 5.72 mmol) and triphenylphosphoranylidene acetaldehyde (1.74 g, 5.72 mmol) were dissolved in toluene (15 mL) and stirred at 70 °C for 24 hours. Conversion to products was confirmed by TLC, and the mixture evaporated before purification by flash column chromatography (90:10 Hexanes–EtOAc) to obtain the title compound<sup>123</sup> as an amorphous white solid (670 mg, 3.35 mmol, 59%).  $\delta_{\text{H}}$  (**500MHz, CDCl<sub>3</sub>**): 9.70 (1H, d, *J* 7.5, 1'-H), 7.64 (1H, d, *J* 2.1, 2-H), 7.50 (1H, d, *J* 8.3, 5-H), 7.40 (1H, dd, *J* 8.3 and 2.1, 6-H), 7.37 (1H, d, *J* 16.0, 3'-H), 6.68 (1H, dd, *J* 16.0 and 7.5, 2'-H);  $\delta_{\text{C}}$  (**125MHz, CDCl<sub>3</sub>**): 193.1 (C-1), 149.5 (C-3), 135.3 (C-1'), 134.1 (C-4), 133.7 (C-3), 131.2 (C-5), 130.1 (C-2), 130.0 (C-2'), 127.3 (C-6); **IR**  $\nu_{\text{max}}$  (**neat**)/**cm<sup>-1</sup>**: 3312.0, 3090.1, 3070.5, 2849.7, 2760.1, 1682.2, 1667.1, 1626.5, 1586.8, 1554.0; **R<sub>f</sub>** = 0.27 (90:10 Hexanes–EtOAc); **HRMS (ESI)**: C<sub>9</sub>H<sub>6</sub>Cl<sub>2</sub>O requires [M+H]<sup>+</sup> 200.9874, found 200.9868.

#### 6.2.4 Synthesis of Round 2 co-substrates

##### (2E)-3-(Pyridin-2-yl)prop-2-enal (D1)

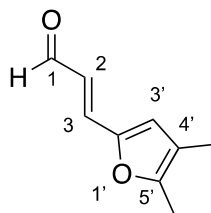


Pyridine-2-carboxaldehyde (238  $\mu\text{L}$ , 2.50 mmol) and triphenylphosphoranylidene acetaldehyde (761 mg, 2.50 mmol) were dissolved in THF (7.5 mL) and stirred at 70 °C for 24 hours. Conversion to products was confirmed by TLC, and the mixture evaporated before purification by flash column chromatography (50:50 Pentane–Diethyl Ether) to obtain the title compound<sup>124</sup> as an amorphous brown solid (75 mg, 0.56 mmol, 22%).  $\delta_{\text{H}}$  (**400MHz, CDCl<sub>3</sub>**): 9.79 (1H, d, *J* 7.7, 1-H), 8.69 (1H, dd, *J* 4.8 and 1.7, 6'-H), 7.76 (1H, td, *J* 7.8 and 1.7, 4'-H), 7.54 (1H, d, *J* 7.8, 3'-H), 7.52 (1H, d, *J* 15.8, 3-H), 7.31 (1H, dd, *J* 7.8 and 4.8, 5'-H), 7.08 (1H, dd, *J* 15.8 and 7.8, 2-H);  $\delta_{\text{C}}$  (**100MHz, CDCl<sub>3</sub>**): 193.7 (C-1), 152.9 (C-2'), 151.3 (C-



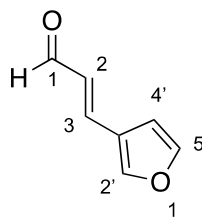
3), 150.5 (C-6'), 137.0 (C-4'), 131.8 (C-2), 124.9 (C-5'), 124.3 (C-3'); **IR**  $\nu_{\max}$  (**neat**)/ $\text{cm}^{-1}$ : 3045.8, 3006.3, 2920.1, 2846.0, 2756.6, 1668.9, 1629.3, 1579.5, 1565.4; **R<sub>f</sub>** = 0.22 (50:50 Hexanes–Diethyl Ether); **HRMS (ESI)**:  $\text{C}_8\text{H}_7\text{NO}$  requires  $[\text{M}+\text{H}]^+$  267.1128, found 267.1126.

**(2E)-3-(4,5-Dimethylfuran-2-yl)prop-2-enal (D2)**



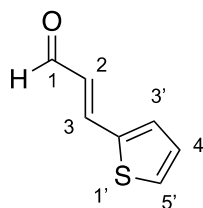
4,5-Dimethylfuran-2-carbaldehyde (305  $\mu\text{L}$ , 2.5 mmol) and triphenylphosphoranylidene acetaldehyde (761 mg, 2.5 mmol) were dissolved in THF (7.5 mL) and stirred at 70  $^{\circ}\text{C}$  for 24 hours. Conversion to products was confirmed by TLC, and the mixture evaporated before purification by flash column chromatography (80:20 Hexane–Diethyl Ether) to obtain the *title compound* as a deep red oil (148 mg, 0.99 mmol, 40%).  $\delta_{\text{H}}$  (**400MHz,  $\text{CDCl}_3$** ): 9.55 (1H, d,  $J$  7.9, 1-H), 7.08 (1H, d,  $J$  15.5, 3-H), 6.57 (1H, s, 3'-H), 6.47 (1H, dd,  $J$  15.5 and 7.9, 2-H), 2.28 (3H, s, 4'- $\text{CH}_3$ ), 1.97 (3H, s, 5'- $\text{CH}_3$ );  $\delta_{\text{C}}$  (**100MHz,  $\text{CDCl}_3$** ): 193.0 (C-1), 153.1 (C-2'), 148.12 (C-5'), 138.1 (C-3), 124.2 (C-2), 121.0 (3'-H), 118.5 (C-4'), 12.0 (C-5 Methyl), 9.8 (C-4 Methyl); **IR**  $\nu_{\max}$  (**neat**)/ $\text{cm}^{-1}$ : 3087.6, 2953.5, 2922.7, 2848.2, 1652.9, 1630.8, 1591.9, 1514.6; **R<sub>f</sub>** = 0.62 (50:50 Hexanes–Diethyl Ether); **HRMS (ESI)**:  $\text{C}_9\text{H}_{10}\text{O}_2$  requires  $[\text{M}+\text{H}]^+$  151.0754, found 151.0749.

**(2E)-3-(Furan-3-yl)prop-2-enal (D3)**

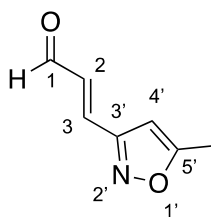


Furan-3-carbaldehyde (216  $\mu\text{L}$ , 2.5 mmol) and triphenylphosphoranylidene acetaldehyde (761 mg, 2.5 mmol) were dissolved in THF (7.5 mL) and stirred at 70 °C for 24 hours. Conversion to products was confirmed by TLC, and the mixture evaporated before purification by flash column chromatography (80:20 Hexane–Diethyl Ether) to obtain the title compound<sup>125</sup> as a brown oil (72 mg, 0.59 mmol, 24%).  $\delta_{\text{H}}$  (400MHz,  $\text{CDCl}_3$ ): 9.61 (1H, d,  $J$  7.8, 1-H), 7.75 (1H, s, 2'-H), 7.47 (1H, d,  $J$  1.9, 5'-H), 7.39 (1H, d,  $J$  15.7, 3-H), 6.61 (1H, d,  $J$  1.9, 4'-H), 6.43 (1H, dd,  $J$  15.7 and 7.8, 2-H);  $\delta_{\text{C}}$  (100MHz,  $\text{CDCl}_3$ ): 193.4 (C-1), 145.4 (C-2'), 145.0 (C-5'), 142.5 (C-3), 128.8 (C-2), 122.9 (C-3'), 107.6 (C-4'); IR  $\nu_{\text{max}}$  (neat)/ $\text{cm}^{-1}$ : 3123.5, 3048.4, 2820.4, 2732.6, 1760.1, 1668.5, 1626.3, 1565.8, 1553.7;  $R_{\text{f}}$  = 0.54 (50:50 Hexanes–Diethyl Ether).

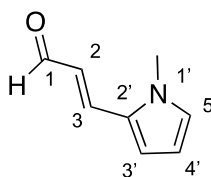
#### (2E)-3-(Thiophen-2-yl)prop-2-enal (D4)



Thiophene-2-carbaldehyde (256 mg, 2.0 mmol) and triphenylphosphoranylidene acetaldehyde (761 mg, 2.1 mmol) were dissolved in chloroform (7 mL) and stirred at 70 °C for 24 hours. Conversion to products was confirmed by TLC, and the mixture evaporated before purification by flash column chromatography (85:15 Pentane–Diethyl Ether) to obtain the title compound<sup>126</sup> as a brown oil (128 mg, 0.93 mmol, 47%).  $\delta_{\text{H}}$  (400MHz,  $\text{CDCl}_3$ ): 9.62 (1H, d,  $J$  7.7, 1-H), 7.58 (1H, d,  $J$  15.6, 3-H), 7.50 (1H, d,  $J$  5.0, 5'-H), 7.36 (1H, dd,  $J$  3.7 and 1.0, 3'-H), 7.11 (1H, dd,  $J$  5.1 and 3.7, 4'-H), 6.51 (1H, dd,  $J$  15.6 and 7.7, 2-H);  $\delta_{\text{C}}$  (100MHz,  $\text{CDCl}_3$ ): 193.0 (C-1), 144.5 (C-3), 139.4 (C-2'), 132.2 (C-3'), 130.5 (C-5'), 128.6 (C-4'), 127.5 (C-2); IR  $\nu_{\text{max}}$  (neat)/ $\text{cm}^{-1}$ : 3324.98, 3104.0, 2814.6, 2721.6, 1662.9, 1606.4, 1513.1;  $R_{\text{f}}$  = 0.64 (50:50 Pentane–Diethyl Ether); HRMS (ESI):  $\text{C}_7\text{H}_6\text{O}_2\text{S}$  requires  $[\text{M}-\text{H}]^-$  153.0016, found 153.0011.

**(2E)-3-(5-Methyl-1,2-oxazol-3-yl)prop-2-enal (D5)**

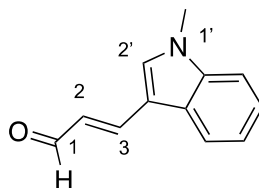
5-Methylisoxazole-3-carbaldehyde (444 mg, 4.0 mmol) and triphenylphosphoranylidene acetaldehyde (1.278 g, 4.2 mmol) were dissolved in THF (12.5 mL) and stirred at 70 °C for 24 hours. Conversion to products was confirmed by TLC, and the mixture evaporated before purification by flash column chromatography (85:15 Hexane–Diethyl Ether) to obtain the title compound<sup>124</sup> as an amorphous white solid (420 mg, 3.06 mmol, 77%).  $\delta_{\text{H}}$  (400MHz,  $\text{CDCl}_3$ ): 9.72 (1H, d,  $J$  7.7, 1-H), 7.47 (1H, d,  $J$  16.2, 3-H), 6.62 (1H, dd,  $J$  16.2 and 7.7, 2-H), 6.23 (1H, s, 4'-H), 2.45 (3H, s, 5'- $\text{CH}_3$ );  $\delta_{\text{C}}$  (100MHz,  $\text{CDCl}_3$ ): 192.9 (C-1), 171.0 (C-5'), 159.8 (C-3'), 138.9 (C-3), 134.1 (C-2), 99.5 (C-4'), 12.3 (5'- $\text{CH}_3$ ); IR  $\nu_{\text{max}}$  (neat)/ $\text{cm}^{-1}$ : 3338.8, 3128.6, 3040.1, 2854.3, 2836.4, 2752.0, 1681.0, 1597.1;  $R_f$  = 0.40 (75:25 Hexanes–ethyl Ether); HRMS (ESI):  $\text{C}_7\text{H}_7\text{NO}_2$  requires  $[\text{M}+\text{H}]^+$  138.0555, found 138.0544.

**(2E)-3-(1-Methyl-1H-pyrrol-2-yl)prop-2-enal (D6)**

*N*-Methylpyrrole (500 mg, 6.2 mmol) and 3-dimethylacrolein (561  $\mu\text{L}$ , 5.6 mmol) were dissolved in chloroform (2 mL), before dropwise addition of a solution of phosphoryl chloride (517  $\mu\text{L}$ , 5.6 mmol) in chloroform (1 mL) at  $-10$  °C. After 1 hour, a 30% solution of sodium perchlorate (3 mL) was added, and the mixture filtered and evaporated under reduced pressure. The residue was then stirred vigorously with an aqueous solution of potassium

hydroxide (1 mL, 5 M) and chloroform (6 mL). After 2 hours, the mixture was filtered, the phases separated, and the organic layer washed twice with water (2 x 5 mL). The organic layer was then evaporated and purified by flash column chromatography (DCM) to obtain the title compound<sup>127</sup> as an amorphous off-white solid (234 mg, 1.73 mmol, 28%).  $\delta_{\text{H}}$  (**400MHz, CDCl<sub>3</sub>**): 9.54 (1H, d, *J* 7.7, 1-H), 7.31 (1H, d, *J* 15.5, 3-H), 6.87 – 6.83 (1H, m, 5'-H), 6.74 (1H, d, *J* 4.1, 3'-H), 6.43 (1H, dd, *J* 15.5 and 7.7, 2-H), 6.25 – 6.17 (1H, m, 4'-H), 3.74 (3H, s, NCH<sub>3</sub>);  $\delta_{\text{C}}$  (**100MHz, CDCl<sub>3</sub>**): 193.1 (C-1), 139.9 (C-3), 129.3 (C-2'), 129.1 (C-5'), 123.6 (C-2), 114.7 (C-3'), 110.2 (C-4'), 34.7 (NCH<sub>3</sub>); **IR**  $\nu_{\text{max}}$  (**neat**)/cm<sup>-1</sup>: 3072.8, 2916.8, 2847.1, 1653.1, 1607.8, 1521.2; **R<sub>f</sub>** = 0.39 (DCM); **HRMS (ESI)**: C<sub>8</sub>H<sub>9</sub>NO requires [M+Na]<sup>+</sup> 158.0573, found 158.0576.

**(2E)-3-(1-Methyl-1H-indol-3-yl)prop-2-enal (D7)**



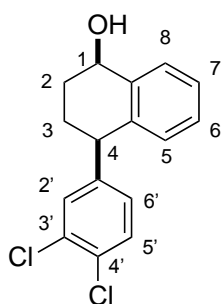
*N*-Methylindole (420  $\mu$ L, 3.29 mmol) and 3-dimethylacrolein (300  $\mu$ L, 2.99 mmol) were dissolved in chloroform (1.5 mL), before dropwise addition of a solution of phosphoryl chloride (277  $\mu$ L, 5.60 mmol) in chloroform (0.5 mL) at  $-10$  °C. After 1 hour, a 30% solution of sodium perchlorate (2 mL) was added, and the mixture filtered and evaporated under reduced pressure. The residue was then stirred vigorously with an aqueous solution of potassium hydroxide (1 mL, 5M) and chloroform (4 mL). After 2 hours, the mixture was filtered, the phases separated, and the organic layer washed twice with water (5 mL). The organic layer was then evaporated and purified by flash column chromatography (DCM) to obtain the title compound<sup>128</sup> as an amorphous off-white solid (173 mg, 0.93 mmol, 28%).  $\delta_{\text{H}}$  (**500MHz, CDCl<sub>3</sub>**): 9.60 (1H, d, *J* 7.8, 1-H), 7.89 (1H, dt, *J* 7.8 and 1.0, Ar-H), 7.64 (1H, d, *J* 15.7, 3-H), 7.44 (1H, s, 2'-H), 7.40 – 7.28 (3H, m, Ar-H), 6.74 (1H, dd, *J* 15.7 and 7.8, 2-H), 3.84 (3H, s, NCH<sub>3</sub>);  $\delta_{\text{C}}$  (**125MHz, CDCl<sub>3</sub>**): 194.2 (C-1),

146.4 (C-3), 138.4 (Ar), 134.2 (Ar), 126.0 (Ar), 124.3 (C-2), 123.6 (Ar), 122.1 (Ar), 120.6 (Ar-H), 112.5 (C-3'), 110.3 (C-2'), 33.5 (NCH<sub>3</sub>); **IR**  $\nu_{\text{max}}$  (neat)/cm<sup>-1</sup>: 3090.2, 3053.6, 2910.0, 2817.2, 2725.6, 1649.1, 1605.0, 1570.9, 1520.2; **R<sub>f</sub>** = 0.46 (DCM); **HRMS (ESI)**: C<sub>12</sub>H<sub>11</sub>NO requires [M+H]<sup>+</sup> 186.0913, found 186.0911.

### 6.2.5 Syntheses for Compounds Isolated from ADS

#### 4-(3,4-Dichlorophenyl)-1,2,3,4-tetrahydronaphthalen-1-ol

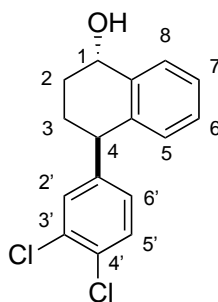
To a stirring mixture of 4-(3,4-dichlorophenyl)-1-tetralone (200 mg, 0.68 mmol) in methanol (1.5 mL) was added sodium borohydride (39 mg, 1.02 mmol) in portions. The mixture was stirred at ambient temperature for 3 hours. Water was added and the mixture evaporated under reduced pressure to remove the volatile components. The remaining aqueous portion was extracted with ethyl acetate. The organic phase was then washed with water, dried with sodium sulfate and evaporated to dryness under reduced pressure to obtain the crude alcohol (50:50 mixture of diastereomers determined *via* <sup>1</sup>H NMR). Purification by flash column chromatography (75:25 Hexane–EtOAc) gave the diastereomers<sup>114</sup>, *rac*-**35a** (73 mg, 0.25 mmol, 37%) and *rac*-**35b** (82 mg, 0.28 mmol, 41%) as colourless oils.



#### (1*R*\*,4*R*\*)-4-(3,4-Dichlorophenyl)-1,2,3,4-tetrahydronaphthalen-1-ol

(*rac*-**35a**) -  $\delta_{\text{H}}$  (500MHz, CDCl<sub>3</sub>): 7.46 (1H, dd, *J* 7.8 and 1.4, 8-H), 7.36 (1H, d, *J* 8.2, 5'-H), 7.28 (2H, m, 2'-H and 7-H), 7.18 (1H, td, *J* 7.6 and 1.4, 6-H), 6.98 (1H, dd, *J* 8.2 and 2.1, 6'-H), 6.82 (1H, app dt, *J* 7.6 and 1.4, 5-H), 4.87 (1H, br q, *J* 4.7, 1-H), 3.99 (1H, dd, *J* 9.0 and 5.6, 4-H), 2.23 – 1.95 (4H, m,

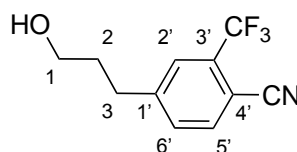
2-H and 3-H), 1.90 (1H, br d,  $J$  4.7, OH);  $\delta_c$  (**125MHz, CDCl<sub>3</sub>**): 147.1 (C-1'), 139.1 (C-8a), 138.6 (C-4a), 132.5 (C-4'), 130.8 (Ar), 130.5 (Ar), 130.4 (C-3'), 129.9 (Ar), 129.2 (Ar), 128.4 (Ar), 128.3 (Ar), 127.2 (Ar), 68.0 (C-1), 45.2 (C-4), 30.2 (C-2), 28.3 (C-3); **IR**  $\nu_{\max}$  (**neat**)/**cm<sup>-1</sup>**: 3311.7, 3023.2, 2939.3, 2865.1, 2830.4, 1588.6, 1560.6; **R<sub>f</sub>** = 0.50 (75:25 Hexanes–EtOAc); **HRMS (ESI)**: C<sub>16</sub>H<sub>14</sub>Cl<sub>2</sub>O requires [M+Na]<sup>+</sup> 315.0314, found 315.0312.



**(1S\*,4R\*)-4-(3,4-Dichlorophenyl)-1,2,3,4-tetrahydronaphthalen-1-ol**

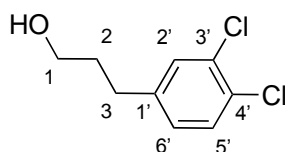
(**rac-35b**) -  $\delta_H$  (**500MHz, CDCl<sub>3</sub>**): 7.64 – 7.48 (1H, d,  $J$  7.8, 8-H), 7.33 (1H, d,  $J$  8.3, 5'-H), 7.28 (1H, td,  $J$  7.5 and 1.4, 7-H), 7.18 (1H, td,  $J$  7.5 and 1.4, 6-H), 7.12 (1H, d,  $J$  2.1, 2'-H), 6.88 – 6.82 (2H, m, 6'-H and 5-H), 4.89 (1H, br q,  $J$  6.0, 1-H), 4.14 (1H, t,  $J$  6.3, 4-H), 2.43 – 2.27 (1H, m, 2-H<sub>a</sub>), 2.16 – 2.08 (1H, m 3-H<sub>a</sub>), 1.86 (1H, br d,  $J$  6.4, OH), 1.84 – 1.76 (2H, m, 2-H<sub>b</sub> and 3-H<sub>b</sub>);  $\delta_c$  (**125MHz, CDCl<sub>3</sub>**): 147.0 (C-1'), 139.8 (C-8a), 137.9 (C-4a), 132.5 (C-4'), 130.7 (Ar), 130.4 (Ar), 130.3 (C-3'), 130.1 (Ar), 128.3 (Ar), 128.2 (Ar), 128.1 (Ar), 127.3 (Ar), 68.3 (C-1), 44.6 (C-4), 30.1 (C-3), 29.1 (C-2); **IR**  $\nu_{\max}$  (**neat**)/**cm<sup>-1</sup>**: 3319.5, 2940.6, 2862.2, 2831.3; **R<sub>f</sub>** = 0.31 (75:25 Hexanes–EtOAc); **HRMS (ESI)**: C<sub>16</sub>H<sub>14</sub>Cl<sub>2</sub>O requires [M+Na]<sup>+</sup> 315.0314, found 315.0308.

**3-(4-Cyano-3-trifluoromethylphenyl)propan-1-ol (36)**



4-[(1*E*)-3-Oxoprop-1-en-1-yl]-2-(trifluoromethyl)benzonitrile (100 mg, 0.45 mmol), sodium borohydride (17 mg, 0.45 mmol) and palladium (II) acetate (4.98 mg, 0.023 mmol) were added to a flask with a magnetic stirrer, with a deflated balloon attached to the neck. Methanol (5 mL) was slowly added into the flask *via* a syringe. The mixture was stirred at room temperature until the reaction was observed to be completed by TLC. The mixture was filtered, and the organic phase evaporated under reduced pressure. Brine was added, and the product extracted with chloroform. The organic layer was dried over magnesium sulfate, filtered and concentrated using a rotary evaporator. The crude mixture was purified by flash column chromatography (75:25 Hexane–EtOAc) to obtain the title compound<sup>115</sup> as an amorphous white solid (83 mg, 0.36 mmol, 80%).  $\delta_{\text{H}}$  (500MHz, CDCl<sub>3</sub>): 7.76 (1H, d, *J* 7.9, 5'-H), 7.67 – 7.61 (1H, m, 2'-H), 7.52 (1H, dd, *J* 7.9 and 1.6, 6'-H), 3.70 (2H, td, *J* 6.0 and 4.0, 1-H), 2.92 – 2.82 (2H, m, 3-H), 1.99 – 1.85 (2H, m, 2-H), 1.40 (1H, br s, O-H); (125MHz, CDCl<sub>3</sub>): 148.5 (C-1'), 134.9 (C-5'), 133.0 (q, *J* 32.5, C-3'), 132.3 (C-6'), 127.0 (d, *J* 4.6, C-2'), 122.6 (q, *J* 273.8, CF<sub>3</sub>), 115.8 (CN), 107.6 (d, *J* 2.2, C-4'), 61.6 (C-1), 33.5 (C-2), 32.3 (C-3); IR  $\nu_{\text{max}}$  (neat)/cm<sup>-1</sup>: 3289.7, 2939.4, 2867.1, 2231.6, 1614.8, 1578.1, 1502.3; *R*<sub>f</sub> = 0.27 (75:25 Hexanes–EtOAc); HRMS (ESI): C<sub>11</sub>H<sub>10</sub>F<sub>3</sub>NO requires [M+H]<sup>+</sup> 230.0787, found 230.0789.

### 3-(3,4-Dichlorophenyl)propan-1-ol (37)

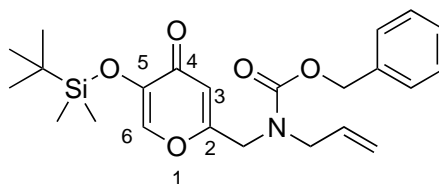


3-(3,4-Dichlorophenyl)propanoic acid (500 mg, 2.25 mmol) was stirred in THF (10 mL), and borane-THF (1M in THF, 4.60 mL, 4.50 mmol) added at room temperature. After stirring for 12 hours, the mixture was cooled to 0 °C and quenched by addition of 1M NaOH. The mixture was diluted with ether and washed with water twice followed by brine. The organic phase was separated and dried over magnesium sulfate, filtered and concentrated under reduced pressure. The residue was purified by flash

column chromatography (75:25 Hexane–EtOAc) to obtain the title compound<sup>116</sup> as an amorphous white solid (360 mg, 1.65 mmol, 73%).  $\delta_{\text{H}}$  (500MHz,  $\text{CDCl}_3$ ): 7.34 (1H, d,  $J$  8.2, 5'-H), 7.29 (1H, d,  $J$  2.0, 2'-H), 7.03 (1H, dd,  $J$  8.2 and 2.0, 6'-H), 3.71 – 3.59 (2H, m, 1-H), 2.71 – 2.63 (2H, m, 3-H), 1.93 – 1.81 (2H, m, 2-H), 1.33 (1H, br s, O-H);  $\delta_{\text{C}}$  (125MHz,  $\text{CDCl}_3$ ): 142.2 (C-1'), 132.4 (C-3'), 130.5 (5'-H), 130.4 (C-2'), 129.9 (C-4'), 128.1 (6'-H), 61.9 (C-1), 33.9 (C-2), 31.3 (C-3); IR  $\nu_{\text{max}}$  (neat)/ $\text{cm}^{-1}$ : 3318.3, 2939.8, 2865.4, 1593.4, 1561.3;  $R_{\text{f}}$  = 0.39 (75:25 Hexanes–EtOAc). HRMS (ESI):  $\text{C}_9\text{H}_8\text{Cl}_2\text{O}_2$  requires  $[\text{M}-\text{H}]^-$  216.9829, found 216.9824.

### 6.2.6 Synthesis of Exemplar Screening Compounds

**Benzyl *N*-({5-[(*tert*-butyldimethylsilyl)oxy]-4-oxo-4H-pyran-2-yl)methyl)-*N*-(prop-2-en-1-yl)carbamate (41)**



To a suspension of 5-hydroxy-2-(hydroxymethyl)-4H-pyran-4-one **38** (9.99 g, 70.3 mmol) in dichloromethane (150 mL) at 0 °C was added triethylamine (10.8 mL, 77.3 mmol), *tert*-butylchlorodimethylsilane (10.7 g, 71.0 mmol) and *N,N*-dimethylpyridin-4-amine (0.258 g, 2.11 mmol). Following addition, the ice bath was removed and the reaction warmed to room temperature and stirred for 90 minutes. The reaction was quenched with saturated  $\text{NH}_4\text{Cl}$  solution (100 mL) and water (100 mL). Following separation, the aqueous phase was extracted using  $\text{CH}_2\text{Cl}_2$  (2 x 150 mL). The organic extracts were combined, filtered through a phase separation funnel and concentrated *in vacuo*. The crude residue was used as substrate for the second part of the experiment. To the crude starting material (70.3 mmol) diluted in dichloromethane (150 mL) at 0 °C was added triethylamine (12.1 mL, 86.45 mmol) then methanesulfonyl chloride (5.98 mL, 77.3 mmol) dropwise. The ice bath was then removed, and the reaction mixture warmed



to room temperature and left to stir for 45 mins. The reaction was then quenched with water (150 mL), then the phases separated before extracting the aqueous phase with dichloromethane (2 x 150 mL). The organic extracts were combined, filtered through a phase separation funnel and concentrated *in vacuo*. The crude residue of **39** was used in next step without purification.

**{5-[(*tert*-Butyldimethylsilyl)oxy]-4-oxo-4H-pyran-2-yl)methyl**

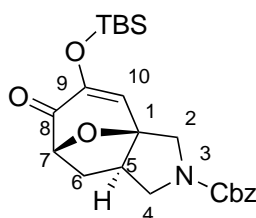
**methanesulfonate (39) -  $\delta_{\text{H}}$  (400MHz,  $\text{CDCl}_3$ ):** 7.69 (1H, s, 6-H), 6.48 (1H, s, 3-H), 4.97 (1H, s,  $\text{CH}_2$ ), 3.10 (3H, s,  $\text{SO}_2\text{CH}_3$ ), 0.96 (9H, s,  $\text{SiC}(\text{CH}_3)_3$ ), 0.23 (6H, s, 2 x  $\text{SiCH}_3$ ); **LC-MS ( $\text{ES}^+$ ):**  $\text{C}_{13}\text{H}_{22}\text{O}_6\text{SSi}$  requires  $[\text{M}+\text{H}]^+$  335.09, found 335.09.

To a crude residue of (5-((*tert*-butyldimethylsilyl)oxy)-4-oxo-4H-pyran-2-yl)methyl methanesulfonate **39** (23.5 g, 70.3 mmol) diluted in dichloromethane (150 mL) at 0 °C was added triethylamine (9.80 mL, 70.3 mmol) and slow addition of prop-2-en-1-amine (20 mL, 267 mmol). Following addition, the ice bath was removed, and the mixture stirred at room temperature overnight (17 hours). The reaction was quenched with water (150 mL), and following separation of the phases, the aqueous phase extracted with dichloromethane (2 x 150 mL). The organic extracts were then combined and filtered through a phase separation funnel before concentrating *in vacuo*. The crude residue of **40** was used in next step without purification. **5-[(*tert*-Butyldimethylsilyl)oxy]-2-[(prop-2-en-1-yl)amino]methyl)-4H-pyran-4-one (40) -  $\delta_{\text{H}}$  (400MHz,  $\text{CDCl}_3$ ):** 7.64 (1H, s, 6-H), 6.35 (1H, s, 3-H), 5.86 (1H, ddt,  $J$  17.1, 10.3 and 6.0,  $\text{CH}=\text{CH}_2$ ), 5.24 – 5.08 (2H, m,  $\text{CH}=\text{CH}_2$ ), 3.62 (2H, s,  $\text{C}_\alpha\text{CH}_2\text{NH}$ ), 3.27 (2H, dt,  $J$  6.0 and 1.3,  $\text{NHCH}_2\text{CH}=\text{CH}_2$ ), 0.96 (9H, s,  $\text{SiC}(\text{CH}_3)_3$ ), 0.23 (6H, s, 2 x  $\text{SiCH}_3$ ); **LC-MS ( $\text{ES}^+$ ):**  $\text{C}_{15}\text{H}_{25}\text{NO}_3\text{Si}$  requires  $[\text{M}+\text{H}]^+$  296.16, found 296.16.

To the crude residue 2-((allylamino)methyl)-5-((*tert*-butyldimethylsilyl)oxy)-4H-pyran-4-one **40** (20.8 g, 70.3 mmol) diluted in dichloromethane (150 mL) at 0 °C was slowly added triethylamine (16.9 mL, 121 mmol) followed by dropwise addition of benzyl carbonochloridate (15.1 mL, 105 mmol). The ice bath was then removed, and the reaction mixture warmed to room temperature, stirring for 3 hours. The reaction was

quenched with saturated  $\text{NH}_4\text{Cl}$  solution (150 mL) and water (150 mL), then the phases separated, and the aqueous phase extracted with dichloromethane (2 x 150 mL). The organic extracts were combined, filtered through a phase separation funnel and concentrated *in vacuo* to give the title product<sup>34</sup> as a pale yellow amorphous solid (16.8 g, 39.1 mmol, 56% over 3 steps from kojic acid).  $\delta_{\text{H}}$  (400MHz,  $\text{CDCl}_3$ , 330 K): 7.56 (1H, s, 6-H), 7.39-7.27 (5H, m, Cbz Ar-H), 6.23 (1H, s, 3-H), 5.81-5.70 (1H, m,  $\text{CH}=\text{CH}_2$ ), 5.21-5.10 (4H, m,  $\text{CH}=\text{CH}_2$  and  $\text{OCH}_2\text{Ph}$ ), 4.26 (2H, s,  $\text{C}_q\text{CH}_2\text{N}$ ), 3.96 (2H, s,  $\text{NCH}_2\text{CH}=\text{CH}_2$ ), 0.97 (9H, s,  $\text{SiC}(\text{CH}_3)_3$ ), 0.24 (6H, s, 2 x  $\text{SiCH}_3$ );  $\delta_{\text{C}}$  (100MHz,  $\text{CDCl}_3$ , 330 K): 175.3 (C-4), 163.3 (C-2), 156.1 (N(CO)O), 145.8 (C-5), 144.0 (C-6), 136.5 ( $\text{CH}=\text{CH}_2$ ), 132.9 (Ar- $\text{C}_q$ ), 128.7 (Ar-C), 128.4 (Ar-C), 128.2 (Ar-C), 118.2 ( $\text{CH}=\text{CH}_2$ ), 113.7 (C-3), 65.6 ( $\text{OCH}_2\text{Ph}$ ), 50.3 ( $\text{CH}_2\text{CH}=\text{CH}_2$ ), 47.6 ( $\text{C}_q\text{CH}_2\text{NH}$ ), 25.8 ( $\text{SiC}(\text{CH}_3)_3$ ), 18.7 ( $\text{SiC}_q$ ), -4.3 (2 x  $\text{SiCH}_3$ ); **LC-MS (ES<sup>+</sup>)**:  $\text{C}_{23}\text{H}_{31}\text{NO}_5\text{Si}$  requires  $[\text{M}+\text{H}]^+$  430.20, found 430.20.

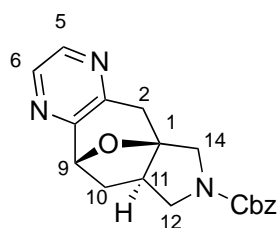
**Benzyl (1R\*, 5S\*, 7S\*)-9-[(*tert*-butyldimethylsilyl)oxy]-8-oxo-11-oxa-3-azatricyclo [5.3.1.0<sup>1,5</sup>]undec-9-ene-3-carboxylate (42)**



A stirred solution of benzyl *N*-({5-[(*tert*-butyldimethylsilyl)oxy]-4-oxo-4H-pyran-2-yl)methyl)-*N*-(prop-2-en-1-yl)carbamate **41** (9.50g, 22.1 mmol) in xylenes (24 mL) was heated to reflux and stirred for 14 hours. The crude reaction mixture was then concentrated *in vacuo* and the residue purified by flash column chromatography (gradient to 40% EtOAc in Heptane over 35 mins) to give the title compound<sup>34</sup> as a colourless amorphous solid (8.98 g, 20.9 mmol, 95%).  $\delta_{\text{H}}$  (400MHz,  $\text{CDCl}_3$ , 50:50 mixture of rotamers): 7.39 – 7.28 (5H, m, Cbz Ar-H), 6.29 (0.5H, s, 10-H), 6.26 (0.5H, s, 10-H), 5.14 (1H, s,  $\text{OCH}_a\text{H}_b\text{Ph}$ ), 5.13 (1H, s,  $\text{OCH}_a\text{H}_b\text{Ph}$ ), 4.78 (1H, d,  $J$  8.1, 7-H), 4.07 – 3.88 (2H, m, 2- $\text{H}_b$  and 4- $\text{H}_a$ ), 3.68 (0.5H, d,  $J$  13.1, 2- $\text{H}_a$ ), 3.64 (0.5H, d,  $J$  12.8, 2- $\text{H}_a$ ), 3.17 (1H, q,  $J$  11.0, 4- $\text{H}_b$ ), 2.87 – 2.72 (1H, m, 5-H), 2.36 – 2.18 (1H, m,

6-H<sub>b</sub>), 1.89 (1H, dt, *J* 13.7 and 9.4, 6-H<sub>a</sub>), 0.93 (9H, s, SiC(CH<sub>3</sub>)<sub>3</sub>), 0.17 (6H, s, 2 x SiCH<sub>3</sub>);  $\delta_c$  (**100MHz, CDCl<sub>3</sub>, 50:50 mixture of rotamers**): 193.7 (C-8), 154.5 (N(CO)O), 154.3 (N(CO)O), 148.1 (C-9), 136.8 (Ar-C<sub>q</sub>), 138.7 (Ar C-<sub>q</sub>), 128.7 (Ar-C), 128.3 (Ar-C), 128.2 (Ar-C), 128.1 (Ar-C), 127.3 (C-10), 127.2 (C-10), 90.6 (C-1), 89.8 (C-1), 83.4 (C-7), 67.2 (OCH<sub>2</sub>Ph), 53.9 (C-2 or C-4), 53.5 (C-2 or C-4), 53.1 (C-2 or C-4), 52.7 (C-2 or C-4), 47.1 (C-5), 46.2 (C-5), 31.6 (C-6), 31.5 (C-6), 25.7 (SiC(CH<sub>3</sub>)<sub>3</sub>), 18.6 (SiC<sub>q</sub>), -4.5 (2 x SiCH<sub>3</sub>) (28 of 36 expected peaks observed); **LC-MS (ES<sup>+</sup>)**: C<sub>23</sub>H<sub>31</sub>NO<sub>5</sub>Si requires [M+H]<sup>+</sup> 430.20, found 430.20.

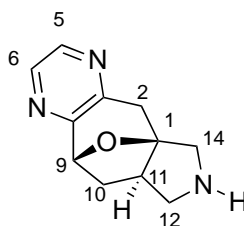
**Benzyl (1R\*, 9R\*, 11R\*)-15-oxa-4,7,13-triazatetracyclo[7.5.1.0<sup>1,11</sup>.0<sup>3,9</sup>]pentadeca-3(8),4,6-triene-13-carboxylate (43)**



In two equally sized batches, ethane-1,2-diamine (2.18 ml, 32.6 mmol) was added to a suspension of benzyl (1R\*, 5S\*, 7S\*)-9-[(tert-butyl dimethylsilyl)oxy]-8-oxo-11-oxa-3-azatricyclo[5.3.1.0<sup>1,5</sup>]undec-9-ene-3-carboxylate **42** (7.00 g, 16.3 mmol) in acetic acid (7.5 mL). Following stirring at room temperature for 10 minutes, the reaction mixture was then heated at 160 °C under microwave irradiation for 30 minutes. The two batches were then combined and concentrated *in vacuo*. The residue was diluted in DCM (70 mL) and washed with saturated NaHCO<sub>3</sub> solution (70 mL). The aqueous layer was extracted further with dichloromethane (4 x 30 mL), then the organic extracts combined, washed with water (2 x 30 mL) and brine (30 mL) before filtering through a phase separation funnel and concentrating *in vacuo*. The product was then purified by chromatography, eluting with DCM–10% NH<sub>3</sub>/MeOH in DCM (0% to 30%), to give the title compound<sup>34</sup> as a viscous orange oil (2.02 g, 5.99 mmol, 37%).  $\delta_H$  (**400MHz, CDCl<sub>3</sub>**): 8.39 (1H, d, *J* 2.6, 5/6-H), 8.28 (1H, d, *J* 2.5, 5/6-H), 7.39 – 7.28 (5H, m, Cbz Ar-H), 5.29 (1H, d, *J* 6.9, 9-H), 5.14 (2H, d, *J* 3.0, OCH<sub>2</sub>Ph), 4.08 (1H, d, *J* 12.7, 14-

H<sub>a</sub>), 3.88 (1H, dd, *J* 11.4 and 9.3, 12-H<sub>b</sub>), 3.47 (3H, m, 2-H<sub>a</sub>, 12-H<sub>a</sub> and 14-H<sub>b</sub>), 2.92 (1H, d, *J* 17.6, 2-H<sub>b</sub>), 2.69 (1H, s, 11-H), 2.39 (1H, d, *J* 7.2, 10-H<sub>a</sub>), 2.26 (1H, s, 10-H<sub>b</sub>);  $\delta_c$  (**100MHz, CDCl<sub>3</sub>, mixture of two rotamers**): 155.4 (C-8), 154.6 (N(CO)O), 149.3 (C-3), 143.6 (C-5 or C-6), 141.7 (C-5 or C-6), 136.8 (Ar-C<sub>q</sub>), 128.6 (Ar-C), 128.2 (Ar-C), 128.1 (Ar-C), 91.2 (C-1), 90.3 (C-1), 80.6 (C-9), 67.2 (OCH<sub>2</sub>Ph), 66.9 (OCH<sub>2</sub>Ph), 55.1 (C-14), 54.7 (C-14), 54.4 (C-12), 54.1 (C-12), 46.7 (C-11), 45.7 (C-11), 43.4 (C-10), 43.2 (C-10), 39.5 (C-2) (23 of 34 expected peaks observed); **IR**  $\nu_{\max}$  (**neat**)/cm<sup>-1</sup>: 2953.4, 2880.2, 1703.0; **LC-MS (ES<sup>+</sup>)**: C<sub>19</sub>H<sub>19</sub>N<sub>3</sub>O<sub>3</sub> requires [M+H]<sup>+</sup> 338.14, found 338.14.

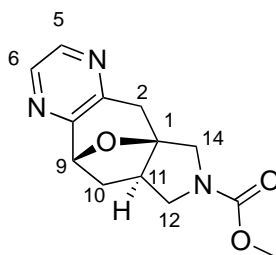
**(1R\*, 9R\*, 11R\*)-15-Oxa-4,7,13-triazatetracyclo[7.5.1.0<sup>1,11</sup>.0<sup>3,8</sup>]pentadeca-3(8),4,6-triene (44)**



Sodium hydroxide (1.79 g, 44.8 mmol) was added to a stirred solution of benzyl (1R\*, 9R\*, 11R\*)-15-oxa-4,7,13-triazatetracyclo[7.5.1.0<sup>1,11</sup>.0<sup>3,8</sup>]pentadeca-3(8),4,6-triene-13-carboxylate **43** (0.72 g, 2.13 mmol) in methanol (25 mL). The reaction mixture was heated at reflux for 15 hours, then acidified to pH 7 with concentrated hydrochloric acid, before reverse phase purification (10 to 30% MeCN in H<sub>2</sub>O(1% NH<sub>4</sub>OH)) to obtain the title compound<sup>34</sup> as a brown oil (0.261 g, 1.28 mmol, 60%).  $\delta_H$  (**400MHz, MeOD**): 8.50 (1H, d, *J* 2.7, 5/6-H), 8.41 (1H, d, *J* 2.6, 5/6-H), 5.22 (1H, d, *J* 6.5, 9-H), 3.46 (1H, d, *J* 17.3, 2-H<sub>a</sub>), 3.32 (1H, d, *J* 12.6, 14-H<sub>a</sub>), 3.13 (1H, dd, *J* 12.0 and 7.6, 12-H<sub>a</sub>), 3.01 (1H, d, *J* 17.4, 2-H<sub>b</sub>), 2.90 (1H, d, *J* 12.1, 12-H<sub>b</sub>), 2.81 (1H, d, *J* 12.7, 14-H<sub>b</sub>), 2.65 – 2.50 (2H, m, 10-H<sub>a</sub> and 11-H), 2.17 (1H, m, 10-H<sub>b</sub>);  $\delta_c$  (**100MHz, MeOD**): 157.0 (C-8), 151.9 (C-3), 144.3 (C-5 or C-6), 142.6 (C-5 or C-6), 94.1 (C-1), 81.2 (C-9), 56.4 (C-12), 54.9 (C-14), 48.1 (C-11), 44.6 (C-10), 39.5 (C-2); **IR**  $\nu_{\max}$

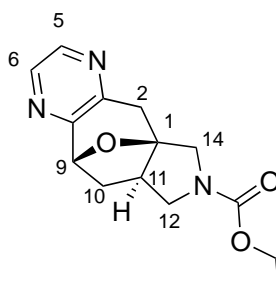
(neat)/cm<sup>-1</sup>: 3324.5, 2977.4, 2901.4; **LC-MS (ES<sup>+</sup>)**: C<sub>11</sub>H<sub>13</sub>N<sub>3</sub>O requires [M+H]<sup>+</sup> 204.11, found 204.11.

**Methyl (1*R*\*,9*R*\*,11*R*\*)-15-oxa-4,7,13-triazatetracyclo[7.5.1.0<sup>1,11</sup>.0<sup>3,8</sup>]pentadeca-3(8),4,6-triene-13-carboxylate (45)**



Methyl carbonochloridate (0.171 mL, 2.21 mmol) was added dropwise to a solution of (1*R*\*, 9*R*\*, 11*R*\*)-15-oxa-4,7,13-triazatetracyclo[7.5.1.0<sup>1,11</sup>.0<sup>3,8</sup>]pentadeca-3(8),4,6-triene **44** (300 mg, 1.48 mmol) and *N*-ethyl-*N*-isopropylpropan-2-amine (0.514 mL, 2.95 mmol) in acetonitrile (5 mL) at 0 °C. Following the addition, the reaction was stirred at room temperature for 17 hours. The mixture was then diluted with brine (5 mL) and extracted with DCM (3 x 5 mL). Purified by reverse phase purification (10% to 30% MeCN in H<sub>2</sub>O (1% NH<sub>4</sub>OH)) to obtain the title compound<sup>34</sup> as a colourless viscous oil (0.248 g, 0.949 mmol, 64.3 %).  $\delta_{\text{H}}$  (**400MHz, CDCl<sub>3</sub>**): 8.40 (1H, d, *J* 2.6, 5/6-H), 8.28 (1H, d, *J* 2.6, 5/6-H), 5.28 (1H, d, *J* 6.9, 9-H), 4.03 (1H, d, *J* 10.3, 12-H<sub>a</sub>), 3.88 – 3.80 (1H, m, 14-H<sub>a</sub>), 3.71 (3H, s, CO<sub>2</sub>CH<sub>3</sub>), 3.46 (3H, m, 2-H<sub>a</sub>, 12-H<sub>b</sub> and 14-H<sub>b</sub>), 2.92 (1H, d, *J* 17.8, 2-H<sub>b</sub>), 2.73 – 2.63 (1H, m, 11-H), 2.46 – 2.36 (1H, m, 10-H<sub>a</sub>), 2.25 (1H, m, 10-H<sub>b</sub>);  $\delta_{\text{C}}$  (**100MHz, CDCl<sub>3</sub>, mixture of two rotamers**): 155.3 (C-8), 155.2 (N(CO)O), 149.2 (C-3), 143.5 (C-5 or C-6), 141.6 (C-5 or C-6), 91.0 (C-1), 90.1 (C-1), 80.4 (C-9), 54.9 (C-12), 54.6 (C-12), 54.1 (C-14), 54.0 (C-14), 52.6 (NCO<sub>2</sub>CH<sub>3</sub>), 46.6 (C-11), 45.6 (C-11), 43.2 (C-10), 39.4 (C-2) (17 of 26 expected peaks observed); **IR**  $\nu_{\text{max}}$  (neat)/cm<sup>-1</sup>: 3047.7, 2974.1, 2879.3, 1693.6, 1541.4; **HRMS (ESI)**: C<sub>13</sub>H<sub>15</sub>N<sub>3</sub>O<sub>3</sub> requires [M+H]<sup>+</sup> 262.1191, found 262.1187.

**Ethyl (1*R*\*,9*R*\*,11*R*\*)-15-oxa-4,7,13-triazatetracyclo[7.5.1.0<sup>1,11</sup>.0<sup>3,8</sup>]pentadeca-3(8),4,6-triene-13-carboxylate (46)**



Ethyl carbonochloridate (0.073 mL, 0.77 mmol) was added dropwise to a solution of (1*R*\*, 9*R*\*, 11*R*\*)-15-oxa-4,7,13-triazatetracyclo[7.5.1.0<sup>1,11</sup>.0<sup>3,8</sup>]pentadeca-3(8),4,6-triene **44** (130 mg, 0.64 mmol) and triethylamine (0.178 mL, 1.28 mmol) in DMF (2 mL) at 0 °C. Following the addition, the reaction was stirred at room temperature for 17 hours. The mixture was then diluted with water (5 mL) and extracted with EtOAc (3 x 5 mL). Purified by reverse phase purification (15% to 35% MeCN in H<sub>2</sub>O (1% NH<sub>4</sub>OH)) to obtain the *title product* as a pale yellow viscous oil (85 mg, 0.309 mmol, 48%).  $\delta_{\text{H}}$  (500MHz, CDCl<sub>3</sub>): 8.40 (1H, d, *J* 2.6, 5/6-H), 8.29 (1H, d, *J* 2.6, 5/6-H), 5.29 (1H, d, *J* 6.8, 9-H), 4.15 (2H, q, *J* 7.1, OCH<sub>2</sub>CH<sub>3</sub>), 4.04 (1H, d, *J* 12.7, 12-H<sub>a</sub>), 3.85 (1H, m, 14-H<sub>a</sub>), 3.52 – 3.32 (3H, m, 2-H<sub>a</sub>, 12-H<sub>b</sub> and 14-H<sub>b</sub>), 2.93 (1H, d, *J* 17.6, 2-H<sub>b</sub>), 2.69 (1H, m, 11-H), 2.41 (1H, m, 10-H<sub>a</sub>), 2.31–2.20 (1H, m, 10-H<sub>b</sub>), 1.26 (3H, t, *J* 7.1, OCH<sub>2</sub>CH<sub>3</sub>);  $\delta_{\text{C}}$  (125MHz, CDCl<sub>3</sub>): 155.4 (C-8), 154.9 (N(CO)O), 149.4 (C-3), 143.6 (C-5 or C-6), 141.7 (C-5 or C-6), 91.2 (C-1), 90.3 (C-1), 80.6 (C-9), 61.4 (OCH<sub>2</sub>CH<sub>3</sub>), 55.0 (C-12), 54.7 (C-12), 54.1 (C-14), 46.7 (C-11), 45.7 (C-11), 43.4 (C-10), 43.2 (C-10), 39.6 (C-2), 14.9 (OCH<sub>2</sub>CH<sub>3</sub>) (18 of 28 expected peaks observed); IR  $\nu_{\text{max}}$  (neat)/cm<sup>-1</sup>: 3049.1, 2975.3, 2877.2, 1691.0, 1539.8; HRMS (ESI): C<sub>14</sub>H<sub>17</sub>N<sub>3</sub>O<sub>3</sub> requires [M+H]<sup>+</sup> 276.1343, found 276.1339.

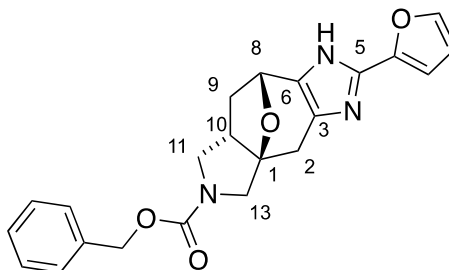
**General Procedures for Synthesis of Imidazole Analogues:****A**

Ammonium acetate (10.0 equiv.) was added to a stirred suspension of the silyl enol ketone **42** (1.0 mmol, 1.0 equiv.) and the appropriate aldehyde (1.0 equiv.) in acetic acid (70 mM reaction concentration). The resulting mixture was heated to 60 °C and stirred for 17 hours. The reaction was allowed to cool to room temperature, then added to a saturated aqueous solution of sodium hydrogen carbonate (20 mL). The mixture was extracted with ethyl acetate (4 x 20 mL) and the combined organic layers dried over magnesium sulphate, before filtering and concentrating under reduced pressure.

**B**

Ammonium acetate (5.0 equiv.) was added to a stirred suspension of the silyl enol ketone **42** (1.0 mmol, 1.0 equiv.), the appropriate aldehyde (1.0 equiv.) and the appropriate aniline (5.0 equiv.) in acetic acid (70 mM reaction concentration). The resulting mixture was heated to 60°C and stirred for 17 hours. The reaction was allowed to cool to room temperature, then added to a saturated aqueous solution of sodium hydrogen carbonate (20 mL). The mixture was extracted with ethyl acetate (4 x 20 mL) and the combined organic layers dried over magnesium sulphate, before filtering and concentrating under reduced pressure.

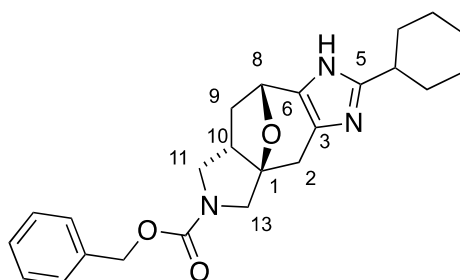
**Benzyl (1*R*\*, 8*R*\*, 10*S*\*)-5-(furan-2-yl)-14-oxa-4,6,12-triazatetracyclo[6.5.1.0<sup>1,10</sup>.0<sup>3,7</sup>]tetradeca-3(7),4-diene-12-carboxylate (47)**



By general procedure **A**, using furfural, eluting with 50% to 100% EtOAc in Hexane, afforded the *title compound* (76 mg, 0.194 mmol, 65%) as a brown amorphous solid.  $\delta_{\text{H}}$  (**400MHz, CDCl<sub>3</sub>**): 7.40-7.28 (6H, m, Ar-H and furan 5-H), 6.82 (1H, d, *J* 3.4, furan 3-H), 6.48 (1H, dd, *J* 3.5 and 1.8, furan 4-H), 5.26 (1H, d, *J* 5.9, 8-H), 5.21-5.07 (2H, m, OCH<sub>2</sub>Ph), 4.07 (1H, d, *J* 12.6, 13-H<sub>a</sub>), 3.83-3.72 (1H, m, 11-H<sub>a</sub>), 3.55-3.36 (2H, m, 11-H<sub>b</sub> and 13-H<sub>b</sub>), 3.27-3.14 (1H, m, 2-H<sub>a</sub>), 2.71-2.64 (1H, m, 10-H), 2.61 (1H, d, *J* 15.5, 2-H<sub>b</sub>), 2.56-2.45 (1H, m, 9-H<sub>a</sub>), 2.16- 2.05 (1H, m, 9-H<sub>b</sub>);  $\delta_{\text{C}}$  (**100MHz, CDCl<sub>3</sub>**, **mixture of two rotamers**): 154.9 (N(CO)O), 146.1 (Ar-C<sub>q</sub>), 142.1 (furan C-5), 138.2 (Ar-C<sub>q</sub>), 136.7 (Ar-C<sub>q</sub>), 128.6 (Ph-C), 128.1 (Ph-C), 128.0 (Ph-C), 112.0 (furan C-4), 106.7 (furan C-3), 91.1 (C-1), 90.2 (C-1), 67.1 (OCH<sub>2</sub>Ph), 55.0 (C-13), 53.3 (C-11), 53.5 (C-11), 47.1 (C-10), 46.1 (C-10), 45.7 (C-9), 45.6 (C-9), 32.8 (C-2) (21 of 40 expected peaks observed); **IR**  $\nu_{\text{max}}$  (**neat**)/**cm<sup>-1</sup>**: 3117.7, 3031.2, 2952.7, 2874.3, 1694.2, 1589.6; **HRMS (ESI)**: C<sub>22</sub>H<sub>21</sub>N<sub>3</sub>O<sub>4</sub> requires [M+H]<sup>+</sup> 392.1605, found 392.1608.

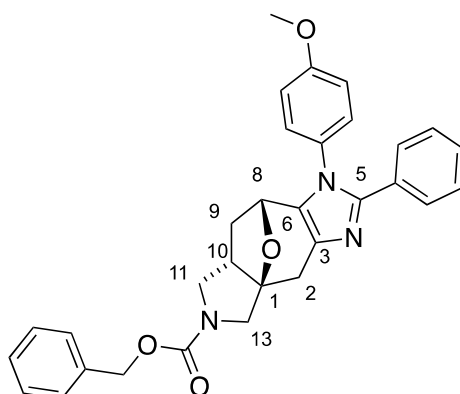


**Benzyl (1*R*\*, 8*R*\*, 10*S*\*)-5-cyclohexyl-14-oxa-4,6,12-triazatetracyclo[6.5.1.0<sup>1,10</sup>.0<sup>3,7</sup>]tetradeca-3(7),4-diene-12-carboxylate (48)**



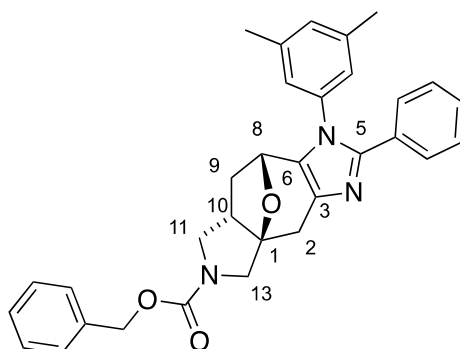
By general procedure **A**, using cyclohexane carboxaldehyde, eluting with 50% to 100% EtOAc in Hexane, afforded the *title compound* (143 mg, 0.351 mmol, 38%) as a brown amorphous solid.  $\delta_H$  (**400MHz, CDCl<sub>3</sub>**): 7.36-7.28 (5H, m, Ar-H), 5.18-5.09 (3H, m, OCH<sub>2</sub>Ph and 8-H), 4.01 (1H, dd, *J* 12.6 and 2.4, 13-H<sub>a</sub>), 3.80-3.70 (1H, m, 11-H<sub>a</sub>), 3.48-3.31 (2H, m, 11-H<sub>b</sub> and 13-H<sub>b</sub>), 3.14-3.03 (1H, m, 2-H<sub>a</sub>), 2.68-2.59 (2H, m, Cy 1-H and 10-H), 2.48-2.35 (2H, m, 9-H<sub>a</sub> and 2-H<sub>b</sub>), 2.04-1.88 (3H, m, 9-H<sub>b</sub> and Cy 2-H<sub>a</sub>), 1.78-1.59 (3H, m, Cy-H), 1.47-1.08 (5H, m, Cy 2-H<sub>b</sub> and Cy-H);  $\delta_C$  (**100MHz, CDCl<sub>3</sub>, mixture of two rotamers**): 154.7 (N(CO)O), 151.6 (Ar-C<sub>q</sub>), 136.7 (Ar-C<sub>q</sub>), 128.5 (Ar-C), 128.0 (Ar-C), 127.9 (Ar-C), 91.1 (C-1), 90.0 (C-1), 67.0 (OCH<sub>2</sub>Ph), 55.0 (C-13), 53.5 (C-11), 47.0 (C-10), 46.0 (C-10), 45.7 (C-9), 45.5 (C-9), 37.9 (Cy C-1), 32.7 (C-2), 32.2 (Cy C-2), 32.1 (Cy C-2), 26.0 (Cy C-3 or Cy C-4), 25.8 (Cy C-3 or Cy C-4) (21 of 40 expected peaks observed); **IR**  $\nu_{\max}$  (**neat**)/cm<sup>-1</sup>: 3064.6, 2925.2, 2850.7, 1684.4, 1611.5, 1521.8; **HRMS (ESI)**: C<sub>24</sub>H<sub>29</sub>N<sub>3</sub>O<sub>3</sub> requires [M+H]<sup>+</sup> 408.2282, found 408.2283.

**Benzyl (1*R*\*, 8*R*\*, 10*S*\*)-6-(4-methoxyphenyl)-5-phenyl-14-oxa-4,6,12-triazatetracyclo[6.5.1.0<sup>1,10</sup>.0<sup>3,7</sup>]tetradeca-3(7),4-diene-12-carboxylate (49)**



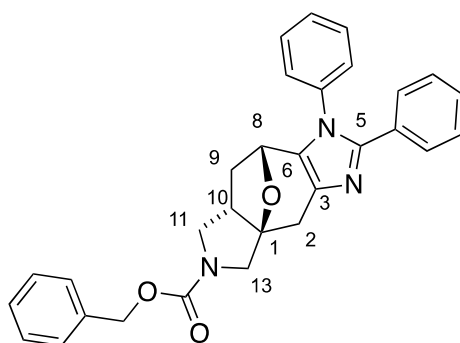
By general procedure **B**, using benzaldehyde and *p*-anisidine, eluting with 50% to 100% EtOAc in Hexane, afforded the *title compound* (125 mg, 0.246 mmol, 58%) as a dark brown amorphous solid.  $\delta_{\text{H}}$  (**400MHz, CDCl<sub>3</sub>**): 7.39-7.28 (7H, m, Ar-H), 7.25-7.17 (3H, m, Ar-H), 7.08 (2H, d, *J* 8.8, PMP 2-H), 6.92 (2H, d, *J* 8.8, PMP 3-H), 5.35 (1H, d, *J* 5.9, 8-H), 5.18-5.08 (2H, m, OCH<sub>2</sub>Ph), 4.10-3.99 (1H, m, 13-H<sub>a</sub>), 3.84 (3H, s, OCH<sub>3</sub>), 3.77 (1H, dd, *J* 11.6 and 8.9, 11-H<sub>a</sub>), 3.55-3.42 (1H, m, 13-H<sub>b</sub>), 3.41-3.30 (1H, m, 11-H<sub>b</sub>), 3.10-2.97 (1H, m, 2-H<sub>a</sub>), 2.79-2.56 (2H, m, 9-H<sub>a</sub> and 10-H), 2.38 (1H, d, *J* 15.6, 2-H<sub>b</sub>), 2.21-2.09 (1H, m, 9-H<sub>b</sub>).  $\delta_{\text{C}}$  (**100MHz, CDCl<sub>3</sub>, mixture of two rotamers**): 159.7 (PMP C-4), 154.8 (N(CO)O), 145.9 (Ar-C<sub>q</sub>), 141.4 (Ar-C<sub>q</sub>), 136.9 (Ar-C<sub>q</sub>), 130.6 (Ar-C<sub>q</sub>), 129.8 (Ar-C<sub>q</sub>), 128.6 (Ar-C), 128.3 (2 peaks, Ar-C), 128.2 (Ar-C), 128.1 (2 peaks, Ar-C), 128.0 (Ar-C), 125.1 (Ar-C), 115.0 (PMP C-3), 90.9 (C-1), 90.0 (C-1), 77.5 (C-8), 67.1 (OCH<sub>2</sub>Ph), 55.7 (OCH<sub>3</sub>), 55.4 (C-13), 55.1 (C-11), 53.5 (C-11), 47.4 (C-10), 46.4 (C-10), 45.5 (C-9), 32.5 (C-2) (28 of 50 expected peaks observed).; **IR**  $\nu_{\text{max}}$  (**neat**)/cm<sup>-1</sup>: 3060.0, 2952.9, 2837.0, 1697.7, 1608.1, 1583.7, 1511.3; **HRMS (ESI)**: C<sub>31</sub>H<sub>29</sub>N<sub>3</sub>O<sub>4</sub> requires [M+H]<sup>+</sup> 508.2231, found 508.2226.

**Benzyl (1*R*\*, 8*R*\*, 10*S*\*)-6-(3,5-dimethylphenyl)-5-phenyl-14-oxa-4,6,12-triazatetracyclo[6.5.1.0<sup>1,10</sup>.0<sup>3,7</sup>]tetradeca-3(7),4-diene-12-carboxylate (50)**



By general procedure **B**, using benzaldehyde and 3,5-dimethyl aniline, eluting with 50% to 100% EtOAc in Hexane, afforded the *title compound* (74 mg, 0.146 mmol, 42%) as a light yellow amorphous solid.  $\delta_{\text{H}}$  (**400MHz, CDCl<sub>3</sub>**): 7.45-7.27 (7H, m, Ar-H), 7.25-7.16 (3H, m, Ar-H), 7.10-7.00 (1H, m, Ar-H), 6.77 (2H, s, Ar-H), 5.34 (1H, d, *J* 5.9, 8-H), 5.20-5.05 (2H, m, OCH<sub>2</sub>Ph), 4.15-3.99 (1H, m, 13-H<sub>a</sub>), 3.77 (1H, dd, *J* 11.5 and 8.8, 11-H<sub>a</sub>), 3.55- 3.31 (2H, m, 11-H<sub>b</sub> and 13-H<sub>b</sub>), 3.13-2.95 (1H, m, 2-H<sub>a</sub>), 2.76-2.60 (2H, m, 10-H and 9-H<sub>a</sub>), 2.38 (1H, d, *J* 15.8, 2-H<sub>b</sub>), 2.30 (6H, s, CH<sub>3</sub>), 2.20-2.09 (9-H<sub>b</sub>);  $\delta_{\text{C}}$  (**100MHz, CDCl<sub>3</sub>, mixture of two rotamers**): 154.7 (N(CO)O), 145.6 (Ar-C), 141.3 (Ar-C), 139.7 (Ar-C), 139.6 (Ar-C), 136.9 (Ar-C), 136.8 (Ar-C), 130.2 (Ar-C), 130.3 (Ar-C), 128.5 (Ar-C), 128.2 (Ar-C), 128.1 (2 peaks, Ar-C), 128.0 (2 peaks, Ar-C), 124.8 (Ar-C), 124.4 (Ar-C), 90.8 (C-1), 89.9 (C-1), 73.8 (C-8), 67.0 (OCH<sub>2</sub>Ph), 55.3 (C-13), 55.0 (C-13), 53.5 (C-11), 47.3 (C-10), 46.3 (C-10), 45.4 (C-9), 32.4 (C-2), 21.2 (CH<sub>3</sub>) (29 of 50 expected peaks observed); **IR**  $\nu_{\text{max}}$  (**neat**)/cm<sup>-1</sup>: 3057.7, 3018.4, 2973.4, 2944.3, 2877.4, 1700.6, 1611.7, 1596.7, 1510.1; **HRMS (ESI)**: C<sub>32</sub>H<sub>31</sub>N<sub>3</sub>O<sub>3</sub> requires [M+H]<sup>+</sup> 506.2438, found 506.2432.

**Benzyl (1*R*\*, 8*R*\*, 10*S*\*)-5,6-diphenyl-14-oxa-4,6,12-triazatetracyclo[6.5.1.0<sup>1,10</sup>.0<sup>3,7</sup>]tetradeca-3(7),4-diene-12-carboxylate (51)**



By general procedure **B**, using benzaldehyde and aniline, eluting with EtOAc, afforded the *title compound* (127 mg, 0.266 mmol, 62%) as a light yellow amorphous solid.  $\delta_H$  (**400 MHz, CDCl<sub>3</sub>**): 7.46-7.40 (3H, m, Ar-H), 7.38-7.29 (7H, m, Ar-H), 7.24-7.19 (3H, m, Ar-H), 7.19-7.14 (2H, m, Ar-H), 5.36 (1H, d, *J* 5.9, 8-H), 5.19-5.07 (2H, m, OCH<sub>2</sub>Ph), 4.06 (1H, d, *J* 12.0, 13-H<sub>a</sub>), 3.77 (1H, dd, *J* 11.5 and 8.9, 11-H<sub>a</sub>), 3.56-3.43 (1H, m, 13-H<sub>b</sub>), 3.41-3.30 (1H, m, 11-H<sub>b</sub>), 3.16-2.99 (1H, m, 9-H<sub>a</sub>), 2.78-2.60 (2H, m, 2-H<sub>a</sub> and 10-H), 2.39 (1H, d, *J* 15.7, 2-H<sub>b</sub>), 2.20- 2.10 (1H, m, 9-H<sub>b</sub>);  $\delta_C$  (**400 MHz, CDCl<sub>3</sub>, mixture of two rotamers**): 154.8 (N(CO)O), 145.8 (Ar-C), 141.4 (Ar-C), 136.9 (Ar-C), 136.8 (Ar-C), 130.2 (Ar-C), 130.0 (Ar-C), 129.9 (Ar-C), 128.8 (Ar-C), 128.6 (Ar-C), 128.4 (2 peaks, Ar-C), 128.3 (Ar-C), 128.1 (Ar-C), 128.0 (Ar-C), 126.9 (Ar-C), 124.9 (Ar-C), 90.9 (C-1), 89.9 (C-1), 73.8 (C-8), 67.1 (OCH<sub>2</sub>Ph), 55.3 (C-13), 55.0 (C-13), 53.5 (2 x peaks, C-11), 47.3 (C-10), 46.4 (C-10), 45.4 (C-9), 32.5 (C-2) (29 of 48 expected peaks observed); **IR**  $\nu_{max}$  (**neat**)/cm<sup>-1</sup>: 3061.6, 2952.8, 2873.5, 1696.2, 1596.8; **HRMS (ESI)**: C<sub>30</sub>H<sub>27</sub>N<sub>3</sub>O<sub>3</sub> requires [M+H]<sup>+</sup> 478.2125, found 478.2123.

### 6.3 Procedures for Transfer to Plate Format

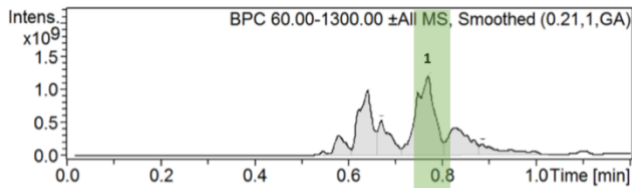
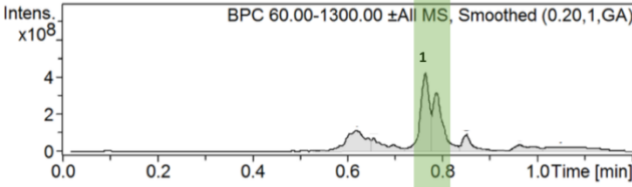
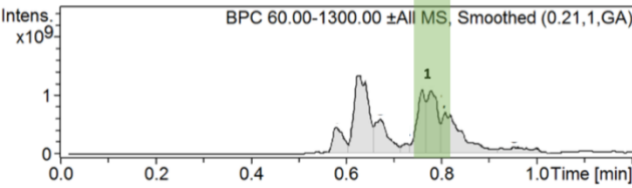
#### Plate Based Synthesis of Compound 22

Cinnamaldehyde (1 M solution in  $\text{CHCl}_3$ , 10  $\mu\text{L}$ ) and 4-methoxyphenacyl chloride (1 M solution in  $\text{CHCl}_3$ , 20  $\mu\text{L}$ ) were added to a 300  $\mu\text{L}$  reaction vial, and the solutions were allowed to evaporate. A solution of *rac*-2-{diphenyl[(trimethylsilyl)oxy]methyl}pyrrolidine (0.002 mM) and triethylamine (0.01 mM) in chloroform was added (100  $\mu\text{L}$ ), and the reaction vial sealed for 24 hours. LC-MS analysis was obtained, and compared to that of the same reaction performed in a flask on a 50 fold higher scale. NMR analysis of the purified product of the flask-based reaction was obtained, and the crude LC-MS analyses compared.

<p style="text-align: center;"> <b>22</b>            75%            Exact Mass = 280.1099         </p>			
Format	LC-MS Trace	Retention Time (Mins)	Mass Found
Flask		<b>0.60 (1)</b> <b>0.67 (2)</b>	<b>474.26</b> <b>474.19</b>
Isolated Product		<b>0.60 (1)</b>	<b>281.21</b>
Plate		<b>0.59 (1)</b> <b>0.62 (2)</b>	<b>474.25</b> <b>474.27</b>

### Plate Based Synthesis of Compound 23

Crotonaldehyde (1 M solution in CHCl<sub>3</sub>, 10 μL) and *N*-methylindole (1 M solution in CHCl<sub>3</sub>, 20 μL) were added to a 300 μL reaction vial, and the solutions were allowed to evaporate. A solution of (2*R*\*,5*R*\*)-5-benzyl-2-tert-butyl-3-methylimidazolidin-4-one (0.002 mM) and trifluoroacetic acid (0.0002 mM) in chloroform was then added (100 μL), and the reaction wells sealed for 24 hours. LC-MS analysis was obtained, and compared to that of the same reaction performed in a flask on a 50 fold higher scale. NMR analysis of the purified product of the flask-based reaction was obtained, and the crude LC-MS analyses compared.

Format	LC-MS Trace	Retention Time (Mins)	Mass Found
Flask	 <p>BPC 60.00-1300.00 ±All MS, Smoothed (0.21,1,GA)</p>	0.78 (1)	588.35
Isolated Product	 <p>BPC 60.00-1300.00 ±All MS, Smoothed (0.20,1,GA)</p>	0.78 (1)	217.73
Plate	 <p>BPC 60.00-1300.00 ±All MS, Smoothed (0.21,1,GA)</p>	0.78 (1)	588.33

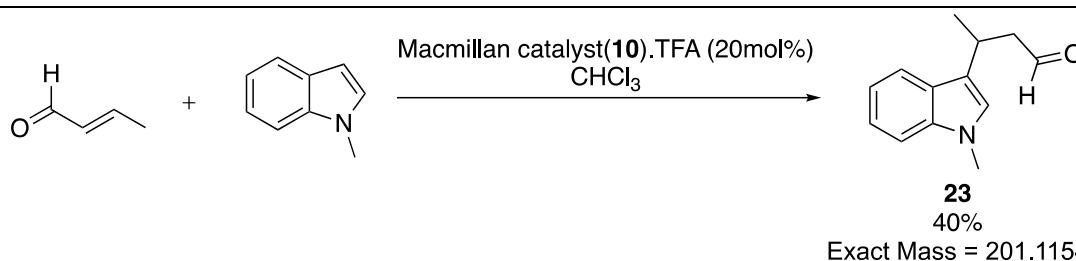


### Plate Based Synthesis of Compound 31

Crotonaldehyde (1 M solution in  $\text{CHCl}_3$ , 10  $\mu\text{L}$ ) and 3-phenyl-1 $\lambda^6$ ,2-benzothiazole-1,1-dione (1 M solution in  $\text{CHCl}_3$ , 20  $\mu\text{L}$ ) were added to a 300  $\mu\text{L}$  reaction vial, and the solutions were allowed to evaporate. A solution of 2-Mesityl-2,5,6,7-tetrahydropyrrolo[2,1-c][1,2,4]triazol-4-ium chloride (0.0006 mM) and 1,8-diazabicyclo(5.4.0)undec-7-ene (0.00012 mM) in DCM was then added (100  $\mu\text{L}$ ), and the reaction wells sealed for 24 hours. LC-MS analysis was obtained, and compared to that of the same reaction performed in a flask on a 50 fold higher scale. NMR analysis of the purified product of the flask-based reaction was obtained, and the crude LC-MS analyses compared.

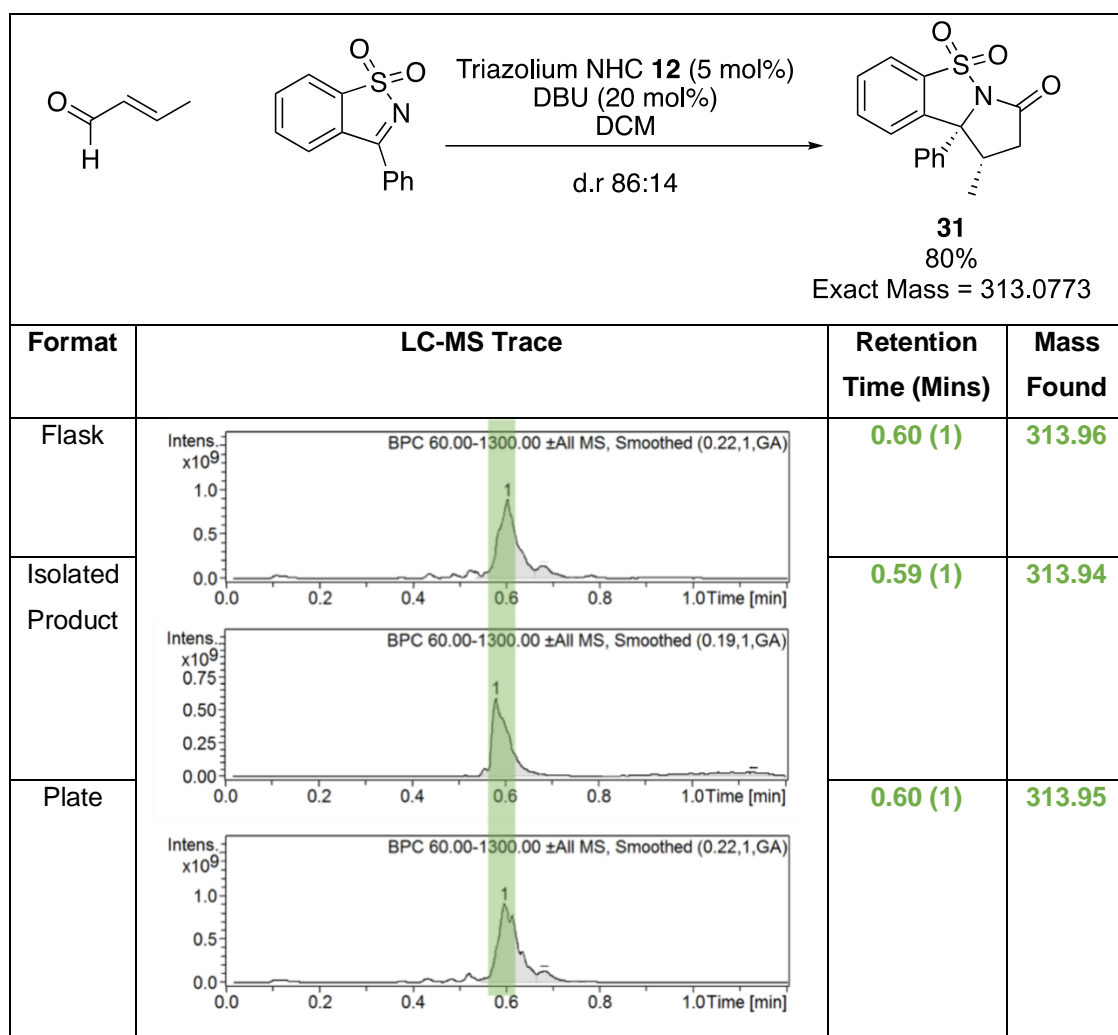
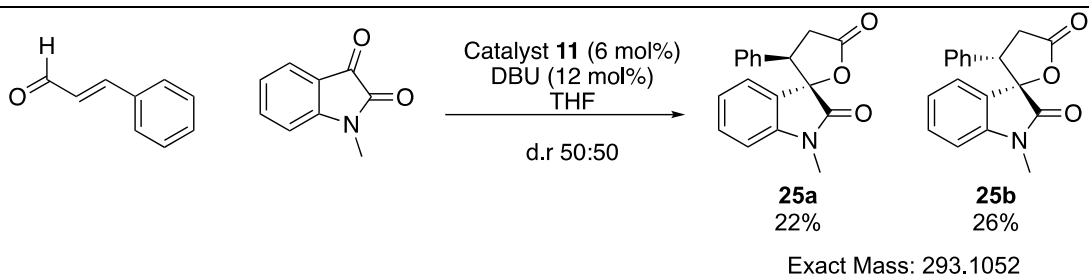


### Plate Based Synthesis of Compounds 25a and 25b

Cinnamaldehyde (1 M solution in  $\text{CHCl}_3$ , 10  $\mu\text{L}$ ) and methylisatin (1 M solution in  $\text{CHCl}_3$ , 20  $\mu\text{L}$ ) were added to a  $\mu\text{L}$  reaction vial, and the solutions were allowed to evaporate. A solution of 1,3-Bis(2,4,6-trimethylphenyl)imidazolium chloride (0.0006 mM) and 1,8-diazabicyclo(5.4.0)undec-7-ene (0.00012 mM) in THF was then added (100  $\mu\text{L}$ ), and the reaction wells sealed for 24 hours. LC-MS analysis was obtained, and compared to that of the same reaction performed in a flask on a 50 fold higher scale. NMR analysis of the purified product of the flask-based reaction was obtained, and the crude LC-MS analyses compared.

Format	LC-MS Trace	Retention Time (Mins)	Mass Found
Flask		0.59 (1)	294.14
Isolated Product		0.59 (1)	293.93
Plate		0.59 (1)	294.14





## 6.4 Procedures for Post-Reaction Protocol Development

### **Reduction with Sodium Borohydride**

The standard, 1,2,4-trichloro-5-methoxybenzene (7.4 mg, 0.035 mmol), and the selected carbonyl substrate (0.035 mmol) were weighed into a vial. Deuterated chloroform (400  $\mu\text{L}$ ) was added, and the solutions transferred into NMR tubes. Following an initial  $^1\text{H}$  NMR experiment to obtain a spectrum of the reaction components, 40  $\mu\text{L}$  (0.0525 mmol, 1.5 equiv.) of a solution of sodium borohydride (11.9 mg in 240  $\mu\text{L}$  of methanol) was added into the NMR tube and the solution left for one hour. A final  $^1\text{H}$  NMR (400 MHz) spectrum was obtained, and the integral ratios of the initial and final spectra compared to determine percentage conversion.

### **Reductive Amination with Secondary Amines**

The standard, 1,2,4-trichloro-5-methoxybenzene (7.4 mg, 0.027 mmol), and carbonyl substrate (0.027 mmol) were weighed into vial. Deuterated chloroform (400  $\mu\text{L}$ ) was added, and the solutions transferred into NMR tubes. Following an initial  $^1\text{H}$  NMR run to obtain a spectrum of the reaction components, the appropriate amine (0.030 mmol) was added to the NMR tubes, followed by 40  $\mu\text{L}$  (0.0405 mmol, 1.5 equiv.) of a solution of tetramethylammonium triacetoxyborohydride (63.9 mg, 0.243 mmol) in acetic acid (240  $\mu\text{L}$ ). The mixture was left for 24 hours before obtaining a  $^1\text{H}$  NMR spectrum, and then another  $^1\text{H}$  NMR (400 MHz) spectrum after 48 hours. The integral ratios of the spectra were compared to determine percentage conversion, and LC-MS analysis confirmed the presence of the expected products.

## 6.5 Procedures for Assembly of ADS Reaction Arrays

### 6.5.1 Stock Solutions of Reaction Components

Stock solutions of components were made up to enable the efficient setup of ADS reaction arrays. Solutions varied in their concentrations, and their addition volumes to the reaction vial to make up a 100  $\mu\text{L}$  scale reaction (**Table 6.1**).

Component	Stock Solution	Volume ( $\mu\text{L}$ )	Reaction Concentration
Substrate	1 M (in chloroform)	10	100 mM
Co-substrate	1 M (in chloroform)	20	200 mM
Catalyst System	10 mM (chloroform for amine catalysts, THF for NHCs; concentration relative to catalyst)	100	10 mM

**Table 6.1 – An outline of the solutions used in reaction array setup, their concentrations, addition volumes and their final reaction concentration.**

### 6.5.2 Mock Array

Mock arrays were executed to determine the activity of the individual components at the same concentration at which the array was to be screened. This array was carried out on components that had been subjected to the work-up procedures, and their relative bioactivities relative to the testosterone positive control were determined. Components exhibiting biological activity at the reaction array screening concentration were identified and removed from the array to prevent interference so bioactive

mixtures as a result of productive reaction combinations could readily be identified. The mock array protocol is outlined graphically in **Figure 3.5**, and concentrations and volumes required of solutions are defined in **Table 6.1**.

1. For the desired component, add the specified volume of solution to reaction vial.
2. Allow evaporation.
3. Add either:
  - a. 50  $\mu\text{L}$  of chloroform, followed by 50  $\mu\text{L}$  of a 0.62 M solution of sodium borohydride in ethanol.
  - b. 75  $\mu\text{L}$  of a 0.4 M solution of  $\text{Me}_2\text{NH}$  in chloroform, and sealing the vessel for 45 minutes. Following this, 25  $\mu\text{L}$  of a 0.62 M solution of  $\text{Me}_4\text{N.BH}(\text{OAc})_3$  in AcOH is added.
4. After 4 hours, add 25  $\mu\text{L}$  of a 5 M solution of acetaldehyde in chloroform to quench unreacted reductant.
5. Leave the plate to evaporate, before further evaporation in a GeneVac apparatus for 4 hours.
6. Follow single-point assay protocol specified in **Section 6.6.3** to obtain bioactivity % of reduced component relative to testosterone.

### **6.5.3 Reaction Arrays**

The full reaction array protocol is outlined graphically in **Figure 3.8**, and was used for both the exhaustive and targeted reaction arrays. Concentrations of solutions are defined in **Table 6.1**

1. For the desired reaction in each well, add first 10  $\mu\text{L}$  of the substrate solution, followed by 20  $\mu\text{L}$  of the co-substrate solution.
2. Allow evaporation.
3. Add 100  $\mu\text{L}$  of the desired catalytic system, before sealing the reaction vial. Leave to react for 24 hours.
4. Remove lids to vials, leave to evaporate.
5. Add either:

- a. 50  $\mu\text{L}$  of chloroform, followed by 50  $\mu\text{L}$  of a 0.62 M solution of sodium borohydride in ethanol.
  - b. 75  $\mu\text{L}$  of a 0.4 M solution of  $\text{Me}_2\text{NH}$  in chloroform, and sealing the vessel for 45 minutes. Following this, 25  $\mu\text{L}$  of a 0.62 M solution of  $\text{Me}_4\text{N.BH}(\text{OAc})_3$  in AcOH is added.
6. After 4 hours, add 25  $\mu\text{L}$  of a 5 M solution of acetaldehyde in chloroform to quench unreacted reductant.
7. Leave the plate to evaporate naturally, before evaporation in a GeneVac apparatus for 4 hours.
8. Follow single-point assay protocol specified in **Section 6.6.3** to obtain bioactivity % of crude product mixture relative to testosterone.

## 6.6 Assay Experimental Procedures

### 6.6.1 General Assay Procedure

The assay kit was purchased from Fischer Scientific and used as instructed in black 384-well Corning assay plates (#4514). The kit contained:

- **AR-LBD GST:** Rat AR-LBD in a buffer pH 7.5, containing protein, stabilising reagents and glycerol, concentration batch dependent.
- **Fluorescein-tagged peptide:** 100  $\mu$ M in 50 mM HEPES buffer, pH 7.5, sequence: VESGSSRFMQLFMANDLLT.
- **Tb<sup>3+</sup> anti-GST antibody:** Concentration batch dependent. 10 mM HEPES buffered saline 137 mM NaCl, 2.7 mM KCl, pH 7.5.
- **TR-FRET co-regulator buffer:** proprietary buffer, pH 7.5, 20% glycerol.
- **DTT:** 1 M in water.

The 1M DTT solution was diluted to 5 mM in TR-FRET co-regulator buffer. This solution was then used as the buffer for all other assay components.

The final DMSO concentration for all ligands screened was 1%. The assay included three additions per well, in which 2.5  $\mu$ L of AR-LBD was added to 5  $\mu$ L of the ligand in buffer (1% DMSO), followed by the addition of 2.5  $\mu$ L of a pre-mixed fluorescein-tagged peptide/Tb<sup>3+</sup> anti-GST antibody solution.

A 20  $\mu$ M solution of testosterone was prepared for use as the positive control, by adding 5  $\mu$ L of a 5000  $\mu$ M solution to 45  $\mu$ L of DMSO to make a 500  $\mu$ M (100 x final screening concentration) solution. 1  $\mu$ L of the 500  $\mu$ M solution was then diluted with 49  $\mu$ L of the prepared buffer to make a 20  $\mu$ M solution, of which 5  $\mu$ L was added to the assay plate in triplicate to give a

final assay concentration of 10  $\mu\text{M}$ . For the negative control, 5  $\mu\text{L}$  of the prepared buffer (2% DMSO) was added to each well, leading to a final DMSO concentration of 1% when screened.

Other ligands to be assayed were diluted to a concentration twice that of the desired screening concentration with a solution of prepared buffer (2% DMSO). Dilution of the controls or ligands with the other assay components would lead to a final concentration of 1% DMSO in all assay wells.

A solution of the AR-LBD was prepared, diluting with the prepared buffer, the concentration of which was dependent upon the batch of protein used during the assay. 2.5  $\mu\text{L}$  of a solution that was four times the final desired screening concentration was added to the well to be assayed.

A solution of the  $\text{Tb}^{3+}$  anti-GST antibody and the fluorescein-tagged peptide was prepared, diluting with the prepared buffer. Both these components in the solution were 4x the final concentration to be used in the assay: 2000 nM for the fluorescein-tagged peptide, and either 40 or 20 nM of the  $\text{Tb}^{3+}$  anti-GST antibody, depending on the requirements of each batch of antibody used. 2.5  $\mu\text{L}$  of this solution was added to all wells, leading to final concentrations of 500 nM, and either 10 or 5 nM, for the fluorophore and antibody components respectively.

The plate was then left to incubate for 4 hours, and read using a Perkin-Elmer Envision 2103 Multilabel reader, equipped with a 320 nM excitation filter (14 nM bandwidth, excites  $\text{Tb}^{3+}$ ), and 495 nM (14 nM bandwidth, detects  $\text{Tb}^{3+}$  fluorescence) and 520 nM (10 nM bandwidth, detects fluorescein fluorescence) emission filters. A 400 nM dichroic mirror with a delay window of 100  $\mu\text{s}$  and an integration window of 200  $\mu\text{s}$  were used to detect the fluorescence at an excitation light percentage of 50%. 3 repeat measurements were obtained, and the results of each measurement averaged during processing.

Three repeat measurements were obtained, and the results of each measurement averaged, before combining to generate the final data. In the rare case of there being a clear inconsistent outlier within the three points, it was deleted to create a duplicate point. Each data point was normalised relative to the controls, obtaining percentage activity relative to the 10  $\mu$ M testosterone positive control ( $EC_{50} = 17$  nM).

### **6.6.2 Procedure for Dose-Response Assay**

DMSO solutions of compounds to be tested were prepared at a concentration 100 times that of the desired final screening concentration. This solution was then subject to serial dilution with DMSO across 12 points in either a three-fold or four-fold manner (see specific dose response assay for detail). The 100x solutions were then diluted to 2x that of the final screening concentration with the prepared buffer, before addition of 5  $\mu$ L to the desired wells in triplicate. The general assay procedure specified in **6.6.1** was then followed, and the data analysed to produce the observed results.

### **6.6.3 Procedure for Single Point Assays**

DMSO solutions of the product mixtures were made relative to the concentration of the armed substrate in the reaction array ( $\Sigma[P_n] = 100$  mM). This solution was diluted to 100x the final screening concentration with DMSO, before preparation of a 2x the final screening concentration solution of each with the prepared buffer. 5  $\mu$ L of each solution was added to the assay plate in triplicate. The general assay procedure specified in **6.6.1** was then followed, and the data analysed to produce the observed results. The relevant final screening concentration is described in the main text relevant for each single-point assay executed.

## 6.7 Structural Data used for Cheminformatics Pipeline

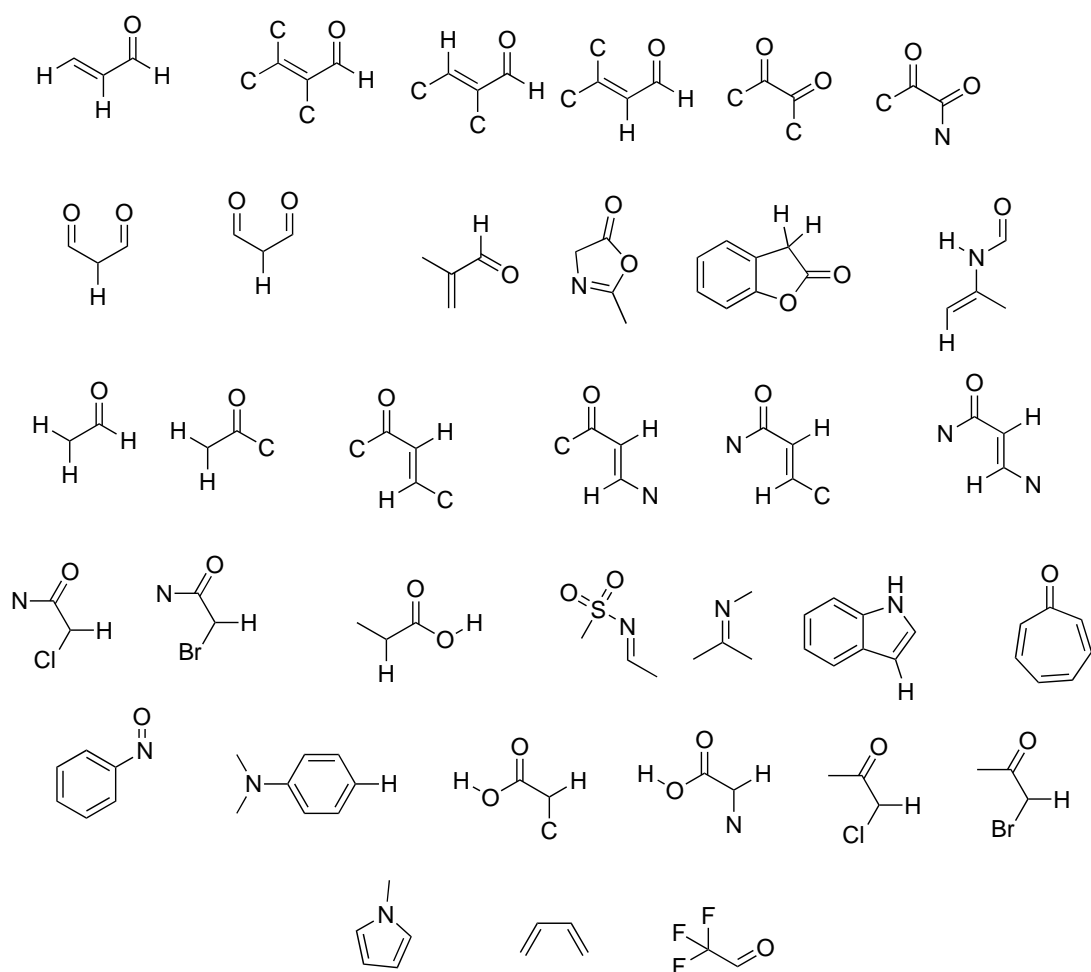
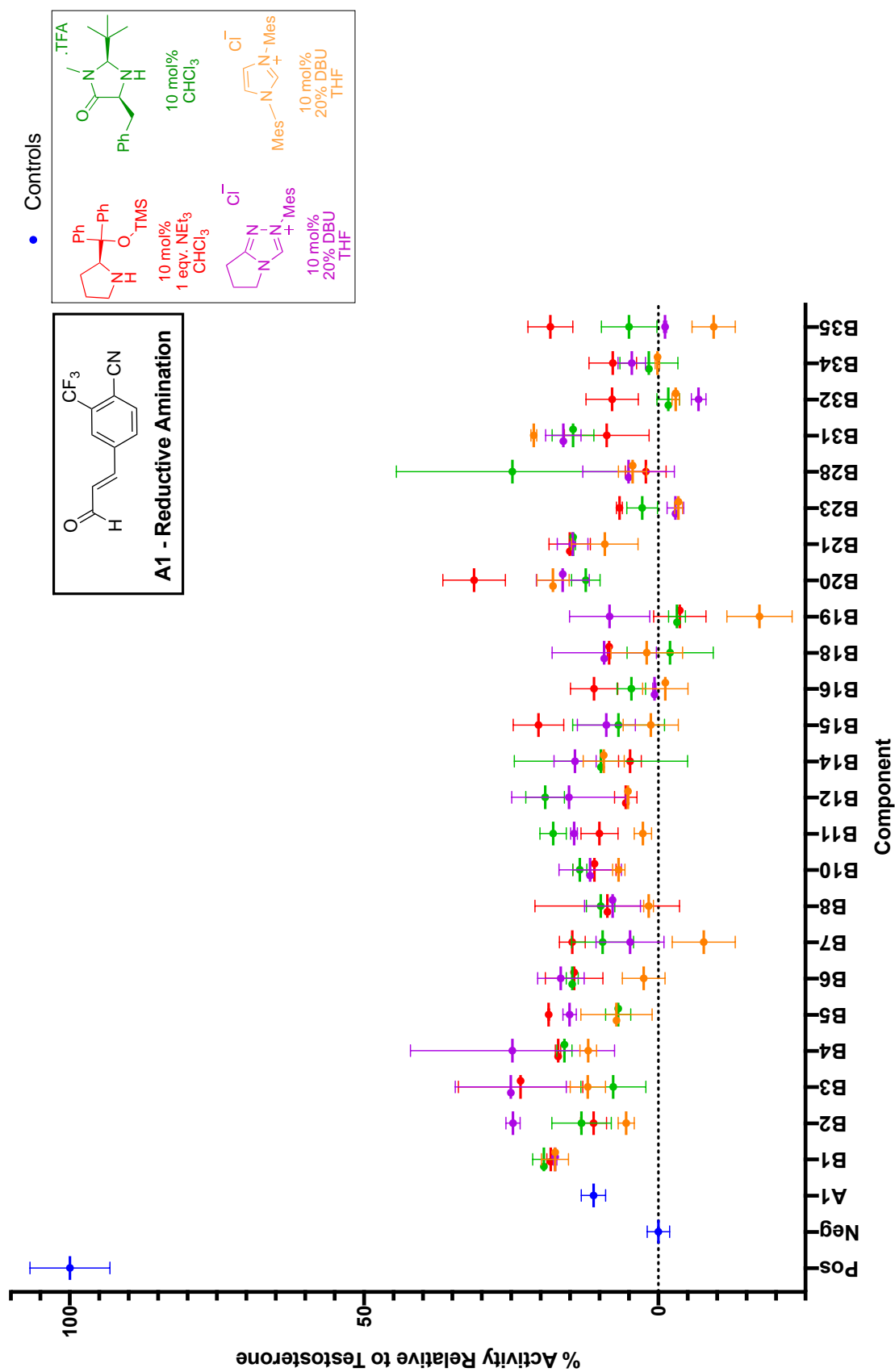


**Figure 6.1** – Structural motifs that were used to filter for potential co-substrates for the first round of exhaustive ADS.

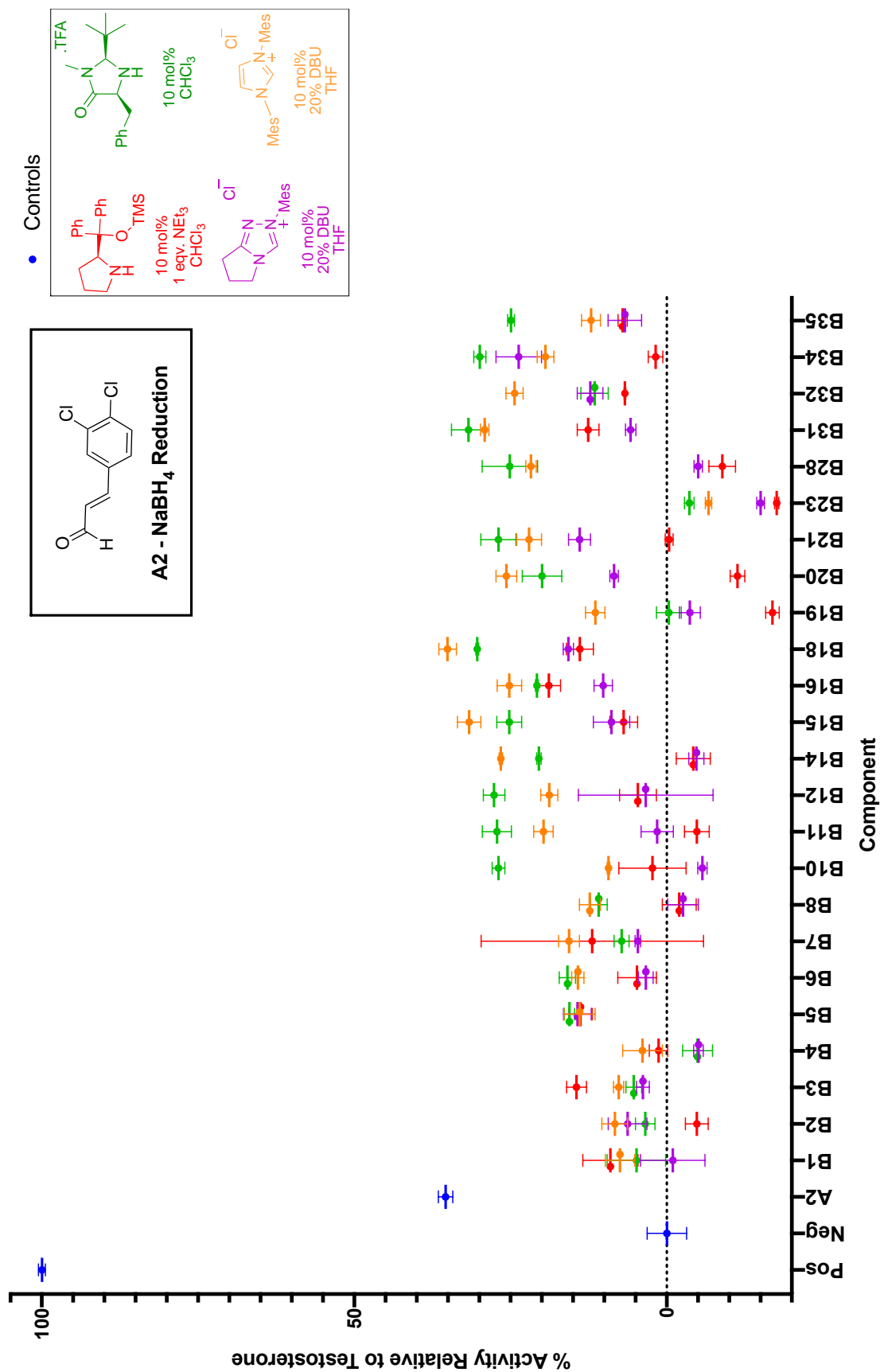
The cheminformatics workflow enabled a library of 250,000 commercially available compounds from Sigma-Aldrich and Fluorochem to be filtered, allowing selection of suitable co-substrates for ADS reaction arrays. The compounds selected had desirable structural motifs with potential for organocatalytic reactions, in addition to possessing desirable physiochemical parameters (**Figure 3.4**). The structural motifs used to filter the library are shown in **Figure 6.1**: they demonstrate good diversity with regard to their potential reactivity with both secondary amine and NHC catalyst classes.





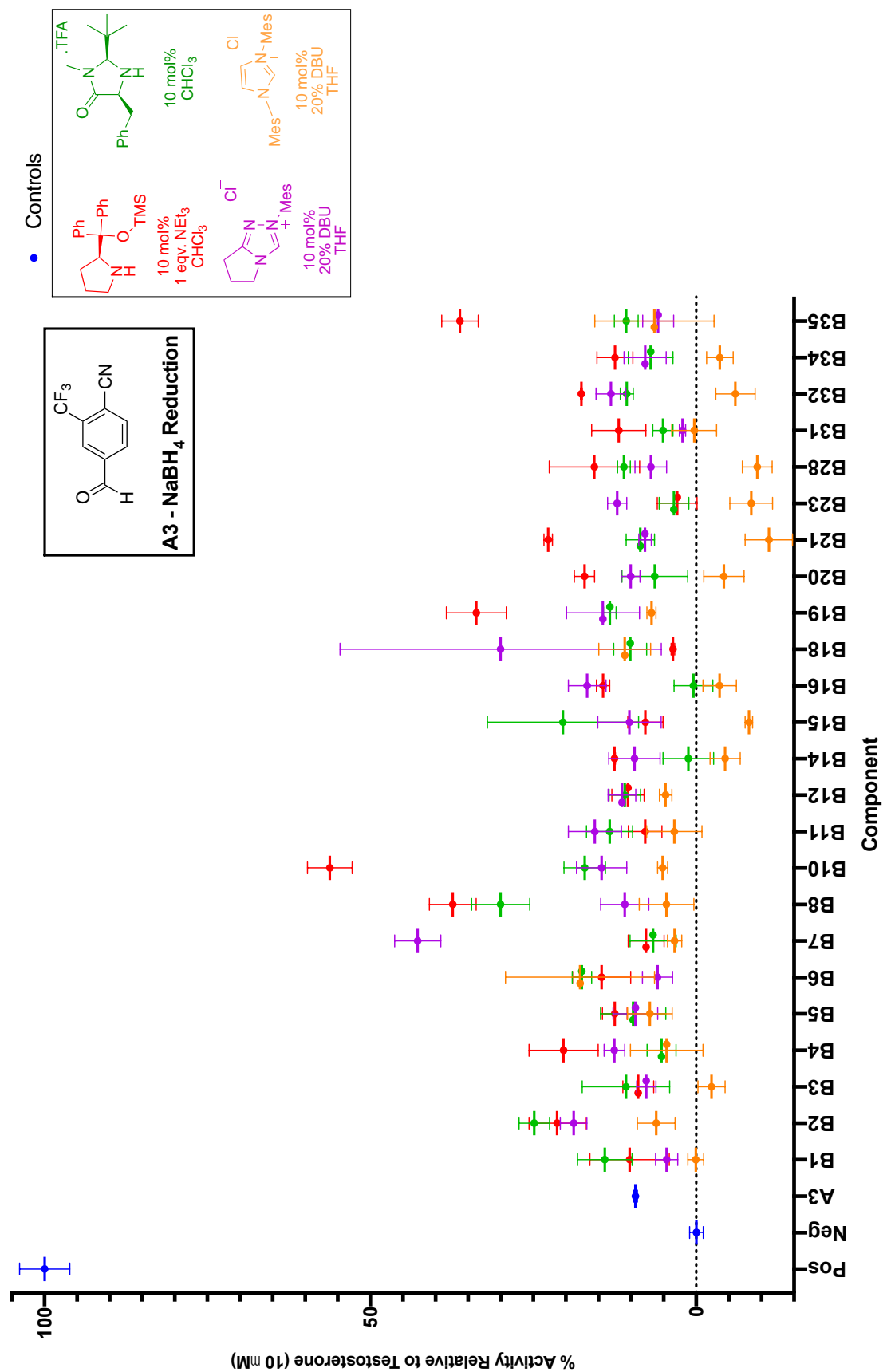


**Figure 6.3** - Assay data for reactions involving substrate **A1** with the reductive amination protocol, screened at  $\Sigma[P_n] = 10 \mu\text{M}$ .

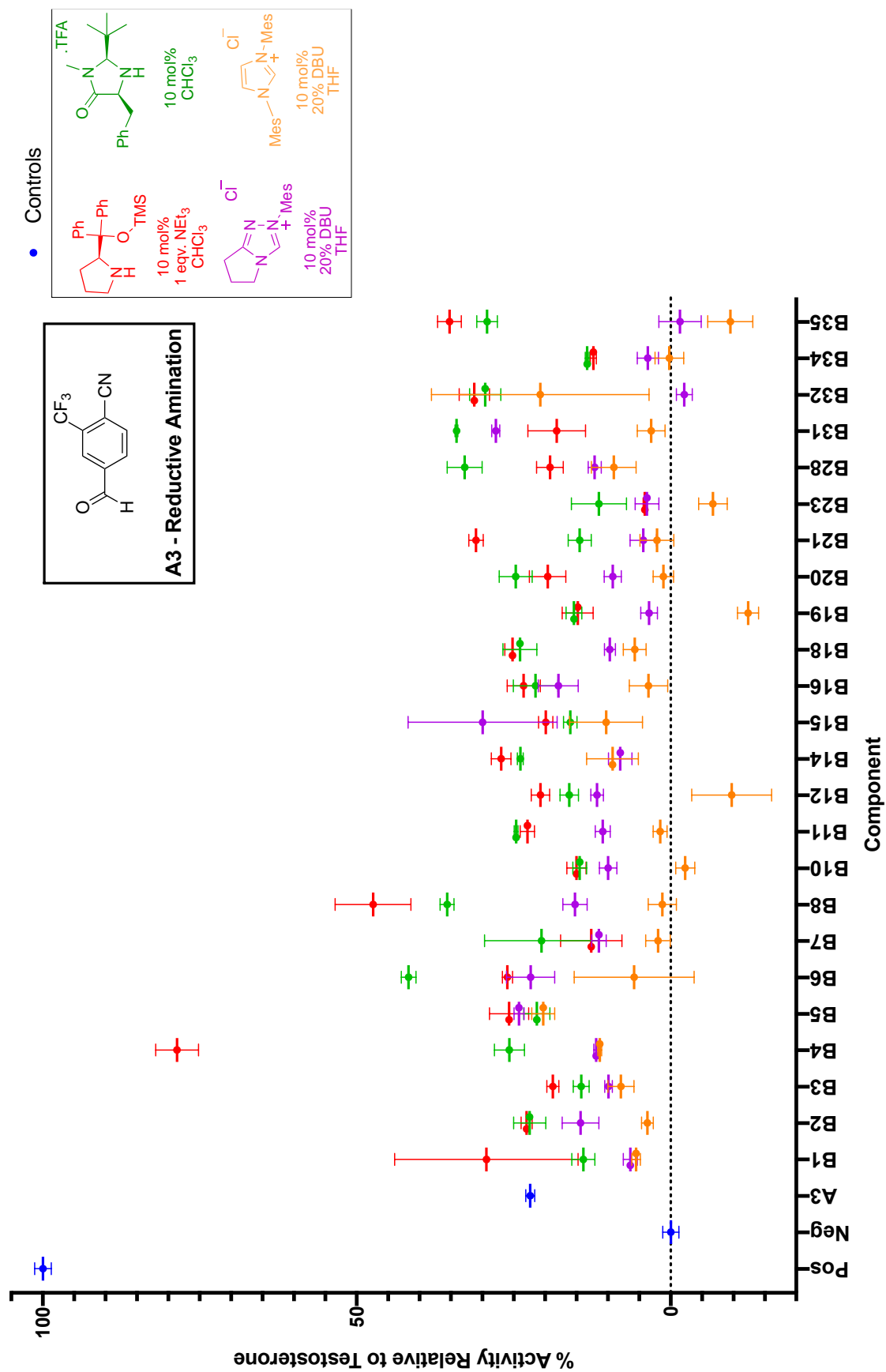


**Figure 6.4** - Assay data for the reactions involving substrate **A2** with the sodium borohydride reduction protocol, screened at  $\Sigma[P_n] = 10 \mu\text{M}$ .

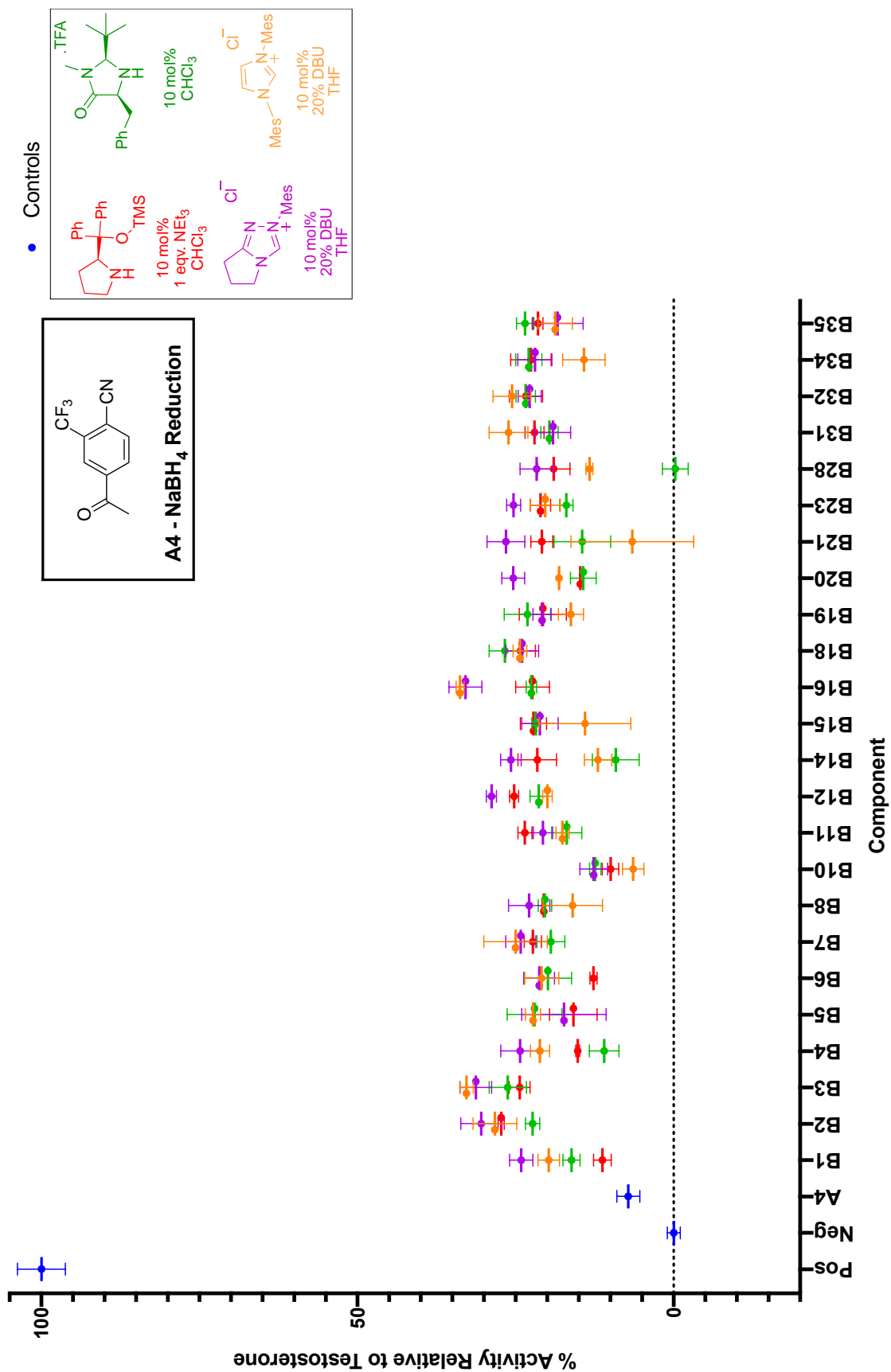




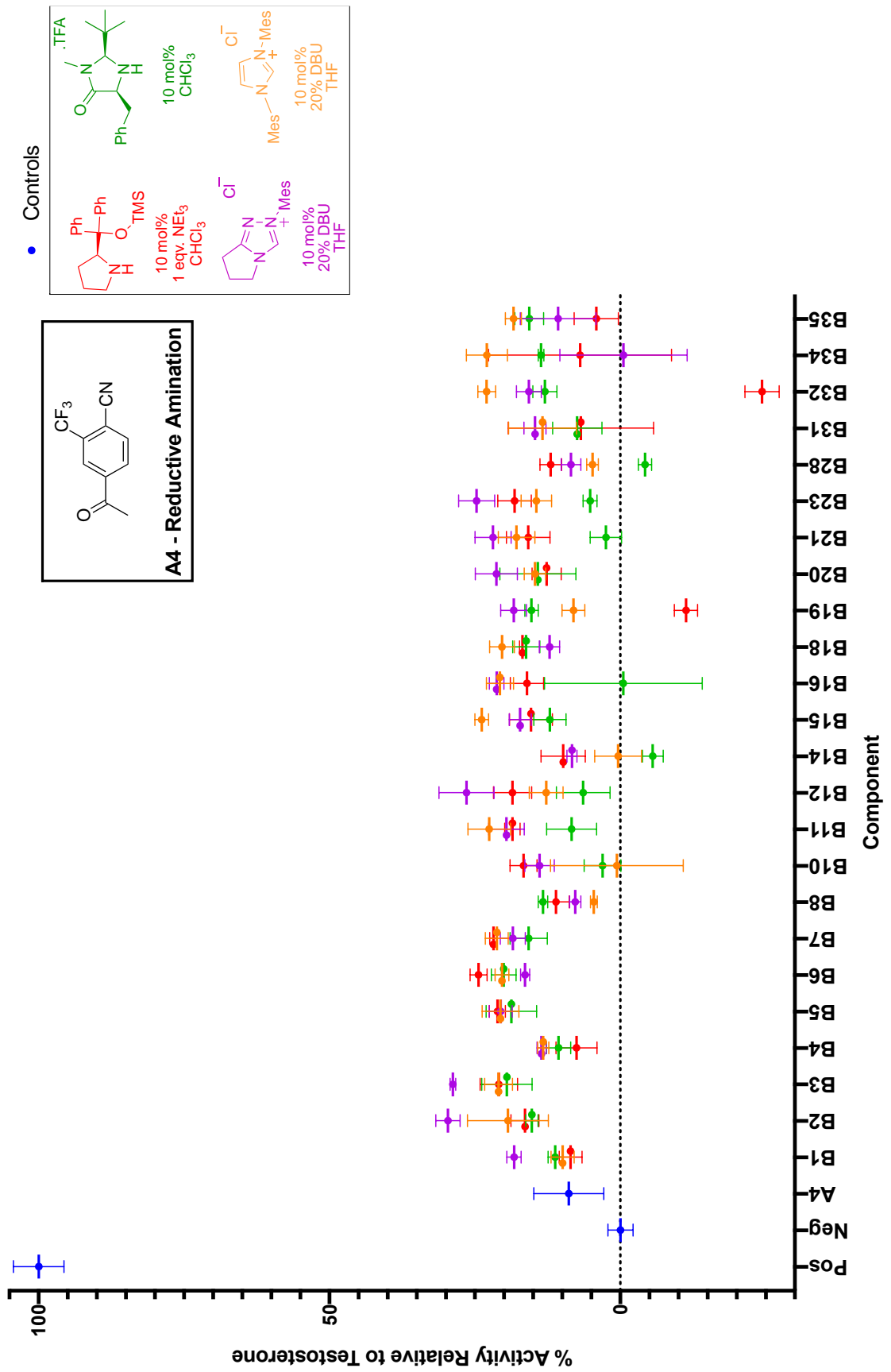
**Figure 6.6** - Assay data for reactions involving **A3** with the sodium borohydride reduction protocol, screened at  $\Sigma[P_n] = 10 \mu\text{M}$ .



**Figure 6.7** - Assay data for reactions involving the substrate **A3** with the reductive amination protocol, screened at  $\Sigma[P_n] = 10 \mu\text{M}$ .

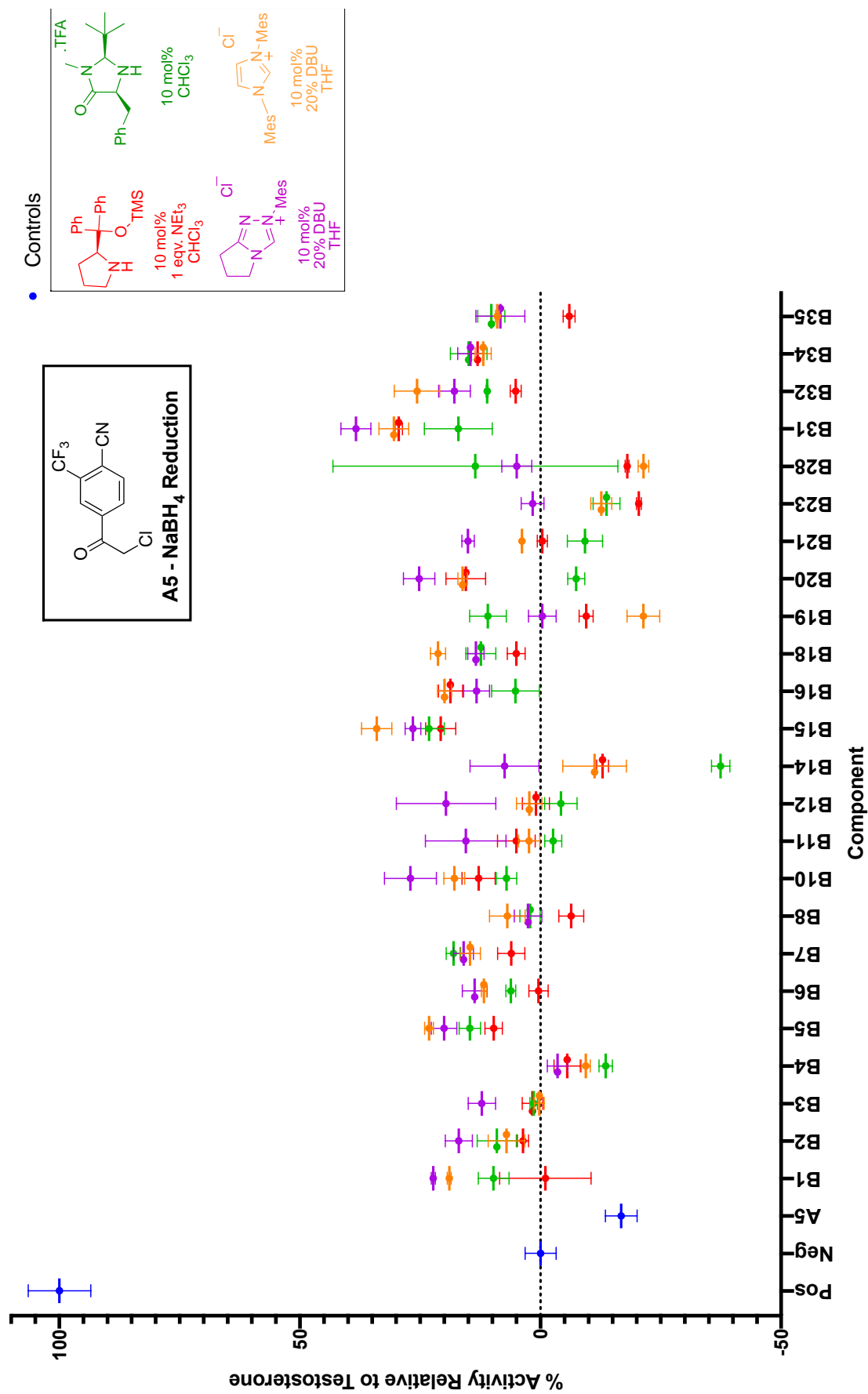


**Figure 6.8** - Assay data for reactions involving substrate **A4** with the sodium borohydride reduction protocol, screened at  $\Sigma[P_n] = 10 \mu\text{M}$ .

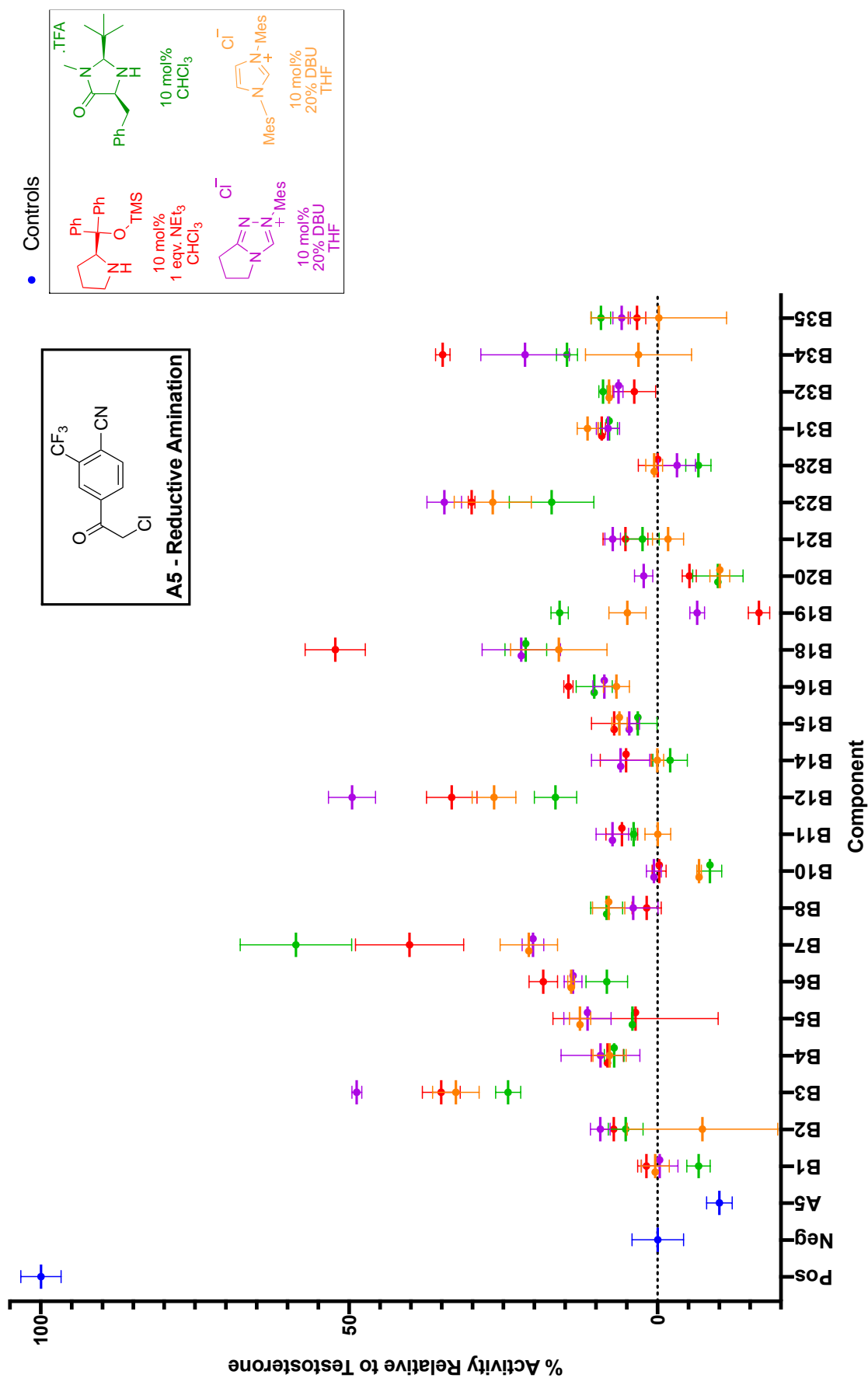


**Figure 6.9** - Assay data for reactions involving the substrate **A4** with the reductive amination protocol, screened at  $\Sigma[P_n] = 10 \mu\text{M}$ .





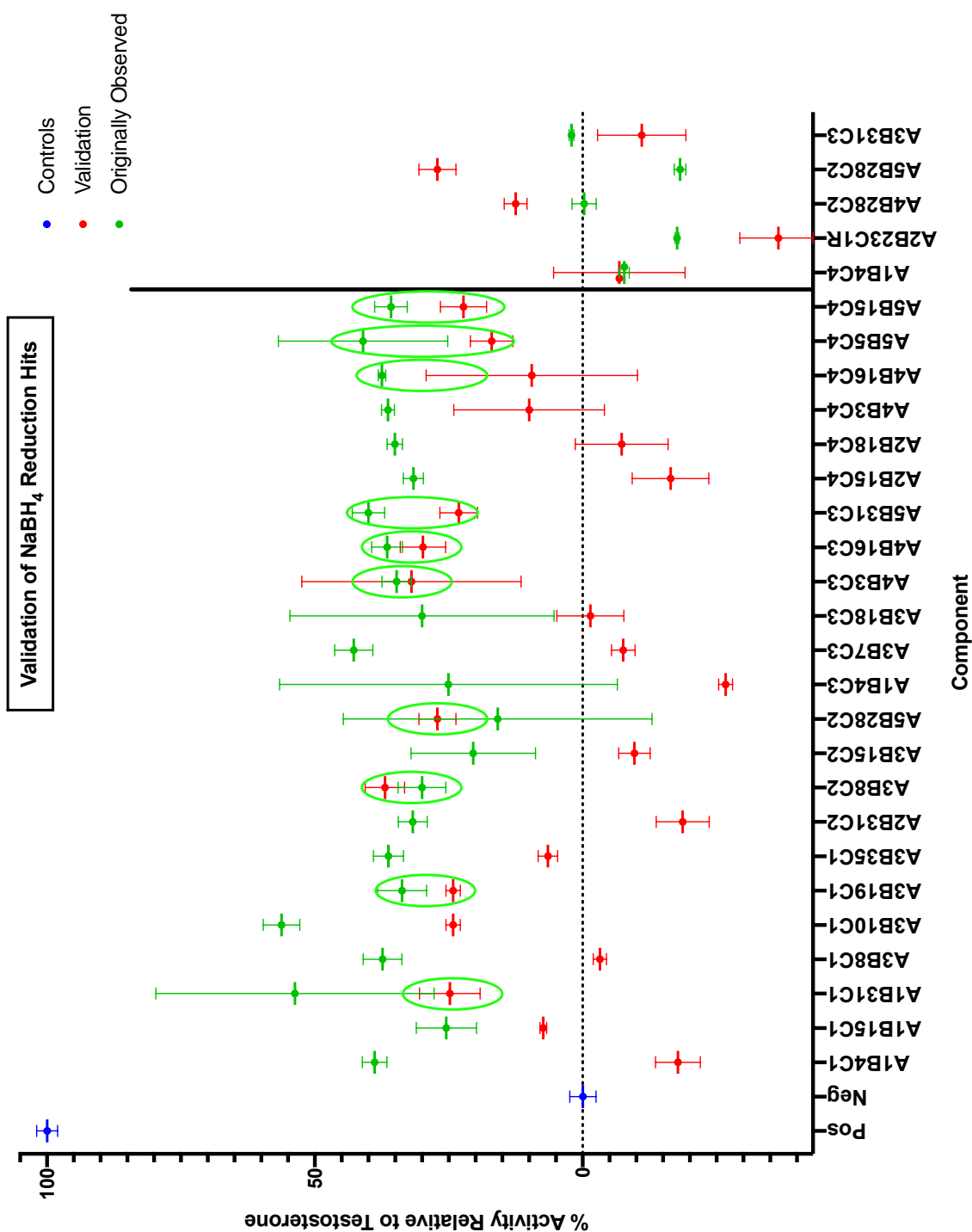
**Figure 6.10** - Assay data for reactions involving substrate **A5** with the sodium borohydride reduction protocol, screened at  $\Sigma[P_n] = 10 \mu\text{M}$ .

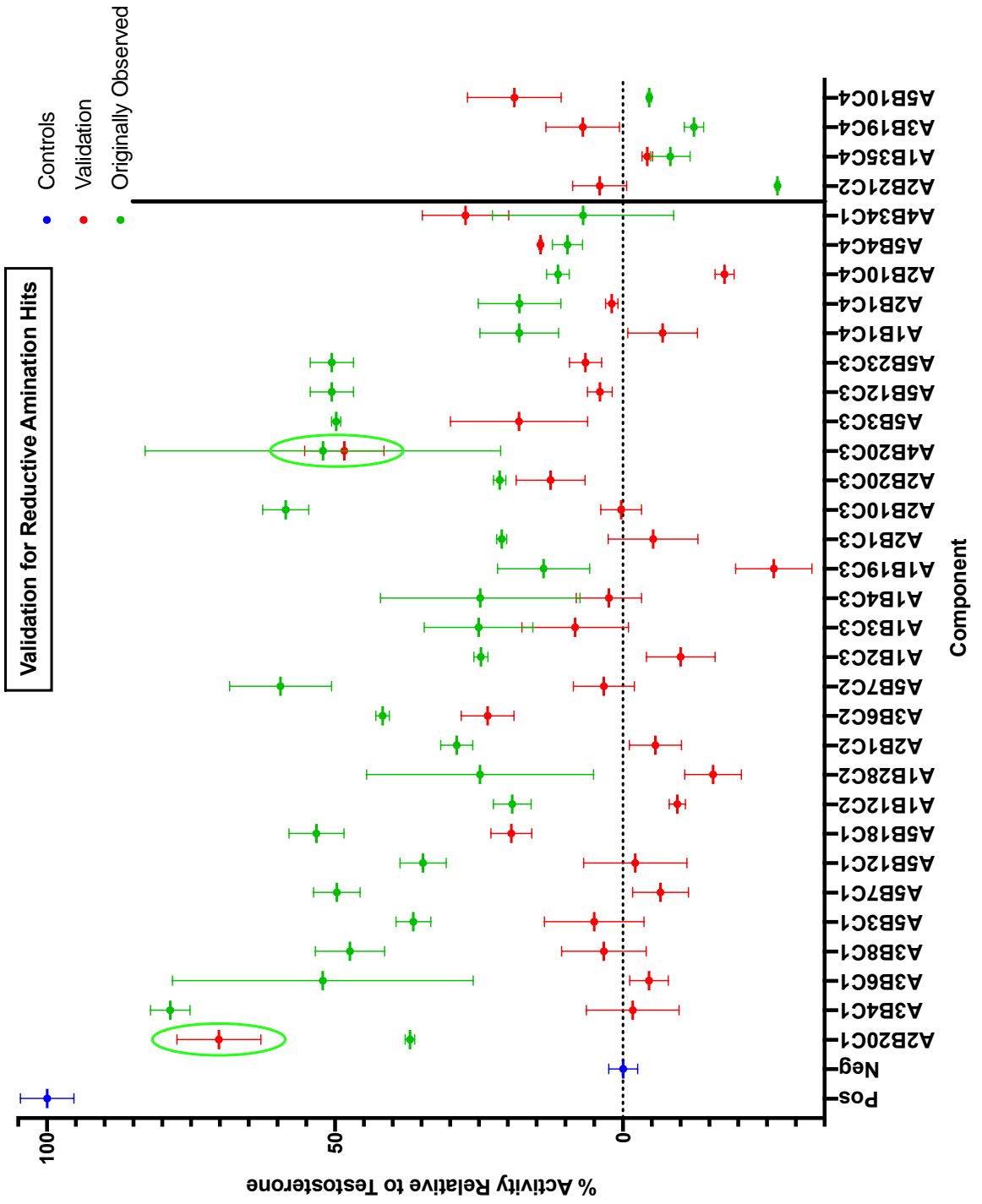


**Figure 6.11** - Assay data for reactions involving the substrate **A5** with the reductive amination protocol, screened at  $\Sigma[P_n] = 10 \mu\text{M}$ .

### 6.8.1 Round 1 Validation Study

The following data shows the validation arrays for the hits identified from the first round reaction arrays using organocatalytic ADS. The reactions were repeated identically to the first round reactions and screened again using the single-point assay protocol at a screening concentration of  $\Sigma[P_n] = 10 \mu\text{M}$ . Reactions that were highlighted to develop a new reaction array are highlighted, and summarised in **Table 3.2**.

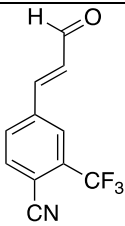
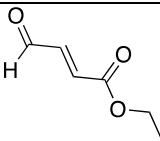
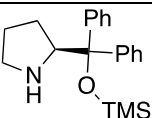
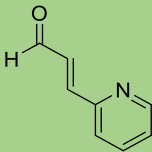
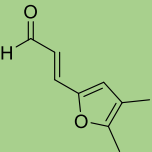
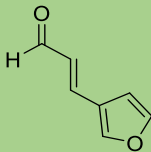
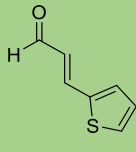
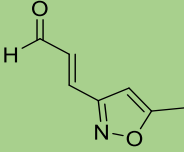
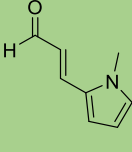
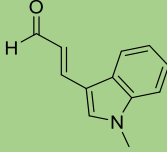


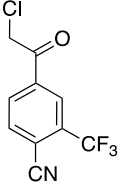
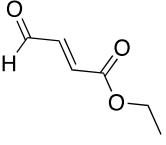
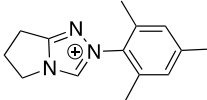


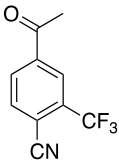
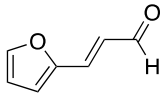
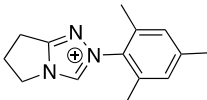
## 6.9 Design of Round 2 ADS Reaction Arrays

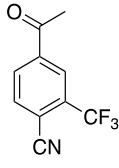
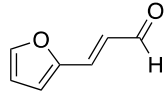
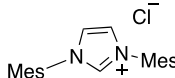
Substrates for Round 2 are shown in the following tables. For each active combination identified from the first round of the exhaustive reaction arrays, up to 7 structurally-related analogues of the co-substrate were selected with the aid of cheminformatics tools such as Pipeline Pilot and Knime. The co-substrates had favourable properties, in addition to exhibiting structural similarity to the co-substrate present in the original active combination.

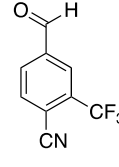
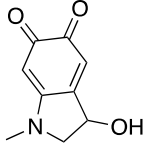
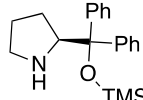
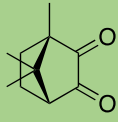
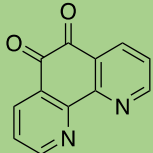
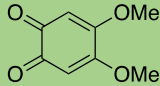
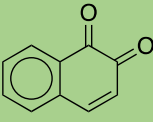
Additionally, each new reaction featured both catalysts within the class that was used in the original hit. For example, if NHC catalyst system was used in the original hit, both NHC systems (**C3** + **C4**) were used in the new reaction. The substrate and work-up protocol in each reaction remained the same for each new combination.

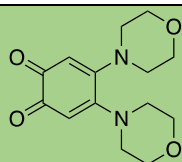
<b>A1B31C1R</b>	 <p><b>A1</b></p>	 <p><b>B31</b></p>	 <p>+ <i>ent</i>, 1 equiv. NEt<sub>3</sub> CHCl<sub>3</sub> <b>C1</b></p>
 <p><b>D1</b></p>	 <p><b>D2</b></p>	 <p><b>D3</b></p>	 <p><b>D4</b></p>
 <p><b>D5</b></p>	 <p><b>D6</b></p>	 <p><b>D7</b></p>	
<p><i>As the hit reaction used a secondary amine catalyst system, both secondary amine catalysts (C1 + C2) were used in all new combinations, with D1-D7 replacing B31.</i></p>			

<b>A5B31C3R</b>	 <p><b>A5</b></p>	 <p><b>B31</b></p>	 <p>DBU, THF <b>C3</b></p>
<b>D1 – D7</b>			
<i>As the hit reaction used an NHC catalyst system, both NHC catalyst systems (C3 + C4) were utilised for all new combinations, with D1-D7 replacing B31.</i>			

<b>A4B16C3R</b>	 <p><b>A4</b></p>	 <p><b>B16</b></p>	 <p>DBU, THF <b>C3</b></p>
<b>D1 – D7</b>			
<i>As the hit reaction used an NHC catalyst system, both NHC catalyst systems (C3 + C4) were utilised for all new combinations, with D1-D7 replacing B31.</i>			

<b>A4B16C4R</b>	 <p><b>A4</b></p>	 <p><b>B16</b></p>	 <p>DBU, THF <b>C4</b></p>
<b>D1 – D7</b>			
<i>As the hit reaction used an NHC catalyst system, both NHC catalyst systems (C3 + C4) were utilised for all new combinations, with D1-D7 replacing B31.</i>			

<b>A3B19C1R</b>	 <p><b>A3</b></p>	 <p><b>B19</b></p>	 <p>+ <i>ent</i>, 1 equiv. NEt<sub>3</sub> CHCl<sub>3</sub> <b>C1</b></p>
 <p><b>E1</b></p>	 <p><b>E2</b></p>	 <p><b>E3</b></p>	 <p><b>E4</b></p>



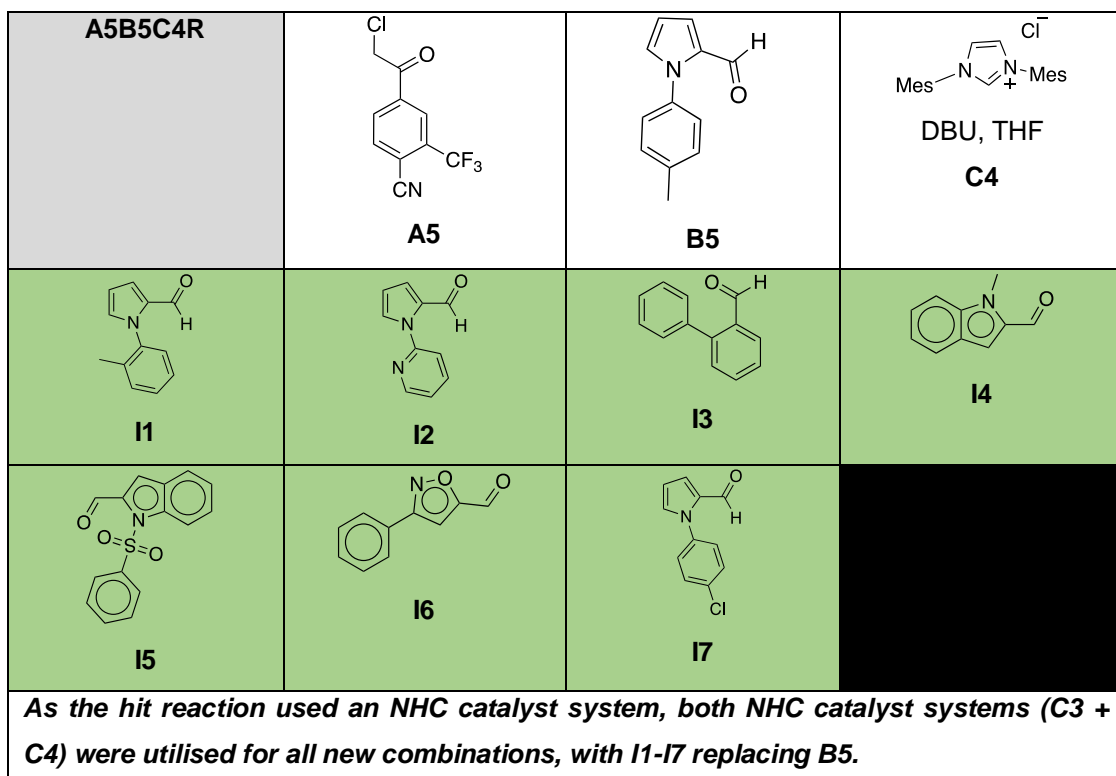
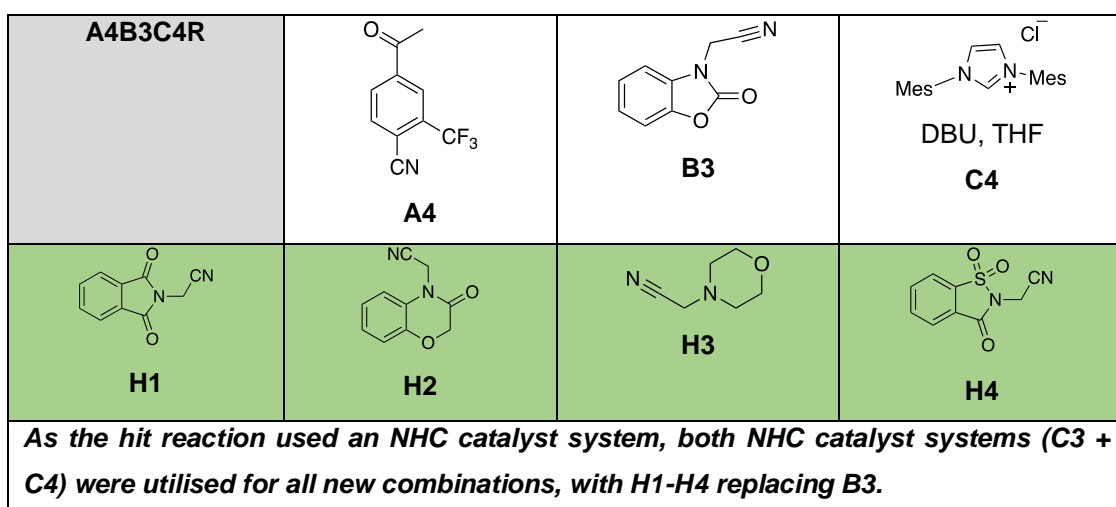
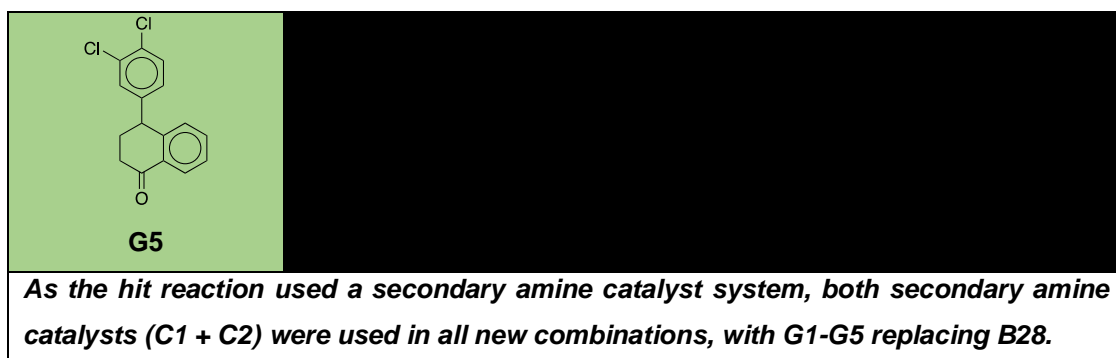
E5

*As the hit reaction used a secondary amine catalyst system, both secondary amine catalysts (C1 + C2) were used in all new combinations, with E1-E5 replacing B19.*

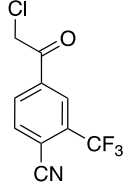
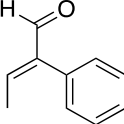
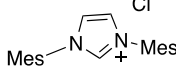
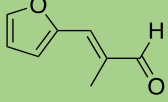
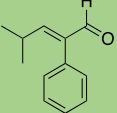
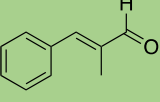
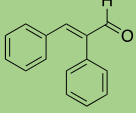
A3B8C2R	<p>A3</p>	<p>B8</p>	<p>+ ent, CHCl<sub>3</sub> C2</p>
<p>F1</p>	<p>F2</p>	<p>F3</p>	<p>F4</p>
<p>F5</p>	<p>F6</p>	<p>F7</p>	

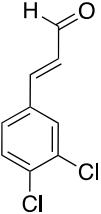
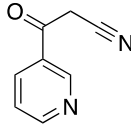
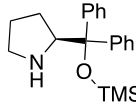
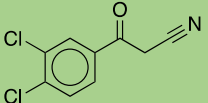
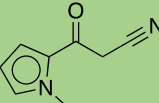
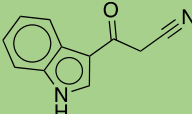
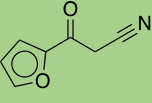
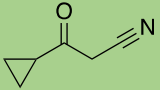
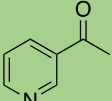
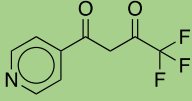
*As the hit reaction used a secondary amine catalyst system, both secondary amine catalysts (C1 + C2) were used in all new combinations, with F1-F7 replacing B8.*

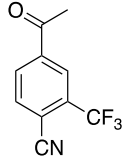
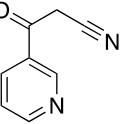
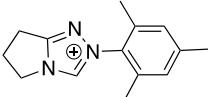
A5B28C2R	<p>A5</p>	<p>B28</p>	<p>+ ent, CHCl<sub>3</sub> C2</p>
<p>G1</p>	<p>G2</p>	<p>G3</p>	<p>G4</p>





<b>A5B15C4R</b>	 <p><b>A5</b></p>	 <p><b>B15</b></p>	 <p>DBU, THF <b>C4</b></p>
 <p><b>J1</b></p>	 <p><b>J2</b></p>	 <p><b>J3</b></p>	 <p><b>J4</b></p>
<p><i>As the hit reaction used an NHC catalyst system, both NHC catalyst systems (C3 + C4) were utilised for all new combinations, with J1-J4 replacing B15.</i></p>			

<b>A2B20C1RA</b>	 <p><b>A2</b></p>	 <p><b>B20</b></p>	 <p>+ <i>ent</i>, 1 equiv. NEt<sub>3</sub> CHCl<sub>3</sub> <b>C1</b></p>
 <p><b>K1</b></p>	 <p><b>K2</b></p>	 <p><b>K3</b></p>	 <p><b>K4</b></p>
 <p><b>K5</b></p>	 <p><b>K6</b></p>	 <p><b>K7</b></p>	
<p><i>As the hit reaction used a secondary amine catalyst system, both secondary amine catalysts (C1 + C2) were used in all new combinations, with K1-K7 replacing B20.</i></p>			

<b>A4B20C3RA</b>	 <p><b>A4</b></p>	 <p><b>B20</b></p>	 <p>DBU, THF <b>C3</b></p>
<b>K1-K7</b>			
<p><i>As the hit reaction used an NHC catalyst system, both NHC catalyst systems (C3 + C4) were utilised for all new combinations, with K1-K7 replacing B20.</i></p>			

## 6.10 Methods for Evaluation and Scale-Up

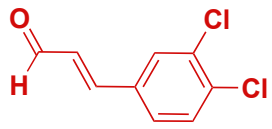
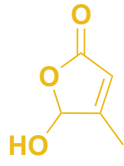
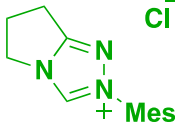
To evaluate reactions that indicated bioactivity in the ADS reaction arrays, a number of methods were used to identify both reaction conversion and bioactivity of components, that are outlined in **Section 1.1**.

### ***6.10.1 NMR Analysis Reaction Tracing Experiments***

Reactions were recreated as they were carried out in the original reaction arrays, albeit on a scale five times larger, and utilising deuterated solvents to facilitate NMR analysis. Analysis of the reactions was only carried out prior to execution of the work-up conditions, as this would allow validation that any products that were formed were the result of intermolecular organocatalytic reactions.

1. Obtain  $^{13}\text{C}$  NMR (125 MHz) analyses for the separate components in deuterated solvents.
2. For the desired reaction in each well, add first 50  $\mu\text{L}$  of the substrate solution, followed by 100  $\mu\text{L}$  of the co-substrate solution.
3. Allow evaporation.
4. Add 500  $\mu\text{L}$  of the desired catalytic system in deuterated solvent, before transferring to an NMR tube and sealing.
5.  $^{13}\text{C}$  NMR (125 MHz) was carried out at 6 hour, 24 hour and 48 hour intervals to allow observation of changes in reaction mixture composition.

Analyses for the reaction mixtures **A5G5C1R** and **A1TB20C3R** are shown in **Figure 3.20** and **Figure 3.21** respectively. Analysis for the reaction mixture **A2TB20C3R** can be observed below.

Armed Substrate	Co-Substrate	Catalyst/Additive
		 10 mol% 20% DBU in d <sup>8</sup> -THF

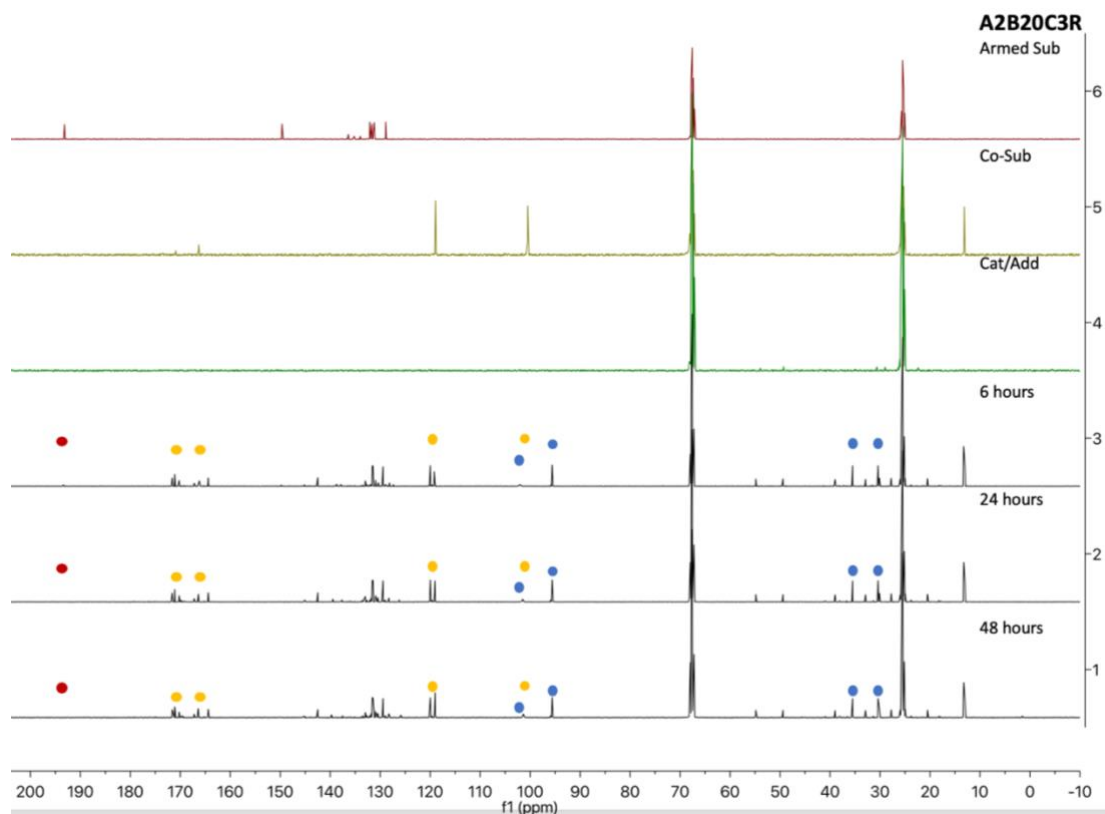


**Table 6.2** - Analysis of the **A2TB20C3R** combination *via* 500 MHz <sup>13</sup>C-NMR demonstrated conversion of both **substrate** and **co-substrates**, and formation of new peaks prior to being subjected to the sodium borohydride reduction. **Blue** dots indicate new peaks in NMR spectra.

### 6.10.2 Crude Dose-Response Experiments

The reaction mixtures from the NMR analysis were subjected to the relevant work-up protocols, before evaporating to obtain the residue of the crude product mixture. This crude product mixture was then assayed using the dose-response protocol outlined in **Section 6.6.2**, with the concentration screened at remaining relative to the limiting substrate.

### 6.10.3 Fractionation of Reactions

The reactions outlined in **Table 3.3** and **Table 3.4** were repeated as they had been in the reaction arrays, albeit in a round-bottomed flask and scaled up by a factor of 50. Following execution of the work-up, the product mixtures were evaporated under reduced pressure, and subsequently fractionated *via* flash column chromatography, eluting with slow-running solvent systems to attempt to isolate individual components within the reaction mixture. All columns were flushed with DCM–MeOH (98:2) following the fractionation to obtain any remaining polar fractions from the column. The fractions were then evaporated under reduced pressure, and each fraction of the reaction screened using the single-point assay procedure outlined in **Section 6.6.3** at a concentration of 20  $\mu\text{M}$  relative to the limiting substrate.

Reaction	Fraction 1	Fraction 2	Fraction 3	Fraction 4	Fraction 5	Fraction 6	Fraction 7
A5G5C1R	30	60	45	16	5	13	
A2K1C1RA	3	1	1	11	8	15	9
A4K1C3RA	6	6	-1	19	0		
A5J4C3R	12	5	-2	7	-3	1	
A4D5C4R	7	14	8	3	-6	-9	
A4H4C4R	6	7	7	1	-5	-9	
A1TB6C1R	5	3	7	19	18	0	
A1TB20C3R	2	14	24	8	2		
A1TB22C3R	-17	11	7	6	14		
A2TB20C3R	19	28	14	18	5		
A2TB22C3R	9	11	7	6	14		

**Table 6.3** – Bioactivity (% value relative to that of testosterone (10  $\mu\text{M}$ )) of the fractions at a 20  $\mu\text{M}$  screening concentration

The results from the NMR reaction tracking by  $^{13}\text{C}$  NMR, the crude-dose response curves and the fractionation (**Table 6.3**) were interpreted to indicate that bioactive components were in the product mixtures **A5G5C1R**, **A1TB20C3R** and **A2TB20C3R**. The  $^1\text{H}$  NMR analysis of the relevant fractions indicated that they were the same as compounds **35**, **36** and **37** respectively, each of which were synthesised *via* an independent method.

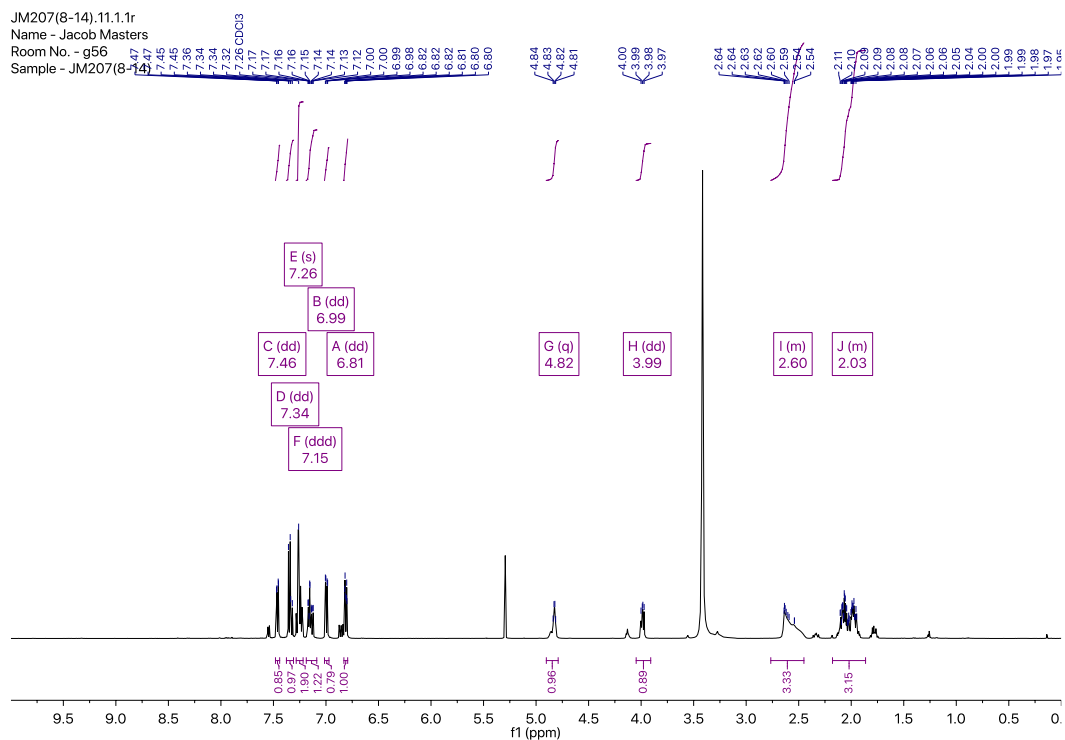


**Figure 6.12** -  $^1\text{H}$  NMR spectrum (500 MHz) of the bioactive Fraction 2 of **A5G5C1R** – the NMR is the same as observed for **35a**.

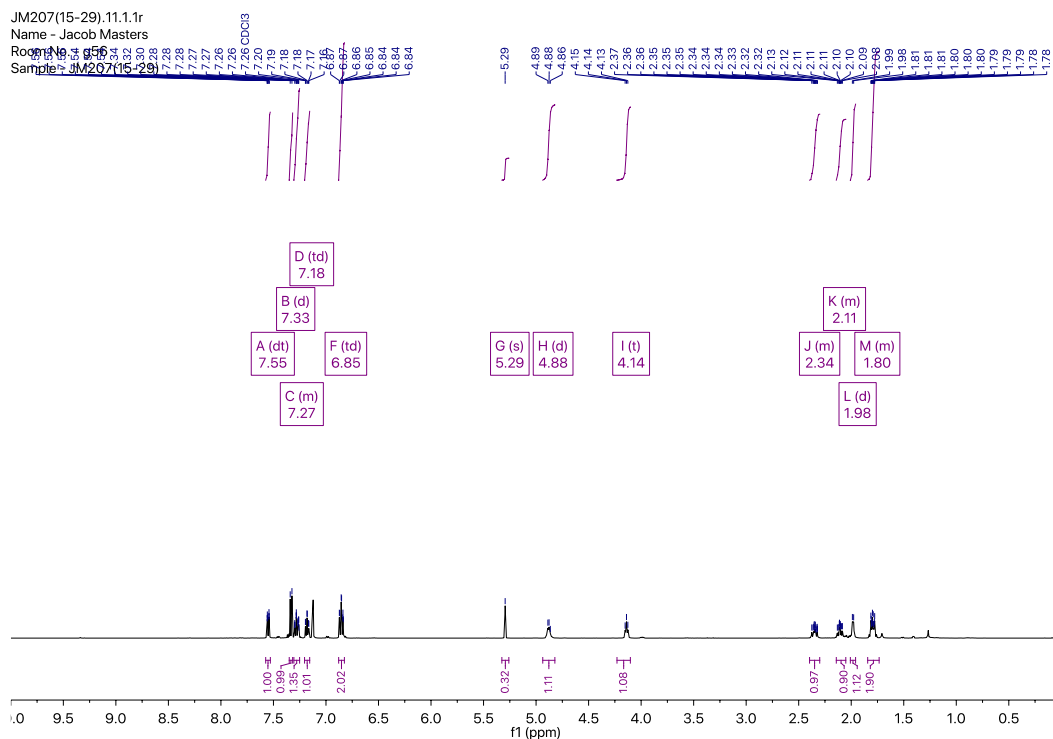


**Figure 6.13** -  $^1\text{H}$  NMR spectrum (500 MHz) of the bioactive Fraction 2 of **A5G5C1R** – the NMR is the same as observed for **35b**.

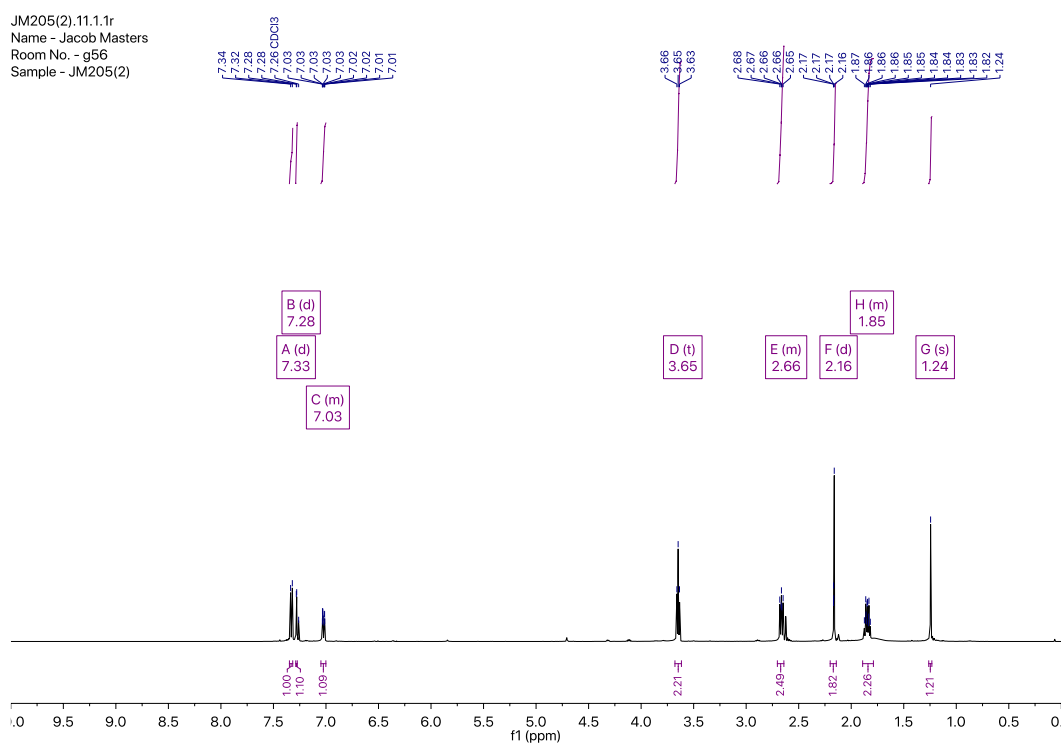


**Figure 6.14** -  $^1\text{H}$  NMR spectrum (500 MHz) of the bioactive Fraction 2 of A1TB20C3R – the NMR is the same as observed for 36.

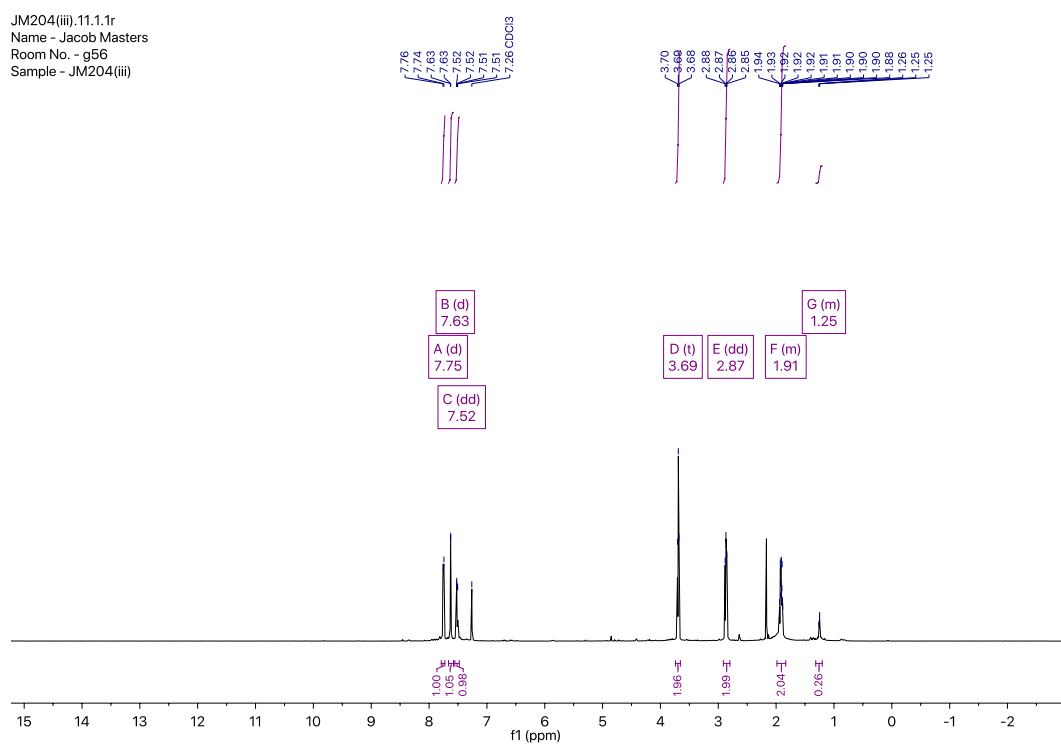


**Figure 6.15** –  $^1\text{H}$  NMR spectrum (500 MHz) of the bioactive Fraction 2 of A2TB20C3R – the NMR is the same as observed for 37.

## 7 References

- 1 E. Patridge, P. Gareiss, M. S. Kinch and D. Hoyer, *Drug Discov. Today*, 2015, **00**, 8–11.
- 2 S. D. Roughley and A. M. Jordan, *J. Med. Chem.*, 2011, **54**, 3451–3479.
- 3 A. H. Lipkus, Q. Yuan, K. A. Lucas, S. A. Funk, W. F. Bartelt, R. J. Schenck and A. J. Trippe, *J. Org. Chem.*, 2008, **73**, 4443–4451.
- 4 M. E. Bunnage, *Nat. Chem. Biol.*, 2011, **7**, 335–339.
- 5 P. Ertl, S. Roggo and A. Schuffenhauer, *J. Chem. Inf. Model.*, 2008, **48**, 68–74.
- 6 T. Henkel, R. M. Brunne, H. Müller and F. Reichel, *Angew. Chemie Int. Ed.*, 1999, **38**, 643–647.
- 7 D. G. Brown and J. Boström, *J. Med. Chem.*, 2018, **61**, 9442–9468.
- 8 D. G. Brown and J. Boström, *J. Med. Chem.*, 2016, **59**, 4443–4458.
- 9 S. Y. Chow and A. Nelson, *J. Med. Chem.*, 2017, **60**, 3591–3593.
- 10 W. P. Walters, J. Green, J. R. Weiss and M. A. Murcko, *J. Med. Chem.*, 2011, **54**, 6405–6416.
- 11 C. Lipinski and A. Hopkins, *Nature*, 2004, **432**, 855–861.
- 12 T. Cernak, K. D. Dykstra, S. Tyagarajan, P. Vachal and S. W. Krska, *Chem. Soc. Rev.*, 2016, **45**, 546–576.
- 13 T. Gensch, M. N. Hopkinson, F. Glorius and J. Wencel-Delord, *Chem. Soc. Rev.*, 2016, **45**, 2900–2936.
- 14 M. H. Shaw, J. Twilton and D. W. C. MacMillan, *J. Org. Chem.*, 2016, **81**, 6898–6926.
- 15 J. Boström, D. G. Brown, R. J. Young and G. M. Keserü, *Nat. Rev. Drug Discov.*, 2018, **17**, 709–727.
- 16 K. R. Campos, P. J. Coleman, J. C. Alvarez, S. D. Dreher, R. M. Garbaccio, N. K. Terrett, R. D. Tillyer, M. D. Truppo and E. R. Parmee, *Science*, 2019, **363**, eaat0805.
- 17 R. Macarron, M. N. Banks, D. Bojanic, D. J. Burns, D. a Cirovic, T. Garyantes, D. V. S. Green, R. P. Hertzberg, W. P. Janzen, J. W. Paslay, U. Schopfer and G. S. Sittampalam, *Nat. Rev. Drug Discov.*, 2011, **10**, 188–195.

- 18 K. H. Bleicher, H.-J. Böhm, K. Müller and A. I. Alanine, *Nat. Rev. Drug Discov.*, 2003, **2**, 369–378.
- 19 S. Fox, S. Farr-Jones, L. Sopchak, A. Boggs, H. W. Nicely, R. Khoury and M. Biro, *J. Biomol. Screen.*, 2006, **11**, 864–869.
- 20 S. Wilhelm, C. Carter, M. Lynch, T. Lowinger, J. Dumas, R. a Smith, B. Schwartz, R. Simantov and S. Kelley, *Nat. Rev. Drug Discov.*, 2006, **5**, 835–844.
- 21 W. Kolch, A. Kotwaliwale, K. Vass and P. Janosch, *Expert Rev. Mol. Med.*, 2002, **4**, 1–18.
- 22 O. B. McDonald, W. J. Chen, B. Ellis, C. Hoffman, L. Overton, M. Rink, A. Smith, C. J. Marshall and E. R. Wood, *Anal. Biochem.*, 1999, **268**, 318–329.
- 23 A. van Oeveren, M. Motamedi, N. S. Mani, K. B. Marschke, F. J. López, W. T. Schrader, A. Negro-Vilar and L. Zhi, *J. Med. Chem.*, 2006, **49**, 6143–6146.
- 24 F. Lovering, J. Bikker and C. Humblet, *J. Med. Chem.*, 2009, **52**, 6752–6756.
- 25 T. E. Nielsen and S. L. Schreiber, *Angew. Chemie Int. Ed.*, 2008, **47**, 48–56.
- 26 D. S. Tan, *Nat. Chem. Biol.*, 2005, **1**, 74–84.
- 27 S. Dandapani, A. R. Germain, I. Jewett, S. le Qument, J.-C. Marie, G. Muncipinto, J. R. Duvall, L. C. Carmody, J. R. Perez, J. C. Engel, J. Gut, D. Kellar, J. L. Siqueira-Neto, J. H. McKerrow, M. Kaiser, A. Rodriguez, M. A. Palmer, M. Foley, S. L. Schreiber and B. Munoz, *ACS Med. Chem. Lett.*, 2014, **5**, 149–153.
- 28 M. D. Burke and S. L. Schreiber, *Angew. Chemie Int. Ed.*, 2004, **43**, 46–58.
- 29 W. R. J. D. Galloway, A. Isidro-Llobet and D. R. Spring, *Nat. Commun.*, 2010, **1**, 1–13.
- 30 R. J. Spandl, A. Bender and D. R. Spring, *Org. Biomol. Chem.*, 2008, **6**, 1149.
- 31 B. M. Ibbeson, L. Laraia, E. Alza, C. J. O' Connor, Y. S. Tan, H. M. L. Davies, G. McKenzie, A. R. Venkitaraman and D. R. Spring, *Nat. Commun.*, 2014, **5**, 3155.



- 32 R. Doveston, S. Marsden and A. Nelson, *Drug Discov. Today*, 2014, **19**, 813–819.
- 33 A. Nadin, C. Hattotuwigama and I. Churcher, *Angew. Chemie Int. Ed.*, 2012, **51**, 1114–1122.
- 34 D. J. Foley, P. G. E. Craven, P. M. Collins, R. G. Doveston, A. Aimon, R. Talon, I. Churcher, F. von Delft, S. P. Marsden and A. Nelson, *Chem. - A Eur. J.*, 2017, **23**, 15227–15232.
- 35 A. Aimon, G. Karageorgis, J. Masters, M. Dow, P. G. E. Craven, M. Ohsten, A. Willaume, R. Morgentin, N. Ruiz-Llamas, H. Lemoine, T. Kalliokoski, A. J. Eatherton, D. J. Foley, S. P. Marsden and A. Nelson, *Org. Biomol. Chem.*, 2018, **16**, 3160–3167.
- 36 A. C. Anderson, *Chem. Biol.*, 2003, **10**, 787–797.
- 37 B. D. Dorsey, R. B. Levin, S. L. McDaniel, J. P. Vacca, J. P. Guare, P. L. Darke, J. A. Zugay, E. a Emini and W. a Schleif, *J. Med. Chem.*, 1994, **37**, 3443–3451.
- 38 B. K. Shoichet, S. L. McGovern, B. Wei and J. J. Irwin, *Curr. Opin. Chem. Biol.*, 2002, **6**, 439–446.
- 39 J. Lyu, S. Wang, T. E. Balius, I. Singh, A. Levit, Y. S. Moroz, M. J. O'Meara, T. Che, E. Alga, K. Tolmachova, A. A. Tolmachev, B. K. Shoichet, B. L. Roth and J. J. Irwin, *Nature*, 2019, **566**, 224–229.
- 40 P. M. Colman, *Curr. Opin. Struct. Biol.*, 1994, **4**, 868–874.
- 41 S. B. Shuker, P. J. Hajduk, R. P. Meadows and S. W. Fesik, *Science (80-. )*, 1996, **274**, 1531–1534.
- 42 D. A. Erlanson, S. W. Fesik, R. E. Hubbard, W. Jahnke and H. Jhoti, *Nat. Rev. Drug Discov.*, 2016, **15**, 605–619.
- 43 T. Fink, H. Bruggesser and J.-L. Reymond, *Angew. Chemie Int. Ed.*, 2005, **44**, 1504–1508.
- 44 L. Ruddigkeit, R. van Deursen, L. C. Blum and J.-L. Reymond, *J. Chem. Inf. Model.*, 2012, **52**, 2864–2875.
- 45 A. L. Hopkins, G. M. Keserü, P. D. Leeson, D. C. Rees and C. H. Reynolds, *Nat. Rev. Drug Discov.*, 2014, **13**, 105–121.
- 46 M. Congreve, G. Chessari, D. Tisi and A. J. Woodhead, *J. Med. Chem.*, 2008, **51**, 3661–3680.
- 47 J. D. Scott, S. W. Li, A. P. J. Brunskill, X. Chen, K. Cox, J. N.

- Cumming, M. Forman, E. J. Gilbert, R. A. Hodgson, L. A. Hyde, Q. Jiang, U. Iserloh, I. Kazakevich, R. Kuvelkar, H. Mei, J. Meredith, J. Misiaszek, P. Orth, L. M. Rossiter, M. Slater, J. Stone, C. O. Strickland, J. H. Voigt, G. Wang, H. Wang, Y. Wu, W. J. Greenlee, E. M. Parker, M. E. Kennedy and A. W. Stamford, *J. Med. Chem.*, 2016, **59**, 10435–10450.
- 48 T. Cernak, N. J. Gesmundo, K. Dykstra, Y. Yu, Z. Wu, Z.-C. Shi, P. Vachal, D. Sperbeck, S. He, B. A. Murphy, L. Sonatore, S. Williams, M. Madeira, A. Verras, M. Reiter, C. H. Lee, J. Cuff, E. C. Sherer, J. Kuethe, S. Goble, N. Perrotto, S. Pinto, D.-M. Shen, R. Nargund, J. Balkovec, R. J. DeVita and S. D. Dreher, *J. Med. Chem.*, 2017, **60**, 3594–3605.
- 49 M. Werner, C. Kuratli, R. E. Martin, R. Hochstrasser, D. Wechsler, T. Enderle, A. I. Alanine and H. Vogel, *Angew. Chemie - Int. Ed.*, 2014, **53**, 1704–1708.
- 50 N. J. Gesmundo, B. Sauvagnat, P. J. Curran, M. P. Richards, C. L. Andrews, P. J. Dandliker and T. Cernak, *Nature*, 2018, **557**, 228–232.
- 51 G. Karageorgis, S. Warriner and A. Nelson, *Nat. Chem.*, 2014, **6**, 872–876.
- 52 R. A. Dixon, *Nature*, 2001, **411**, 843–847.
- 53 R. a Maplestone, M. J. Stone and D. H. Williams, *Gene*, 1992, **115**, 151–157.
- 54 N. P. Keller, G. Turner and J. W. Bennett, *Nat. Rev. Microbiol.*, 2005, **3**, 937–947.
- 55 S. Liver, J. Masters and A. Nelson, in *Chemical and Biological Synthesis: Enabling Approaches for Understanding Biology*, eds. N. J. Westwood and A. Nelson, Royal Society of Chemistry, Cambridge, 2018, pp. 138–152.
- 56 H. M. L. Davies and D. Morton, *Chem. Soc. Rev.*, 2011, **40**, 1857.
- 57 H. M. L. Davies and R. E. J. Beckwith, *Chem. Rev.*, 2003, **103**, 2861–2904.
- 58 S. Fujii, K. Ohta, T. Goto, A. Oda, H. Masuno, Y. Endo and H. Kagechika, *Medchemcomm*, 2012, **3**, 680.
- 59 G. Karageorgis, M. Dow, A. Aimon, S. Warriner and A. Nelson,

- Angew. Chemie Int. Ed.*, 2015, **54**, 13538–13544.
- 60 Y. Huang and J. W. Bode, *Nat. Chem.*, 2014, **6**, 877–884.
- 61 W. Gao and J. T. Dalton, *Drug Discov. Today*, 2007, **12**, 241–248.
- 62 W. Gao, C. E. Bohl and J. T. Dalton, *Chem. Rev.*, 2005, **105**, 3352–3370.
- 63 C. E. Brown-Sequard, *BMJ*, 1893, **1**, 1212–1214.
- 64 H. Fang, W. Tong, W. S. Branham, C. L. Moland, S. L. Dial, H. Hong, Q. Xie, R. Perkins, W. Owens and D. M. Sheehan, *Chem. Res. Toxicol.*, 2003, **16**, 1338–1358.
- 65 R. Narayanan, C. C. Coss and J. T. Dalton, *Mol. Cell. Endocrinol.*, 2018, **465**, 134–142.
- 66 A. L. Handlon, L. T. Schaller, L. M. Leesnitzer, R. V. Merrihew, C. Poole, J. C. Ulrich, J. W. Wilson, R. Cadilla and P. Turnbull, *ACS Med. Chem. Lett.*, 2016, **7**, 83–88.
- 67 D. W. C. MacMillan, *Nature*, 2008, **455**, 304–308.
- 68 E. Knoevenagel, *Chem. Ber.*, 1898, **31**, 2596–2619.
- 69 G. Bredig and P. S. Fiske, *Biochem. Z.*, 1912, **46**, 7–23.
- 70 Z. G. Hajos and D. R. Parrish, *J. Org. Chem.*, 1974, **39**, 1615–1621.
- 71 N. A. Paras and D. W. C. MacMillan, *J. Am. Chem. Soc.*, 2001, **123**, 4370–4371.
- 72 B. List, R. a Lerner and C. F. Barbas, *J. Am. Chem. Soc.*, 2000, **122**, 2395–2396.
- 73 B. List, *J. Am. Chem. Soc.*, 2000, **122**, 9336–9337.
- 74 K. A. Ahrendt, C. J. Borths and D. W. C. MacMillan, *J. Am. Chem. Soc.*, 2000, **122**, 4243–4244.
- 75 P. W. Hickmott, *Tetrahedron*, 1982, **38**, 3363–3446.
- 76 S. V Ley, *Asymmetric Organocatalysis*, Springer Berlin Heidelberg, Berlin, Heidelberg, 2009, vol. 291.
- 77 A. G. Doyle and E. N. Jacobsen, *Chem. Rev.*, 2007, **107**, 5713–5743.
- 78 P. Dinér, A. Kjærsgaard, M. A. Lie and K. A. Jørgensen, *Chem. - A Eur. J.*, 2008, **14**, 122–127.
- 79 U. Eder, G. Sauer and R. Wiechert, *Angew. Chemie Int. Ed. English*, 1971, **10**, 496–497.
- 80 W. S. Jen, J. J. M. Wiener and D. W. C. MacMillan, *J. Am. Chem.*

- Soc., 2000, **122**, 9874–9875.
- 81 S. Brandau, A. Landa, J. Franzén, M. Marigo and K. A. Jørgensen, *Angew. Chemie Int. Ed.*, 2006, **45**, 4305–4309.
- 82 G. Lelais and D. W. C. MacMillan, *Aldrichimica Acta*, 2006, **39**, 79–87.
- 83 B. List, *Tetrahedron*, 2002, **58**, 5573–5590.
- 84 J. F. Austin and D. W. C. MacMillan, *J. Am. Chem. Soc.*, 2002, **124**, 1172–1173.
- 85 D. Enders and U. Kallfass, *Angew. Chemie Int. Ed.*, 2002, **41**, 1743–1745.
- 86 H. Stetter, *Angew. Chem. Int. Ed. Engl.*, 1976, **15**, 639–647.
- 87 X. Bugaut and F. Glorius, *Chem. Soc. Rev.*, 2012, **41**, 3511.
- 88 A. J. Arduengo, R. L. Harlow and M. Kline, *J. Am. Chem. Soc.*, 1991, **113**, 361–363.
- 89 J. C. Sheehan and D. H. Hunneman, *J. Am. Chem. Soc.*, 1966, **88**, 3666–3667.
- 90 R. Breslow, *J. Am. Chem. Soc.*, 1958, **80**, 3719–3726.
- 91 K. L. Jensen, G. Dickmeiss, H. Jiang, Ł. Albrecht and K. A. Jørgensen, *Acc. Chem. Res.*, 2012, **45**, 248–264.
- 92 M. Schelhaas and H. Waldmann, *Angew. Chemie Int. Ed. English*, 1996, **35**, 2056–2083.
- 93 L. Samulis and N. C. O. Tomkinson, *Tetrahedron*, 2011, **67**, 4263–4267.
- 94 X.-F. Huang, Z.-M. Liu, Z.-C. Geng, S.-Y. Zhang, Y. Wang and X.-W. Wang, *Org. Biomol. Chem.*, 2012, **10**, 8794.
- 95 Y. Zhang, S. Wang, S. Wu, S. Zhu, G. Dong, Z. Miao, J. Yao, W. Zhang, C. Sheng and W. Wang, *ACS Comb. Sci.*, 2013, **15**, 298–308.
- 96 C. Cassani, X. Tian, E. C. Escudero-Adán and P. Melchiorre, *Chem. Commun.*, 2011, **47**, 233–235.
- 97 S. Agrawal, N. Molleti and V. K. Singh, *Chem. Commun.*, 2015, **51**, 9793–9796.
- 98 W. Li, X. Li, T. Ye, W. Wu, X. Liang and J. Ye, *Tetrahedron Lett.*, 2011, **52**, 2715–2718.
- 99 A. Medvedev, O. Buneeva and V. Glover, *Biologics*, 2007, **1**, 151–62.
- 100 V. Nair, S. Vellalath, M. Poonoth, R. Mohan and E. Suresh, *Org. Lett.*,

- 2006, **8**, 507–509.
- 101 S. S. Sohn, E. L. Rosen and J. W. Bode, *J. Am. Chem. Soc.*, 2004, **126**, 14370–14371.
- 102 V. Nair, S. Vellalath, M. Poonoth and E. Suresh, *J. Am. Chem. Soc.*, 2006, **128**, 8736–8737.
- 103 R. N. Reddi, P. K. Prasad and A. Sudalai, *Angew. Chemie Int. Ed.*, 2015, **54**, 14150–14153.
- 104 M. Rommel, T. Fukuzumi and J. W. Bode, *J. Am. Chem. Soc.*, 2008, **130**, 17266–17267.
- 105 T. Rodrigues, D. Reker, P. Schneider and G. Schneider, *Nat. Chem.*, 2016, **8**, 531–541.
- 106 R. Sink, S. Gobec, S. Pecar and A. Zega, *Curr. Med. Chem.*, 2010, **17**, 4231–4255.
- 107 C. F. Lo, K. Karan and B. R. Davis, *Ind. Eng. Chem. Res.*, 2007, **46**, 5478–5484.
- 108 A. Heydari, S. Khaksar, J. Akbari, M. Esfandyari, M. Pourayoubi and M. Tajbakhsh, *Tetrahedron Lett.*, 2007, **48**, 1135–1138.
- 109 B.-C. Chen, J. E. Sundeen, P. Guo, M. S. Bednarz and R. Zhao, *Tetrahedron Lett.*, 2001, **42**, 1245–1246.
- 110 S. Sato, T. Sakamoto, E. Miyazawa and Y. Kikugawa, *Tetrahedron*, 2004, **60**, 7899–7906.
- 111 J. Strovel, S. Sittampalam, N. P. Coussens, M. Hughes, J. Inglese, A. Kurtz, A. Andalibi, L. Patton, C. Austin, M. Baltezor, M. Beckloff, M. Weingarten and S. Weir, *Early Drug Discovery and Development Guidelines: For Academic Researchers, Collaborators, and Start-up Companies*, 2004.
- 112 Biotek Instruments, *An Introduction to Fluorescence Resonance Energy Transfer (FRET) Technology and its Application in Bioscience*, 2012, 1–6.
- 113 G. Karageorgis, University of Leeds, 2015.
- 114 G. Wang, C. Zheng and G. Zhao, *Tetrahedron: Asymmetry*, 2006, **17**, 2074–2081.
- 115 J. A. Gurak and K. M. Engle, *ACS Catal.*, 2018, **8**, 8987–8992.
- 116 H. J. Finlay, R. M. Lawrence, C. S. Huang, J. J. Hangeland, P. G.

- Sleph, A. Y. A. Chen, D. A. Gordon, L. E. Haque, D. S. Taylor, T. J. Friends, R. R. Wexler, M. D. Basso, R. Yang, L. M. Abell, X. Yin, L. P. Adam, T. W. Harrity, J. M. Onorato, J. Jiang and J. Neels, *ACS Med. Chem. Lett.*, 2018, **9**, 673–678.
- 117 T. Gensch and F. Glorius, *Science*, 2016, **352**, 294–295.
- 118 K. D. Collins and F. Glorius, *Nat. Chem.*, 2013, **5**, 597–601.
- 119 K. D. Collins, A. Rühling and F. Glorius, *Nat. Protoc.*, 2014, **9**, 1348–1353.
- 120 T. Gensch, M. Teders and F. Glorius, *J. Org. Chem.*, 2017, **82**, 9154–9159.
- 121 D. Gao and C. Cui, *Chem. - A Eur. J.*, 2013, **19**, 11143–11147.
- 122 C. Kashima, H. Harada, I. Kita, I. Fukuchi and A. Hosomi, *Synthesis (Stuttg.)*, 1994, **1994**, 61–65.
- 123 T. Haemers, J. Wiesner, R. Busson, H. Jomaa and S. Van Calenbergh, *European J. Org. Chem.*, 2006, **2006**, 3856–3863.
- 124 R. Wang, X. Zhang, C. Chen, G. Chen, Q. Zhong, Q. Zhang, S. Zheng, G. Wang and Q.-H. Chen, *Eur. J. Med. Chem.*, 2016, **110**, 164–180.
- 125 P. Valenta, N. A. Drucker, J. W. Bode and P. J. Walsh, *Org. Lett.*, 2009, **11**, 2117–2119.
- 126 T.-T. Xu, T.-S. Jiang, X.-L. Han, Y.-H. Xu and J.-P. Qiao, *Org. Biomol. Chem.*, 2018, **16**, 5350–5358.
- 127 H. T. Kim, W. Lee, E. Kim and J. M. Joo, *Chem. - An Asian J.*, 2018, **13**, 2418–2422.
- 128 B. Yin, C. Cai, G. Zeng, R. Zhang, X. Li and H. Jiang, *Org. Lett.*, 2012, **14**, 1098–1101.